SVENSKA GEOFYSISKA FÖRENINGEN

VOLUME 8, NUMBER 3 **Tellus** AUGUST 1956

A QUARTERLY JOURNAL OF GEOPHYSICS

Theorie zur Errechnung des Wasserstandes und der Strömungen in Randmeeren nebst Anwendungen[1]

Von WALTER HANSEN

Deutsches Hydrographisches Institut, Hamburg,
International Meteorological Institute in Stockholm

(Manuscript received July 10, 1956)

Abstract

For the detection of non-stationary movements in the ocean there exists, at present, no theory that could by observation stand a test with regard to its practical applicability. As there is available an abundant material of sea-level- and current observations from the marginal and adjacent seas and as in such areas maximum values of movements occur, the study of which deserves a special practical interest, a method is developed for determining the movements in such areas; morever, the results of a numerical computation of an especially heavy storm surge (Holland-Orkan) and of the tides in an estuary (the Ems river) are discussed. By combining these results with numerical weather prediction it is, in principle, possible to carry out numerical prediction of sea level.

Die Problemstellung

Die wesentlichen Ursachen für die Strömungen und die damit verbundenen Wasserstände im Meere liegen in den windschub-, den gezeiten- und den dichtegradienterzeugenden Kräften. Abgesehen von den instationären Gezeiten und Oberflächenwellen, sind die grossen permanenten Stromsysteme der Ozeane, seit jeher das Kernproblem der dynamischen Ozeanographie, fast immer als stationäre Bewegungen behandelt worden. Wenn auch V. W. Ekman bereits vor dreissig Jahren die Grundzüge einer rationellen Theorie derartiger stationärer Meeresströmungen entwickelt hat, ist es aber erst in den letzten 8 bis 10 Jahren gelungen, vor allem durch die Arbeiten von Stommel und Munk, Lösungen anzugeben, die zum mindesten in grossen Zügen mit den Beobachtungen übereinstimmen.

Die sehr zahlreichen Beobachtungen zeigen indessen, dass die grossen Stromsysteme nur im statistischen Mittel stationär sind. Die wellenartigen Mäander, die sich längs des Golfstroms fortpflanzen und zu Abschnürungen von Warm- und Kaltwasserkörpern führen können, geben schöne Beispiele für dynamisch interessante aber zur Zeit noch nicht erfassbare kleinmassstäbige, instationäre Vorgänge im offenen Meer. Ohne Zweifel besteht an der Entwicklung von Verfahren zur Vorhersage der Lage und Intensität etwa des Golfstromes ein lebhaftes wissenschaftliches und praktisches Interesse. Zur Ent-

[1] Die Untersuchungen wurden finanziell gefördert durch Bereitstellung von Mitteln des Bundesverkehrsministeriums aus Zuschüssen des ERP-Sondervermögens und der Deutschen Forschungsgemeinschaft.

wicklung und Anwendung eines derartigen Verfahrens bedarf es aber einer so ausserordentlichen Vermehrung des bereits vorhandenen sehr umfangreichen Beobachtungsmaterials, dass diese Forderung in naher Zukunft kaum wird verwirklicht werden können. Es ist deshalb verständlich, dass die Theoretiker, sofern sie sich überhaupt mit instationären Vorgängen beschäftigen, „Transient"-Probleme bevorzugen. Darunter sind hier Probleme etwa wie die langfristigen Änderungen der grossen permanenten Stromsysteme zu verstehen, die von Änderungen der allgemeinen atmosphärischen Windzirkulation hervorgerufen werden. Untersuchungen in dieser Richtung sind von CHARNEY (1955), MORGAN und VERONIS (1953) und VERONIS (1956) in Angriff genommen worden.

Anders liegen die Verhältnisse in den Rand- und Nebenmeeren wie etwa in der Nordsee.

Es ist zu hoffen, dass es mit der Entwicklung von Methoden zur numerischen Vorausberechnung des atmosphärischen Druckfeldes in 5 km Höhe, und später an der Meeresoberfläche, für 24, 48 und unter Umständen auch 72 Stunden, möglich sein wird, die Schubspannung an der Meeresoberfläche von Rand- und Nebenmeeren vorauszusagen. In Verbindung mit einer rationellen Theorie der Wasserbewegungen eröffnet sich damit erstmalig die Möglichkeit zum Aufbau eines theoretisch begründeten meteorologisch-ozeanographischen Verfahrens zur Vorhersage von Wasserständen und Strömungen in Rand- und Nebenmeeren. Die zahlreichen und routinemässig ausgeführten Beobachtungen des Wasserstandes an den Küsten eines Randmeeres wie der Nordsee geben die Möglichkeit, die Ergebnisse einer derartigen Theorie systematisch zu prüfen, und damit das Vertrauen in die dynamischen Methoden der Ozeanographie zu festigen.

Der praktische Wert derartiger Verfahren liegt vor allem darin, dass regelmässige und zuverlässige Wasserstandsvorhersagen rechtzeitig vor schweren Sturmfluten warnen können. Als Beispiel sei die als Folge des Holland-Orkans 1953 aufgetretene Sturmflut genannt, die schwere Verluste an Menschenleben und umfangreiche Verwüstungen hervorgerufen hat. Andere Anwendungen des Verfahrens zur Ermittlung der Wasserstände und Strömungen für Aufgaben der Praxis, etwa des Seewasserbaues, werden weiter unten beleuchtet.

Die Entwicklung eines Verfahrens zur Errechnung der Wasserstände und Stromgeschwindigkeiten in einem Randmeer wie der Nordsee wird dadurch erleichtert, dass mit homogenen Wassermassen gerechnet werden kann, da hohe Windgeschwindigkeiten die Sturmfluten zur Folge haben, im Verein mit den Gezeitenströmen für eine weitgehende horizontale und vertikale Vermischung sorgen. Schwierigkeiten, die aber überwunden werden können, bereitet die regional und in extremen Fällen wegen der Wasserstandsänderungen auch zeitlich variable Tiefe. Vielleicht noch grössere Schwierigkeiten können dadurch entstehen, dass die lateralen und vertikalen Reibungskoeffizienten nur mangelhaft bekannt sind.

Es ist heute noch nicht zu übersehen, in welcher Weise die Verknüpfung der Wasserstands- mit der numerischen Wettervorhersage am zweckmässigsten erfolgen soll. Nach den guten Ergebnissen, die die barotrope Theorie ergeben hat, ist vielleicht zu hoffen, dass eine barokline Theorie die benötigten Gradientwindwerte an der Meeresoberfläche liefern wird. Erwähnt sei in diesem Zusammenhang, dass nicht nur 24-, 48- und 72-stündige, sondern auch kurzfristigere Vorhersagen der Sturmflutwasserstände von wenigen Stunden in aktuellen Fällen sehr wichtig sein können.

Wegen dieser noch offenen Fragen ist das Schwergewicht der vorliegenden Untersuchung auf den ozeanographischen Teil der Theorie gelegt, und diese unter Verwendung von meteorologischen Beobachtungen an Hand von Wasserstandsbeobachtungen geprüft worden. Ausserdem wurde das Verfahren zur Ermittlung der Gezeiten und Gezeitenströme in einer Flussmündung der deutschen Nordseeküste verwendet, da in diesem Fall eine gute Kontrolle durch die vorhandenen Beobachtungen möglich war, und derartigen Untersuchungen ein besonderes praktisches Interesse zukommt.

Die Ableitung der Theorie

Die hier mitgeteilten Verfahren sind Verallgemeinerungen von solchen, die der Verfasser vor einer Reihe von Jahren zur Ermittlung von rein harmonischen Gezeitenschwin-

gungen und stationären Meeresströmungen abgeleitet hat. Ein wesentlicher Gesichtspunkt war dabei, Methoden zu finden, die unmittelbar an Hand vorliegender Beobachtungen geprüft und damit für praktische Aufgaben nutzbar gemacht werden können.

Grundlage der Untersuchungen sind die hydrodynamischen Differentialgleichungen:

$$\frac{\partial u}{\partial t} - fv + g\frac{\partial \zeta}{\partial x} - \nu\frac{\partial^2 u}{\partial z^2} - \nu^\star \triangle u + u\frac{\partial u}{\partial x} + v\frac{\partial u}{\partial y} + w\frac{\partial u}{\partial z} = k^{(x)}$$

$$\frac{\partial v}{\partial t} + fu + g\frac{\partial \zeta}{\partial y} - \nu\frac{\partial^2 v}{\partial z^2} - \nu^\star \triangle v + u\frac{\partial v}{\partial x} + v\frac{\partial v}{\partial y} + w\frac{\partial v}{\partial z} = k^{(y)} \qquad (1)$$

$$\frac{\partial u}{\partial x} + \frac{\partial v}{\partial y} + \frac{\partial w}{\partial z} = 0$$

Es bedeuten: x, y, z, t Raum- und Zeitkoordinaten, z von der ungestörten Meeresoberfläche positiv aufwärts gerechnet.

h Wassertiefe bei ungestörter Wasseroberfläche.

u, v, w Geschwindigkeitskomponenten.

U, V Komponenten der über die Tiefe gemittelten Geschwindigkeiten, also

$$U = \frac{1}{H}\int_{-h}^{\zeta} u\,dz, \quad V = \frac{1}{H}\int_{-h}^{\zeta} v\,dz$$

Ferner wird gesetzt:

$$u = U(1 + u'), \quad v = V(1 + v')$$

so dass

$$\int_{-h}^{\zeta} u'\,dz = \int_{-h}^{\zeta} v'\,dz = 0$$

Es ist hydrostatischer Druck und konstante Dichte angesetzt. In den ersten zwei Gleichungen ist durch diese konstante Dichte dividiert, sämtliche Glieder besitzen dann die Dimension einer Beschleunigung m sec^{-2}. Zur Abkürzung ist dieser Faktor nicht hingeschrieben worden. $k^{(x)}$ und $k^{(y)}$ sind die Komponenten der äusseren Beschleunigungen. Der Index *Ob* bezieht sich auf die Oberfläche, der Index *Bd* auf den Boden. Es sind f Coriolisparameter, g Erdbeschleunigung, $z = \zeta$ ist die Abweichung der Oberfläche vom ungestörten Meeresniveau, $z = -h$ der Meeresboden, $H = h + \zeta$ Gesamttiefe, ν, $\nu^\star$ vertikale und horizontale virtuelle Viskositätszahlen mit der Dimension m^2/sec. $\triangle = \frac{\partial^2}{\partial x^2} + \frac{\partial^2}{\partial y^2}$ Laplace-Operator.

Die Integration dieser Gleichungen von $z = -h(x, y)$ bis zu $z = \zeta$ (x, y) liefert drei neue Gleichungen für die Komponenten der mittleren Geschwindigkeit U, V und für den Wasserstand ζ, die nach einigen Umformungen den Ausgangsgleichungen in den wesentlichen Ausdrücken sehr ähnlich sind. Die ausserdem auftretenden Integrale über u'^2, $u'v'$ und v'^2 werden aus einer vorzugebenden vertikalen Geschwindigkeitsverteilung (Potenz- oder logarithmische Gesetze) ermittelt. Bei den hier zu behandelnden Aufgaben spielen diese Terme aber keine Rolle. Die Umformung erfolgt unter Verwendung der Randbedingungen:

$$w_{Ob} = \frac{\partial \zeta}{\partial t} + u_{Ob}\frac{\partial \zeta}{\partial x} + v_{Ob}\frac{\partial \zeta}{\partial y} \text{ an der Oberfläche}$$

und $$w_{Bd} = -\left(u_{Bd}\frac{\partial h}{\partial x} + v_{Bd}\frac{\partial h}{\partial y}\right) \text{ am Boden.}$$

Hiernach stimmt die Normalkomponente der Geschwindigkeit mit der entsprechenden Geschwindigkeitskomponente der Grenzfläche überein. Zur Abkürzung wird noch gesetzt:

$$A^{(x)} = k^{(x)} + \nu^\star \triangle U + \frac{\nu^\star}{H}\int_{-h}^{\zeta} \triangle(Uu')\,dz - \frac{1}{H}\frac{\partial}{\partial x}\left(U^2\int_{-h}^{\zeta} u'^2 dz\right) - \frac{1}{H}\frac{\partial}{\partial y}\left(UV\int_{-h}^{\zeta} u'v'\,dz\right),$$

$$A^{(y)} = k^{(y)} + \nu^\star \triangle V + \frac{\nu^\star}{H}\int_{-h}^{\zeta} \triangle(Vv')\,dz - \frac{1}{H}\frac{\partial}{\partial x}\left(UV\int_{-h}^{\zeta} u'v'dz\right) - \frac{1}{H}\frac{\partial}{\partial y}\left(V^2\int_{-h}^{\zeta} v'^2 dz\right).$$

Sämtliche τ, die hier als Schub bezeichnet werden, besitzen, da durch die nicht aufgeschriebene Dichte dividiert worden ist, die Dimension $m^2/sec.^2$

Es resultieren die Gleichungen:

$$\frac{\partial U}{\partial t} - fV + g\frac{\partial \zeta}{\partial x} + \frac{\tau_{Bd}^{(x)}}{H} + U\frac{\partial U}{\partial x} + V\frac{\partial U}{\partial y} = \frac{\tau_{Ob}^{(x)}}{H} + A^{(x)},$$

$$\frac{\partial V}{\partial t} + fU + g\frac{\partial \zeta}{\partial y} + \frac{\tau_{Bd}^{(y)}}{H} + U\frac{\partial V}{\partial x} + V\frac{\partial V}{\partial y} = \frac{\tau_{Ob}^{(y)}}{H} + A^{(y)}, \quad (2)$$

$$\frac{\partial \zeta}{\partial t} + \frac{\partial}{\partial x}(HU) + \frac{\partial}{\partial y}(HV) = 0$$

Dieses System wird als Grundlage der Untersuchung in zweidimensional ausgedehnten Meeresgebieten benutzt. Beträgt die Breite (y-Koordinate) nur einen Bruchteil der Länge (x-Koordinate), wie etwa in kanalartigen Buchten und Flussmündungen, dann wird die Anzahl der Unbekannten durch Integration über die Breite abermals vermindert. Es werden eingeführt:

Die Breite $B = b_1 + b_2$, der Querschnitt $Q = \int_{-b_2}^{b_1} H\,dy$, $\bar{u} = \frac{1}{Q} \cdot \int_{-b_2}^{b_1} HU\,dy$. Entsprechende Umformungen wie oben führen hier zu dem System für eindimensionale Gebiete:

$$\frac{\partial \bar{u}}{\partial t} + g\frac{\partial \zeta}{\partial x} + \frac{B}{Q} \cdot \tau_{Ob} + \bar{u}\frac{\partial \bar{u}}{dx} = \frac{B}{Q} \cdot \tau_{Bd} + A \quad (3)$$

$$\frac{\partial \zeta}{\partial t} + \frac{1}{B} \cdot \frac{\partial}{\partial x}(Q\bar{u}) = 0$$

$\bar{u}$, ζ und τ sind definitionsgemäss Mittelwerte über den Querschnitt oder die Breite, A entspricht dem $A^{(x)}$ im zweidimensionalen Fall. Numerische Rechnungen und theoretische Abschätzungen zeigen, dass in Rand- und Nebenmeeren $A^{(x)}$ und $A^{(y)}$, in Flussmündungen A, im Vergleich mit den anderen Termen in den Gleichungen klein und demnach zu vernachlässigen sind. Entsprechendes gilt für die konvektiven Terme. Angemerkt sei, dass keine grundsätzlichen Schwierigkeiten entstehen, wenn diese Ausdrücke mitgeschleppt werden.

Die in den Gleichungen (2) und (3) auftretenden tangentialen Schübe am Boden und an der Oberfläche werden hier, physikalischen Gepflogenheiten entsprechend, proportional dem Quadrat der Geschwindigkeit gesetzt. Für den Schub an der Meeresoberfläche τ_{Ob} wird nach dem Vorgang von Ekman, Palmén u. a. (vgl. SVERDRUP 1942):

$$\tau_{Ob} = \lambda \cdot W|W| \quad \text{mit } \lambda = 3{,}2 \cdot 10^{-6} \quad (4)$$

wo W die Windgeschwindigkeit über dem Wasser ist. Die Dimension von W ist $m\,sec^{-1}$ und von τ $m^2\,sec^{-2}$.

Der Tangentialschub am Boden τ_{Bd} wird proportional dem Quadrat der mittleren Stromgeschwindigkeit gesetzt:

$$\tau_{Bd} = r \cdot \bar{u}|\bar{u}|. \quad (5)$$

Hier ist r ebenso wie λ eine dimensionslose Grösse. Aus Beobachtungen ist r zu $2{,}6 \times 10^{-3}$ ermittelt worden.

Da die Anzahl der Windbeobachtungen von der freien Nordsee für die hier vorzunehmende Untersuchung der Sturmflut am 31. 1. und 1. 2.1953 nicht ausreicht, musste auf die Luftdruckverteilung zurückgegriffen und daraus der geostrophische Wind ermittelt werden. Der Umrechnungsfaktor wurde mit 0,7 angesetzt; damit ist in Gleichung (4) an Stelle von λ mit ausreichender Genauigkeit der Faktor $0{,}5 \cdot \lambda$ einzutragen, wenn W die Windgeschwindigkeit des geostrophischen Windes bedeutet. Die Faktoren λ und r können räumlich und zeitlich variieren. Das Ausmass dieser Änderungen auch in Abhängigkeit von den massgebenden Parametern ist mit Hilfe eigens dafür angestellter Beobachtungen untersucht worden. Diese speziellen Ergebnisse lassen sich aber zur Zeit noch nicht für Untersuchungen der unten folgenden Art verwerten, da bei den hier zu behandelnden aktuellen Fällen (Holland-Orkan) nur die normalen Routinebeobachtungen zur Verfügung stehen. Aus dem Grunde werden hier die Koeffizienten λ und r als Konstante aufgefasst, was in erster Approximation gerechtfertigt sein wird.

WELANDER (1956) hat im International Meteorological Institute, Stockholm, in jüngster Zeit lineare Theorien der winderzeugten Wasserbewegungen entwickelt, die an Stelle der Verknüpfung gemäss Gleichung (5) von der

Voraussetzung ausgehen, dass die Geschwindigkeit am Boden gleich Null ist. Lineare ebenso wie nicht lineare Theorien (HANSEN, 1950) dieser Art liefern funktionale Zusammenhänge zwischen den Tangentialschüben, den Geschwindigkeiten am Meeresboden und an der Oberfläche, der mittleren Geschwindigkeit und dem Oberflächengefälle. Ausserdem tritt die virtuelle Viskositätszahl als Koeffizient der Geschwindigkeit auf. Derartige Theorien können dazu dienen, mit Hilfe von gleichzeitigen Wind-, Strom- und Gefällsbeobachtungen die numerischen Werte der Zahlen λ und r zu berechnen.

Ursprünglich war vorgesehen, in der hier dargestellten Theorie den Schub am Boden im nichtstationären Fall so anzusetzen, dass beim Übergang zum stationären Zustand eine Lösung erhalten wird, die mit der Lösung des nichtlinearen eindimensionalen Falles übereinstimmt. Da hier die mittlere Geschwindigkeit Null ist, wird der Schub dem Oberflächengefälle proportional. Auf den zweidimensionalen Fall übertragen ergibt sich ein Faktor von 1,5 mit dem der Schub an der Oberfläche multipliziert werden sollte. Da aber in zweidimensional ausgedehnten Meeresgebieten veränderlicher Tiefe die Komponenten der mittleren Geschwindigkeit im allgemeinen von Null verschieden sind, wurde dieser Faktor nachträglich aus den Rechnungen eliminiert. Das bedeutet, dass abgesehen von der Nichtlinearität der Gleichungen, praktisch der Schub am Boden proportional dem Quadrat der Stromgeschwindigkeit gesetzt wird.

Die hier zu behandelnden Aufgaben führen für die Gleichungssysteme (2) und (3) zu Rand- und Anfangswertaufgaben. Eine auch für praktische Zwecke ausreichende Reproduktion der natürlichen Bewegungsvorgänge im Meere mittels dieser Differentialgleichungen ist nur dann zu erwarten, wenn keine die Allgemeinheit wesentlich einschränkenden Vereinfachungen vorgenommen werden. Aus diesem Grund ist das Hauptaugenmerk auf die Entwicklung von Verfahren gelegt, die unter unmittelbarer Verwendung der vorgegebenen Rand- und Anfangswerte numerische Lösungen liefern.[1] Analytische Lösungen können nur unter unvergleichlich höherem Aufwand den Anforderungen gerecht werden, der etwa aus einer natürlichen Tiefenverteilung entspringt. Hierzu werden in der üblichen Weise (vgl. etwa HANSEN, 1954) zunächst die in den Gleichungen (2) und (3) auftretenden Differentialquotienten nach x und y durch Differenzenquotienten approximiert, die einem bestimmten Gitter der Maschenweite l zugeordnet sind. Es entsteht ein System gewöhnlicher Differentialgleichungen in bezug auf die Differentialquotienten nach der Zeit t, die sämtlich linear auftreten. Das bedeutet: Die zeitlichen Änderungen der Geschwindigkeitskomponenten und der Wasserstände in den Gitterpunkten sind bekannt, wenn die Funktionswerte vorgegeben sind. Werden auch die Ableitungen nach der Zeitkoordinate t durch finite Ausdrücke ersetzt, dann können ausgehend von bekannten Funktionswerten zu einem Anfangszeitpunkt diese Funktionswerte zu einem darauffolgenden numerisch ermittelt werden.

Das im Eindimensionalen verwendete Gitter ist in den Abb. 1 und 2 dargestellt. Das Nordseegitter ist in Abb. 3 zu erkennen. Die partiellen Ableitungen nach x oder x und y sind jeweils durch zentrale Differenzen in der Weise ersetzt, dass in den durch Kreuze gekennzeichneten Punkten die Geschwindigkeiten und in den durch ausgefüllte Kreise dargestellten Punkten die Wasserstände errechnet werden. Auch die Ableitungen nach der Zeit werden durch zentrale Differenzen approximiert. In den Zeitpunkten $t=t_0$, $t=t_0+2\,\Delta\,t$ usw. werden die Geschwindigkeitskomponenten, in den Zeitpunkten $t=t_0+\Delta t$, $t=t_0+3\Delta t$ usw. die Wasserstände numerisch ermittelt. Die Rechnung wird so angelegt, dass mit den bereits für t_0 und $t_0+\Delta t$ bekannten Geschwindigkeiten und Wasserständen unter Benutzung der Bewegungsgleichungen die Geschwindigkeiten für $t=t_0+2\,\Delta t$ erhalten werden. Diese Werte werden in der Kontinuitätsgleichung zusammen mit den Wasserständen für $t=t_0+\Delta t$ zur Ermittlung der Wasserstände im Zeitpunkt $t=t_0+3\,\Delta t$ benutzt. In dieser Weise fortfahrend werden Schritt für Schritt die Geschwindigkeiten und Wasserstände bestimmt, wobei die Randbedingungen wesentlich in die Rechnung eingehen.

Im eindimensionalen Fall werden als Rand-

[1] KIVISILD (1954) hat ein graphisches Verfahren mitgeteilt und zur Ermittlung des Windstaus im Binnensee Okeechokee benutzt.

werte vorgegeben: Der Wasserstand an der Mündung und der Süsswasserzufluss an der Landseite als Funktionen der Zeit. Im zweidimensionalen Fall werden als Randbedingungen verwendet: Auf der Nordgrenze des Gebietes, die von Schottland nach Norwegen verläuft, bleiben die Wasserstände ungestört. Längs den Küsten ist die Normalkomponente der Geschwindigkeit Null. Das gilt auch für den Eingang zum Skagerrak, das hier nicht berücksichtigt wird. Die Durchflussmenge durch die Doverstrasse ist proportional dem Wasserstand gesetzt. Angemerkt sei, dass keine Beobachtungen des Wasserstandes oder der Durchflussmenge in die Rechnung eingesetzt werden.

Courant, Friedrich und Levy haben darauf hingewiesen, dass derartige Verfahren nur dann brauchbar sind, wenn $\frac{\Delta t}{l}$ kleiner ist als eine Zahl, die von der Wahl der verwendeten finiten Ausdrücke abhängt. Ist ein Reibungsterm vorhanden – wie bei den hier zu behandelnden Aufgaben –, dann existiert nicht nur eine eindeutig bestimmte Lösung, sondern diese ist auch – jedenfalls nach hinreichend langer Zeit – von den Anfangswerten unabhängig. Das Ausmass dieses Abklingens hängt einmal vom Betrag der Reibung, dann aber auch von der Struktur des approximierenden Gleichungssystems ab. Das Koeffizientenschema dieses Systems als Matrix aufgefasst besitzt Eigenwerte χ und Eigenvektoren.

Durch geeignete Wahl des Zeitschrittes Δt wird $|\chi| < 1$. Sind die Eigenwerte χ einfach, dann erfolgt das Abklingen gemäss $|\chi|^k$ für grosse k, treten aber mehrfache Eigenwerte auf, dann tritt zu diesem Wert ein Faktor der Grössenordnung k, der zum mindesten zu Beginn das Abklingen verzögern kann. Diese Zusammenhänge sind nur dann bis in alle Einzelheiten klar zu erkennen, wenn die Eigenwerte des Systems der Differenzengleichungen bekannt sind. Bei Gittern mit mehreren hundert inneren Punkten ist deren Ermittlung ausserordentlich aufwendig. Nach den bisher in diesem Zusammenhang angestellten Überlegungen und den praktischen Erfahrungen werden folgende Vermutungen nahegelegt. Im eindimensionalen Fall besitzt die Matrix nur einfache Eigenwerte. Im zweidimensionalen Fall kommen unter den Eigenwerten der Matrix mehrfache vor, sofern die Coriolisbeschleunigung unberücksichtigt bleibt. Wird dagegen f mitgenommen, dann treten zwar keine mehrfachen aber offenbar nahe beieinander gelegene Eigenwerte auf, so dass sich trotzdem Konvergenzverzögerungen bemerkbar machen. Zur Erprobung des Verfahrens wurden die Mitschwingungsgezeiten in einem rechteckigen Becken von der Grösse und der Tiefenverteilung der Nordsee errechnet. Vor allem in den tiefen im Norden gelegenen Teilen zeigten die Wasserstände Aufrauhungen. Erst nach einer Mittelung benachbarter Werte betrug der mittlere Fehler etwa ein drittel Meter. Dieses Ergebnis deutet jedenfalls darauf hin, dass das Verfahren noch nicht voll geeignet ist, Schwingungsvorgänge mit der Periode der Halbtagsgezeiten, das sind rund 12 Stunden, zu untersuchen. Wie bereits erwähnt, treten die Störungen vornehmlich in tiefem Wasser auf, das mag auch seinen Grund darin haben, dass hier die dämpfende Wirkung der Reibung wegen der grossen Tiefe geringer als im flachen Küstenbereich ist. Andererseits scheint eine in jedem Zeitschrittvorgenommene Mittelbildung räumlich benachbarter Funktionswerte die Konvergenz zu verbessern. Da diese Zusammenhänge heute noch nicht in voller Allgemeinheit durchschaubar sind, kann nicht immer auf eine experimentelle Erprobung dieser numerischen Verfahren verzichtet werden, und gelegentliche Misserfolge müssen in Kauf genommen werden. Auf jeden Fall ist im Zweidimensionalen eine kritische Verwendung des numerischen Verfahrens angezeigt.

Bemerkenswert ist, dass das Auftreten mehrfacher Eigenwerte auch im zweidimensionalen Fall vermieden werden kann, wenn die aus den Gleichungen (2) abzuleitende Vorticity und Divergenz zusammen mit dem Wasserstand zur Aufstellung des Systems finiter Ausdrücke verwendet werden. Im einfachsten linearen Fall konstanter Tiefe, linearer Reibung und verschwindender Erdrotation findet keine räumliche Ausbreitung der Rotation statt und diese ist durch ihren Anfangswert und die Rotation der äusseren Kräfte bestimmt. Damit reduziert sich das System auf zwei Gleichungen für die Divergenz und den Wasserstand. Das zweidimensionale Problem ist damit auf die Lösung eines eindimensionalen zurückgeführt.

Die Anwendung der Theorie auf die Ermittlung von Wind- und gezeitenbedingten Bewegungen

Mit Hilfe der hier dargestellten Theorie wurden seit mehreren Jahren eine grössere Anzahl von ein- und zweidimensionalen Fällen vom Verfasser in der Abteilung Ozeanographie des Deutschen Hydrographischen Instituts in Hamburg mit der Hand und ab 1955 in enger Zusammenarbeit mit dem International Meteorological Institute in Stockholm unter Benutzung der BESK untersucht. In diesem Institut wurden auch die Maschinenprogramme sowohl für die eindimensionalen wie auch für die zweidimensionalen Fälle geschrieben. Ein umfassender Arbeitsbericht ist in Vorbereitung und erscheint gesondert. KREISS (1956) hat die Gezeiten und Gezeitenströme in geometrisch einfach gestalteten Kanälen untersucht. Im Zusammenhang mit Aufgaben des praktischen Wasserbaus wurden nach dem hier abgeleiteten Verfahren die Gezeiten und Gezeitenströme in einigen Flüssen mit der Hand gerechnet. Die Ergebnisse zeigen gute Übereinstimmung mit den Beobachtungen. Für zweidimensionale rechteckige Gebiete konstanter Tiefe sind Handrechnungen mit Gittern geringer Punktzahl zur Ermittlung der Gezeiten und der windbedingten Bewegungen durchgeführt worden. Die Ergebnisse waren unterschiedlich. Während die winderzeugten Wasserstände der Grössenordnung nach und die Phasen der Gezeiten recht gut mit den Beobachtungen übereinstimmten, waren zwischen beobachteten und errechneten Amplituden grössere Differenzen vorhanden.

Bei Rechnungen mit eindimensionalen Gebieten fanden, wie es die Theorie erwarten lässt, keine Konvergenzverzögerungen statt, auch dann nicht, wenn gleichzeitig Gezeiten und windbedingte Bewegungen gerechnet wurden. Dasselbe gilt für die Handrechnungen für zweidimensionale Gebiete, sofern die Anzahl der Gitterpunkte klein ist. Konvergenzverzögerungen machten sich überhaupt erst bemerkbar bei grosser Anzahl der Gitterpunkte. Der Grad der Konvergenzverzögerung wird nach den Erfahrungen mit den numerischen Rechnungen von der zeitlichen Änderung der steuernden Funktionen wie etwa der Windschubkraft oder den Gezeitenwasserständen auf dem Rande beeinflusst. Ist etwa das vorgegebene Windfeld zeitlich konstant, dann werden praktisch keine Schwierigkeiten auftreten. Erstrecken sich die zeitlichen Änderungen über einen Zeitraum von grössenordnungsmässig zwei Tagen, wie etwa im Falle des Holland-Orkans, dann scheinen die Schwierigkeiten nicht allzu gross. Sie wachsen aber offenbar an, wenn die Dauer der zeitlichen Änderungen bei einem halben Tag liegt, wie die Nachrechnung der Halbtagsgezeiten für die Nordsee zeigt.

Zur Hauptsache werden im folgenden die Lösungen zweier Aufgaben besprochen und mit den Beobachtungen verglichen. Die erste betrifft die Nachrechnung der Gezeiten und Gezeitenströme in der Ems, die zweite die Ermittlung der vom Holland-Orkan bedingten Wasserbewegungen in der Nordsee.

Bei der Vorbereitung numerischer Rechnungen muss die Maschenweite des Gitters so gewählt werden, dass auf der einen Seite alle wesentlichen Einflüsse der Küsten- und Tiefengestalt erfasst werden. Auf der anderen Seite ist zu vermeiden, dass die Anzahl der Gitterpunkte und damit der Rechenaufwand zu gross werden. Die Maschenweite beträgt auf der Ems 2, auf der Nordsee 37 km. Im eindimensionalen Fall kann bei Maschinenrechnungen die Maschenweite ohne weiteres herabgesetzt werden. In der Nordseerechnung würde durch eine wesentliche Verkleinerung des Gitterpunktabstandes die Rechenarbeit aber erheblich ansteigen. Die hier für die Nordsee gewählte Maschenweite von 37 km gestattet die Küsten- und Tiefengestalt in den wesentlichen Zügen zu erfassen. Andererseits bleibt die Rechenarbeit noch in erträglichen Grenzen.

Es ist selbstverständlich, dass die Rechnung keine detaillierten Angaben für Gebiete liefert, deren Längen oder Breiten kleiner als die Maschenweite sind. In morphologisch reich gegliederten Gebieten, wie etwa im Wattenmeer, können aber die örtlichen Änderungen des Windstaus von Interesse sein. Zur Lösung dieser Aufgabe wären zunächst durch eine Rechnung für das gesamte Randmeer mit relativ grosser Maschenweite die windbedingten Wasserstände vor der Küste zu ermitteln. Diese können dann als vorgegebene Randwerte in einer Rechnung für ein Gitter mit kleinerer Maschenweite benutzt werden, und damit wird dann der Windstau

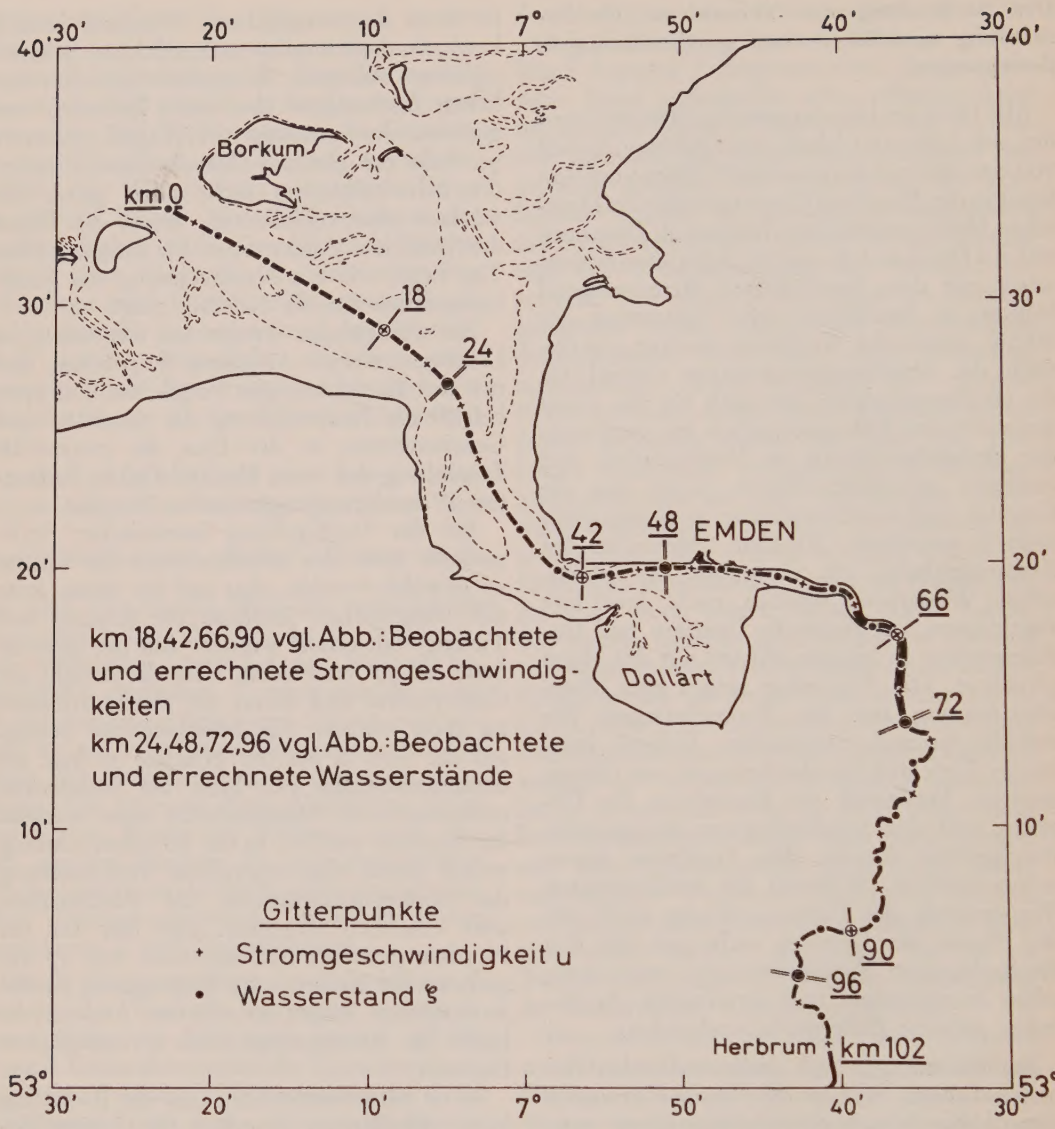

Abb. 1. Gezeitenästuar Ems. Das Gitter fällt mit der Stromachse zusammen. Zahlen geben Entfernung in Kilometern flussaufwärts, gerechnet von der Mündung bei Borkum. Die Wasserstände sind in den Punkten, die mit einem •, die Stromgeschwindigkeiten in den Punkten, die mit einem + bezeichnet sind, errechnet. Der Abstand aufeinander folgender Punkte beträgt 2 km. Vergleich zwischen beobachteten und errechneten Wasserständen erfolgt in den Punkten ⊙ mit 24, 48, 72 und 96 km Entfernung, für beobachtete und errechnete Stromgeschwindigkeiten in den Punkten ⊕ mit 18, 42, 66 und 90 km Entfernung von Borkum (vgl. Abb. 2).

auch in Gebieten geringer Ausdehnung aber örtlich stark veränderlicher Morphologie erhalten. In speziellen eindimensionalen Fällen kann das etwa nach dem hier gegebenen Beispiel von der Ems ausgeführt werden.

Das Gezeitenästuar der Ems erstreckt sich von der Mündung in die Nordsee bei der Insel Borkum bis zum etwa 100 km flussaufwärts gelegenen Ort Herbrum, wo ein Wehr errichtet ist. (Vergleiche Abb. 1.) Als Rand-

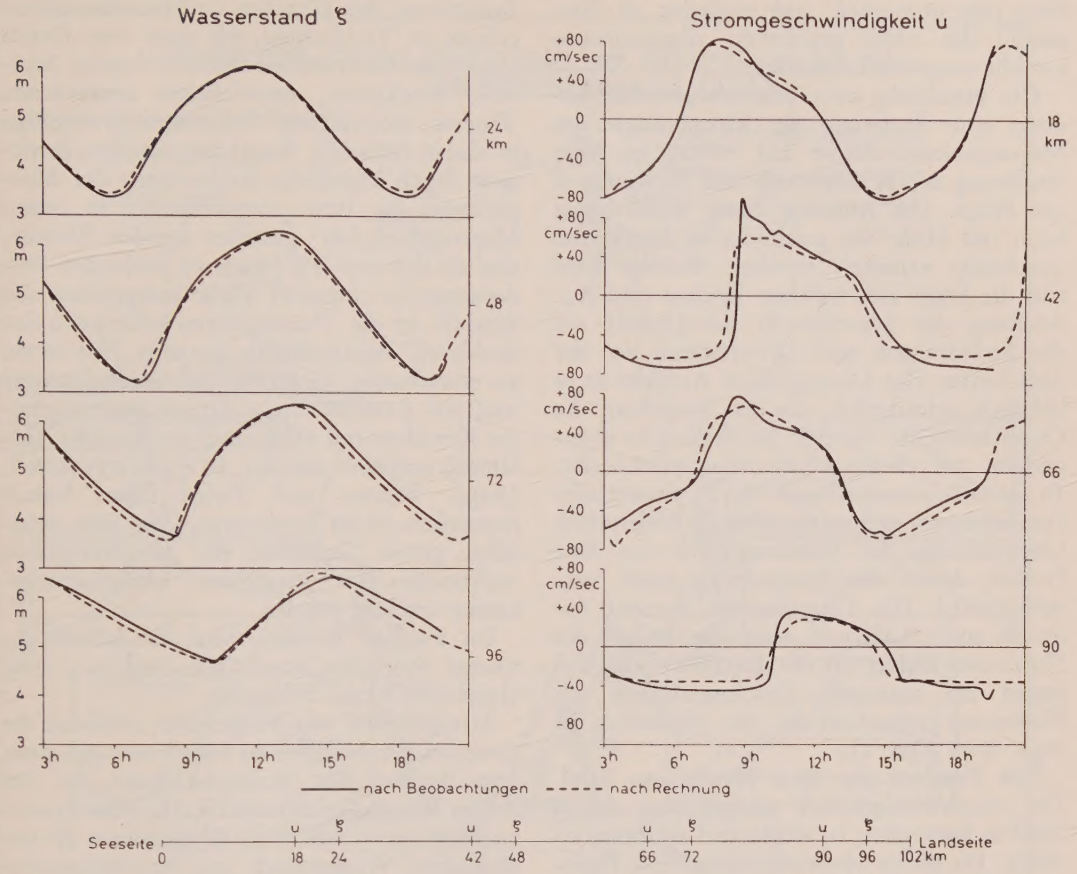

Abb. 2. Beobachtete (———) und errechnete (– – –) Wasserstände und Stromgeschwindigkeiten auf der Ems am 25.6.1949. Zum Vergleich sind die Wasserstände in 24, 48, 72 und 96 km, die Stromgeschwindigkeiten in 18, 42, 66 und 90 km Entfernung von der Mündung dargestellt.

bedingungen wurden die am 25. 6. 1949 bei Borkum beobachteten Wasserstände und die bei Herbrum zufliessende Süsswassermenge verwendet. Die 102 km lange Strecke wurde in Abschnitte von je 2 km Länge eingeteilt, und die Wasserstände in Entfernungen von 4, 8, 12 usw. bis 100 km und die Stromgeschwindigkeiten in Entfernungen von 2, 6, 10 usw. bis 98 km, von der Mündung ab gerechnet, numerisch ermittelt. Breiten, Querschnitte und Oberflächen waren vorgegeben. Die Wasserstände in Entfernungen von 24, 48, 72 und 96 km und die über den Querschnitt gemittelten Stromgeschwindigkeiten in Entfernungen von 18, 42, 66 und 90 km wurden aus Beobachtungen für den 25. 6. 1949 entnommen und mit den errechneten Werten zum Vergleich in Abb. 2 dargestellt. Die Übereinstimmung zwischen beobachteten und errechneten Wasserständen und Stromgeschwindigkeiten ist bemerkenswert und umfasst sogar Feinheiten im Kurvenverlauf.

An dieser Stelle sei angemerkt, dass von den Wasserbauingenieuren vor allem in Holland – es seien nur die Namen von H. A. Lorenz, Thiysse, Dronkers und Schönfeldt genannt –, eine Reihe von Methoden zur Ermittlung der Gezeiten in Flussmündungen entwickelt worden sind, die entweder auf einer Linearisierung beruhen, Potenzreihenentwicklungen oder die Charakteristiken-Theorie benutzen. Das hier verwendete Verfahren ist demgegen-

über rein numerisch und erscheint als Spezialfall des oben gegebenen allgemeineren zweidimensionalen Ansatzes.

Die Errichtung von Wasserbauwerken bedingt eine Änderung der Morphologie des Meeresgebietes. Diese hat wiederum eine Änderung der Wasserstände und Strömungen zur Folge. Das Ausmass dieser Änderungen kann mit Hilfe des geschilderten Verfahrens quantitativ ermittelt werden. An der Ems tritt die Frage auf, welchen Einfluss eine Abdeichung der Meeresbucht des Dollart auf die Strömungen und Wasserstände in der Ems besitzt. Zur Lösung dieser Aufgabe ist es lediglich erforderlich, in der Rechnung die Querschnitte im Bereich des Dollart so abzuändern, wie es die Eindeichung vorschreibt. Es ist zu erwarten und durch numerische Handrechnungen bestätigt, dass die vorhandene Unsymmetrie des Gezeitenstroms vor dem Dollart durch die Eindeichung noch verstärkt wird. Die Unsymmetrie kommt dadurch zum Ausdruck, dass die Dauer des Flutstroms kleiner als die des Ebbstroms, dagegen die maximale Geschwindigkeit des Flutstroms grösser als die des Ebbstroms ist (vgl. etwa Abb. 2).

Das Flussbett der Ems besteht aus Sand. Die Geschwindigkeiten reichen aus, diesen Sand in Bewegung zu setzen und zu transportieren. Da dieser Materialtransport eine Funktion der Geschwindigkeit ist, wird er im Mittel über eine Gezeitenperiode wegen der Unsymmetrie der Gezeitenströme nur dann verschwinden, wenn das Fluss- oder Meeresgebiet im Gleichgewicht steht. Da bei der Eindeichung des Dollart die Unsymmetrie des Gezeitenstroms verstärkt wird, ist mit einem landwärts gerichteten Materialtransport zu rechnen, der das Fahrwasser der Ems verschlechtern kann. Bisher scheint es nur gelungen zu sein, aus den quantitativ ermittelten Stromgeschwindigkeiten den Materialtransport qualitativ abzuschätzen. Eine Theorie des resultierenden Materialtransportes über eine Gezeitenperiode scheint nicht vorzuliegen. Es wäre denkbar, eine solche auf der Grundlage der Transportgleichung zu entwickeln. Aber die Kenntnis der Stromgeschwindigkeit allein gestattet bereits wichtige Schlüsse auf die daraus folgenden Tendenzen zur Umgestaltung der Morphologie.

Das vorstehend geschilderte Verfahren zur Ermittlung der Gezeiten und Gezeitenströme erlaubt in Verbindung mit einer von KREISS (1956) im International Meteorological Institute, Stockholm, entwickelten analytischen Theorie nichtlinearer Schwingungsvorgänge in einem einfachen Kanal festzustellen, inwieweit durch künstliche Änderungen der Morphologie die Bewegungsvorgänge in einem Meeresgebiet so gestaltet werden können, dass sie den von der Praxis zu stellenden Forderungen in optimaler Weise entsprechen. Als Beispiel sei die Planung eines schleusenfreien (sea-level) Panamakanals genannt. Die hierin zu erwartenden Gezeiten und Gezeitenströme sind von LAMOEN (1949) für ein angenommenes Kanalbett mit Hilfe eines graphischen Verfahrens ermittelt worden. Es erscheint reizvoll, Länge, Breiten und Tiefen dieses Kanals numerisch so zu bestimmen, dass eine möglichst grosse Sicherheit für die Navigation verbunden mit geringsten Unterhaltungskosten erreicht werden.

Im zweiten Beispiel wird die bereits genannte Sturmflut vom 31. 1. und 1. 2. 1953 (Holland-Orkan) behandelt.

Ursprünglich war vorgesehen, zunächst die Gezeiten der Nordsee zu berechnen und dann mit Beginn des Holland-Orkans die aus dessen Windfeld folgenden Kräfte dem System zu überlagern. Auf diese Weise hätten die tatsächlichen Wasserstände und Stromgeschwindigkeiten erhalten und mit den aktuellen Beobachtungen verglichen werden können. Da aber, wie oben bereits erwähnt, das hier zur Verfügung stehende, unmittelbar aus den Bewegungsgleichungen abgeleitete Verfahren die Gezeiten der Nordsee nur mit einer für praktische Zwecke noch nicht immer ausreichenden Genauigkeit wiedergibt, wurden in der Rechnung die windbedingten Bewegungen allein ermittelt.

Die meteorologischen Beobachtungen wurden dankenswerter Weise vom Seewetteramt Hamburg bearbeitet und für die Rechnung vorbereitet. Aus den eigens für diese Aufgabe gezeichneten Wetterkarten von 3 zu 3 Stunden wurden dort der Luftdruck und der geostrophische Wind für die Gitterpunkte gewonnen. Die Prüfung der Theorie wird dadurch erleichtert, dass sowohl GROEN (1953) als auch ROSSITER (1954) die während des Holland-Orkans aufgetretenen Wasserstände für eine grosse Zahl von Orten an den Küsten

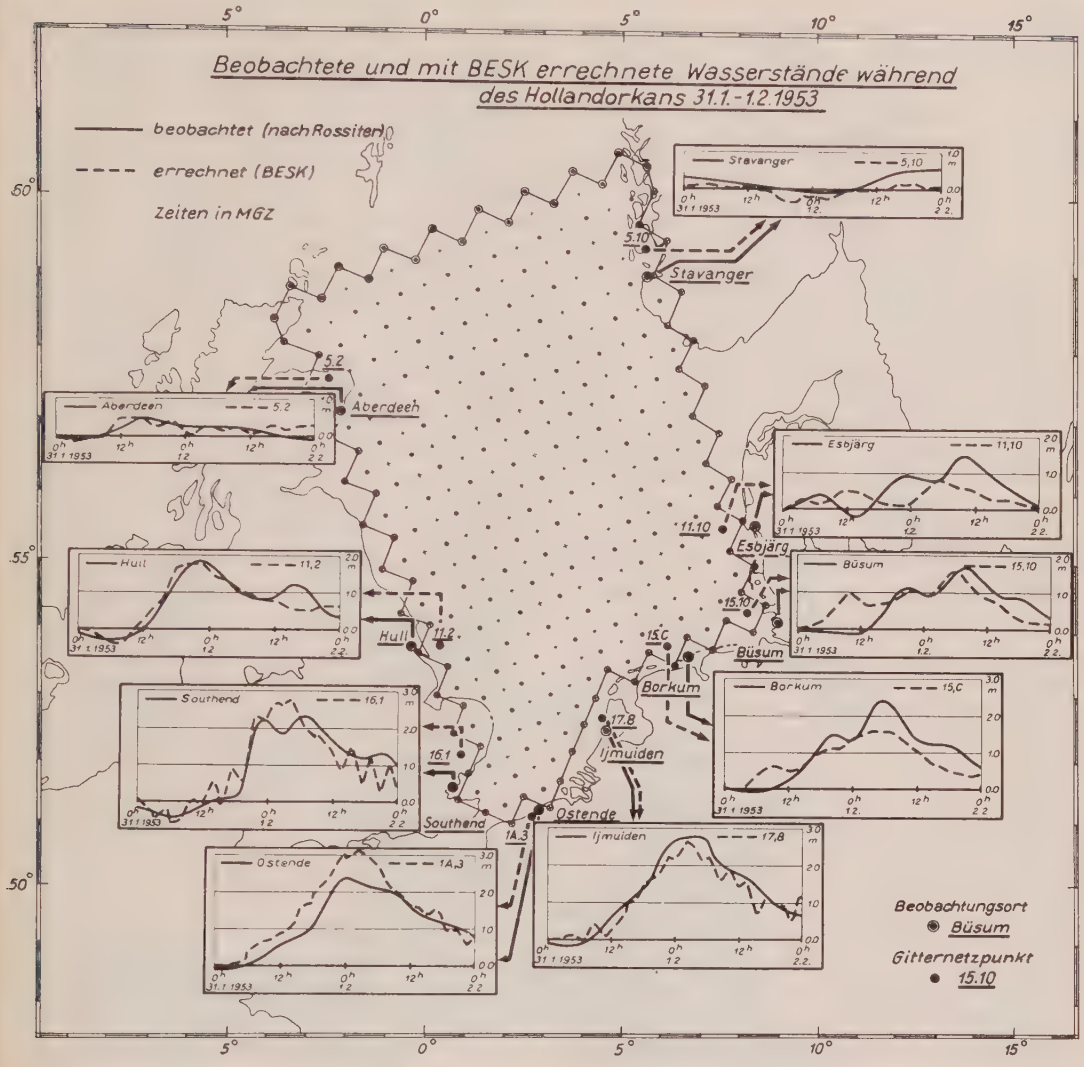

Abb. 3. Gitternetz für die Nordsee zur Nachrechnung des Hollandorkans. Die Wasserstände sind in den durch ●, die Stromgeschwindigkeiten in den durch + bezeichneten Punkten errechnet. Darstellungen geben beobachtete (———, nach Rossiter) und errechnete (— — —, nach B E S K) Wasserstände. Die Beobachtungen auf die Orte mit unterstrichenen Namen, die Rechnungen auf die durch Ziffern bezeichneten Glitterpunkte, Pfeile weisen auf die zugehörige Darstellung.

der Nordsee bearbeitet haben. Rossiter hat nach Elimination der Gezeiten Windstaukurven für diese Küstenorte mitgeteilt, die in Auswahl in Abb. 3 wiedergegeben sind.

D e Rechnung liefert für die Dauer des Holland-Orkans die Wasserstände und die mittleren Geschwindigkeiten in den durch Vollkreise und Kreuze bezeichneten Gitterpunkten (vgl. Abb. 3 und 4). In Abb. 3 sind für Gitterpunkte, die Beobachtungsorten benachbart sind, die errechneten gemeinsam mit den von Rossiter gegebenen Werten über der Zeit eingetragen. Besonders für die Orte an der englischen Küste und für Ijmuiden gibt die Rechnung die Beobachtungen relativ gut wieder. Ausgesprochen schlecht ist das Ergebnis nur für einen Ort, nämlich Esbjerg. Das ist mög-

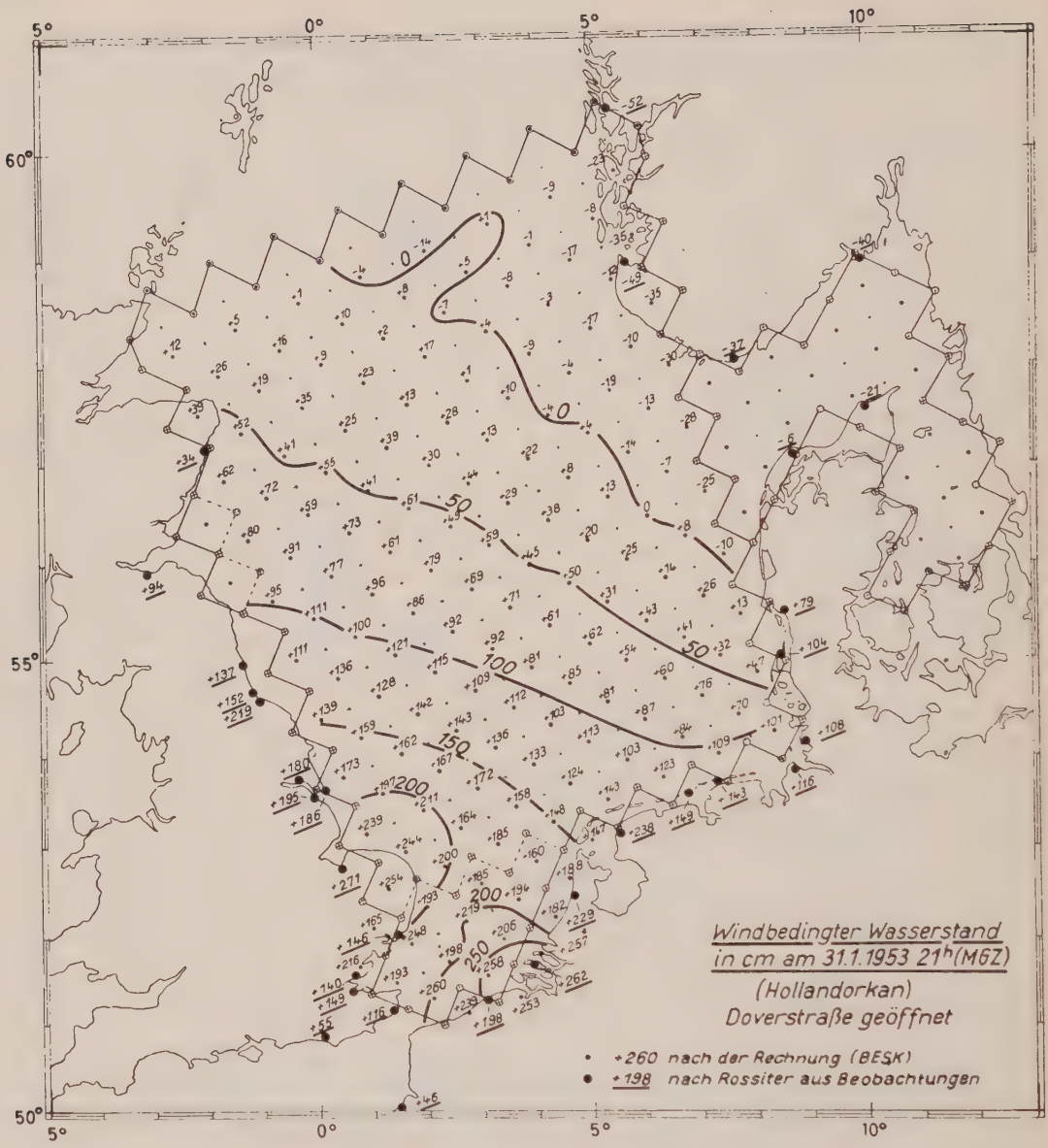

Abb. 4. Linien gleichen Wasserstandes in Zentimetern am 31.1.1953 um 21h MGZ, Zahlen geben mit BESK errechnete, unterstrichene Zahlen die von Rossiter aus den Beobachtungen abgeleiteten Wasserstände.

licherweise darauf zurückzuführen, dass das Skagerrak nicht in die Rechnung einbezogen wurde. Die an einigen Orten in den Rechnungen auftretenden Schwingungen von etwa 3 bis 4 Stunden Dauer können entweder in der Struktur des verwendeten Verfahrens oder in einer zeitlichen Unstetigkeit des verwendeten Windfeldes begründet sein. Diese Unstetigkeit kann dadurch zustande gekommen sein, dass die Werte, den meteorologischen Beobachtungsterminen entsprechend für jeweils 3 Stunden in der Rechnung konstant gesetzt wurden. Eine lineare Interpolation kann diesen Mangel beheben.

Eine Vorstellung von der Gestalt der errechneten Meeresoberfläche zur Zeit der höchsten Windgeschwindigkeit vermittelt Abb. 4. Die unterstrichenen Werte längs der Küste geben den beobachteten Windstau für diesen Zeitpunkt. Die Abweichungen erreichen nur in wenigen Punkten 0,5 m und überschreiten diesen Betrag selten. Da für den Holland-Orkan keine für einen Vergleich geeigneten Strombeobachtungen vorliegen, sind die errechneten Stromgeschwindigkeiten hier nicht dargestellt.

Gewisse Abweichungen zwischen beobachteten und errechneten Wasserständen können möglicherweise auch darauf zurückzuführen sein, dass nicht immer eine ausreichende Anzahl meteorologischer Beobachtungen vorhanden war, um das Windfeld auf der freien Nordsee eindeutig festzulegen. Bei schweren Stürmen wird die Schiffahrt erfahrungsgemäss stark eingeschränkt und zum Teil müssen sogar die Feuerschiffe die Beobachtungen einstellen. Es wäre deshalb sehr nützlich eine Methode zu entwickeln, die es gestattet, aus den meteorologischen Beobachtungen längs den Küsten der Nordsee etwa unter Verwendung eines hydrodynamischen Interpolationsverfahrens brauchbare Windangaben für das freie Seegebiet abzuleiten. Der Gedanke, aus den bekannten Werten am Rande eines Meeresgebietes, die Werte im Innern mit Hilfe der hydrodynamischen Differentialgleichungen zu ermitteln, ist in der Ozeanographie mehrfach verwendet worden. Selbst dann, wenn es gelingen sollte, in der freien Nordsee Wetterstationen einzurichten, kann eine derartige Methode noch von Nutzen sein.

Das Ergebnis dieser ersten Nachrechnung einer schweren Sturmflut für ein Randmeer, wenn auch in einigen Einzelheiten noch nicht voll befriedigend, gibt doch Anlass, den Ausbau und die Vervollkommung der hier entwickelten Theorie voranzutreiben. Dazu ist zunächst eine Verbesserung des numerischen Verfahrens in dem oben dargelegten Sinne erforderlich. Vorarbeiten sind in Angriff genommen. Insbesondere werden die Möglichkeiten untersucht, die die Verwendung der Vorticity-, Divergenz- und Kontinuitätsgleichung bietet. Da in der Ozeanographie bei den hier zu behandelnden Aufgaben die konvektiven Terme unberücksichtigt bleiben, werden die in der Meteorologie damit in Zusammenhang auftretenden Komplikationen vermieden. Allerdings ergibt sich für das ozeanographische Problem ein System von fünf partiellen Differentialgleichungen, da Strom- und Potentialfunktionen zusätzlich eingeführt werden müssen, um die Randbedingungen in einfacher Weise zu berücksichtigen. Zur Prüfung der verbesserten Verfahren sollten sowohl die Gezeiten wie auch die schweren Sturmfluten nachgerechnet werden, die in der Vergangenheit aufgetreten sind. Hierfür könnten auch synoptische Messungen von Schiffen und registrierenden Geräten auf See im Verein mit den routinemässig anfallenden Beobachtungen der Küsten- und Feuerschiffstationen ein wertvolles Material liefern. Im Zusammenhang mit der Weiterentwicklung der Theorie muss untersucht werden, in welcher Weise der Windstau von der räumlichen und zeitlichen Struktur des Windfeldes abhängt. Aus Beobachtungen ist bekannt, dass extrem hohe Wasserstände in Flachwassergebieten rasch auf Änderungen des lokalen Windes reagieren, andererseits an der durchweg tieferen englischen Ostküste Wasserstandsänderungen auftreten, deren Zusammenhang mit dem lokalen Wind nicht erkennbar ist. Zu verstehen sind diese Erscheinungen qualitativ insofern, als die relativ hohe Reibung in Seichtwassergebieten eine so starke Dämpfung bedingt, dass die Bewegungen hier quasistationär erfolgen, auf tiefem Wasser wird die Dämpfung so gering, dass sich Schwingungen entwickeln können. Es ist vorgesehen für einfache, typische Windfelder Wasserstände und Stromgeschwindigkeiten mit der BESK zu rechnen. Für NNW- und WSW-Wind konstanter Geschwindigkeit ist das bereits erfolgt. Die Ergebnisse zeigen den erwähnten Einfluss der Tiefenverteilung und der Erdrotation. Im ersten Fall treten die Maximalwerte im südwestlichen Teil der Nordsee, im zweiten Fall in der Deutschen Bucht auf.

Wie eingangs bereits bemerkt taucht für die Zukunft der Gedanke auf, die Theorie zur Ermittlung der windbedingten Wasserstände mit der Theorie der numerischen Wettervorhersage zu verbinden. Dann könnte im Anschluss an eine numerische Wettervorhersage eine numerische Wasserstandsvorhersage gegeben werden. Die auf dem ozeanographischen Sektor zur Zeit noch vorhandenen

Schwierigkeiten sind vorstehend diskutiert. Für die Meteorologie würde hieraus die Aufgabe folgen, die vorhandenen Methoden so auszubauen, dass hinreichend detaillierte Vorhersagen des tangentialen Windschubes an der Meeresoberfläche geliefert werden können. Damit in Zusammenhang wäre eine Intensivierung der Arbeiten über die Beziehungen einerseits zwischen dem errechneten geostrophischen Wind in 1 000 mb und dem wahren Wind an der Meeresoberfläche, andererseits zwischen diesem und dem Tangentialschub an der Meeresoberfläche erforderlich.

Nach den Erfolgen, die in Stockholm, Washington und anderen Orten mit routinemässig durchgeführten numerischen Vorhersagen der Gestalt der 500 mb-Fläche für weiträumige Gebiete erzielt worden sind, ist zu hoffen, dass es gelingen wird, unter Verallgemeinerung der vorhandenen Theorien auch das hier vorliegende Problem zu lösen. Über einen Versuch die 1 000 mb-Fläche unter Verwendung beobachteter Randwerte zu ermitteln, ist von Bushly und Hinds (1955) berichtet worden. Sie haben neben anderen Fällen auch den Holland-Orkan nachgerechnet.

Professor Rossby gebührt besonderer Dank, da er nicht nur in zahlreichen Diskussionen wertvolle Anregungen gegeben, sondern die Durchführung der Untersuchungen dadurch erst ermöglicht hat, dass sämtliche Maschinenrechnungen mit der leistungsfähigen und schnellrechnenden schwedischen Elektronenrechenmaschine BESK ausgeführt werden konnten.

SCHRIFTTUM

Bushby, F. H., and Hinds, M. K., 1955: Computations of 24-HR pressure changes. *Quarterly Journal Royal Meteorological Society*, **8**, No. 349.

Charney, J. G., 1955: Generation of ocean currents by wind. *J. Mar. Res.* **14**, No. 3.

Groen, P., 1953: Voorlopig Oderzuck van de Waterstanden opgetreden langs de Kusten der Noordzee. *Kon. Ned. Met. Inst.*, Rapport IV, No. 6.

Hansen, W., 1950: Triftstrom und Windstau. *Deutsche Hydrographische Zeitschrift*, **3**, Heft 5/6.

– 1954: Über ein Verfahren zur Ermittlung der Gestalt der Meeresoberfläche bei zeitveränderlichem Windfeld. *Deutsche Hydrographische Zeitschrift*, **7**, Heft 1/2.

Kivisild, H., 1954: Wind effect on shallow bodies of water with special reference to Lake Okeechokee. Dist. Göteborg.

Kreiss, H. O., 1956: Einige Bemerkungen über nichtlineare Schwingungen in Kanälen. *Tellus*, **9**, 1.

Lamoen, J., 1949: Tides and current velocities in a sea-level canal. *Engineering*, July 29.

Rossiter, J. R., 1954: The North Sea storm surge of 31 January and 1 February 1953. *Royal Society, Ser. A, Mathematical and Physical Sciences*, No. 915, Vol. 246.

Sverdrup, H. U., a. a., 1942: *The Oceans*. New York.

Veronis, G., and Morgan, G. W., 1953: A study of the time-dependent wind-driven ocean circulation. *Graduate Division of Applied Mathematics*, Brown University, Providence, R. I.

Veronis, G., 1956: Partition of energy between geostrophic and non-geostrophic oceanic motions. *Deep-Sea Res* **3**.

Welander, P., 1956: On the wind action on shallow seas with particular reference to the problem of numerical sea-level prediction. *Tellus*, **9**, 1.

On the Wind-Driven Ocean Circulation[1]

By G. W. MORGAN, Brown University, Providence

(Manuscript received February 8, revised June 5, 1956)

Abstract

Some aspects of existing theories of the wind-driven ocean circulation are examined with particular emphasis on the question of the need for the inclusion of lateral eddy viscosity to provide a mechanism for balancing the applied wind torque. A new model is proposed according to which the ocean is divided into a southern and a northern portion, attention being restricted to the former which is itself subdivided into an interior region and a boundary region adjacent to the western shore. The equations of motion in terms of spherical coordinates are formally integrated over depth for both a homogeneous and a two-layer ocean. Approximate equations analogous to those used in existing theories are proposed for the interior region. Conditions in the boundary region are considered in an effort to determine the relative importance of the various terms in the equations. Based on these considerations approximate equations are derived for the boundary region. These imply the predominance of the pressure terms, the nonlinear inertia terms and the terms arising from the variation of the Coriolis parameter with latitude.

The approximate equations are transformed to surface coordinates and are applied to the homogeneous ocean and a two-layer ocean subjected to a simple wind distribution, yielding reasonable results. It is shown that the variation of the Coriolis parameter plays a fundamental role in the formation of the stream on the western shore. Simple physical interpretations of the results are presented including an explanation of the facts that no similar stream can be formed on the eastern shore and that the variation of depth in a two-layer ocean, when the Coriolis parameter is assumed constant, cannot give rise to an intense stream. Appropriate curves illustrating the dependence of the solutions on certain dimensionless parameters are given. When applied to the North Atlantic the theory gives reasonable results for the Gulf Stream north to, say, Cape Hatteras.

1. Introduction

Existing theories of the wind-driven circulation in closed ocean basins (SVERDRUP, 1947; MUNK, 1950) are based on the assumption that the principal features of the flow pattern are the result of the balance between wind, Coriolis, lateral friction and pressure forces and that all other contributions to the dynamic equations are, for purposes of an approximate investigation, negligible. This assumption leads to a linear problem, an approximate solution of which is obtained most conveniently by applying boundary layer analysis to the vorticity equation (MUNK and CARRIER, 1950). Although the circulation which is predicted is, at least qualitatively, very reasonable, the theory has been criticized especially on the grounds that the value of the coefficient of lateral eddy viscosity must be chosen empirically, and further, that the value which gives the proper width to the intense current on the western shore is considerably larger than that indicated by other, independent considerations.

In the following, other aspects of the abovementioned theories are considered and attention is devoted to the question of the importance of the lateral eddy viscosity. It has previously been argued that this must be included in every steady-state theory because it provides the forces of friction on the sides of the basin which give rise to the torque that

[1] Contribution No. 811 from the Woods Hole Oceanographic Institution.

must be present to balance the total torque exerted on the ocean by the wind. This problem is discussed in Section 2 where an equation for the balance of total moment of momentum about the center of mass of the ocean is derived and it is seen that this consideration alone is not sufficient to determine whether friction is required in the moment balance.

In Section 3 the equation of vorticity in terms of spherical coordinates is formally integrated over the depth of a layer of water which is considered to have uniform density (either the total ocean depth, if one deals with a homogeneous model, or the depth of the upper layer in a two-layer model). Approximate equations which apply to the interior region of the ocean and stipulate the predominance of wind, Coriolis, and pressure forces are derived in Section 4. In Section 5 the conditions in the boundary region in which an intense current is expected are discussed and we return to the problem of the need for including lateral eddy viscosity. Based on this discussion a model is proposed according to which the ocean is divided into a southern and a northern region. Attention is confined to the former which is again divided into an interior region, to which the equations derived in Section 4 apply, and a boundary region, adjacent to the western shore, for which approximate equations are derived by means of boundary layer analysis. These imply the predominance of the pressure terms, the nonlinear inertia terms, and the terms arising from the variation of the Coriolis parameter with latitude, friction being neglected.[1]

The approximate equations are transformed to surface coordinates in Section 6 and are applied to a homogeneous ocean in Section 7. The theory predicts an intense current flowing northward along the western shore. The reason for the existence of this current from a physical point of view is discussed and it is shown why no similar current can exist on the eastern shore.

In Section 8 the theory is applied to the upper layer of a two-layer ocean. The role of a certain parameter involving the depth of the layer, the magnitude of the westward volume transport into the boundary region, the south-north dimension of the basin, the reduced gravity constant, and the variation of the Coriolis parameter with latitude, is studied. A proof is given that the variation of the Coriolis parameter is essential to the formation of an intense current even in a two-layer system. Numerical solutions are presented and it is concluded that, for reasonable values of the physical quantities involved, the barotropic and baroclinic models are not basically different as far as the formation of the stream is concerned. When applied to the North Atlantic the theory predicts the correct order of magnitude for the width of the Gulf Stream.

2. Moment of Momentum Balance

It has frequently been asserted (e.g. MONTGOMERY, 1940) that, for steady-state conditions, friction must be present on the bounding surfaces of the basin to provide the torque required to balance the total torque applied by the wind. Since it has been held reasonable to assume that the friction on the bottom is negligible, this argument has led to the conclusion that lateral eddy viscosity must be included in the equations of motion in order to give rise to a shear stress on the sides of the basin. In view of the obvious importance of this question, it will be examined in the following. The physical quantity of interest is the total moment of momentum about the center of mass, the momentum referring to the velocity recorder by an observer who is fixed to the earth. For steady-state conditions this moment must be constant.

The equation of motion is

$$\varrho \frac{Dq}{Dt} + \varrho 2 \boldsymbol{\Omega} \times \boldsymbol{q} + \varrho \boldsymbol{\Omega} \times (\boldsymbol{\Omega} \times \boldsymbol{r}) = \\ = - \nabla p + \varrho \nabla \chi' + \boldsymbol{F} \qquad (2.1)$$

where q is the velocity of a particle as seen by an observer fixed to the earth, D/Dt is the material derivative, ϱ is the density (not necessarily uniform), $\boldsymbol{\Omega}$ is the earth's angular

[1] The probability that viscosity is unimportant in the Gulf Stream was suggested by H. Stommel in a discussion following formal papers delivered at the June 1954 Convocation at Woods Hole (the complete proceedings of which are to be published as a supplement to the Journal of Marine Research, Vol. 14, No. 4, Dec. 31, 1955), and in a privately printed pamphlet entitled "Why do our ideas about the ocean circulation have such a peculiarly dream-like quality?", April 1954.

rotation vector, $\boldsymbol{r}$ is the position vector of the particle with respect to the center of the earth and with respect to a coordinate system which rotates with the earth, p is the pressure, χ' is the gravitational potential, and $\boldsymbol{F}$ is the net force on a unit volume due to eddy viscosity and can be written $\nabla \cdot \sigma$ where σ denotes the stress dyad minus the contribution of the pressure p.

The equation of conservation of mass is

$$\frac{\partial \varrho}{\partial t} + \operatorname{div} \varrho \boldsymbol{q} = 0. \tag{2.2}$$

Set

$$\nabla \chi' - \boldsymbol{\Omega} \times (\boldsymbol{\Omega} \times \boldsymbol{r})$$
$$= \nabla \chi' - \nabla \left(\frac{1}{2} \Omega^2 \tilde{\omega}^2 \right) \equiv \nabla \chi \tag{2.3}$$

where $\tilde{\omega}$ is the perpendicular distance of a point from the axis of rotation of the earth, Ω is the absolute value of $\boldsymbol{\Omega}$ and χ is the apparent gravitational potential. Carrying out the vector multiplication of the resulting equation with $\boldsymbol{r}_c$, the position vector of a point with respect to the center of mass, and integrating over the total volume of the ocean, one has

$$\int_V \varrho \boldsymbol{r}_c \times \frac{D\boldsymbol{q}}{Dt} dV + \int_V \varrho \boldsymbol{r}_c \times (2\boldsymbol{\Omega} \times \boldsymbol{q}) \, dV =$$
$$- \int_V \boldsymbol{r}_c \times \nabla p dV + \int_V \varrho \boldsymbol{r}_c \times \nabla \chi dV + \int_V \boldsymbol{r}_c \times \nabla \sigma \cdot dV \tag{2.4}$$

This equation can be transformed by making use of equation (2.2), the relations

$$\frac{D\boldsymbol{r}}{Dt} = \boldsymbol{q},$$
$$\int_V \varrho \frac{D\varphi}{Dt} dV = \frac{D}{Dt} \int_V \varrho \varphi dV, \tag{2.5}$$

φ being any arbitrary continuous function with continuous first derivatives, and the transformation formulae relating volume and surface integrals, to give

$$\frac{D}{Dt} \int_V \boldsymbol{r}_c + \varrho \boldsymbol{q} dV + \int_V \boldsymbol{r}_c \times \varrho (2\boldsymbol{\Omega} \times \boldsymbol{q}) dV =$$
$$\int_V \varrho \boldsymbol{r}_c \times \nabla \chi dV - \int_S \boldsymbol{r}_c \times \boldsymbol{n} p dS + \int_S \boldsymbol{r}_c \times \boldsymbol{T} dS \tag{2.6}$$

where S is the surface enclosing the volume V, $\boldsymbol{n}$ is the unit outer normal vector on S, and $\boldsymbol{T} = \boldsymbol{n} \cdot \sigma$ and denotes that portion of the surface traction which is due to the frictional mechanism. It should be noted that equation (2.6) holds irrespective of the particular nature of the eddy viscosity (or molecular viscosity), the only additional requirement for its derivation being the symmetry of the stress dyad.

The left-hand side of equation (2.6) represents the rate of change of moment of momentum and consists of the rate of change as seen by an observer fixed to the earth and the contribution by the Coriolis forces. The right-hand side represents the moment of all external forces, the gravitational attraction, the pressure on the surfaces and the forces arising from viscosity. The last integral may be split into two portions, one involving integration over the free surface and thus representing the moment due to the wind, the other involving integration over the ocean bottom and sides. The contribution of the pressures to the moment is principally due to the fact that the free surface is disturbed by the motion and that the moments due to the pressures on the sides will then not, in general, add to zero. If one deals with a circular basin having a vertical shore and uniform depth, then the moment due to the pressures acting on the shore will be very small because the center of mass will be very close to the geometrical center.

For a steady-state solution the first term on the left of equation (2.6) must vanish. The contribution of the body force to the moment is negligible. Thus the moment balance involves the contributions of the Coriolis force, the pressure, the wind, and the friction on the shores and bottom, and it is seen that no immediate conclusion can be drawn from this consideration alone concerning the need for including friction on the sides, even if friction on the bottom is neglected from the start. The moment created by the wind may possibly be balanced by the Coriolis and pressure moments, or by the former alone if the basin is circular.

The preceding considerations in no way prove that lateral friction is not required; they only demonstrate that the question cannot be decided on the basis of moment balance alone. The problem will be discussed from a different point of view in Section 5.

3. Equations of Motion in Spherical Coordinates

Since an analytical investigation of the three-dimensional problem is prohibitively complicated, we follow the usual procedure of confining our attention to the integrals over depth of the velocity components and of the vorticity.

Using the spherical coordinates (r, ϑ, φ), the origin being at the center of the earth and ϑ being the colatitude, and corresponding velocity components q_1, q_2, q_3, the momentum equations are

$$\frac{\partial q_1}{\partial t} + \text{non linear terms} - 2\,q_3\Omega \sin\vartheta = $$

$$= -\frac{1}{\varrho}\frac{\partial p}{\partial r} - g + F_1 \tag{3.1}$$

$$\frac{\partial q_2}{\partial t} + q_1\frac{\partial q_2}{\partial r} + \frac{q_2}{r}\frac{\partial q_2}{\partial \vartheta} + \frac{q_3}{r\sin\vartheta}\frac{\partial q_2}{\partial \varphi} + \frac{q_1 q_2}{r} -$$

$$- \frac{{q_3}^2\cot\vartheta}{r} - 2\,q_3\Omega\cos\vartheta = -\frac{1}{\varrho}\frac{1}{r}\frac{\partial p}{\partial \vartheta} + F_2 \tag{3.2}$$

$$\frac{\partial q_3}{\partial t} + q_1\frac{\partial q_3}{\partial r} + \frac{q_2}{r}\frac{\partial q_3}{\partial \vartheta} + \frac{q_3}{r\sin\vartheta}\frac{\partial q_3}{\partial \varphi} + \frac{q_1 q_3}{r} +$$

$$+ \frac{q_2 q_3}{r}\cot\vartheta + 2q_2\Omega\cos\vartheta + 2q_1\Omega\sin\vartheta =$$

$$= \frac{1}{\varrho}\frac{1}{r\sin\vartheta}\frac{\partial p}{\partial \varphi} + F_3 \tag{3.3}$$

Here (F_1, F_2, F_3) denote the contributions of the eddy viscosity, g denotes the gravitational acceleration, and the centrifugal force terms which give rise to the ellipticity of the undisturbed free surface of the ocean have been neglected.

We shall make either of two assumptions concerning the distribution of density; a) we consider the "homogeneous" ocean which has uniform density everywhere and is subsequently assumed to be of uniform depth when undisturbed; b) we consider a "two-layer" ocean which consists of two superposed layers each of uniform density. In the latter case we shall be concerned only with the motion in the upper, lighter layer, and the equations of motion refer to that layer alone. Hence, in both cases, the equation expressing the conservation of mass is that for an incompressible fluid:

$$\frac{\partial}{\partial r}(r^2\sin\vartheta q_1) + \frac{\partial}{\partial \vartheta}(r\sin\vartheta q_2) + \frac{\partial}{\partial \varphi}(r q_3) = 0 \tag{3.4}$$

The radial component of vorticity is

$$\zeta_1 = (\operatorname{curl} \boldsymbol{q})_1 =$$

$$= \frac{1}{r^2\sin\vartheta}\left[\frac{\partial}{\partial \vartheta}(r\sin\vartheta q_3) - \frac{\partial}{\partial \varphi}(r q_2)\right] \tag{3.5}$$

The first component equation of the vorticity equation is obtained by performing the operation appearing on the right side of (3.5) on equations (3.3) and (3.2) in the place of q_3 and q_2, respectively, and making use of equation (3.4):

$$\frac{\partial \zeta_1}{\partial t} + q_1\frac{\partial \zeta_1}{\partial r} + \frac{q_2}{r}\frac{\partial \zeta_1}{\partial \vartheta} + \frac{q_3}{r\sin\vartheta}\frac{\partial \zeta_1}{\partial \varphi} +$$

$$+ \frac{1}{r}\frac{\partial q_1}{\partial \vartheta}\frac{\partial q_3}{\partial r} + \frac{1}{r^2}\frac{\partial q_1}{\partial \vartheta}q_3 - \frac{1}{r\sin\vartheta}\frac{\partial q_1}{\partial \varphi}\frac{\partial q_2}{\partial r} -$$

$$- \frac{1}{r^2\sin\vartheta}\frac{\partial q_1}{\partial \varphi}q_2 + \frac{2}{r}q_1\zeta_1 -$$

$$- \frac{\zeta_1}{r^2\sin\vartheta}\frac{\partial}{\partial r}(r^2\sin\vartheta q_1) + \frac{4}{r}\Omega\cos\vartheta q_1 -$$

$$- \frac{2}{r^2}\Omega\cot\vartheta\frac{\partial}{\partial r}(r^2\sin\vartheta q_1) +$$

$$+ \frac{2}{r}\Omega\sin\vartheta\frac{\partial q_1}{\partial \vartheta} - \frac{2}{r}\Omega\sin\vartheta q_2 =$$

$$= \frac{1}{r^2\sin\vartheta}\left[\frac{\partial}{\partial \vartheta}(r\sin\vartheta F_3) - \frac{\partial}{\partial \varphi}(rF_2)\right] \tag{3.6}$$

The rate of change of the first component of vorticity as we follow a particle is

$$\frac{D\zeta_1}{Dt} = \frac{\partial \zeta_1}{\partial t} + q_1\frac{\partial \zeta_1}{\partial r} + \frac{q_2}{r}\frac{\partial \zeta_1}{\partial \vartheta} + \frac{q_3}{r\sin\vartheta}\frac{\partial \zeta_1}{\partial \varphi} \tag{3.7}$$

Note that this is not the same as the first component of $D\boldsymbol{\zeta}/Dt$, $\boldsymbol{\zeta}$ being the vorticity vector. We shall find it convenient to focus our attention on that portion of the rate of change of ζ_1 which is associated with the particle's horizontal motion only and therefore define

$$\frac{d}{dt} \equiv \frac{\partial}{\partial t} + \frac{q_2}{r}\frac{\partial}{\partial \vartheta} + \frac{q_3}{r\sin\vartheta}\frac{\partial}{\partial \varphi} \tag{3.8}$$

We now integrate equation (3.6) over the depth of the total ocean in case a) and over the upper layer in case b). In both cases the limits can be written $r = h_b(\vartheta, \varphi, t)$ on the bottom and $r = h_s(\vartheta, \varphi, t)$ on the free surface with h_b being constant in case a). Letting

$$f = 2\Omega \cos \vartheta \tag{3.9}$$

and making use of (3.8) one obtains, after some manipulation

$$\int_{h_b}^{h_s} \frac{d\zeta_1}{dt}\, dr - (q_1\zeta_1)\Big|_{h_b}^{h_s} + 2\int_{h_b}^{h_s} q_1 \frac{\partial \zeta_1}{\partial r}\, dr +$$

$$+ \int_{h_b}^{h_s} \left(\frac{1}{r}\frac{\partial q_1}{\partial \vartheta}\frac{\partial q_3}{\partial r} + \frac{1}{r^2}\frac{\partial q_1}{\partial \vartheta} q_3 - \frac{1}{r \sin \vartheta}\frac{\partial q_1}{\partial \varphi}\frac{\partial q_2}{\partial r} - \right.$$

$$\left. - \frac{1}{r^2 \sin \vartheta}\frac{\partial q_1}{\partial \varphi} q_2 \right) dr + \int_{h_b}^{h_s} \frac{df}{dt}\, dr - (q_1 f)\Big|_{h_b}^{h_s} +$$

$$+ 2\Omega \sin \vartheta \int_{h_b}^{h_s} \frac{1}{r}\frac{\partial q_1}{\partial \vartheta}\, dr =$$

$$= \frac{1}{\sin \vartheta}\int_{h_b}^{h_s} \frac{1}{r^2}\left[\frac{\partial}{\partial \vartheta}(r \sin \vartheta F_3) - \frac{\partial}{\partial \varphi}(rF_2)\right] dr \tag{3.10}$$

where the symbol $(\ )\Big|_{h_b}^{h_s}$ stands for $(\ )_{r=h_s} - (\ )_{r=h_b}$.

We now evaluate the frictional terms in (3.10). Let

$$F_i = \frac{1}{\varrho}\frac{1}{r^2}\frac{\partial}{\partial r}\left(A_r r^2 \frac{\partial q_i}{\partial r}\right) + F_i^*, \quad i = 2, 3 \tag{3.11}$$

where A_r denotes the radial eddy viscosity and F_2^*, F_3^* are used for the sake of brevity to represent the contributions due to the coefficient of lateral eddy viscosity A_L the magnitude of which is so far arbitrary. Assuming that A_r is independent of ϑ and φ and neglecting the variation of r within the range of the integration, one obtains for the right side of equation (3.10)

$$\frac{1}{\varrho}\frac{\cot \vartheta}{r}\left(A_r \frac{\partial q_3}{\partial r}\right)\Big|_{h_b}^{h_s} + \frac{1}{\varrho}\frac{1}{r}\left(A_r \frac{\partial^2 q_3}{\partial r\, \partial \vartheta}\right)\Big|_{h_b}^{h_s} -$$

$$- \frac{1}{\varrho}\frac{1}{r \sin \vartheta}\left(A_r \frac{\partial^2 q_2}{\partial r\, \partial \varphi}\right)\Big|_{h_b}^{h_s} +$$

$$+ \frac{1}{\sin \vartheta}\int_{h_b}^{h_s} \frac{1}{r^2}\left[\frac{\partial}{\partial \vartheta}(r \sin \vartheta F_3^*) - \frac{\partial}{\partial \varphi}(rF_2^*)\right] dr \tag{3.12}$$

The pertinent components of shear stress are

$$\tau_{r\vartheta} = A_r\left(\frac{1}{r}\frac{\partial q_1}{\partial \vartheta} - \frac{q_2}{r} + \frac{\partial q_2}{\partial r}\right)$$

$$\tau_{r\varphi} = A_r\left(\frac{1}{r \sin \vartheta}\frac{\partial q_1}{\partial \varphi} - \frac{q_3}{r} + \frac{\partial q_3}{\partial r}\right) \tag{3.13}$$

Since the depth of the ocean is much smaller than the radius of the earth, only the last term in each of the brackets in equation (3.13) is important. Expression (3.12) can then be written[1]

$$\frac{1}{\varrho}\left\{\frac{1}{r}\frac{\partial}{\partial \vartheta}\left(\tau_{r\varphi}\Big|_{h_b}^{h_s}\right) + \frac{\cot \vartheta}{r}\left(\tau_{r\varphi}\Big|_{h_b}^{h_s}\right) - \right.$$

$$- \frac{1}{r \sin \vartheta}\frac{\partial}{\partial \varphi}\left(\tau_{r\vartheta}\Big|_{h_b}^{h_s}\right) -$$

$$- \frac{1}{r}\left(\left[\frac{\partial}{\partial r}\left(A_r \frac{\partial q_3}{\partial r}\right)\right]\frac{\partial h}{\partial \vartheta}\right)\Big|_{h_b}^{h_s} +$$

$$\left. + \frac{1}{r \sin \vartheta}\left(\left[\frac{\partial}{\partial r}\left(A_r \frac{\partial q_2}{\partial r}\right)\right]\frac{\partial h}{\partial \varphi}\right)\Big|_{h_b}^{h_s}\right\} +$$

$$+ \frac{1}{\sin \vartheta}\int_{h_b}^{h_s} \frac{1}{r^2}\left[\frac{\partial}{\partial \vartheta}(r \sin \vartheta F_3^*) - \frac{\partial}{\partial \varphi}(rF_2^*)\right] dr \tag{3.14}$$

where $\left(\left[\ \right]\frac{\partial h}{\partial \vartheta}\right)\Big|_{h_b}^{h_s}$ is an abbreviation for

$$\left[\ \right]_{r=h_s}\frac{\partial h_s}{\partial \vartheta} - \left[\ \right]_{r=h_b}\frac{\partial h_b}{\partial \vartheta} \quad \text{and} \quad \frac{\partial}{\partial \vartheta}\left(\tau_{r\varphi}\Big|_{h_b}^{h_s}\right)$$

$$= \frac{\partial}{\partial \vartheta}\left[\tau_{r\varphi}(h_s, \vartheta, \varphi, t) - \tau_{r\varphi}(h_b, \vartheta, \varphi, t)\right].$$

[1] For details see: G. W. Morgan; On the integration over depth of the equations for the wind-driven ocean circulation; Reference No. 54 – 89; unpublished manuscript of the Woods Hole Oceanographic Institution, December 1954.

Note that the three terms containing the shear stresses are approximately $\frac{1}{\varrho}(\operatorname{curl}\boldsymbol{\tau})_1\Big|_{h_b}^{h_s}$, where $\boldsymbol{\tau}$ is the shear stress vector on the surfaces h_s or h_b. The additional surface terms arise from the fact that

$$\left(\frac{\partial}{\partial\vartheta}\frac{\partial q_3}{\partial r}\right)\Bigg|_{h_b}^{h_s} \mp \frac{\partial}{\partial\vartheta}\left[\left(\frac{\partial q_3}{\partial r}\right)\Bigg|_{h_b}^{h}\right]$$

4. Interior Equations

In this section we derive approximate equations applicable to the interior of the ocean, i.e. to a region sufficiently far removed from all shores. A more precise definition of the "interior region" will be given in Section 5. We assume, as do other investigators, that all terms which are nonlinear in the velocity components, as well as the contributions of lateral eddy viscosity are negligibly small there. It is further assumed that the pressure is hydrostatic everywhere in the ocean, i.e. that all terms involving velocity components in (3.1) are negligible. These assumptions can be readily justified by examining the orders of magnitude of the terms in the equations. Equation (3.1) becomes

$$\frac{\partial p}{\partial r} = \varrho g \tag{4.1}$$

Integration of equation (4.1) together with the boundary condition $p = 0$ at $r = h_s$ gives

$$p = \varrho g\,(h_s - r). \tag{4.2}$$

For the two-layer model, we assume that all velocities are negligible in the lower layer so that the pressure gradients vanish there. This leads to the two relations

$$\frac{\partial h_b}{\partial\vartheta} = -\frac{\varrho}{\triangle\varrho}\frac{\partial h_s}{\partial\vartheta}, \quad \frac{\partial h_b}{\partial\varphi} = -\frac{\varrho}{\triangle\varrho}\frac{\partial h_b}{\partial\varphi} \tag{4.3}$$

where $\triangle\varrho$ is the density difference between the two layers. Letting

$$D = h_s - h_b \tag{4.4}$$

we can write

$$\frac{\partial h_s}{\partial\vartheta} = \frac{\partial D}{\partial\vartheta}, \quad \frac{\partial h_s}{\partial\varphi} = \frac{\partial D}{\partial\varphi} \tag{4.5}$$

for the homogeneous ocean (h_b having been assumed constant) and

$$\frac{\partial h_s}{\partial\vartheta} = \frac{\triangle\varrho}{\varrho}\frac{\partial D}{\partial\vartheta}, \quad \frac{\partial h_s}{\partial\varphi} = \frac{\triangle\varrho}{\varrho}\frac{\partial D}{\partial\varphi} \tag{4.6}$$

for the two-layer model, where it has been assumed that $\triangle\varrho \ll \varrho$.

The momentum equations (3.2) and (3.3) become, using (3.11) and (4.2)

$$-2\Omega q_3\cos\vartheta = -g\frac{1}{r}\frac{\partial h_s}{\partial\vartheta} + \frac{1}{\varrho}\frac{1}{r^2}\frac{\partial}{\partial r}\left(A_r r^2\frac{\partial q_2}{\partial r}\right) \tag{4.7}$$

$$2\Omega q_2\cos\vartheta + 2\Omega q_1\sin\vartheta = -g\,\frac{1}{r\sin\vartheta}\,\frac{\partial h_s}{\partial\varphi} + \frac{1}{\varrho}\frac{1}{r^2}\frac{\partial}{\partial r}\left(A_r r^2\frac{\partial q_3}{\partial r}\right) \tag{4.8}$$

Before writing the approximate form of the vorticity equation (3.10) it is convenient to evaluate the term $(q_1 f)\Big|_{h_b}^{h_s}$. Applying the kinetic boundary conditions

$$\frac{D}{Dt}(h_s - r) = \frac{D}{Dt}(h_b - r) = 0 \tag{4.9}$$

we have

$$(q_1 f)\Big|_{h_b}^{h_s} = f\left(\frac{q_2}{r}\frac{\partial h}{\partial\vartheta} + \frac{q_3}{r\sin\vartheta}\frac{\partial h}{\partial\varphi}\right)\Bigg|_{h_b}^{h_s} \tag{4.10}$$

Evaluating the right side by means of equations (4.7) and (4.8), we have

$$(q_1 f)\Big|_{h_b}^{h_s} = -\left(\frac{2\Omega}{r}\sin\vartheta q_1\frac{\partial h}{\partial\vartheta}\right)\Bigg|_{h_b}^{h} + \frac{1}{\varrho}\left\{\left(\frac{1}{r^3}\frac{\partial}{\partial r}\left[A_r r^2\frac{\partial q_3}{\partial r}\right]\frac{\partial h}{\partial\vartheta}\right)\Bigg|_{h_b}^{h_s} - \left(\frac{1}{r^3\sin\vartheta}\frac{\partial}{\partial r}\left[A_r r^2\frac{\partial q_2}{\partial r}\right]\frac{\partial h}{\partial\varphi}\right)\Bigg|_{h_b}^{h_s}\right\} \tag{4.11}$$

When this expression is substituted into equation (3.10) the last two terms cancel the corresponding terms on the right side of equation (3.10) as given by expression (3.14), provided we neglect the variation of r in equation (4.11).

The resulting vorticity equation (without nonlinear and lateral eddy viscosity terms) may be simplified further by noting that the slopes of the top and bottom surfaces will be much less than one, so that $q_1 \ll q_2$. Thus, only the term in df/dt is important on the left side and, using (3.8), equation (3.10) becomes approximately

$$-\frac{2\Omega}{r}\sin\vartheta\int_{h_b}^{h_s} q_2\,dr=\frac{1}{\varrho}\left\{\frac{1}{r}\frac{\partial}{\partial\vartheta}\left(\tau_{r\varphi}\Big|_{h_b}^{h_s}\right)+\right.$$

$$\left.+\frac{\cot\vartheta}{r}\left(\tau_{r\varphi}\Big|_{h_b}^{h_s}\right)-\frac{1}{r\sin\vartheta}\frac{\partial}{\partial\varphi}\left(\tau_{r\vartheta}\Big|_{h_b}^{h_s}\right)\right\} \quad (4.12)$$

Integration of the approximate momentum equations (4.7) and (4.8) leads to

$$-2\Omega\cos\vartheta\int_{h_b}^{h_s} q_3\,dr=-g'\frac{1}{r}D\frac{\partial D}{\partial\vartheta}+\frac{1}{\varrho}(\tau_{r\vartheta})\Big|_{h_b}^{h_s} \quad (4.13)$$

$$2\Omega\cos\vartheta\int_{h_b}^{h_s} q_2\,dr=-g'\frac{1}{r\sin\vartheta}D\frac{\partial D}{\partial\varphi}+$$

$$+\frac{1}{\varrho}(\tau_{r\varphi})\Big|_{h_b}^{h_s} \quad (4.14)$$

where we have used (4.4) to (4.6) and have neglected q_1, and

$$\left.\begin{aligned} g' &\equiv g && \text{in the homogeneous ocean}\\ g' &\equiv \frac{\Delta\varrho}{\varrho}g && \text{in the two-layer ocean}\end{aligned}\right\} \quad (4.15)$$

The integrated continuity equation is readily shown to be

$$\frac{\partial}{\partial\vartheta}\int_{h_b}^{h_s}\sin\vartheta\,q_2\,dr+\frac{\partial}{\partial\varphi}\int_{h_b}^{h_s} q_3\,dr=0 \quad (4.16)$$

This relation is approximate in that the variation of r over the range of integration has been neglected. Introducing the "transport" components Q_2, Q_3, equation (4.16) is satisfied by defining the transport stream function ψ by the relations

$$\left.\begin{aligned} Q_2 &\equiv \int_{h_a}^{h_s} q_2\,dr \equiv -\frac{1}{r\sin\vartheta}\frac{\partial\psi}{\partial\varphi}\\ Q_3 &\equiv \int_{h_b}^{h_s} q_3\,dr \equiv -\frac{1}{r}\frac{\partial\psi}{\partial\vartheta}\end{aligned}\right\} \quad (4.17)$$

Equations (4.12) to (4.14) and (4.17) are the equations which we shall apply to the interior of the ocean.

5. Boundary Equations

a) Preliminary discussion.

To conform with reality, the circulation to be predicted by theory will have to exhibit relatively large velocities and velocity gradients at least near the western shore. Hence the approximations made in Section 4 for the interior region of the ocean cannot be expected to hold there. This is otherwise evident from a mathematical point of view since the approximate equations (4.12) to (4.16) do not constitute a system of a sufficiently high order to yield solutions which satisfy all boundary conditions. Hence these equations are not adequate for the entire enclosed ocean.

It has been assumed by other investigators (e.g. MUNK, 1950) that the influence of lateral eddy viscosity, while negligible in the interior, becomes important near the shore. The theory based on this assumption has led to a circulation pattern which looks remarkably realistic. As was already mentioned in the introduction, the theory has been criticized, however, because of the need for the empirical choice of the value of the coefficient of lateral eddy viscosity and the fact that the value which gives the proper width to the stream on the western shore is larger than one might expect from independent considerations. It is useful to consider the merits of this "viscous" theory from other points of view.

It was stated in the introduction that the torque due to the frictional forces on the shores has, at times, been held to be the torque which balances the torque applied by the wind. Now the viscous theory shows that the magnitude of the shore friction torque depends on the value of the viscosity (the shear stress on the shore being proportional to the viscosity and the normal derivative of the tangential

velocity component, and the latter varying as viscosity to the minus two-thirds power). Hence, if the argument were correct, the value of the viscosity should be chosen so as to satisfy the torque balance! Fortunately the discussion in Section 2 relieves us of this requirement. If the friction torque is essential to the torque balance, it is certainly not the only contribution.

Consider now briefly, from a physical point of view, the role of the shore in producing an intense current. The solution of the interior vorticity and continuity equations (4.12) and (4.16) with a realistic wind distribution and neglecting bottom friction (see Section 6) leads to a southward transport component over the southern interior. The equations do not determine the direction of the other component. This evidently depends on the flow near the coast. Whichever it is, in a model which requires that the circulation be confined essentially to the northern hemisphere, the stipulation of an eastern or western shore must give rise to an intense northward current on one of the coasts, since the water which flows toward this coast has to be turned to the north to satisfy continuity. The stream will have to be narrow and hence intense if it is not to interfere with the concept of the interior region. Thus, the boundary condition of vanishing normal velocity on the shore is responsible for turning the current northward; the mechanism which accounts for the narrowness of this current (and which will determine on which of the two shores the current exists) remains to be investigated, but it appears reasonable that the usual viscous boundary condition of no slip will not have to play an essential role in the creation of the stream. This is also indicated by the viscous theory which shows that even if the extreme condition of zero normal derivative of the tangential transport is specified on the coast, the width and intensity of the stream are essentially unaffected. If, however, the no-slip condition is not essential, then the function of viscosity may not be paramount in the formation of the stream. It is only necessary to have a system of equations which is of sufficiently high order to be capable of yielding solutions which can satisfy the condition of vanishing normal transport. This, of course, can be accomplished by including the nonlinear inertia terms. The inclusion of viscosity, on the other hand, leads to a higher order system which requires another and, it seems, extraneous boundary condition.

It is important to note that the preceding discussion, having been restricted to the formative stage of the northward stream, does not necessarily suggest that lateral viscosity will not be important anywhere in the system. Since our study of the moment of momentum balance gave no conclusive answer to this question, it may be useful to examine it here from another point of view.

Imagine that the flow is contained between two solid concentric spheres and that it is created by the application of body forces uniformly distributed over the depth, rather than by surface forces. If there is no top or bottom friction we may expect the motion to be independent of r and to have vanishing radial velocity. The vorticity equation (3.6) then becomes

$$\frac{d}{dt}(\zeta_1 + f) = (\operatorname{curl} \boldsymbol{B})_1 + \begin{matrix}\text{lateral eddy} \\ \text{viscosity terms}\end{matrix} \qquad (5.1)$$

where $\boldsymbol{B}$ represents the body forces. If $(\operatorname{curl} \boldsymbol{B})_1$ is everywhere positive, (as we may expect $(\operatorname{curl} \boldsymbol{\tau})_1\big|_h$, the curl of the wind stress, to be), and if viscosity is absent, then equation (5.1) says that the quantity $\zeta_1 + f$ will always increase as we follow a particle. If the system is closed, this leads to a nonsteady flow. Hence, for steady flow, lateral friction must be important at least in some region through which every particle will have to pass.

This conclusion also follows immediately from energy considerations. The direction of the flow to be expected in the interior is such that the body force would do positive work on the system. In the absence of lateral eddy viscosity, however, there is no mechanism for dissipating the resulting increase in kinetic energy.

The author has so far not succeeded in carrying out an analogous examination of the variation of $\zeta_1 + f$ for the actual problem. It may be noted, however, that in our formulation the transfer of the wind stress to the water occurs by means of vertical eddy viscosity and that, therefore, a mechanism for energy dissipation exists even in the absence of lateral eddy viscosity. Thus, the energy argument breaks down.

b) A new model.

The considerations presented so far suggest that we adopt a new model for our system. Let us imagine the ocean between, say, 10° latitude and 50° latitude to consist of a southern and a northern portion with the dividing circle of latitude at about 35°. The southern portion is further divided as shown. The figure also shows a typical streamline of the anticipated circulation, most, or perhaps all, of the streamlines being expected to pass through all three regions.

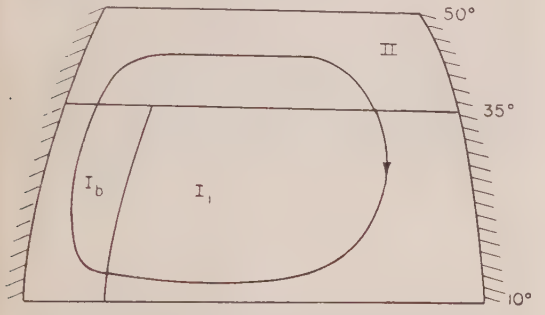

Fig. 1. The three regions of a new ocean model. I_i: interior region; I_b: frictionless stream region; II: northern region; nonsteady and lateral friction effects possibly important.

Our theory will apply to the interior region I_i and the boundary region I_b; (it will be seen that no boundary region is required on the eastern shore). In I_i the equations of Section 4 are applicable. In I_b nonlinear inertia, but not viscosity, will be included. In the Atlantic, I_b is to include the Gulf Stream north to about Cape Hatteras. In region II nonlinear, viscous and nonsteady effects may be important. This region includes the Gulf Stream meanders. If it turns out that lateral viscosity must be present somewhere in the system, its influence will be confined to region II. It is quite possible that the analysis of the problem in regions I and II together may have to include instability of the meanders, i.e. nonsteady effects. These, too, are assumed to be present in II only. The analysis of the flow in I is based on the assumption that this flow can be studied without inquiring into the conditions in II. Thus, whatever occurs in II, the flow which emerges from there into I_i is such that it obeys our interior equations. Similarly, the flow entering II from I_b is supposed to be determined by conditions in I_i and I_b alone.

c) Order of magnitude estimates.

The terms in the vorticity equation (3.10) may be grouped into three categories: (i) terms nonlinear in the velocities, (ii) terms due to the earth's rotation, (iii) terms resulting from eddy viscosity. The relative importance of each group will be examined in the following subsection by the usual procedures of boundary analysis. In the present section we carry out a preliminary simplification by comparing the relative magnitudes of the terms within each group.

(i) It will be assumed that the shores are given by two meridians. We must then expect that, in the boundary region, $|q_3| \ll |q_2|$ and derivatives parallel to the shore, $\left(\frac{\partial}{\partial\vartheta}\right)$, will be much smaller than those normal to the shore, $\left(\frac{\partial}{\partial\varphi}\right)$. Hence, from equation (3.5), $\zeta_1 \approx -(1/r \sin\vartheta)(\partial q_2/\partial\varphi)$. The magnitude of q_1 is readily estimated from the kinetic boundary condition, equation (4.9), in terms of q_2, q_3 and the slopes of h_s and h_b. For the homogeneous ocean q_1 is very small due to the small surface slope. For the two-layer ocean the principal contribution is due to the slope of h_b, the thermocline, the variation of h_b being of the order of the depth D itself.

Examining the third integral in equation (3.10), it is clear that the first, second and fourth terms are negligible compared with the third.

The contributions of $\int_{h_b}^{h_s} (d\zeta_1/dt)dr$ and $(q_1\zeta_1)\Big|_{h_b}^{h_s}$ are seen to be of equal importance in the two-layer case. To compare these terms with the remaining nonlinear terms involving radial differentiation, we must obtain an estimate of $\partial q_2/\partial r$. The second, third and fourth terms of equation (3.10) have the following orders of magnitude for a two-layer model:

$$[(q_1/r)(\partial q_2/\partial\varphi)]_{r=h_b}; \quad (q_1/r)_{r=h_b}\left[(\partial q_2/\partial\varphi)\Big|_{h_b}^{h_s}\right];$$

$$(\partial q_1/\partial\varphi)_{r=h_b}\left[(q_2/r)\Big|_{h_b}^{h_s}\right].$$

(For a homogeneous ocean q_1 is so small everywhere that all these terms are negligible.) The second and third of the above expressions

involve a difference in the values at h_s and h_b of the quantities $\partial q_2/\partial\varphi$ and q_2, respectively. If these differences are of the order of the quantities themselves, then all terms must be expected to be of equal importance. We assume in the following that these differences are much smaller than the quantities themselves and hence that the term $(q_1\,\zeta_1)\Big|_{h_b}^{h_s}$, predominates. This implies that the top and bottom shear stresses which constitute the principal cause of the radial variation of q_2 are relatively unimportant in the boundary region, thus leaving q_2 essentially uniform with depth. This condition can probably be relaxed somewhat because our estimates of the third and fourth terms are likely to be on the high side, q_1 and $\partial q_1/\partial\varphi$ having been taken out of the integrals and evaluated at $r = h_b$ where they will be greatest. Nevertheless it may be important to note that the justification for omitting the terms under consideration is not beyond question.

(ii) As in (i), the first two terms involving Ω in equation (3.10) are seen to be of the same order, while the third one is negligible.

(iii) We turn to expression (3.12) for the terms due to eddy viscosity. Of the three terms involving radial eddy viscosity the last one will predominate. The principal contribution due to lateral eddy viscosity comes from $F_2{}^*$ and is approximately

$$\frac{1}{\varrho r^3 \sin^3\vartheta}\int_{h_b}^{h_s} A_L \frac{\partial^3 q_2}{\partial\varphi^3}\,dr$$

A_L denoting the lateral eddy viscosity.

The simplified vorticity equation (3.10) now becomes

$$\int_{h_b}^{h}\frac{d}{dt}(\zeta_1 + f)\,dr - [q_1(\zeta_1+f)]\Big|_{h_b}^{h_s} =$$

$$= -\frac{1}{\varrho}\frac{1}{r}\left(A_r\frac{\partial^2 q_2}{\partial r\partial\varphi}\right)\Bigg|_{h_b}^{h_s} -$$

$$- \frac{1}{r^3\sin^3\vartheta}\int_{h_b}^{h_s} A_L\,\partial^2 q_2/\partial\varphi^2\cdot dr \qquad (5.2)$$

with $\zeta_1 \cong -(1/r\sin\vartheta)(\partial q_2/\partial\varphi)$.

d) Boundary layer analysis.

In this subsection the technique of boundary layer analysis is employed to examine the relative magnitudes of the terms in (5.2). This technique assumes that a boundary layer type of solution exists. If it does, then the procedure readily yields an estimate of some of the properties of the solution; in this case, of the width and intensity of the stream.

We first assume that the essence of the phenomenon of interest to us will not be lost if we neglect the radial variation of the velocity components and of A_L within the boundary layer for the purpose of evaluating the integrals in equation (5.2). We also assume that the radial eddy viscosity term is not important. This assumption may not be valid for a homogeneous or a two-layer ocean, or perhaps even for a more realistic model, but an argument in its favor might be as follows. At the top surface the radial velocity gradient will be zero in the absence of a meridional wind. At the bottom surface the radial eddy viscosity may be sufficiently small to keep $(A_r\,\partial^2 q_2/\partial r\partial\varphi)_{r=h_b}$ small. We make the assumption in spite of the uncertainty of its validity because of the desirability of investigating the boundary solution in the complete absence of friction. Equation (5.2) becomes

$$D\frac{d(\zeta_1+f)}{dt} - [q_1(\zeta_1+f)]\Big|_{h_b}^{h_s} =$$

$$= -\frac{D}{\varrho r^3\sin^3\vartheta}A_L\frac{\partial^2 q_2}{\partial\varphi^2} \qquad (5.3)$$

or, using the kinetic boundary conditions (4.9),

$$\frac{d}{dt}\left(\frac{\zeta_1+f}{D}\right) = -\frac{1}{D\varrho r^3\sin^3\vartheta}A_L\frac{\partial^3 q_2}{\partial\varphi^3} \qquad (5.4)$$

Equation (5.4) is rendered dimensionless by the following transformations

$$\left.\begin{aligned} q_2 &= q^* q_2' \qquad q_3 = q^* q_3' \\ \frac{1}{r}\frac{\partial}{\partial\vartheta} &\approx \frac{1}{s}\frac{\partial}{\partial\vartheta'} \qquad \frac{1}{r}\frac{\partial}{\partial\varphi} \approx \frac{1}{s}\frac{\partial}{\partial\varphi'} \\ \beta &= \frac{2\Omega}{r} \end{aligned}\right\} \qquad (5.5)$$

where q^* is a characteristic velocity taken to be a measure of the zonal velocity in the transition

region from the interior to the boundary layer, s is the south-north extent of region I, and $\sin\vartheta$ is approximated by one. We further restrict ourselves for the moment to an homogeneous ocean or to a two-layer model with such a deep upper layer that the depth may be regarded as uniform. Equation (5.4) then becomes approximately

$$\frac{q^*}{s^2\beta}\left(q_2'\frac{\partial^2 q_2'}{\partial\vartheta'\partial\varphi'}+q_3'\frac{\partial^2 q_2'}{\partial q_3'^2}-\cos\vartheta\, q_2'\frac{\partial q_2'}{\partial\varphi'}\right)+ \\ +q_2'=\frac{A_L}{s^3\beta}\frac{\partial^3 q_2'}{\partial q_3'^3} \qquad (5.6)$$

According to our discussion in Sections 5 a) and 5 b), we expect that the nonlinear terms will be important in the boundary layer. Since they are negligible in the interior, the parameter

$$N\equiv\frac{q^*}{s^2\beta} \qquad (5.7)$$

must be much less than one. Hence the terms cannot be important in the boundary layer unless the derivatives, and possibly the functions themselves, are large there. We therefore set

$$\varphi'=N^m\varphi'', \quad q_2'=N^{-n}q_2'' \qquad (5.8)$$

where m, n are to be determined and are expected to be positive. We hope to find a transformation (5.8) such that q_2'' $(\vartheta_1'\varphi'')$, q_3' (ϑ',φ'') and their derivatives are of order one in the boundary layer. The magnitude of each term will then be indicated by its coefficient.

The continuity equation (4.16) shows that $m=n$ and equation (5.6) becomes

$$N^{1-3m}\left(q_2''\frac{\partial^2 q_2''}{\partial\vartheta'\partial\varphi''}+q_3'\frac{\partial^2 q_2''}{\partial\varphi''^2}-\cos\vartheta\, q_2''\frac{\partial q_2''}{\partial\varphi''}\right)+ \\ +N^{-m}q_2''=N^{-4m}\frac{A_L}{\varrho s^3\beta}\frac{\partial^3 q_2''}{\partial\varphi''^3} \qquad (5.9)$$

Since we expect nonlinear and Coriolis terms to balance, we must have $m=\frac{1}{2}$. The terms due to lateral eddy viscosity will be unimportant if $N^{-3/2}A_L/\varrho s^3\beta=\beta^{1/2}A_L/\varrho q^{*3/2}\ll 1$. The width of the stream will be of order $sN^{1/2}=(q^*/\beta)^{1/2}$, and the meridional velocity component will be of order $q^*N^{-1/2}=s(q^*\beta)^{1/2}$. With $\beta=2\times10^{-13}\cdot(\text{cm sec})^{-1}$, $q^*=10$ cm sec^{-1} this gives approximately 70 km for the width of the stream, which is the correct order of magnitude. The condition for smallness of the friction terms places an upper bound of approximately 5×10^6 cm^2 sec^{-1} on the magnitude of A_L. Assuming that this corresponds to actual conditions and that, therefore, lateral eddy viscosity is negligible, the vorticity equation (5.4) becomes

$$\frac{d}{dt}\left(\frac{\zeta_1+f}{D}\right)=0 \qquad (5.10)$$

Since, in this equation, the variation of ζ_1, q_2, q_3 with depth has, effectively, been neglected, the derivative d/dt may be interpreted as the rate of change as one follows a vertical column of water in its horizontal motion, and the equation (5.10) states that the potential vorticity associated with such a column is conserved during its motion in the boundary region. Using equation (4.17), equation (5.10) can be integrated along a "transport line", i.e. a line of constant ψ, to give

$$\frac{\zeta_1+f}{D}=F(\psi) \qquad (5.11)$$

where F is a function which must be determined by matching the distribution of $(\zeta_1+f)/D$ in the boundary with the distribution in the interior near the edge of the boundary layer.

e) The momentum equations in the boundary layer.

The considerations contained in the preceding sections may now be applied to the integrals over depth of the momentum equations (3.2) and (3.3) to derive approximate equations which are consistent with the assumptions made in deriving the vorticity equation. They are

$$\int_{h_b}^{h_s}\left(\frac{q_2}{r}\frac{\partial q_2}{\partial\vartheta}+\frac{q_3}{r\sin\vartheta}\frac{\partial q_2}{\partial\varphi}\right)dr-2\Omega\cos\vartheta\int_{h_b}^{h_s}q_3\,dr= \\ =-g'\frac{1}{r}D\frac{\partial D}{\partial\vartheta} \qquad (5.12)$$

$$2\Omega\cos\vartheta\int_{h_b}^{h}q_2\,dr=-g'\frac{1}{r\sin\vartheta}D\frac{\partial D}{\partial\varphi} \qquad (5.13)$$

We note that the meridional transport component is geostrophic, but that the zonal component is not, the nonlinear terms being as important as the Coriolis contribution.

Neglecting the variation of the integrands with depth, we derive an approximate Bernoulli equation by multiplying equation (5.12) by q_2, equation (5.13) by q_3, adding the resulting equations to obtain

$$\frac{d}{dt}\left(\frac{q_2^2}{2}\right)+g'\frac{dD}{dt}=0, \tag{5.14}$$

and finally integrating along a streamline (or transport line), giving

$$\frac{q_2^2}{2}+g'D=B(\psi) \tag{5.15}$$

where B is an arbitrary function which must be determined by matching the boundary with the interior solution.

6. Transformation to Surface Coordinates

Having derived the equations in terms of spherical coordinates in an effort not to lose any important effects of the spherical ocean shape by premature introduction of plane coordinates, we are now ready to make this transformation to give the equations a more familiar appearance.

Our boundary layer analysis has been based on the assumption that the derivative $\partial/\partial\varphi$ represents differentiation normal to the coast. Hence two meridians are taken to represent the coast lines. The simplest coordinate system will then be one in which these are coordinate lines. Hence, set

$$\left.\begin{array}{llll} x=R\varphi, & y=R(K-\vartheta) & z=r-R & \\ u=q_3, & v=-q_2 & & \\ U=Q_3, & V=-Q_2 & & \\ \tau_x=\tau_{r\varphi}, & \tau_y=-\tau_{r\vartheta} & & \end{array}\right\} \tag{6.1}$$

where K is the colatitude of the southern boundary of region I, R is the radius of the undisturbed ocean surface. Note that while y measures distance along a meridian of a sphere of radius R, x does not measure exact distance along a circle of latitude. We have

$$\frac{\partial}{\partial r}=\frac{\partial}{\partial z};\quad \frac{\partial}{\partial\vartheta}=-R\frac{\partial}{\partial y};\quad \frac{\partial}{\partial\varphi}=R\frac{\partial}{\partial x} \tag{6.2}$$

If, instead of x, an alternative coordinate x' which does measure distance along a circle of latitude were chosen, (e.g. $x'=\varphi R\sin\vartheta$), then the most convenient geometrical shape in the x'—y plane, the rectangle, would represent a less realistic configuration than does the rectangle in the x—y plane which corresponds to an ocean whose east and west shores are meridians. Moreover, the velocity component v would then be an inconvenient variable since it would not represent the velocity in the direction of the constant x' curves.[1]

The interior equations (4.12), (4.13), (4.14), (4.17) become

$$\beta\sin\vartheta\int_{h_3-R}^{h_1-R}v\,dz=$$

$$=\frac{1}{\varrho}\left(-\frac{\partial\tau_x}{\partial y}+\frac{\cot\vartheta}{R}\tau_x+\frac{1}{\sin\vartheta}\frac{\partial\tau_y}{\partial x}\right)_{z=h_1-R} \tag{6.3}$$

$$2\Omega\cos\vartheta\int_{h_3-R}^{h-R}u\,dz=-\frac{g'}{2}\frac{\partial D^2}{\partial y}+\frac{1}{\varrho}(\tau_y)_{z=h_1-R} \tag{6.4}$$

$$-2\Omega\cos\vartheta\int_{h_3-R}^{h_2-R}v\,dz=$$

$$-\frac{g'}{2\sin\vartheta}\frac{\partial D^2}{\partial x}+\frac{1}{\varrho}(\tau_x)_{z=h_1-R} \tag{6.5}$$

$$V=\int_{h_3-R}^{h_2-R}v\,dz=\frac{1}{\sin\vartheta}\frac{\partial\psi}{\partial x},\quad U=\int_{h_3-R}^{h_2-R}u\,dz=-\frac{\partial\psi}{\partial y} \tag{6.6}$$

[1] The reader may wish to contrast our system with that of MUNK 1950 and MUNK-CARRIER 1950 whose x coordinate measures distance, with the result that the rectangle in the x—y plane does not correspond to a realistic ocean shape. This leads Munk-Carrier to consider a triangle. The rectangle in our x—y plane is perhaps an equally good approximation to the real ocean shape.

The agreement of corresponding terms in Munk's equations and in ours is not complete. This is due to the fact that Munk's equations have apparently not been derived by a systematic transformation of variables and coordinates from a spherical system; hence there is some question concerning the relation of Munk's variables to those in the actual spherical system.

where we have approximated $1/r$ by $1/R$ and, consistent with the assumption already made in the derivation of the boundary equations, have neglected the shear stress at the bottom surface $z = h_b - R$.

The boundary equations (5.11), (5.12), (5.13), (5.15) become

$$\frac{\frac{1}{\sin\vartheta}\frac{\partial v}{\partial x} + 2\Omega\cos\vartheta}{D} = F(\psi) \qquad (6.7)$$

$$\int_{h_b-R}^{h_s-R}\left(v\frac{\partial v}{\partial y} + \frac{u}{\sin\vartheta}\frac{\partial v}{\partial x}\right)dz + 2\Omega\cos\vartheta\int_{h_b-R}^{h_s-R} u\,dz = -\frac{g'}{2}\frac{\partial D^2}{\partial y} \qquad (6.8)$$

$$-2\Omega\cos\vartheta\int_{h_b-R}^{h_s-R} v\,dz = -\frac{g'}{2\sin\vartheta}\frac{\partial D^2}{\partial x} \qquad (6.9)$$

$$\frac{v^2}{2} + g'D = B(\psi) \qquad (6.10)$$

Just as in the derivation of the vorticity equation (6.7), the integrals appearing in equations (6.8) to (6.9) will be evaluated approximately by neglecting the z variation of the integrands.

7. The homogeneous Ocean with simple Wind Distribution

The homogeneous model is important principally because of the insight that will be gained into the role of density stratification in the formation of the western stream by comparing the behaviour of this model with that of a two-layer ocean. The most important question to be investigated in this connection is whether either the variation of the Coriolis parameter with latitude, or the density stratification, or both, are indispensable. Because of its simplicity, the homogeneous model also readily affords insight into the entire phenomenon of the coastal stream.

Assume the wind stresses

$$\tau_x = -W\left(1 - \frac{\gamma^2}{s^2}\right), \quad \tau_y = 0, \quad 0 \le \gamma \le s \qquad (7.1)$$

s being the south-north extent of region I and W being a constant. Equation (6.3) becomes

$$\beta\sin\vartheta V_i = \frac{W}{\varrho}\left[-\frac{2\gamma}{s^2} + \frac{\cot\vartheta}{R}\left(1 - \frac{\gamma^2}{s^2}\right)\right] \qquad (7.2)$$

where the subscript i is used to denote quantities in the interior region I_i. For $\vartheta \ge 55°$ and $K = 75°$, $\cot\vartheta \le .7$ and $s \approx .35\ R$, so that the second term due to the curl of the wind is considerably smaller than the first term over most of the range. Accordingly, we neglect it. Using equation (6.6)

$$\frac{\partial\psi_i}{\partial x} = -\frac{2\gamma W}{\varrho\beta s^2} \qquad (7.3)$$

$$\psi_i = -\frac{2\gamma W}{\varrho\beta s^2}[x + l(\gamma)] \qquad (7.4)$$

$$U_i = \frac{2W}{\varrho\beta s^2}(x + l) + \frac{2\gamma W}{\varrho\beta s^2}\frac{dl}{d\gamma} \qquad (7.5)$$

where $l(\gamma)$ is an arbitrary function. Since we do not expect a strong current on the eastern coast, (the impossibility of such a current will shortly be demonstrated), we anticipate that the interior solution will be valid all the way to this coast. Hence, we want $U = 0$ at $x = a$, $x = 0$ and $x = a$ denoting the western and eastern shores. Thus in the region I_i

$$\psi_i = \frac{2\gamma W}{\varrho\beta s^2}(a - x) \qquad (7.6)$$

$$U_i = -\frac{2W}{\varrho\beta s^2}(a - x) \qquad (7.7)$$

We now examine the boundary equations. From equations (6.6) and (6.7) and neglecting the radial variation of v,

$$\frac{\frac{1}{\sin^2\vartheta}\frac{\partial}{\partial x}\left(\frac{1}{D}\frac{\partial\psi}{\partial x}\right) + 2\Omega\cos\vartheta}{D} = F(\psi). \qquad (7.8)$$

Since $g' = g$ in the homogeneous case, it is clear from equations (6.8) and (6.9) that the surface slopes will be very small and that, for a reasonable average depth, the depth will be essentially uniform. Expanding $\cos\vartheta$ in a power series about $\vartheta = K$ and retaining the first two terms

$$2\Omega\cos\vartheta \approx 2\Omega\cos K + 2\Omega\frac{\gamma}{R}\sin K \qquad (7.9)$$

or

$$f \approx f_K + \beta_K\gamma, \quad \beta_K \equiv \frac{2\Omega}{R}\sin K, \quad f_K \equiv 2\Omega\cos K \qquad (7.10)$$

and equation (7.8) becomes

$$\frac{1}{\sin^2\vartheta}\frac{1}{D}\frac{\partial^2\psi}{\partial x^2}+f_K+\beta_K\gamma=G(\psi) \quad (7.11)$$

where $G(\psi)=DF(\psi)$, D being regarded constant.

According to boundary layer analysis, as discussed in Section 5, the $\partial/\partial x$ derivatives are large only in the boundary layer and decrease as one approaches the interior. The transition from boundary to interior regions is, of course, continuous, but, to simplify the terminology, let us define some suitable distance $x=L$ as the "edge" of the boundary layer, L being large enough so that the boundary layer solution there is essentially equal to the interior solution in the same neighborhood. We then have

$$f_K+\beta_K\gamma=G(\psi_i) \text{ at } x=L \quad (7.12)$$

But, from equation (7.6),

$$\psi_i(L,\gamma)\approx\frac{2Wa}{\varrho\beta s^2}\gamma\equiv U^*\gamma \quad (7.13)$$

since we expect $L\ll a$, and where U^* denotes the zonal transport into the boundary layer. Hence

$$f_K+\beta_K\gamma=G(U^*\gamma) \quad (7.14)$$

and

$$G(\psi)=f_K+\frac{\beta_K}{U^*}\psi \quad (7.15)$$

Substitution into equation (7.11) yields

$$\frac{\partial^2\psi}{\partial x^2}-\frac{\sin^2\left(K-\frac{\gamma}{R}\right)D\beta_K}{U^*}\psi=$$
$$=-\sin^2\left(K-\frac{\gamma}{R}\right)D\beta_K\gamma \quad (7.16)$$

If we consider a closed ocean basin, the coast $x=0$ and the southern boundary $\gamma=0$ form a continuous transport line so that $\psi(0,\gamma)=0$. This boundary condition together with the matching condition as the interior is approached (equation 7.13) determine the constants of integration. The solution is

$$\psi=U^*\gamma\left[1-e^{-\left(\frac{\sin^2(K-\gamma/R)\,D\beta_K}{U^*}\right)^{1/2}x}\right] \quad (7.17)$$

and, from equation (6.6)

$$V=(U^*D\beta_K)^{1/2}\gamma e^{-\left(\frac{\sin^2(K-\gamma/R)\,D\beta_K}{U^*}\right)^{1/2}x} \quad (7.18)$$

Thus the theory predicts an intense northward stream on the western coast, the width of the stream being given by, say,

$$\sin\left(K-\frac{\gamma}{R}\right)\cdot L\approx 4\left(\frac{u^*}{\beta_K}\right)^{1/2}$$

and the intensity of the northward velocity being of order $s(u^*\beta_K)^{1/2}$, where $u^*=U^*/D$. These results are seen to agree with the orders of magnitude previously derived directly from boundary analysis considerations in Section 5 d). Expressions (7.17), (7.18) are simpler and more revealing if we set

$$x\sin\left(K-\frac{\gamma}{R}\right)=X \quad (7.19)$$

X measuring true distance along a circle of latitude.

Curves 1 a of Figures 2 and 3 show the variation of ψ/Us and V/U^* with dimensionless distance X/s from the western shore at $\gamma=s$ for values of U^* (10^5 cm^2 sec^{-1}) and s (2×10^8 cms) corresponding to the North Atlantic and for a depth D (or D^* in the terminology of Section 8) of 4×10^5 cms which corresponds to the total depth of the ocean. Hence the graphs may be interpreted as representing the Gulf Stream which would exist if the motion were barotropic. The stream is quite narrow (its width is about 40 km); the transport is very large near the coast and decreases very rapidly as the distance from the coast increases. The predicted flow is seen to exhibit what might be regarded as the principal qualitative property of the observed circulation—a westward interior transport being turned into a narrow, intense stream near the western coast—and the width of this stream has the appropriate order of magnitude.

The results obtained may be given a very simple physical interpretation. The vorticity equation (6.7), for D essentially constant, states that the absolute vorticity of a particle, ζ_1+f, is conserved. Since f increases as the particle travels northward, ζ_1 must decrease, and since ζ_1 $\left(\text{or } \frac{\partial v}{\partial X}\right)$ is approximately zero

when the particle enters the boundary region it must become negative. Particles which approach the coast at low latitude, i.e. with small f, must undergo a large increase in f to reach a certain more northerly latitude, and hence acquire a large negative value of ζ_1 (or $\partial v/\partial X$). Those approaching with larger f need not suffer such a great change in f to reach the same northerly latitude and hence acquire less negative $\partial v/\partial X$. This gives rise to the exponential type of decline in current intensity from the coast to the interior.

It is now clear that the interior transport approaching the west coast could equally well be turned into an intense southward current if we did not stipulate that $\gamma = 0$ be a streamline in the boundary region, i.e. that the circulation be enclosed on the south. Following the same physical reasoning as before, a southward current means a decrease in f and hence positive $\partial v/\partial X$ to conserve vorticity. Further, the particles approaching the coast with larger f must acquire larger positive $\partial v/\partial X$ than must those approaching with smaller f. Hence we obtain a boundary layer solution with v having its greatest negative value at the coast and increasing to zero as the interior is approached.

Any flow pattern intermediate between the two already discussed, with a portion of the westward interior current being turned into an intense northward stream and the balance into an intense southward stream is also possible. The entire infinite family of solutions is obtained by stipulating the boundary condition

$$\psi(0, \gamma) = \gamma s U^*, \quad 0 \leq \gamma \leq 1. \qquad (7.20)$$

This gives

$$\psi = U^*(\gamma s - \gamma)\, e^{-\left(\frac{D\beta_K}{U^*}\right)^{1/2} X} + U^* \gamma \qquad (7.21)$$

$$V = -(U^* D \beta_K)^{1/2} (\gamma s - \gamma)\, e^{-\left(\frac{D\beta_K}{U^*}\right)^{1/2} X} \qquad (7.22)$$

Thus all particles approaching the boundary region north of $\gamma = \gamma s$ (but, of course, south of $\gamma = s$ to remain within region I) turn northward, those approaching between $\gamma = 0$ and $\gamma = \gamma s$ turn southward, the transport line $\psi = U^* \gamma s$ dividing at $x = 0$ to form the shoreline both south and north of $\gamma = \gamma s$.

Which of all these solutions is the appropriate one depends on the appropriate choice of the boundary condition and this in turn is governed by considerations of mass conservation in the overall system.

Other solutions may be obtained, for example, by giving $\psi(o, \gamma)$ a negative value. This gives a northward stream consisting not only of the water approaching the coast from the interior and being turned north, but also of water introduced into the stream in the boundary region across $\gamma = 0$, this extra flow preventing the transport line $\psi = 0$ from reaching the coast.

Another important result which is evident immediately on physical grounds is that the factors which create an intense stream on the west coast could not create a similar stream on the east coast. To show this, let us suppose that the zonal transport component in the interior is eastward. If this transport is to turn northward, f must increase along a transport line, hence $\partial v/\partial X$ must become negative. Further, particles approaching with smaller f must acquire larger negative $\partial v/\partial X$, than those approaching with greater f. Hence the solution would require positive v, negative $\partial v/\partial X$, and v tending to zero as one leaves the boundary region and approaches the interior region. Obviously, these are incompatible conditions. A similar argument rules out a southward stream. Thus we see that a boundary layer type solution is possible in region I if the zonal transport is westward, but not if the zonal transport is eastward.

Mathematically, this is seen as follows. Since ψ_i is zero on $\gamma = 0$, and since $U_i = -\partial \psi_i/\partial \gamma > 0$ for an eastward interior current, ψ_i would be negative for $\gamma > 0$; in particular ψ_i would be negative at the edge of the intense stream on the east coast. The matching with the boundary layer solution, analogous to equation (7.12), would then lead to an expression for $G(\psi)$ analogous to (7.15) with a minus sign in front of the term containing ψ. This gives rise to a plus sign for the ψ term in the equation analogous to (7.16) for the boundary layer stream function, and hence to trigonometric instead of exponential solutions. Hence no boundary layer type solution is possible.

To avoid confusion, it should be emphasized that the above conclusion does not in any way conflict with the well known problem of ideal, irrotational fluid theory, in which a flow impinges on a solid boundary placed normal to the undisturbed flow at infinity. This flow is

not of the boundary layer type and the tangential current is just as wide and no more intense than the normal current. This type of flow was excluded from our investigations as soon as we made approximations appropriate to boundary layer type solutions.

It appears that the simple homogeneous ocean model contains the essential features of the type of circulation one expects. In the following section we investigate to what extent the two-layer model alters the phenomenon.

8. The Two-Layer Ocean with Simple Wind Distribution[1]

We consider the same problem as in Section 7 and make the same approximations except that now the variation of the depth D is taken into account. The interior relations (7.3) to (7.7) remain unchanged. We shall require a relation between U^x and D_i at the edge of the boundary layer. From equations (6.4) and (7.7), and setting $2\Omega \cos\vartheta = f \approx f_K + \beta_K y$, we have

$$D_i^2 = \left(f_K y + \frac{\beta_K y^2}{2}\right)\frac{4W}{\varrho\beta s^2 g'}\,(a-x) + C(x) \tag{8.1a}$$

where $C(x)$ is still arbitrary. If D^* is the depth at $y=0$ and at the edge of the boundary layer $x=L$, then $C(L)=D^{*2}$ and

$$D_i^2(L,y) = \frac{2U^x}{g'}\left(f_K y + \frac{\beta_K y^2}{2}\right) + D^{*2} \tag{8.1b}$$

Another expression for $D_i^2(x,y)$ may be derived by using the momentum equation (6.5). It is approximately

$$D_i^2 = -\left(f_K y + \frac{\beta_K y^2}{2}\right)\frac{4W}{\varrho\beta s^2 g'}\,x - \frac{2W\sin K}{\varrho g'}\,x + C_1(y) \tag{8.1c}$$

Comparison with equation (8.1 a) yields

$$C(x) = D_a^2 + \frac{2W\sin K}{\varrho g'}\,(a-x) \tag{8.2}$$

where D_a is a constant and denotes $D_i(a,y)$.

Instead of using the vorticity equation (6.7) it is more convenient, in the two-layer case, to use the momentum equation (6.9) and the Bernoulli equation (6.10). From equations (6.9) and (6.6)

$$\psi = \frac{g'}{2f}D^2 + C_3(y) \tag{8.3}$$

where $C_3(y)$ is arbitrary and is determined by matching ψ and D with the interior solutions. We have from equations (7.13), (8.1) and (8.3)

$$U^* y = \frac{g'}{2f}\left[\frac{2U^*}{g'}\left(f_K y + \frac{\beta_K y^2}{2}\right) + D^{*2}\right] + C_3 \tag{8.4}$$

whence

$$C_3(y) = \frac{\beta_K y^2 U^*}{2f} - \frac{g' D^{*2}}{2f} \tag{8.5}$$

Substituting in equation (8.3) and solving for D^2 we obtain

$$D^2 = D^{*2} + \frac{2f}{g'}\psi - \frac{\beta_K y^2 U^*}{g'} \tag{8.6}$$

Equation (8.6) provides one relation between the unknowns ψ and D. A second relation is obtained from the Bernoulli equation (6.10). The unknown function $B(\psi)$ is again determined by matching with the interior solution. As one leaves the boundary region, equation (6.10) becomes

$$g'\left[D^{*2} + \frac{2U^*}{g'}\left(f_K y + \frac{\beta_K y^2}{2}\right)\right]^{1/2} = B(U^* y) \tag{8.7}$$

[1] Some weeks following the final preparation of this paper Dr. J. G. Charney (1955) published a theory of the Gulf Stream much like the one contained in the following section. Charney's aim is to study a two-layer model which is fashioned to fit as closely as possible the observed topography of the thermocline between the Florida Straits and Cape Hatteras and the observed volume transports in the Stream, in order to determine how closely the theory can reproduce the observed flow. By contrast, this author's primary goal has been to critically analyze some of the questions connected with the formulation of a suitable theory and the development of the pertinent equations, and to investigate the mechanism which gives rise to the intense coastal current. This is done with a view to clarifying such problems as the roles of density stratification and the variation of the Coriolis parameter, the possibility of the existence of a current on the eastern boundary, the direction of the intense current, etc. In order not to obscure any of these aspects of the problem the simple model used to study the homogeneous ocean is retained in this section, where our theory is applied to the two-layer system, and no attempt is made to fit the model more closely to the Gulf Stream.

giving

$$B(\psi) = g'\left[D^{*2} + \frac{2f_K}{g'}\psi + \frac{\beta_K}{g'U^*}\psi^2\right]^{1/2} \quad (8.8)$$

Substitution into equation (6.10) yields

$$\frac{v^2}{2} = g'\left\{\left[D^{*2} + \frac{2f_K}{g'}\psi + \frac{\beta_K}{g'U^*}\psi^2\right]^{1/2} - D\right\} \quad (8.9)$$

Finally, replacing v by $(1/D\sin\vartheta)\,\partial\psi/\partial x$ from equation (6.6) and eliminating D by using equation (8.6), the following equation for ψ is obtained:

$$\left(\frac{\partial\psi}{\partial x}\right)^2 =$$

$$= 2g'\sin^2\left(K - \frac{\gamma}{R}\right)\left[D^{*2} + \frac{2f}{g'}\psi - \frac{\beta_K\gamma^2U^*}{g'}\right]$$

$$\left\{\left[D^{*2} + \frac{2f_K}{g'}\psi + \frac{\beta_K}{g'U^*}\psi^2\right]^{1/2} - \right.$$

$$\left. - \left[D^{*2} + \frac{2f}{g'}\psi - \frac{\beta_K\gamma^2U^*}{g'}\right]^{1/2}\right\} \quad (8.10)$$

The appropriate boundary condition is that $x=0$ be a streamline. As in Section 7 the particular value to be chosen for $\psi(o, \gamma)$ depends on continuity considerations for the entire system. We shall restrict our numerical solutions to the model discussed in Section 7, i.e. to the case where the circulation is confined to a region north of $\gamma=0$, so that

$$\psi(o, \gamma) = 0 \quad (8.11)$$

We first note the very important result $\partial\psi/\partial x=0$ for all x if $\beta_K=0$. Thus, if the variation of the Coriolis parameter with latitude were neglected, no boundary stream could be produced. From a different point of view, the result shows that the variation in depth alone and its effect on the potential vorticity (equation (6.7)) cannot give rise to an intense stream. Thus, in the two-layer ocean, as in the homogeneous model, the variation of f is the essential phenomenon and it remains to investigate how the resulting flow pattern is modified by density stratification. More physical insight into this conclusion can perhaps be gained by the following consideration. Consider the change of relative vorticity ζ_1 $\left(\text{or } \frac{1}{\sin\vartheta}\frac{\partial v}{\partial x}\right)$ as one follows a streamline. Since, according to equation (6.7), potential vorticity is conserved, a change in ζ_1 will be due either to a change in f or to a change in D. We see from equation (8.6), however, that a change of D along a given streamline is due solely to a change in f. Hence, if f is constant, ζ_1 is constant along each streamline and since it is approximately zero near the edge of the boundary layer it must be zero everywhere. Thus the existence of β_K is the primary cause of the phenomenon. Inasmuch as β_K together with the small value of g' in the two-layer model give rise to a considerable change of depth along a streamline, and this change in turn effects the potential vorticity and hence the current, the latter is actually dependent on the depth (and hence on the density stratification) as well as on β_K.

Proceeding now with the analysis of the differential equation (8.10), we replace x by X according to equation (7.19) and then introduce the non-dimensional quantities $\bar{X}$, $\bar{\gamma}$, $\bar{\psi}$ by the relations

$$X = s\bar{X}, \quad \gamma = s\bar{\gamma}, \quad \psi = U^*s\bar{\psi}$$

so that $\bar{\psi}$ approaches $\bar{\gamma}$ as one approaches the interior. Equation (8.10) becomes

$$\left(\frac{\partial\bar{\psi}}{\partial\bar{X}}\right)^2 = \frac{2\beta_K{}^{3/2}s^3}{U^{*1/2}g'^{1/2}}\left[\varepsilon + \delta\bar{\psi} + 2\bar{\gamma}\bar{\psi} - \bar{\gamma}^2\right]$$

$$\left\{\left[\varepsilon + \delta\bar{\psi} + \bar{\psi}^2\right]^{1/2} - \left[\varepsilon + \delta\bar{\psi} + 2\bar{\gamma}\bar{\psi} - \bar{\gamma}^2\right]^{1/2}\right\} \quad (8.13)$$

where

$$\varepsilon = \frac{D^{*2}g'}{U^*\beta_Ks^2} = \frac{D^*g'}{u^*\beta_Ks^2}, \quad \delta = \frac{2f_K}{\beta_Ks} \quad (8.14)$$

Introducing the transformation

$$\xi = \left(\frac{\beta_K{}^{3/2}s^3}{U^{*1/2}g'^{1/2}}\right)^{1/2}\bar{X}, \quad (8.15)$$

equation (8.13) becomes

$$\left(\frac{\partial\bar{\psi}}{\partial\xi}\right)^2 = 2\left[\varepsilon + \delta\bar{\psi} + 2\bar{\gamma}\bar{\psi} - \bar{\gamma}^2\right]$$

$$\left\{\left[\varepsilon + \delta\bar{\psi} + \bar{\psi}^2\right]^{1/2} - \left[\varepsilon + \delta\bar{\psi} + 2\bar{\gamma}\bar{\psi} - \bar{\gamma}^2\right]^{1/2}\right\} \quad (8.16)$$

In this form all the parameters of the problem appear in the two dimensionless groupings ε and δ only. The meaning of δ is evident. The

significance of ε is readily seen from equation (8.6). In terms of the dimensionless variables we have

$$D^2 = D^{*2} + \frac{2\,(f_K + \beta_K s\bar{\gamma})}{g'}\,U^* s\bar{\psi} - \frac{U^*\beta_K s^2\bar{\gamma}^2}{g'} \tag{8.17}$$

Thus $U^*\,\beta_K s^2/g'$ is a measure of the change of the square of the depth along a streamline and $\varepsilon^{1/2}$ is the ratio of the characteristic depth D^* to the characteristic change of depth.

In Section 7 the equations were applied to the homogeneous ocean by neglecting the variation in depth. Hence, it is to be expected that equation (8.16) will yield the solution for the homogeneous ocean when $\varepsilon \gg 1$; i.e. as far as the boundary region is concerned, a two-layer model, the depth of whose upper layer is very great compared to the change of that depth, behaves like a homogeneous model. The approximate analytical solution for $\varepsilon \gg 1$ is obtained in the following manner. The first bracket on the right-hand side of equation (8.16) is approximated by ε. The expressions inside each of the other brackets are divided by ε and the brackets expanded in binomial series retaining terms of order ε^{-1}. This yields

$$\left(\frac{\partial\bar{\psi}}{\partial\xi}\right)^2 \approx \varepsilon^{1/2}(\bar{\gamma} - \bar{\psi})^2 \tag{8.18}$$

Imposing the boundary condition $\bar{\psi}\,(o, \bar{\gamma}) = o$, the solution of equation (8.18) is

$$\bar{\psi} = \bar{\gamma}(1 - e^{-1/4\,\xi}) \tag{8.19}$$

which becomes identical with the solution obtained previously (equation 7.17) upon transformation to the appropriate variables.

If we deal with a homogeneous ocean, ε will in general be large because $g' = g$ and this quantity is of the order of 500 times as great as g' in a usual two-layer model. If we deal wthi a two-layer model ε may be made large by making D^* large. The preceding analysis

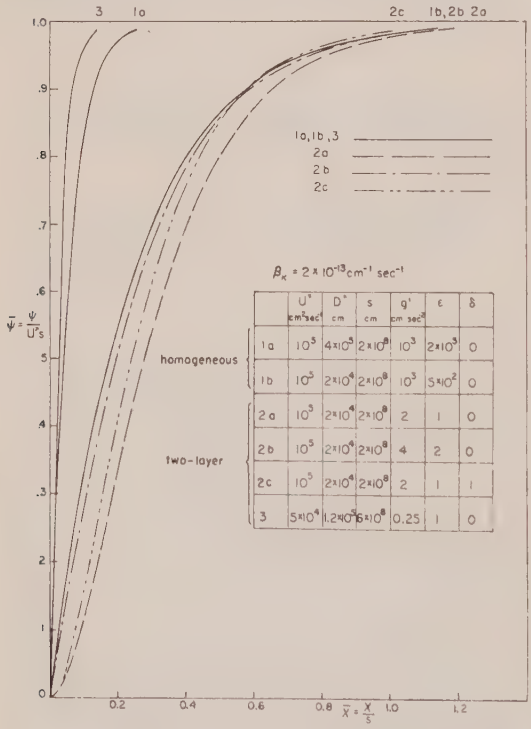

	U^* $cm^2 sec^{-1}$	D^* cm	s cm	g' cm sec^{-2}	ε	δ
1a	10^3	4×10^5	2×10^8	10^3	2×10^5	0
1b	10^5	2×10^4	2×10^8	10^3	5×10^2	0
2a	10^3	2×10^4	2×10^8	2	1	0
2b	10^5	2×10^4	2×10^8	4	2	0
2c	10^3	2×10^4	2×10^8	2	1	1
3	5×10^4	1.2×10^5	6×10^8	0.25	1	0

Fig. 2. Dimensionless transport function $\bar{\psi}$ vs. dimensionless distance from western coast at northern boundary of region I_b for various values of the pertinent paramaters.

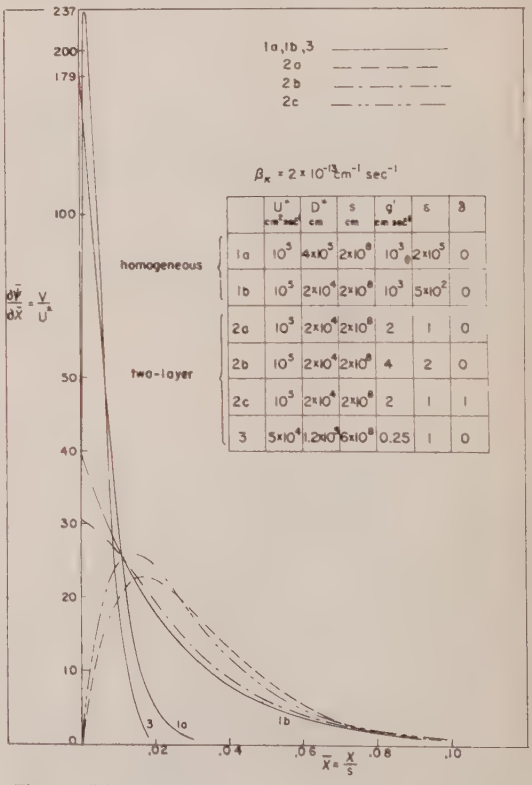

	U^* $cm^2 sec^{-1}$	D^* cm	s cm	g' cm sec^{-2}	ε	δ
1a	10^3	4×10^5	2×10^8	10^3	2×10^5	0
1b	10^5	2×10^4	2×10^8	10^3	5×10^2	0
2a	10^3	2×10^4	2×10^8	2	1	0
2b	10^5	2×10^4	2×10^8	4	2	0
2c	10^3	2×10^4	2×10^8	2	1	1
3	5×10^4	1.2×10^5	6×10^8	0.25	1	0

Fig. 3. Dimensionless northward transport vs. dimensionless distance from western coast at northern boundary of region I_b for various values of the pertinent parameters.

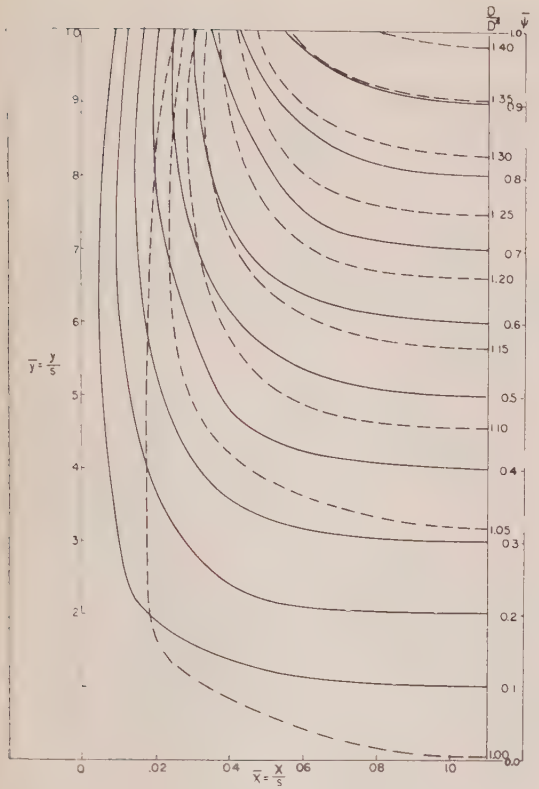

Fig. 4. Constant depth lines (dashed) and "transport" lines (solid) in region I_b for case 2 a of Figs. 2 and 3 corresponding approximately of the formation of the Gulf Stream.

shows that in terms of the variables of equation (8.16) the boundary solutions $\bar{\psi}$ for a homogeneous ocean and a two-layer model are identical provided ε is large and has the same value in the two cases.

Equation (8.16) has been solved numerically for various values of ε and δ and pertinent results are plotted in Figures 2 to 4.

Figure 2 shows the variation of the dimensionless transport function $\bar{\psi}$ with dimensionless distance $\bar{X}$ from the coast at the northern boundary of region I_b. The magnitudes of β_K, U^*, s, g', D^*, ε (see legends of Figs. 2, 3) for Curve 2 a correspond to a baroclinic model of the Gulf Stream except for the fact that the southern boundary of the region I is at the equator ($\delta = 0$). The width of the Stream is, say, 150 km, a very reasonable value. Curve 2 c represents the same situation with $\delta = 1$, i.e. with the southern boundary at approximately 15° latitude. This northward shift of the southern boundary tends to produce a somewhat narrower stream, but the effect is quite small. Curve 1 b corresponds to a homogeneous ocean with the values of U^*, D^*, s and δ equal to those of the upper layer of the two-layer model of Curve 2 a. These curves thus afford a revealing comparison of the behavior of the two models. The widths of the Streams are practically the same. Thus, the question of whether the bottom surface is solid, or an interface between two layers of slightly different density in a baroclinic model, does not have much bearing on the formation of the Stream and its width. Another interesting comparison may be made between Curves 2 a and 1 a, the latter (see Section 7) corresponding to a homogeneous ocean whose depth is that of the total two-layer model with the same values of U^*, s, and δ and which therefore represents the Stream that would exist if the motion were barotropic.

Curve 2 b represents the same situation as 2 a except that the density difference is double. Comparison of the two curves demonstrates the relative insensitivity of the stream formation to this factor.

Curve 3 applies to an ocean with the same values of ε and δ as 2 a but different U^*, s, g', D^*. The drastic decrease in the width of the current may be seen from equation (8.15) to be due primarily to the increase in s.

In Figure 3 the dimensionless transport $\partial\bar{\psi}/\partial X$ is plotted against $\bar{X}$ for the systems discussed above. The transport shows a general tendency to decrease monotonically with $\bar{X}$ due to the decrease in velocity. This tendency, however, is counterbalanced by the monotonic increase of the depth, so that in some cases the transport first increases to a maximum and then decreases. This is the case in 2 a, 2 c and 3 where the transport starts from zero due to the fact that the depth vanishes at $\bar{y} = s$, $\bar{X} = 0$ in these cases; (see the following discussion of this point). The narrow streams of cases 1 a and 3 give rise to very large transports extending over a very narrow region. The transport adjacent to the coast in the homogeneous model 1 b is much greater than that in the corresponding baroclinic model 2 a due to the latter's very small depth near the coast. The transport in 1 b drops off much more rapidly with $\bar{X}$, however, so that the widths of the streams are about equal (Fig. 2).

Figure 4 represents a typical pattern of transport and constant depth lines (case 2 a). The transport lines near the coast tend to bend away from the latter after first approaching it due to the decrease in depth near the coast. This decrease tends to cut down the transport near the coast and hence to force the stream seawards.

Our results indicate that the density stratification influences certain aspects of the stream formation, but that it is a modifying factor rather than a fundamental one insofar as our problem is concerned. One important point must be discussed in this connection, however.

Equation (8.17) shows that, for fixed γ, the depth is smallest at the boundary and that it becomes zero when

$$\bar{\gamma} = \varepsilon^{1/2} \text{ or } \gamma^2 = \frac{D^{*2} g'}{U^* \beta_K s} \qquad (8.20)$$

Thus, if $\varepsilon < 1$, the solution cannot be valid for $\bar{\gamma} > \varepsilon^{1/2}$ and the value $\bar{\gamma} = \varepsilon^{1/2}$ might be interpreted as the latitude north of which a new regime of flow must take over. Since the velocity remains non-zero at that point we must actually except that the solution will break down at some distance south of $\bar{\gamma} = \varepsilon^{1/2}$.

The preceding remarks apply to the behavior of the boundary solution when an arbitrarily fixed transport U^* with arbitrary depth D^* at $\gamma = 0$ flows into the boundary region. If, however, we require that the boundary solution be matched to an interior solution the validity of which is to extend up to the eastern shore, then D^* and U^* are not independent. From equation (8.2)

$$C(L) = D^{*2} \approx D_a^2 + \frac{2 Wa \sin K}{\varrho g'} \qquad (8.21)$$

whence, using the definitions of ε and U^x,

$$\varepsilon = \frac{D^{*2}}{D^{*2} - D_a^2} \qquad (8.22)$$

Hence, in this case $\varepsilon \geqslant 1$ and takes on its smallest value, one, only in the extreme case when $D_a = 0$. Since the meridional transport is independent of x in the interior, this extreme case would imply infinite meridional velocity at $x = a$.

It is worth noting that when the model under investigation does not represent an enclosed ocean, but rather a system in which northward flow is allowed to enter the stream across the boundary $\gamma = 0$ so that the value of ψ on the western shore is negative, then, from equation (8.17), the depth will become zero for a value of $\bar{\gamma}$ which is smaller than $\varepsilon^{1/2}$, so that the solution may break down for $\bar{\gamma} < 1$ even if it is matched to an interior solution which is valid right up to $x = a$. It appears that this breakdown of the solution when ε is sufficiently small constitutes the major difference in the dynamics of the streams in a two-layer and a homogeneous model.

The theory predicts that the meridional velocity is a maximum at the western shore. This appears to violate completely the condition that a viscous fluid should adhere to a solid boundary, a condition which was specifically excluded by our approximate analysis. This violation becomes less serious than appears at first sight when one considers that the boundary may be interpreted as a water boundary with the region between the stream and the coast acting as sub-layer similar to the laminar sub-layer encountered in turbulent boundary layer flows.

Acknowledgment

The author wishes to express his gratitude to Mr. Henry Stommel of the Woods Hole Oceanographic Institution for the comments and advice offered in the course of valuable discussions without which this investigation would not have been possible.

REFERENCES

CHARNEY, J. G., 1955: The Gulf Stream as an inertial boundary layer. *Proc. N.A.S.* (USA). **41**, No. 10, pp. 731 – 740.

MONTGOMERY, R. B., 1940: The present evidence on the importance of lateral mixing processes in the Ocean. *Bull. Amer. Met. Soc.* **21**, p. 87.

MUNK, W. H., 1950: On the wind-driven ocean circulation. *J. Met.* **7**, p. 79.

MUNK, W. H., and CARRIER, G. F., 1950: The wind-driven circulation in ocean basins of various shapes. *Tellus*, **2**, No. 3, pp. 158 – 167.

STOMMEL, H., 1955: Discussion published as a supplement to the *Journal of Marine Research*, **14**, No. 4. Also, "Why do our ideas about the ocean circulation have such a peculiarly dream-like quality?", April 1954.

SVERDRUP, A. U., 1947: Wind-driven currents in a baroclinic ocean with application to the equatorial currents of the Eastern Pacific. *Proc. N.A.S.* (USA) **33**, p. 318.

Direction of Faulting in the Deep-Focus Spanish Earthquake of March 29, 1954[1]

By J. H. HODGSON and J. IRMA COCK, Dominion Observatory, Ottawa

(Manuscript received October 21, 1955)

Abstract

An earthquake of magnitude 7.1 occurred off the south coast of Spain on March 29, 1954. The earthquake was remarkable in that it had a focal depth of about 650 km; no earthquake with focal depth greater than normal is known to have occurred in this area previously.

Using methods already established but here reviewed, the mechanism at the focus is investigated. The method defines two planes, without determining which is the fault. There are thus two possibilities. Under the first possibility the fault is approximately vertical and strikes north-south. The movement is vertical, such that the eastern side of the fault rises with respect to the western side. Under the second possibility the fault is approximately horizontal, and the movement is also horizontal, the material above the focus moving due east (that is, in the sense of the earth's rotation) with respect to the material below the focus.

Introduction

Detailed studies of the earth's seismicity have shown that earthquakes with deeper than normal focus ordinarily occur in well defined and very limited areas of the earth's surface. They are associated particularly with many of the circum-Pacific seismic zones, although earthquakes with intermediate focal depths are found in the Hindu Kush and in the eastern Mediterranean. The occurrence of a deep-focus earthquake outside of these established zones is a definitely unusual event.

Such an earthquake occurred on March 29, 1954, in the vicinity of Granada, Spain. No earthquake with focal depth greater than normal is known to have occurred in this area before, yet it is clear that this shock had a focal depth of about 650 km. It was, moreover, larger than any shock previously known in the vicinity, having had a Richter magnitude of 7.1, sufficient to cause property damage in Granada and Malaga despite the great depth of focus.

It seems desirable that such an unusual earthquake should be studied as extensively as possible. As a contribution to this study we here present the results of an investigation into the direction of faulting in the earthquake.

Method used

The method used in this research, which was developed in a series of earlier papers (HODGSON and MILNE, 1951; HODGSON and STOREY, 1953), is based on the premise that the earthquake is due to slipping along a fault. Fig. 1 provides a simple example. Suppose that FF represents, in plan, the trace of a vertical fault which undergoes displacement during an earthquake in the sense shown by the arrows. By the simple argument that points ahead of an arrow will be pushed by the impulse while points behind an arrow

[1] Published by permission of the Acting Deputy Minister, Department of Mines and Technical Surveys, Ottawa, Canada.

will be pulled, one sees intuitively that the area in the vicinity of the earthquake will be divided into four zones in which the initial motion will be alternately compressional and dilatational as shown in the figure. The boundaries between the zones are provided by the trace of the fault and by the line perpendicular to the motion couple. Conversely, given a suitable distribution of seismograph stations close to the epicentre, it should be possible to separate those recording an initial compression from those recording an initial dilatation by two lines at right angles; one of these lines will represent the trace of the fault.

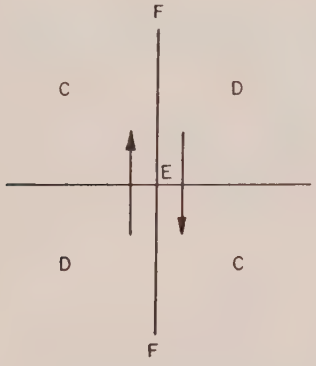

Fig. 1. Zones of compression and dilatation set up around the epicentre.

This very simple example serves to illustrate the principle, established rigorously by NAKANO (1923), that the volume surrounding an earthquake focus is divided into four sectors, alternately compressional and dilatational with respect to first motion. The boundaries of the sectors are defined by the fault plane and by a second plane, perpendicular to the displacement couple, called the *auxiliary* plane. In particular, if one were dealing with a homogeneous earth, its surface would be divided by these planes into four lunes, two of which would receive the initial motion as a compression, the alternate two receiving a dilatation.

Actually of course the earth is not homogeneous, and this simple distribution is complicated by the curvature of the seismic ray. In Fig. 2, for example, a station S lying to the right of the fault plane receives its initial impulse from a ray originating to the left of the fault. This difficulty is overcome by a device due to Byerly. Instead of plotting S in its true position it is plotted at the point S′, known as the extended position, the point where the tangent to the ray meets the earth. In this way the orientation relative to the planes is maintained, so that the expected separation of the earth's surface into lunes is achieved.

In practice the mapping is done on a stereographic projection, the point at the antipodes of the earthquake being used as the pole of projection and the corresponding diametral plane as the mapping surface. The epicentre becomes the centre of the map, and the extended position S′ of the station S plots into the point B, at the same azimuth as S but at a distance OB from the centre. OB is called the *extended distance*.

It is a property of the stereographic projection that circles on the globe project into circles on the map. The boundaries separating compressions from dilatations on the earth are circular, being the intersections of the sphere with the fault plane and the auxiliary plane. Hence the boundaries on the map must

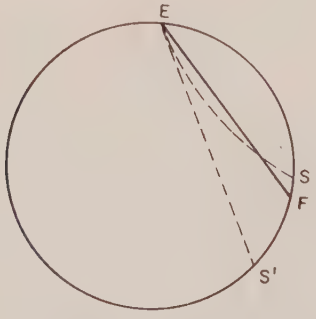

Fig. 2. Definition of Extended position.

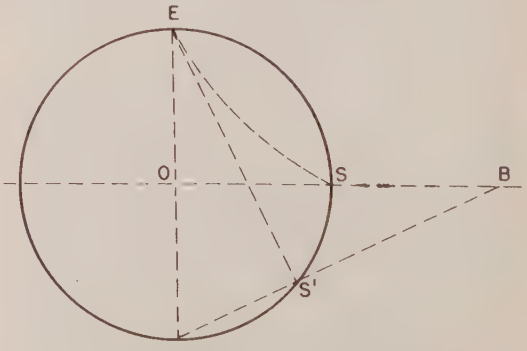

Fig. 3. Definition of Extended distance.

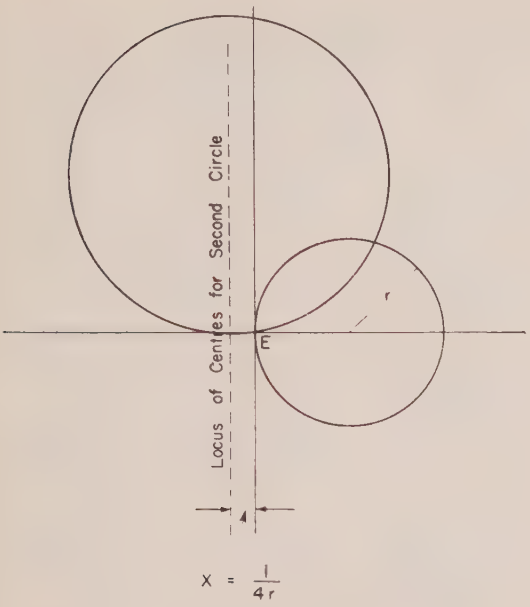

Fig. 4. A typical fault-plane solution.

also be circles. The technique of the research is thus to plot stations on the map at their extended distances and to separate those receiving initial dilatations from those receiving initial compressions by a pair of circles. One of these circles will represent the fault plane, the other the auxiliary plane. It may be shown that the diameters of the circles are equal to the tangent of the dip of the corresponding plane.

In drawing the solution circles it must be remembered that the circles represent orthogonal planes. There is therefore a limitation on their relative positions. This may be expressed as follows. Suppose that one circle of radius r is defined. Then the other circle must have its centre on a line drawn parallel to the tangent to the first circle and at a distance $1/(4r)$ from it.

A typical fault plane solution is shown in Fig. 4. The orthogonality relationship has been shown in the diagram.

In obtaining fault plane solutions one is frequently hampered by the poor distribution of data, owing, for example, to the presence of oceans or of uninhabited land areas. This difficulty has been overcome to some extent through the use of secondary phases. The extended distance of a station is a function of the angle at which the ray leaves the focus to reach the station. As will be apparent from Fig. 5, this angle is different for different phases, so that the extended distance of the station is different for the different phases. One well defined record can thus provide several points on a map.

Before using a secondary phase it is of course necessary to know whether it has suffered any phase change in the course of its path, by reflection, for example, at the surface of the earth or at the boundary of the core. A recent paper by INGRAM and HODGSON (1956) shows that for a focal depth of 0.10 R both PP and pP must have suffered a phase change on reflection, no matter what distance they may be recorded at. It is also assumed, in the light of work by BÅTH (1954), that P_cP does not suffer phase change on reflection at the earth's core.

It should be particularly noted in Figure 5

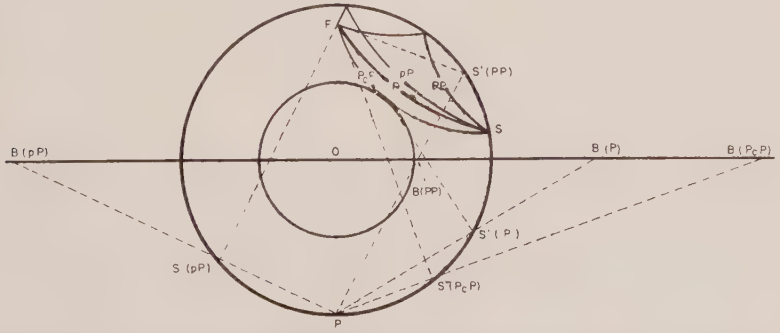

Fig. 5. The phases P_cP, P, pP and PP leave the focus at different angles. Their extended distances OB(P_cP), OB(P), OB(pP) and OB(PP) are thus quite different. Note that pP, arising from an upward-rising ray, has a negative distance.

Table 1. Data on Which Solution is Based

Station	Distance in Degrees from Epicentre	Azimuth in Degrees Epicentre to station	Phase Reported	Direction of Motion
Cartuja	0.1	90.0 W	P	C
Toledo	2.6	7.5 W	P	D
Alicante	2.7	61.5 E	P	C
Lisbon	4.6	68.8 W	P	D
Tortosa	4.7	39.3 E	P	(D)
Coimbra	4.8	50.0 W	P	D
Alger Univ.	5.5	91.5 E	P	C
Barcelona	5.9	44.5 E	P	C
Oropa	11.7	42.7 E	P	C
Paris	12.3	18.1 E	P	C
Pavia	12.3	46.1 E	P	(D)
Prato	12.7	54.6 E	P	D
Basel	13.0	35.0 E	P	D
Rome	13.0	64.6 E	P	D
Rocca di Papa	13.2	65.3 E	P	D
Bologna	13.3	52.1 E	P	D
Salo	13.3	46.8 E	P	D
Chur	13.5	41.4 E	P	D
Zürich	13.5	37.6 E	P	D
Strasbourg	13.9	32.2 E	P	D
Ravensbourg	14.2	38.2 E	P	D
Kew	14.3	7.6 E	P	D
Meszstetten	14.3	36.5 E	P	D
Karlsruhe	14.4	32.3 E	P	D
Stuttgart	14.6	34.4 E	P	D
Uccle	14.7	19.8 E	P	D
ReggioCalabria	15.0	81.1 E	P	D
Messina	15.1	80.3 E	P	D
Trieste	15.4	51.8 E	P	D
De Bilt	15.8	19.6 E	P	D
Rathfarnham	16.3	5.4 W	P	C
Witteveen	17.0	21.0 E	P	D
Durham	17.9	9.3 E	P	D
Prague	18.0	39.2 E	P	D
Vienna	18.2	46.3 E	P	(C)
Stara Dala	18.9	49.9 E	P	D
Aberdeen	19.9	2.0 E	P	D
Skalnate Pleso	20.7	47.7 E	P	D
Copenhagen	21.3	24.8 E	P	D
			P_cP	D
Athens	21.6	79.4 E	P	D
Bergen	24.0	10.4 E	P	D
Istanbul	25.4	71.4 E	P	(C)
M'Bour	25.6	148.8 W	P	C
Uppsala	26.4	23.9 E	P	D
Reykjavik	29.2	16.4 W	P	C
Helwan	29.7	93.8 E	P	(C)
Kiruna	33.4	16.0 E	P	D
Lwiro	49.5	135.5 E	P	D
Seven Falls	49.5	56.1 W	P	C
Shawinigan Falls	50.8	56.2 W	P	C
Ottawa	53.3	57.0 W	P	C
New York C.C.	53.6	62.9 W	P	(D)
			pP	(D)
Palisades	53.6	62.7 W	P	C
Philadelphia	54.6	63.5 W	P	C
			pP	C
Resolute Bay	54.9	18.9 W	P	C
Kirkland Lake	55.2	52.6 W	P	C
Morne des Cadets	55.6	97.8 W	P	C
State College	56.2	61.6 W	P	(D)
Washington	56.4	64.2 W	P	C
San Juan	57.5	90.7 W	P	C
Quetta	57.7	74.6 E	P	D
			pP	D
Cleveland	58.4	59.5 W	P	C
Cincinnati	61.5	60.8 W	P	C
Columbia	61.5	67.6 W	P	C
Chicago	62.5	56.8 W	P	C
			pP	C
Lincoln	69.0	54.2 W	P	C
			pP	C
			PP	D
Fayetteville	69.6	59.5 W	P	C
Kimberley	70.7	153.9 E	P	D
Balboa	73.5	91.1 W	P	C
Pietermaritzburg	73.6	149.6 E	P	D
Tananarive	73.6	129.9 E	P	D
College	74.4	14.8 W	P	C
Bozeman	74.7	43.7 W	P	C
Hungry Horse	74.7	40.3 W	P	C
Merida	74.7	75.1 W	P	C
			pP	C
Butte	75.5	42.8 W	P	C
Grahamstown	75.6	154.3 E	P	D
Salt Lake City	78.2	47.2 W	P	C
			pP	(D)
Victoria	79.3	36.0 W	P	C
			pP	(D)
Seattle	79.5	37.1 W	P	C
Vera Cruz	80.4	73.0 W	P	C
La Paz	80.7	118.6 W	P	C
			pP	C
			PP	(C)
Chihuahua	82.1	59.9 W	P	C
Oaxaca	82.4	74.6 W	P	C
Nelson	82.8	64.4 W	P	C
			pP	(D)
Tacubaya	82.8	71.1 W	P	C
Tucson	83.0	54.4 W	P	C
Boulder City	83.2	49.6 W	P	C
Mineral	84.1	42.4 W	P	C
			pP	C
Shasta	84.3	41.9 W	P	C
			pP	(D)
Montezuma	85.6	122.7 W	P	(D)
Fresno	85.7	46.1 W	P	C
			pP	C
Berkeley	86.3	44.0 W	P	C
			pP	C
			PP	D
			PPP	C
Mount Hamilton	86.3	44.6 W	P	C
			pP	C

Station	Distance in Degrees from Epicentre	Azimuth in Degrees Epicentre to Station	Phase Reported	Direction of Motion
Pasadena.....	86.5	49.0 W	P	C
			pP	C
Manzanillo....	86.9	68.6 W	P	C
Sapporo.....	93.9	25.1 E	P	D
			P_cP	D
			PP	(D)
Hong Kong ..	96.4	55.5 E	P	D
			PP	(D)
Matsushiro ...	98.4	30.4 W	P	D
			PP	C
Djakarta.....	109.8	82.6 E	P	(C)
			pP	(C)
			PP	C
Honolulu.....	116.9	26.8 W	PKP_1	C
Riverview....	159.0	88.2 E	PKP_2	D
			PP	C
Christchurch..	173.1	155.0 E	PKP_1	D
			PP	(D)
Wellington ...	175.7	163.3 E	PKP_1	D
			PP	(D)

that the pP ray, which is generated by an upward rising ray, has a negative extended distance. This is true of any phase which derives from an upward rising ray, and applies not only to pP but also to P for stations close to the epicentre. This has the result of distorting the geographical position of stations close to the epicentre, so that they "pass through" the epicentre and appear at an azimuth opposite to their true one. This can be very confusing unless the reason for it is understood.

Tables of extended distances for the phases shown in Fig. 5 and for many others have been published (HODGSON and STOREY, 1953; HODGSON and ALLEN, 1954 a, b; HODGSON, ALLEN and COCK, 1956). These tables have been used in the present problem.

Summary of available data

Questionnaires seeking information on the direction of motion were circulated to the seismograph stations of the world in January, 1955. The response to this appeal has been very satisfactory, and we take this opportunity to thank our collaborators for their help. The information from the returned questionnaire forms is given in Table 1, along with the distance and azimuth of each contributing station. These distances and azimuths were measured using a device developed for the purpose by this Observatory (WILLMORE and HODGSON, 1955). As a check on the computations, the distances and azimuths were measured independently by each of us.

In Table 1, C indicates that the phase in question was recorded as a compression, D that it was recorded as a dilatation. In plotting, pP and PP are shown with the opposite phase, to allow for the phase change on reflection, but the table gives the motion as actually recorded. Phase designations in parentheses are inconsistent with the published solution.

Fault plane solution

The data listed in Table 1 have been used to plot the fault plane solution diagram shown in Figure 6. Not all the data given in the table have been plotted; to do so would have made the diagram too confusing.

Examination of the diagram will show that a line striking N 2° E, passing between Rathfarnham and Aberdeen, separates compressions on the left from dilatations on the right. We shall presently show that this line of separation is not a straight line but the arc of a very large circle, and that a second very small circle exists, too small to show on this diagram. We shall require that the large circle be large enough to include the observation for Wellington. Since Wellington lies at an extended distance of 40.2 units, the radius of the circle is required to be something in excess of 60 units.

Fig. 6 affords an opportunity to observe the "passing through" of the pP phase. In the south-east quadrant of the diagram, for example, will be found the pP observations from many California and Mexico stations, agreeing in their phase designations with the direct P wave recorded at Lwiro, Tananarive and the South African stations. In the same quadrant will be found P observations from Lisbon, Coimbra and Toledo. These stations lie close to the epicentre and have passed through the origin to their opposite azimuth. Again it should be noted that the information from these stations agrees with that obtained directly and from the pP phases. Other examples of passing through will be found in the diagram; Alicante is plotted to the west of La Paz, Alger University and pP Quetta

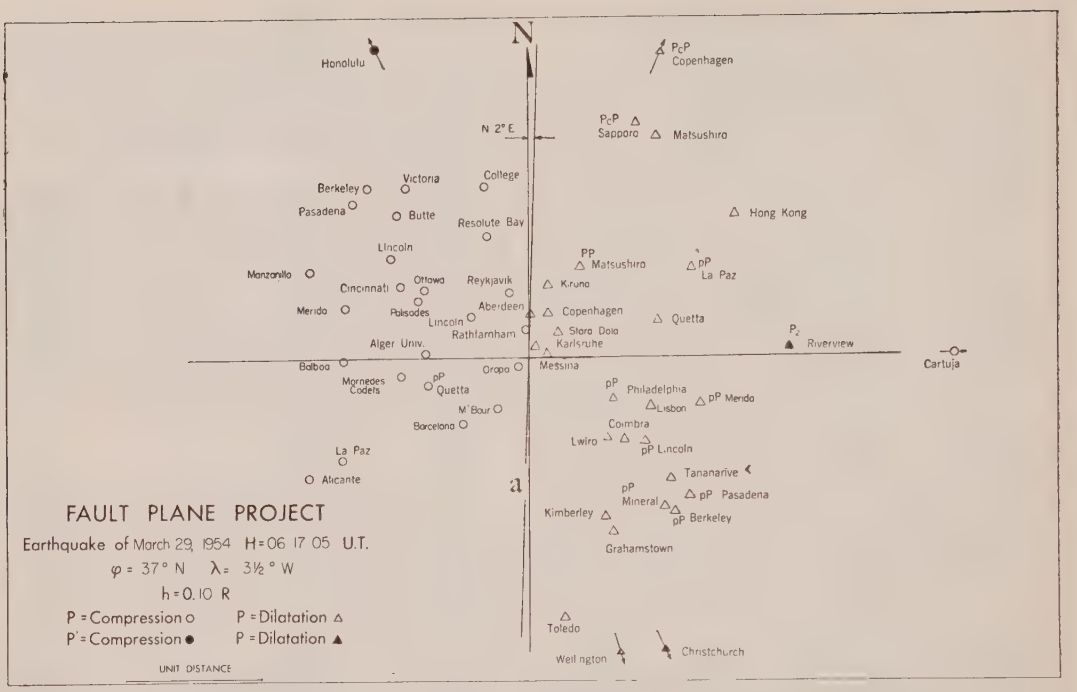

Fig. 6. Fault plane solution diagram. The notation is explained in the legend.

in the vicinity of Morne des Cadets, while Cartuja is plotted off the diagram to the right at a very large distance.

Figure 7 gives the fault plane diagram of the immediate epicentral vicinity on a very large scale. The line through the origin, striking N 2° E has been shown. This line is supposed to separate compressions on the west from dilatations on the east, but on this enlarged diagram it is possible to show a number of dilatations, lying very close to the epicentre, but to the west of it. These dilatations, as well as the compressions for Paris and Oropa, are all from stations which have passed through the origin because of their proximity to the epicentre.

The dilatations at Basel, Prato and Bologne have been separated from the compressions at Paris and Oropa by the small circle shown. This circle has its centre at a distance of 0.004 units from the main circle. According to the formula given earlier the main circle has a radius r given by

$$1/(4r) = 0.004$$

so that $r = 62$ units. We have already pointed out that this radius is sufficient to include the PKP observations at Wellington. The radius corresponds to a dip of about 89°.1.

The small circle represents a plane striking N 78°.5 W and dipping to the south-west at an angle of 3°.4.

The solution presented in Figures 6 and 7 account for all but 20 of 134 observations of motion. The number of observations available, and the numbers of inconsistent observations are summarized in Table 2. This percentage of inconsistencies is somewhat less than normal for a solution of this kind.

Table 2

	P	P_1'	P_2'	pP	PP	PPP	P_cP	Total
Total Number of Observations	100	3	1	17	10	1	2	134
Number of Inconsistent Observations ..	9	0	0	6	5	0	0	20

Fig. 7. Fault plane solution diagram of the immediate epicentre vicinity.

Fig. 8. Cross sections of the earth, through the focus, drawn to scale, showing the two geological possibilities.
a. If plane *a* represents the fault.
b. If plane *b* represents the fault.

Discussion

We have already seen that circle *a* represents a plane striking N 2° E and dipping toward the east at an angle of 89°.1. Circle *b* represents a plane striking N 78°.5 W and dipping to the southwest at an angle of 3°.4. For the purpose of this discussion it seems unwise to say more than that the one plane is vertical and strikes N—S while the other plane is essentially horizontal.

We have then to consider two possibilities. If plane *a* represents the fault, then the fault strikes north-south and is vertical. Plane *b*, under this assumption, will represent the auxiliary plane, which is, by definition, perpendicular to the motion vector. The auxiliary plane being horizontal the motion vector is vertical. The situation is shown, in section, in Fig. 8 a. The western block has dropped relative to the eastern one.

If, on the other hand, the horizontal plane represents the fault, then the vertical plane must represent the auxiliary plane and the motion vector must be horizontal. In this case the motion vector must act in an east-west direction, so that the motion will be as shown in Figure 8 b. Here the material above the focus has moved due east relative to the material below it.

Which of the two possibilities is the true one? This matter can only be solved through the use of S waves, a technique which has not yet progressed to a satisfactory point.

Fault plane solutions have been found for many deep focus earthquakes in the program carried out by this Observatory (Hodgson and Storey, 1954; Hodgson, 1955, 1956 a, b) Most of these have been from earthquakes around the Pacific. In all cases they have shown large transverse components. Indeed this is the first solution obtained for an earthquake of more than normal depth in which there was virtually no transverse displacement. The present solution is therefore unique in the history of the program, further evidence of the unusual nature of this remarkable earthquake.

REFERENCES

Båth, M., 1954: The Density Ratio at the Boundary of the Earth's Core, *Tellus*, **6**, pp. 408—414.

Hodgson, J. H., 1955: Direction of Faulting in Pacific Earthquakes, *Geofisica Pura e Applicata*, Milano, **32**, pp. 31—42.

— 1956 a: Direction of Faulting in Some of the Larger Earthquakes of the Southwest Pacific, 1950—54, *Publications of the Dominion Observatory*, Ottawa, **18**, No. 9.

Hodgson, J. H. 1956 b: Direction of Faulting in Some of the Larger Earthquakes of the North Pacific, 1950—1953, *Publications of the Dominion Observatory*, Ottawa, **18**, No. 10.

Hodgson, J. H., and Allen, J. F. J., 1954 a: Tables of Extended Distances for PKP and P_cP, *Publications of the Dominion Observatory*, Ottawa, **16**, pp. 327—348.

— 1954 b: Tables of Extended Distances for PP and pP, *Publications of the Dominion Observatory*, Ottawa, **16**, pp. 349—362.

Hodgson, J. H., Allen, J. F. J., and Cock, J. Irma, 1956: Tables of Extended Distances for PPP, pPP, pPKP and for P at Very Short Distances, *Publications of the Dominion Observatory*, Ottawa, **18**, No. 5.

Hodgson, J. H., and Milne, W. G., 1951: Direction of Faulting in Certain Earthquakes of the North Pacific, *Bull. Seism. Soc. Amer.*, **41**, pp. 221—242.

Hodgson, J. H., and Storey, R. S., 1953: Tables Extending Byerly's Fault-Plane Techniques to Earthquakes of any Focal Depth, *Bull. Seism. Soc. Amer.*, **43**, pp. 49—61.

— 1954: Direction of Faulting in Some of the Larger Earthquakes of 1949, *Bull Seism. Soc. Amer.*, **44**, pp. 57—83.

Ingram, R. E., S. J., and Hodgson, J. H., 1956: Phase Change of PP and pP on Reflection at a Free Surface, *Bull. Seism. Soc. Amer.*, in press.

Nakano, H., 1923: Notes on the Nature of Forces which Give Rise to the Earthquake Motions, *Seism. Bull. Central Meteorological Observatory of Japan*, 1, pp. 92—120.

Willmore, P. L., and Hodgson, J. H., 1955: Charts for Measuring Azimuth and Distance and for Tracing Seismic Rays Through the Earth, *Publications of the Dominion Observatory*, Ottawa, **16**, No. 14.

On the Local Structural Character of the Earth's Crust

By Eiichi NISHIMURA and Yoshimichi KISHIMOTO
Geophysical Institute, Kyoto University, Kyoto.

(Manuscript received March 7, 1956).

Abstract.

Regional differences in the crustal structure in Japan were investigated, in detail especially around Kyoto, by a duration analysis of the refracted seismic waves of natural earthquakes propagated along the discontinuous surfaces in the crust. Generally speaking the thickness of the earth's crust or, in other words, the depth of the Mohorovičić discontinuity was estimated in our country to be greatly diverse from place to place, its range being nearly 25 ~ 50 km. It was also found that the depth of seismic focus of most frequent occurrence in any region is intimately related to the thickness of the crust in the region concerned.

1. Introduction

For the purpose of investigating the crustal structure in any region, an analysis of the travel time-distance curve obtained from the seismometric observation of natural earthquakes or artificial explosions having occurred in that region, is usually applied in calculating the seismic velocity and thickness of the crustal layer from the apparent velocity and critical distance in the travel time-distance curve. The method is certainly simple and effective for determining the crustal structure in such a case, as the crustal structure to be determined is uniform or monotonously changing in the area concerned, the positions of epicenter and the focal depth of earthquake can be precisely determined, the arrival time of each phase of seismic waves is accurately observed, the effect of locality of the observatories and the instrumental errors of seismographs are negligibly small along with other good observational conditions. But the above conditions are never satisfied in practical cases, especially in relation with natural earthquakes. Consequently the method of analysing the travel time-distance curve for a precise determination of the crustal structure, especially of the heterogeneous distribution, should efficiently be supplemented by other seismometric methods of analysis, for example, the reflected wave, the transformed wave (Wechselwelle), and the refracted wave at and along the discontinuous surfaces in the crust.

2. Method of Analysis

In the present seismometric investigation of the crustal structure, the method of analysing the duration of the seismic refracted wave, which is observed in advance of the direct wave and conveniently designated as "forerunner", was applied to a great many

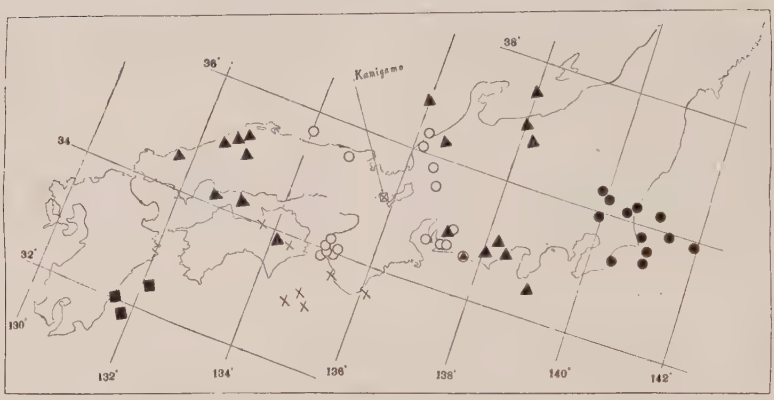

Fig. 1. Positions of the epicenters of earthquakes used in the present investigation and the Kamigamo Geophysical Observatory.

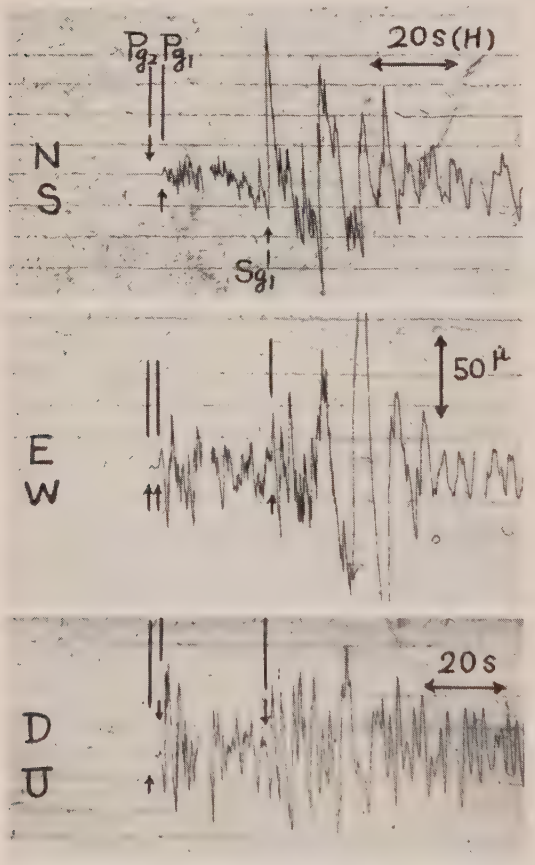

Fig. 2 (a). Wiechert-Seismograms, Jan. 3rd 21h 13m, 1945, Outfall of the Tenryu River (34.7° N, 137.9° E) $Pg_1 \sim Sg_1 = 24.4$ sec, $Pg_2 \sim Pg_1 = 2.0$ sec, focal depth < 10 km (a – group).

Pg_1 and Pg_2 denote the direct wave through the granitic layer and the refracted wave at the interface between the granitic and granodioritic layers.

seismograms obtained at one station of the Kamigamo Geophysical Observatory in Kyoto with the large Wiechert Seismographs for more than forty years. The large Wiechert Seismographs consist of the inertia mass of 1 ton in the horizontal component of inverted pendulum type and 1.3 tons in the vertical component of suspension type with spiral springs, the period of proper oscillation being 12 sec in the horizontal component, and 4 sec in the vertical component, the static magnification of both components being estimated as nearly 200, and both are critically damped with air dampers and mechanically recorded on smoked paper. This method of analysing the duration (the time difference between

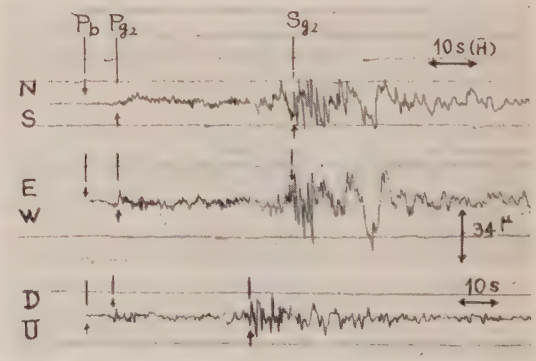

Fig. 2 (b). Wiechert-Seismograms, July 30th 17h 25m, 1953, Western Setoumi (34.1° N, 132.8° E) $Pg_2 \sim Sg_2 = 37.3$ sec, $Pb \sim Pg_2 = 6.9$ sec, focal depth = 20 km (b – group).

Pg_2 and Pb denote the direct wave through the granodioritic layer, and the refracted wave at the interface between the granodioritic and basaltic layers.

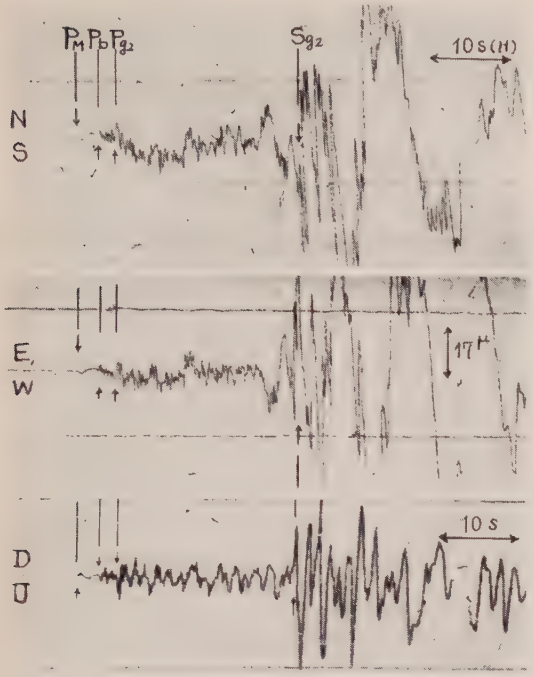

Fig. 2 (c). Wiechert-Seismograms, Jan. 17th 02h 44m, 1947, Tokushima Pref. (33.8° N, 134.2° E), $Pg_2 \sim Sg_2 = 19.7$ sec, $P_M \sim Pg_2 = 4.7$ sec, $Pb \sim Pg_2 = 2.2$ sec, focal depth $\cong$ 10 km (c–group).

Pg_2, Pb and P_M denote the direct wave through the granodioritic layer, the refracted wave at the interface between the granodioritic and basaltic layers and the refracted wave at the Mohorovičić discontinuity, respectively.

the arrival of the forerunner and that of the direct wave) of the forerunner was efficiently supplemented by an analysis of the usual travel time-distance curve, the transformed wave, and other available data. In the following the research procedure and obtained results in the present investigation will be briefly described.

The location of the epicenters of natural earthquakes and some examples of the seismograms used in the present analysis are shown in Fig. 1 and 2 respectively. In Fig. 3 the arrival time differences between forerunners and direct waves of the earthquakes observed at the Kamigamo Geophysical Observatory are plotted taking the P ~ S time as abscissa and value of duration as ordinate. As seen in Fig. 3 these durations are conveniently classified into several groups named the a-, b-, c-, d- and e- group with regard to

Layer	Vp km/sec	Vs km/sec	Thickness km	Remarks
Sedimentary layer	3.8±0.1	2.2±0.2	1.5±0.3	under Kyoto
Granitic layer	5.4±0.1	3.1±0.2	6 ±2	under the area within 200 km distance from Kyoto
Granodioritic layer ..	5.8±0.1	3.4±0.2	14 ±2	»
Basaltic layer	7.0±0.1	4.0±0.2	10 ±2	under Kyoto
Mantle surface ...	8.1±0.1	4.7±0.2	—	probably under whole area in Japan

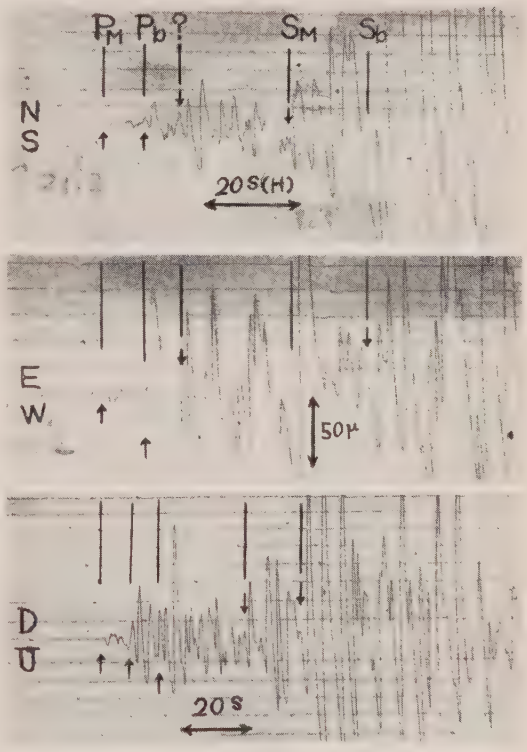

Fig. 2 (d). Wiechert-Seismograms, July 18th 07h 36m, 1954, near Choshi (35.5° N, 141.1° E), $Pb \sim Sb = 50.5$ sec, $P_M \sim Pb = 9.0$ sec, $Pb \sim ? = 8.4$ sec, focal depth $\cong$ 40 km (d-group).

Pb and P_M denote the direct wave through the basaltic layer and the refracted wave at the Mohorovičić discontinuity.

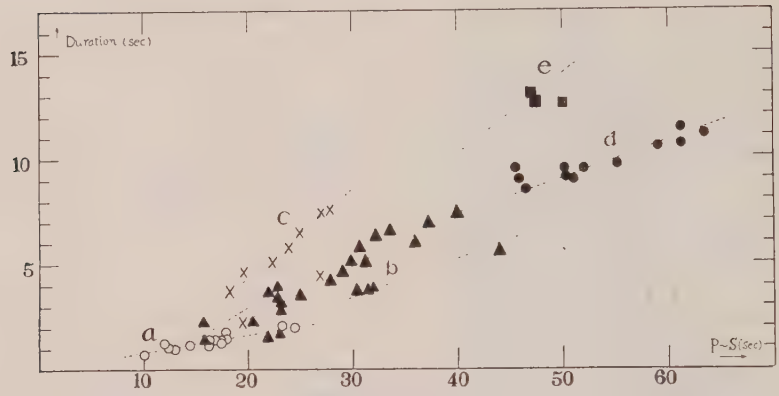

Fig. 3. Relation between the duration of forerunners and the $P \sim S$ time for each group.

the locality, distance of their epicenters seen from the Kamigamo Geophysical Observatory, and moreover duration value observed at Kamigamo. From the analytical treatment on the a-, b- and c-group and some other methods, the crustal structure around Kyoto which was most plausibly determined to fit the observed values of forerunner duration is as follows (KISHIMOTO, 1954, 1955):

However in the above table the propagation velocities of seismic dilatational wave (Vp) and shear wave (Vs) in the sedimentary and granitic layers have been determined from the travel time-distance curves of several selected earthquakes whose epicenters and focal depths were precisely known. The value of velocity for the granodioritic and the deeper layers and all values for the layer thickness except that of basaltic layer were determined from the analysis of duration of forerunner. It ought to be mentioned, particularly in this place, that any method but that of forerunner analysis might perhaps have failed to separate two layers slightly different from one another as those of the granitic and granodioritic layers, because the appearance and number of kind of forerunner (as seen in (a) and (c) of Fig. 2) in the seismograms are the most sensible and unmistakable evidence for existence of any one or two discontinuities under the focal point of earthquake concerned.

3. Results

With regard to the problem of focal depths of earthquakes concerned, all the earthquake foci in the a-group were ascertained in the granitic layer and those in the b- and c-group were estimated to be mainly in the granodioritic layer. But the c-group should clearly be distinguished from the b-group in the point of forerunner duration. The forerunners observed in the seismograms of the b-group may plausibly be explained as refracted waves propagated along the interface between the granodioritic and basaltic layers, but, on the contrary, the forerunners in the c-group could not otherwise be interpreted as the refracted waves along the interface (the Mohorovičić discontinuity) between the basaltic layer and the mantle surface in the point o forerunner duration. Really the distinct appearance of the second forerunner is clearly observed shortly after the first arrival of forerunner in some earthquakes of the c-group, as seen in (c) of Fig. 2, and it may correctly be attributed to the refracted wave along the interface between the granodioritic and basaltic layers, judging from the fact that its duration is precisely plotted on the curve of the b-group as shown in Fig. 3. Then from what causes might be derived the definite difference between the b- and c-groups? Namely, why could not the corresponding forerunner to that of the c-group be observed in the b-group? These can only be explained by the fact that the thickness of the granodioritic layer everywhere under the area within some 200 km distance from Kyoto is nearly the same, but that the thickness of the basaltic layer is considerably different under the area of the c-group earthquakes from that under other areas. Actually the forerunners

along the Mohorovičić discontinuity are clearly observed of the earthquakes in the area of the b-group at the observatories over some 300 km away from the epicenter (KISHIMOTO, 1954, 1955).

4. Local Character of Crustal Thickness

In this way the regional difference in the depth of the Mohorovičić discontinuity or the thickness of the crust might easily and unmistakably be detected by the comparison of duration of earthquake forerunners in one area with that in another area. But this method is invalid for the determination of the absolute value of the crustal thickness under any area, and it should be supplemented by an analysis of the reflected waves of the shallow earthquakes and artificial explosions, or the transformed waves in deep earthquakes occurring under the area concerned. A study of the regional differences in the crustal structure by the analysis of the reflected and transformed waves under various areas in Japan is now in progress and the detailed report will soon be published.

In the present paper an analysis of the transformed waves was tentatively applied for the purpose of determining the crustal thickness under Kyoto. Namely, by the analysis of transformed waves of two similar earthquakes whose focal depths and epicentral distances from Kyoto were nearly 70 km and 100 km respectively, the crustal thickness under Kyoto was estimated as nearly 30 km. Taking the crustal thickness under Kyoto as 30 km, the values of crustal thickness for the respective Districts are schematically obtained as in Fig. 4, under an assumption of a monotonous inclination of the crustal thickness between each District and Kyoto. From this Figure, the crustal thickness may be supposed to vary greatly from place to place in our country, the range of thickness being roughly estimated as from 25 km to 50 km.

5. Focal Depth and Crustal Thickness

It is an attractive problem to examine the relation, if existing, between the focal depths of earthquakes in any area and the crustal thickness under the area concerned. In Fig. 5 the frequency curve of the occurrence of earthquakes having occurred in the last ten years in two areas of the Nankaido District (the c-group) and the Kanto District (the d-group) are plotted according to their focal depths. The difference between the focal depths of maximum occurrence in both areas (20 km and 40 km) corresponds fairly well to that between the estimated crustal thicknesses (25 km and 50 km) under both areas, as seen in the Figure. Roughly speaking, earthquakes in any area are liable to occur at positions a little above the crustal bottom under the area concerned.

6. Conclusion

In conclusion the present article is a report on an attempt to introduce into the research field a method of analysing the forerunner duration appearing in seismograms for in-

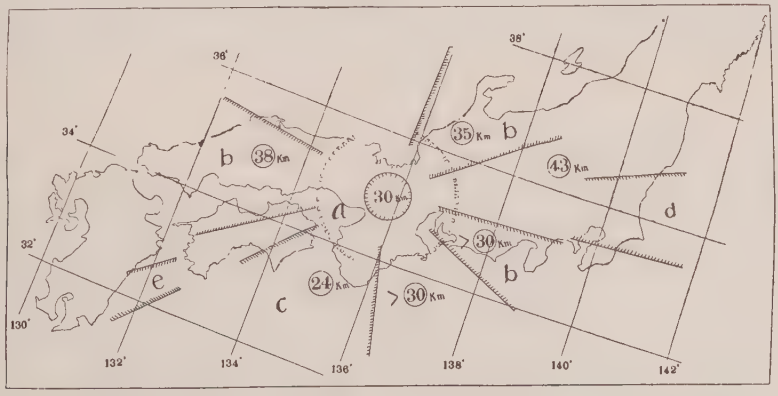

Fig. 4. Schematical representation of the crustal thickness in the various districts.

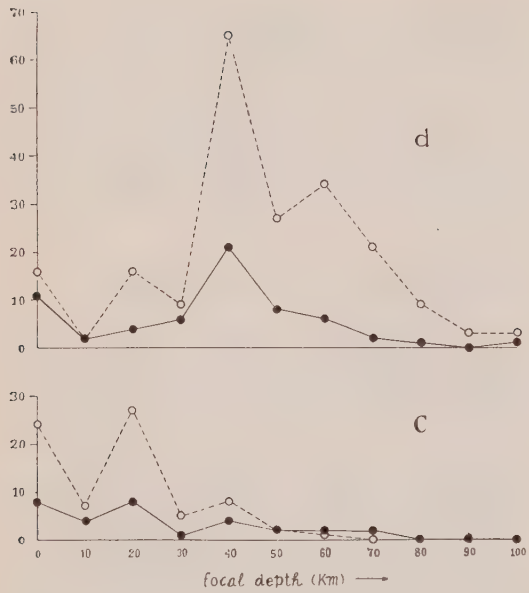

Fig. 5. Relation between frequency of earthquake occurrence and their focal depths in the *c*- and *d*-districts. Dots and circles denote the earthquakes during the last ten years sensible by human feeling at $\triangle > 200$ km and at 200 km $> \triangle \geq$ 100 km, respectively.

vestigating the structure of the earth's crust, especially in heterogeneous distribution. The remarkable regional differences of the crustal thickness roughly estimated in the present investigation are considered to be well in accordance with the heterogeneous distribution of the Mohorovičić discontinuity in U.S.A. observed with the reflected wave of artificial explosion by Tuve, Tatel and Hart (1954), and on the other hand with the anomalous distribution of gravity in our country surveyed by Tsuboi (1954). The synthetic research of various methods of analysing the time-distance curve, forerunner duration, the reflected and transformed waves and other seismometric methods, combined with the gravity and magnetic survey is strongly recommended to be put in operation at many places in the world, as, in case of the Canadian Shield (1950), to classify the local character of the crustal structure. It certainly serves the development of our knowledge on the nature of earthquakes, crustal deformation and many other geophysical phenomena of great importance.

REFERENCES

Kishimoto, Y., 1954: Seismometric Investigation of the Earth's Interior, Part I. *Mem. Coll. Science, Univ. of Kyoto*, Ser. A, **27**, no. 2, pp. 125—143.

— 1955: Ditto, Part II, **27**, no. 3, pp. 243—288.

Tsuboi, C., 1954: Gravity survey along the lines of precise levels throughout Japan by means of a Worden Gravimeter, Part IV. Map of Bouguer anomaly distribution in Japan based on approximately 4,500 measurements. *Bull. Earthq. Res. Inst.*, Supplementary Vol. IV, Part III.

Tuve, M. A., Tatel, H. E., and Hart, P. J., 1954: Crustal structure from seismic explosion, *Journ. Geophys. Res.*, **59**, pp. 415—422.

Wilson, J. T., 1950: Recent applications of geophysical methods to the study of the Canadian Shield, *Trans. Amer. Geophys. Union*, **31**, pp. 101—114.

On the Maintenance of the Trade Winds

By JOANNE STARR MALKUS, Woods Hole Oceanographic Institution[1]

(Manuscript received February 20, revised April 16, 1956)

Abstract

A relation between the large-scale features of the lower trade stream and the effects of small-scale convective motions is investigated. The small-scale processes impose constraints upon the over-all circulation through non-adiabatic heating and the production of shearing stresses. These constraints may be formulated in terms of a theoretical model describing the mean flow in a section along the northern portion of the Pacific trade, which has previously been studied observationally in some detail.

In a simplified frictionless model with non-adiabatic heating the flow exhibits qualitatively many of the important features of the trades, such as subsidence, and a downstream acceleration, increased vertical wind shear, and pressure drop. The motion and pressure fields become numerically related to the heating as observed, however, only upon the introduction of frictional stresses. It is found possible to describe the frictional stress distribution in the lower trades without resorting to direct measurements, which thus provide a later independent check of the model.

The last sections of the paper consider possible quasi-steady rearrangements between the fields of motion, heating, and stress which might be regarded as steps in the slow fluctuations of the system about its average condition. This is done to inquire whether changes in any one of these properties will produce readjustments in the others acting to restore the mean or to accelerate the departure from it. Although such an analysis is handicapped by lack of knowledge concerning the interaction between the heating and stress distributions, one sample calculation suggests that a reduction of heating acts to relieve the subsidence and might thus be expected to restore the convection and thereby the heating. A stable coupling between small- and large-scale motions in the low-level trades is thus indicated, which may play a role in maintaining the high steadiness of the flow. The fact that the wind steadiness vanishes rapidly above the convective layer is clarified if this model is acceptable.

1. Introduction

As the trade winds flow westward and equatorward they accumulate latent heat in the form of water vapor. This stored energy, when released and exported to distant places plays an important part in creating the temperature gradients which drive the general circulation. In the trades themselves, cumulus convection and convective turbulence below cloud base act as the upward distributors of the moisture, originally supplied to the lowest air by evaporation from the sea. These points were brought out in a budget study of the poleward half of the north-east Pacific trade (Riehl, Yeh, Malkus, and La Seur, 1951), hereafter referred to as I. Energy-wise, and as far as mid-latitudes are concerned, vapor ac-

[1] Contribution No. 827 from the Woods Hole Oceanographic Institution.

cumulation is perhaps the most important function of the trades. Nevertheless, they are also accumulating sensible heat in their low levels, as is evidenced by the increase in potential temperature along the air trajectories. Even in the rather northerly section studied in I, the non-adiabatic warming in the bottom 3 km amounts to 3° C in five days (or 2,500 km horizontal travel) and RIEHL (1956) has recently shown that the consequent sensible heat accumulation amounts to about 25% that of the latent. It will be the purpose of this paper to illustrate the importance of this non-adiabatic heat source in the dynamics of the easterly circulation and to suggest the role played by convection in bringing about and distributing the heating. The concomitant role of convective elements in producing frictional stresses also proves important in constructing a theoretical model of the low-level trades.

In order to set up the primary questions which any theoretical model must attempt to answer, we shall begin by reviewing briefly some of the outstanding features of the low-latitude circulation in the northern hemisphere. Between the equator and about 30° N, the existence of a meridional, Hadley-type circulation cell has been confirmed. The work of PISHAROTY (1955) and others has shown that this cell operates in an energy-producing sense. Their figures show that it not only supplies enough energy to overcome its own losses and drive its own motions, but enough to overcome the net energy consumption in the westerlies. Their calculations provide evidence that large amounts of sensible heat and a significant quantity of kinetic energy are exported northward at high levels across latitude 35°. This "driving" cell differs from the other large branches of the general circulation in exhibiting far greater steadiness and relative freedom from travelling disturbances, particularly in the lower and more northerly portions. Its low-level winds, the northeast trades, are in fact the world's most constant wind system, exhibiting steadiness coefficients of 80—90%. The easterlies generally weaken at upper levels and their steadiness gives way to marked fluctuations aloft. The field of vertical motion is as expected, with subsidence in the poleward portions, giving way to ascent as latitude 15° is passed. North of 15°, interaction between the subsidence and counterworking convection from below produces the striking vertically-layered structure which is one of the outstanding features of tropical meteorology. The lower, convection-dominated layer is moist, only slightly stable statically, and contains disturbances of small horizontal scale (from eddies through trade cumuli to convection cells) possessing marked vertical motions. The upper layer is dry, more stable, and contains disturbances of synoptic scale (such as easterly waves) possessing much smaller vertical motions. The upper limit of the convection constitutes the boundary region; it is normally a few hundred meters in thickness, much more stable than either layer, and is called the "trade inversion".

Only that portion of the poleward branch of the Hadley cell will be treated here which was examined in I. That cross section covered a horizontal distance of 2,500 km along the mean summer trajectory of the Pacific trade from 32° N 136° W to Honolulu, Hawaii (21° N 158° W). Vertically, it extended from the sea surface to 3 km, including thus the bottom convective layer, the transition region, and the lowest part of the upper dry layer. By this restricted choice we hope to have selected a simple enough situation, and one covered by sufficient observational material,

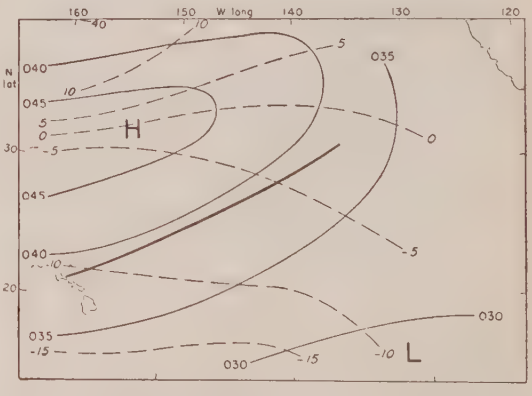

Fig. 1. Map showing orientation of trade-wind section studies. Four sounding stations were spaced out along the heavy solid line, which closely follows the air trajectory for the lowest 3 km. The Hawaiian Islands are shown at the downwind termination, while the U.S. west coast appears in the upper right-hand corner. The lighter solid lines are mean 700 mb contours (10's ft, first digit omitted) while the dashed lines are isopleths of gradient wind speed (m/sec, positive values have component toward east) and thus parallel the sea-level isobars. (After RIEHL et al., 1951.)

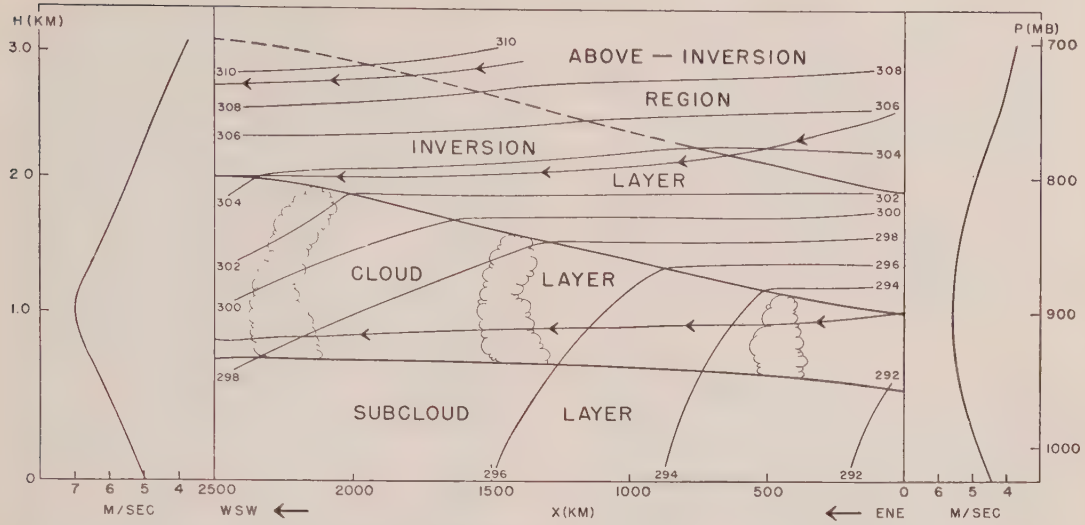

Fig. 2. Vertical structure of the air along the trajectory indicated in Fig. 1. Horizontal distance given in km downstream of entrance end. Vertical coordinate to right in mb, to left in km (approximate). The heavy lines separate the layers described in text. The lines with arrows are trajectories while the lighter solid lines are potential temperature isopleths labelled in degrees absolute. Trade cumulus clouds are entered schematically. To the right is the profile of wind speed (along the section) at the upstream end and to the left is the wind speed profile at the downstream end. Wind speeds are in m/sec.

to frame and test a theoretical model relating several of the predominant processes. To be specific, we shall inquire how the heating, the motions, and the pressure field are related within this section. These relations may in turn provide some clue concerning how this part of the Hadley cell manages to exhibit the structure and perform the transports which the observations tell us that it does. The procedure will be as follows: we shall examine what must happen within such a section to an air-stream which has given properties upon entrance so that it comes out the other end changed in the observed manner. Most importantly, we shall relate the vertical motions to the heating and in so doing demonstrate that the latter is vitally necessary for this portion of the Hadley cell to show subsidence.

In the treatment of a limited section of a larger-scale circulation branch, some features of the over-all flow must be introduced as assumptions. We wish to find out how these over-all features are constrained by the processes going on within this section.

Figures 1—3 summarize the structure of the section, derived from the observations and analyses of I. Those properties which must eventually be related or predicted in a complete theoretical treatment are:

1. The nearly two-dimensional character of the flow. The curvature of the trajectory is not large, and the results of I strongly suggest that the cross-stream divergence is considerably smaller than the downstream divergence.

2. The vertically-layered stability structure. The static stability is close to neutral in the moist layer (nearly dry adiabatic below cloud base and close to moist adiabatic in the cloud layer) with strongest stability in the inversion region, decreasing again above but still positive.

3. The presence of non-adiabatic heating, indicated by the crossing of the parcel trajectories toward higher potential temperature.

4. Downstream increase of east wind speed at all levels below 3 km, with the greatest increase at about 1 km. A vertical profile showing maximum east wind just above cloud base, decreasing upwards and downwards.

5. Subsidence throughout the section, of the order of magnitude of 50 m/day.

6. Extreme wind steadiness in the low levels, decreasing markedly above the cloud tops. Weakness or absence of synoptic disturbances in the summer months. Unlike the westerlies,

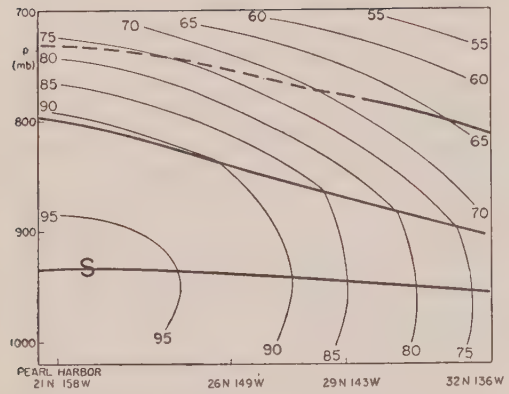

Fig. 3. Vertical cross section of wind steadiness (percent, as defined in I) for the section of Figs. 1 and 2. Heavy lines denote the layers, as in Fig. 2. The vertical coordinate is pressure in mb and the latitude and longitude of the sounding points appear along the bottom. (After RIEHL et al., 1951.)

these can play no role in the maintenance of the flow.

7. A downstream drop in pressure of nearly 5 mb at the ground diminishing upward and disappearing entirely at 3 km. Relative to the trajectory (looking downstream) a counterclockwise rotation of the isobars with height, until they become parallel near the section top. This is another feature of the trades which distinguishes them sharply from the westerlies of middle latitudes.

The problem faced in this paper will be to relate as many as possible of these features theoretically using the hydrodynamic equations. In such a limited treatment as undertaken here, however, it will prove necessary to introduce the first two of the listed properties by assumption and the third, namely the non-adiabatic heating, by "plugging in" observed values. This will result in an overspecified situation, rendering superfluous one equation of motion. The key assumption of the work is probably that of two-dimensional motion, without which the problem would not be soluble. The observations in I, however, provide justification for this limited portion of the atmosphere. The extreme wind steadiness and relatively straight trajectory suggest that the divergence component parallel to the mean motion is very close to the total divergence. This hypothesis was tested in I when the mean vertical motion was computed from this component of the divergence and used satisfactorily in balancing the momentum and water vapor budgets. Estimations of the cross stream divergence (from the slight downstream fanning of trajectories) are in the same sense and about 10 % of the magnitude of the downstream divergence up to the level of the trade inversion, above which it may increase markedly. The reason, if any, for the nearly two-dimensional character of the lower trades must await more fundamental global treatments. Nevertheless, certain important aspects of their structure may be clarified using the restricted approach to be outlined. The types of questions we may hope to shed light upon include the following:

What is the role of the non-adiabatic heating in the dynamics and the thermodynamics of the section? What part do the clouds and smaller-scale turbulent elements play in releasing and distributing the heat? Is the heating vital in maintaining the flow against friction and in accelerating it downstream? Is it purely coincidental that the wind steadiness drops off so rapidly just above the cloud tops and coincidental that the maximum easterly wind is normally observed near cloud base? These questions may be combined in the following one which is tractable to theoretical analysis, namely: Does the heating produced by small-scale convection affect or constrain the larger-scale motions, and if so, is this a stable coupling? For example, if the convection is suppressed will the resulting changes in the large-scale motions be such as to restore it (i.e. perhaps weaken the subsidence rather than strengthen it)?

II. The Premises of the Theory

We are now going to set up a theoretical model for the two-dimensional mean flow in such a section, using the equations of motion, state, continuity, and the first law of thermodynamics containing non-adiabatic heating. Since the velocities solved for occur on a much larger space and time scale than those hypothesized to be responsible for the heating, the latter may, to first order, be introduced as a function of the coordinates only. The fact that the motions in the atmosphere ultimately regulate its heat sources and sinks is of course recognized (MALKUS, 1955 a) and the inter-

action between motion and sources in maintaining the steadiness of the flow will be considered later. We will first show that the heating is necessary to specify the motion field in the average or steady-state condition. To get the observed motion field and pressure drop downstream related correctly to the observed values of the heating, it will also be necessary to include frictional stresses, as will be seen.

Of course, the necessity for subsidence in a broad, equatorward-flowing stream is obvious from other considerations. If the relative vorticity is small compared to the Coriolis parameter, potential vorticity conservation requires descent. But the rate of descent is not prescribed until the exact trajectory and rate of equatorward flow are known. That is to say, the constraint imposed by the requirement of potential vorticity conservation is not sufficient uniquely to determine the motions: we could, in fact, have an infinite number of equatorward trajectories all obeying it. The law of potential vorticity conservation is derived from combining the first two equations of motion and the equation of continuity. There is another constraint, to be derived here, essentially between the first and third equations of motion and the first law of thermodynamics, which will require a specified distribution of subsidence for a given distribution of heating. In other words, for the air to select between the infinite number of equatorward trajectories, each conserving potential vorticity, it is required to prescribe the relation between heating and vertical motion. *The air must pick an equatorward trajectory such that the heating is adequate to give the subsidence which potential vorticity conservation requires for that particular trajectory.* This conclusion is only quantitatively modified by the presence of friction, which in practice merely intensifies the amount of heating required.

To solve the problem in a truly general and complete manner, all these constraints should be applied to the air at once, without specifying the trajectory; and the trajectory, the steady condition, the two-dimensionality, pressure drop, wind-maximum, and so forth should all be derivable. The writer believes that this is beyond tractable analytical methods, at least at present, and that an experimental or numerical attack like that of PHILLIPS (1956) offers the best hope. The present, simple-minded approach may guide such future endeavors.

Here we shall treat the air flow along the *observed* trajectory of Figure 1, which we know from measurement obeys the vorticity conservation law. We shall relate the heating and motion field therein, to see if by assuming the first from observation we can construct a model giving the second. Thus the latitude does not enter explicitly as it would in a more general formulation, but only implicitly via the choice of coordinate axes.

III. The Frictionless Model

When the coordinates are chosen such that the x-axis points downstream along the surface trajectory (the trajectory rotates negligibly with height up to the top of the layer considered), the y-direction points cross stream, and the z-direction upward to form a right-handed system, the hydrodynamic equations of motion, continuity, and state for steady, two-dimensional flow on a rotating system are

$$u\frac{\partial u}{\partial x}+w\frac{\partial u}{\partial z}-fv=-\frac{1}{\varrho}\frac{\partial p}{\partial x} \tag{1}$$

$$u\frac{\partial w}{\partial x}+w\frac{\partial w}{\partial z}=-\frac{1}{\varrho}\frac{\partial p}{\partial z}-g \tag{2}$$

$$\frac{\partial u}{\partial x}+\frac{\partial w}{\partial z}=-\frac{1}{\varrho}\frac{d\varrho}{dt} \tag{3}$$

$$p=\varrho RT \tag{4}$$

where the symbols all have their conventional meanings. The non-adiabatic heating, V, in cal/gm sec, may be evaluated as follows:

$$\frac{V(x,z)}{c_p}\cong\frac{d\Theta}{dt} \tag{5}$$

where c_p is the specific heat of air at constant pressure and Θ is the potential temperature. Since the velocities appearing here to be solved for are steady or average values, the mean cross-trajectory velocity v is by definition zero and the Coriolis term in (1) drops out. A Coriolis term would remain in the y-equation of motion, which is, however, not needed because of the number of assumptions and parameters such as V specified from observations. The test of the presently derived results

will be their agreement with the observed flow, which patently obeys the second equation of motion and the implied latitudinal relations.

Three final simplifications are made. The first is that of hydrostatic equilibrium, which is surely well approximated for motions of the scale considered. The second is the omission of the $1/\varrho \; d\varrho/dt$ term from the equation of continuity, which has been justified in detail by other writers on the steady-state heating problem (MALKUS and STERN, 1953; SMITH, 1955). The third permits linearization of the equations in this particular situation. This is done by noting that the changes in air properties within the section are small compared with the initial values at the entrance end, and in particular the horizontal windspeed, u, changes by only a fraction of itself (at most about 25 %) in the distance of travel considered. It will be assumed that a uniform wind u of 5 m/sec enters the section at the upstream end and that $u'(x, z)$ is the increment within the section. The other variables are similarly broken down into barred quantities referring to the properties of the current at the entrance end and primed quantities referring to the changes occurring within. The vertical velocity is of the magnitude of a primed quantity, being related to u' through the continuity equation. It can be proved[1] that linearization is not vital to the results presented and that these would be nearly identical were this simplification not made, and qualitatively the same for far longer sections where linearization is clearly not justified. The simplest mathematics is used here which brings out the essentials; more formality is not justified in view of the physical restrictions. With the approximations introduced, equations (1) – (4) become

$$\bar{u}\frac{\partial u'}{\partial x} = -\frac{1}{\bar{\varrho}}\frac{\partial p'}{\partial x} \tag{1 a}$$

$$-\frac{1}{\bar{\varrho}}\frac{\partial p'}{\partial z} = \frac{\varrho'}{\bar{\varrho}}g \tag{2 a}$$

$$\frac{\partial u'}{\partial x} + \frac{\partial w'}{\partial z} = 0 \tag{3 a}$$

$$\frac{\varrho'}{\bar{\varrho}} = -\frac{T'}{\bar{T}} \tag{4 a}$$

An additional small term has been left out of equation (4 a). This omission has also been justified in previous work on non-adiabatic heating (STERN, 1954) and its inclusion here gives results so little different from those actually shown that present-day observations could not test the difference.

The heating function V may now be related to the motion and temperature fields through the first law of thermodynamics, as follows:

$$\frac{V}{c_p} = \bar{u}\frac{\partial T'}{\partial x} + w'(\Gamma - \gamma) \tag{5 a}$$

where Γ is the adiabatic lapse rate and γ is the actual (average) lapse rate at the entrance end of the section. Elimination of all other dependent variables is now readily achieved and we obtain a simple differential equation for w', namely

$$\frac{d^2w'}{dz^2} + \frac{gs}{\bar{u}^2}w' = \frac{gV}{c_p\bar{u}^2\bar{T}} \tag{6}$$

where s is $(\Gamma - \gamma)/\bar{T}$, the (average) stability at the upstream end. Since the observations show that $d\Theta/dt$ (and hence V) is very nearly independent of x along this section, the height derivative of w' may be written thus as a total derivative. It is readily shown that under conditions where hydrostatic equilibrium is realized, x-variations in w' would follow any x-variations in V exactly as prescribed by the solutions to this equation.

The heating function is evaluated using Figure 4, which was calculated from the observations of I. It shows the height distribution of the downstream rise in potential temperature along the parcel trajectories, which is readily converted into the individual rate of warming. The z-dependence of V is fairly well approximated by an exponential decay, where $V = V_0e^{-z/h}$ and $h = 1.5$ km. It can be approximated to any higher desired degree of accuracy by a combination of exponential and sinusoidal functions. This was done, with so little difference in result that the added complexity did not justify the labor. If we use the simplest exponential, the differential equation becomes

[1] This has been demonstrated by Melvin Stern, to whom the writer is grateful for many helpful discussions. The formal proof will appear in Stern's Ph. D. dissertation.

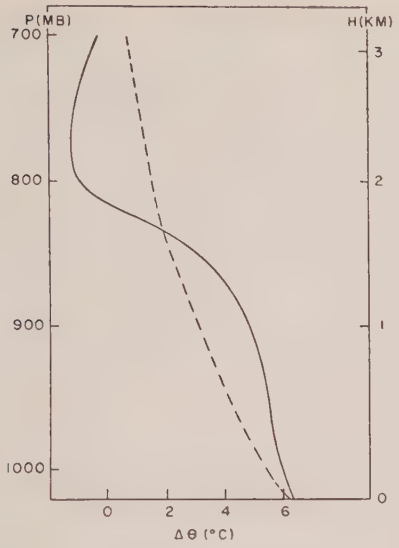

Fig. 4. Graph showing observed net downstream warming, $\triangle\Theta$, of the air parcels, calculated from Fig. 2 as a function of height. Can be converted to the rate of non-adiabatic heating by multiplying by c_p and dividing by the length of time required for the parcels to traverse the section (about 5 days). The potential temperature increment, $\triangle\Theta$, is given in degrees absolute. The dashed curve is the simple exponential function used in the theory to approximate the observed curve.

$$\frac{d^2w'}{dz^2} + B^2w' = Pe^{-z/h} \qquad (6\,a)$$

where

$$B^2 = \frac{gs}{\overline{u}^2}, \quad P = \frac{gV_0}{c_p\overline{u}^2\overline{T}},$$

and where h is chosen as in Figure 4 to give the correct integrated heating for the layer as a whole and $\overline{T}$ is its mean temperature.

SMITH (1955) has shown that the general solution to this equation for a deep air layer bounded below by the ground is given by the real part of the expression

$$\frac{P}{\frac{1}{h^2} + B^2}\left[e^{-z/h} - e^{-iBz}\right]$$

Since h, P, and B are all real, the general solution to (6 a) is

$$w' = \frac{P}{\frac{1}{h^2} + B^2}\left[e^{-z/h} - \cos Bz\right] \qquad (7)$$

The divergence field is prescribed as

$$-\frac{\partial w'}{\partial z} = \frac{\partial u'}{\partial x} = \frac{P}{\frac{1}{h^2} + B^2}\left[\frac{e^{-z/h}}{h} - B\sin Bz\right] \qquad (8)$$

Since the sine function is zero at the ground, the divergence must always be positive there. This means a downstream acceleration of the surface wind and subsidence in the low levels regardless of the value of B, just so long as the heating is positive and decays with height. Equation (1 a) also shows that the surface pressure must drop downstream. What happens to the motion field at higher levels clearly depends both qualitatively and quantitatively on the stability and wind structure through B. With windspeeds of about 5 m/sec in an atmosphere of very low stability, subsidence occurs through a several km-deep layer. For example, if $B = 0.5 \times 10^{-5}$ cm^{-1}, the vertical distribution of w' in dimensionless units is shown in Table 1.

Since it might appear unrealistic to treat an air layer topped by an inversion as "infinitely" deep, we may alternatively investigate a layer in which the damping effect is simulated by a rigid lid placed somewhat higher than the inversion (this is done because the damping by the inversion is more gradual than that by a rigid surface; the precedents have been discussed by MALKUS and STERN, 1953). The solu-

Table 1. Distribution of Vertical Velocity (Dimensionless) with Height for a Deep Layer of Low Stability

Height → (km)	0.2	0.5	1.0	1.5	2.0	2.5	3.0
$\frac{w'(1/h^2+B^2}{P}$	— .073	— .256	— .365	— .363	— .314	— .125	— .065

tion to (6 a) then contains a sine term with an amplitude about 6 % that of the cosine term and the results shown in Table 1 are imperceptibly altered.

Nevertheless, there are difficulties in applying these results directly to the trade winds. In the first place, the observed magnitude of the heating is much greater than necessary. Evaluating P using Figure 4, we find it to be about 1.7×10^{-10} cm^{-1} sec^{-1}, which would lead to rates of subsidence of 400 m/day! We also find faults in the divergence field, $\partial u'/\partial x$, and wind profile, $\bar{u}+u'$. In this theoretical section, the downstream-end wind profile and the divergence profile must have an exactly similar shape since the wind has a constant profile with elevation at the entrance end. Equation (8) tells us that $\partial u'/\partial x$ must be a maximum at the bottom and that the easterly winds will decrease from there upwards. The observations in I show, to be sure, divergence and wind profiles of similar shape but the maximum in both is well above the surface, at about 900 m. Another problem is that the value of B chosen for Table 1 is probably considerably less than the mean stability of the trade-wind moist layer would permit, if the major portion of the processes in the cloud layer are non-saturated.

The first two of the difficulties suggest that something must be working in opposition to the heat source. Examination of the pressure field provides the clue to what it is and what to do about it. Equation (1 a) tells us that a downstream surface pressure drop of only about 0.05 mb in the 2,500 km is required to produce the observed acceleration of the flow. The observations tell us that a pressure drop of nearly 5 mb in fact occurs. This gradient disappears toward the top of the section at 3 km, along which level the pressure is nearly constant. Using this fact and simple hydrostatic considerations, it is evident that the non-adiabatic heating accounts for 80 % of the observed pressure drop at the bottom surface. Adiabatic compression due to sinking accounts for the remainder of the rise of mean temperature in the layer. It seems that a "frictional drag" has been omitted from equation (1 a) which in practice uses up most of the pressure drop produced by the warming. The fact that the pressure gradient disappears at 3 km, at the top of the heated layer, indicates that the stresses may be provided by the same convective elements responsible for the heating. This suggests a method of introducing frictional stresses into the model, with which the next section will be occupied in detail. Even the present oversimplified analysis, however, illustrates the vital role of non-adiabatic heating in the structure, dynamics, and thermodynamics of the trade system. The refinements of the next section make the predicted numbers agree with measurements and tie some previously unrelated observations to the theory, thus providing independent checks of its plausibility.

IV. Model Including Frictional Stresses

If the frictional forces in the plane of the section are hypothesized to be due to the sea surface drag on the bottom and to vertical exchanges of horizontal momentum by small-scale convective elements within the layer, they may be expressed in terms of a shearing stress τ_{xz}. Equation (1 a) should then be written

$$\bar{u}\frac{\partial u'}{\partial x} = -\frac{1}{\bar{\varrho}}\frac{\partial p'}{\partial x} + \frac{1}{\bar{\varrho}}\frac{\partial \tau_{xz}}{\partial z} \qquad (1\,b)$$

Calculations (by SHEPPARD, 1954) from the observations in I and others made in the trades show that the term $1/\bar{\varrho}\,\partial\tau_{xz}/\partial z$ is of the same order of magnitude as $1/\bar{\varrho}\partial p'/\partial x$ and therefore about two orders of magnitude larger than $\bar{u}\partial u'/\partial x$. With the exception of a negligibly small term in the first law of thermodynamics, the remaining equations used here are unchanged. If the shearing stresses within the layer are produced by the same convective and turbulent elements also responsible for the heating, τ_{xz} and its derivatives may be considered functions of the coordinates only, and the elimination carried out as before. Eventually, of course, the shearing stress must be related to the mean wind profile, and be consistent with it.

After elimination, the modified differential equation for w' becomes

$$\frac{d^2w'}{dz^2} + \frac{gs}{\bar{u}^2}w' = -\frac{gV}{c_p\bar{u}^2\bar{T}} - \frac{1}{\bar{\varrho}\bar{u}}\frac{\partial^2\tau_{xz}}{\partial z^2} \qquad (9)$$

We could now proceed with this equation in the straightforward manner of attempting to evaluate $\partial^2\tau_{xz}/\partial z^2$ from the observations and expressing it in some simple functional form

in the equation, as was done earlier for the heating function V. The results would be little better than guesswork, however, for the following combination of reasons: the best observational evidence to date indicates that the two inhomogeneous terms in (9) are very nearly the same size, and the small difference between them is the actual forcing function remaining to determine w'. Although the height distribution of τ_{xz} itself is fairly well depicted by recent measurements, its first derivative is not so certain, and its second derivative even less reliably specified. Therefore an indirect procedure will be followed which employs two independent calculations. Although each of these carries considerable uncertainty, consistency in the results of the two, if it occurs, would prove persuasive.

V. Two-Layer Model with Friction

It will be recalled that the trade-wind moist layer is itself subdivided vertically into two layers of quite different static stability. The subcloud layer, reaching from the sea up to about 650 m, has an average stability of zero. The cloud layer, although its lapse rate is steeper than moist adiabatic is almost surely stable on the average, since active clouds occupy only 10—20 % of the space. If we suppose that 78 % of the processes occurring within the layer are unsaturated, $gs/\overline{u}^2 = B^2 \cong 2 \cdot 10^{-10}$ cm^{-2}. Applying equation (9) to this two-layer system will prove extremely illuminating. For the lower neutral region it takes the simple form

$$\frac{d^2w'}{dz^2} = \frac{gV}{c_p\overline{u}^2\overline{T}} - \frac{1}{\overline{\varrho u}}\frac{\partial^2\tau_{xz}}{\partial z^2} \qquad (10)$$

The two terms on the right are functions of z only and the left-hand term is related to the divergence through the equation of continuity. The height derivative of the divergence in the subcloud layer may thus be expressed as

$$\frac{d}{dz}\left(\frac{\partial u'}{\partial x}\right) = F_1(z) - F_2(z) = F(z) \qquad (11)$$

where

$$F_1(z) = \frac{1}{\overline{\varrho u}}\frac{\partial^2\tau_{xz}}{\partial z^2} \text{ and } F_2(z) = \frac{gV}{c_p\overline{u}^2\overline{T}}.$$

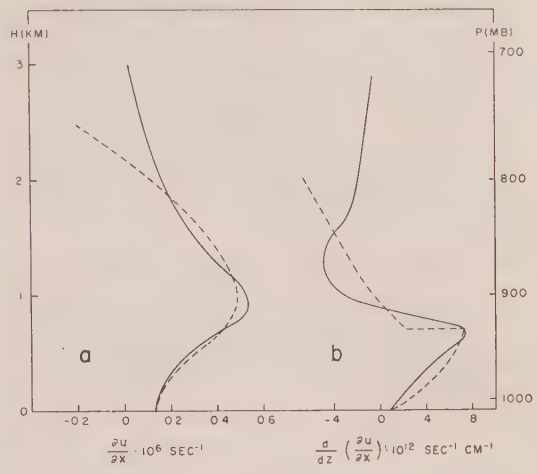

Fig. 5

a. Solid curve is the velocity divergence, $\partial u'/\partial x \cdot 10^6$ sec^{-1}, calculated from the observed wind profiles. It is the component of divergence along the trajectory and averaged over the whole length of the section. The dashed curve is the divergence calculated from the equations of the model.

b. Height derivative of divergence, $d/dz\ (\partial u'/\partial x) \cdot 10^{12}$ sec^{-1} cm^{-1}. The solid curve is calculated from the observed divergence (solid curve in 5a). The dashed curve up to 650 m is constructed (from two exponentials) to fit the observed curve. Its continuation above 650 m is calculated from the results of the model.

Now the observations in I led to a rather good profile of the mean divergence distribution in the section. It was calculated from several wind soundings daily over the four months and was used with consistent results in the previous paper in calculating w' and the transport budgets. This mean divergence profile and its first height derivative are plotted in Figure 5 and will be used here in the following outlined procedures:

(1) Recalling that we know $F_2(z)$ from the heating function, we will establish a functional form of $F(z)$ as a whole from the measurement-calculated profile of $d/dz\ (\partial u'/\partial x)$ in the subcloud layer (that part of the solid curve up to 650 m in Figure 5 b). We will apply the $F(z)$ so obtained to the entire two-layer system via equation (9) written for each layer with appropriate joining boundary conditions. We will solve for w', the divergence field, $d/dz(\partial u'/\partial x)$ above 650 m (not assumed as given), and the pressure field, and compare these with observations.

(2) We will then subtract from the $F(z)$ we took from Figure 5b and used, the $F_2(z)$ evaluated previously from the heating function. This will give a differential equation for τ_{xz}. We may then solve that differential equation and test the results for consistency, both with existing measurements of τ_{xz} in the trades and with the wind profiles.

VI. Solution for the Two-Layer Model

The height derivative of the divergence up to 650 m is well approximated by the dashed curve in Figure 5 b. It is the difference between two exponentials,

$$F(z) = A_1 e^{-z/a_1} - A_2 e^{-z/a_2} \qquad (12)$$

where $A_1 = 1.74 \times 10^{-10}$ cm^{-1} sec^{-1}, $a_1 = 1.715$ km; $A_2 = 1.73 \times 10^{-10}$ cm^{-1} sec^{-1}, $a_2 = 1.5$ km. This expression for $F(z)$ is substituted into equation (9) and the solution is carried out for the two-layered system. The boundary conditions are that w' is zero at the lower surface; that it and its height derivative are continuous at the interface between layers (giving a continuous divergence and wind profile); and that a rigid lid is placed at 4 km. It may be shown that the solution is nearly the same if the upper layer is allowed to be infinitely deep.

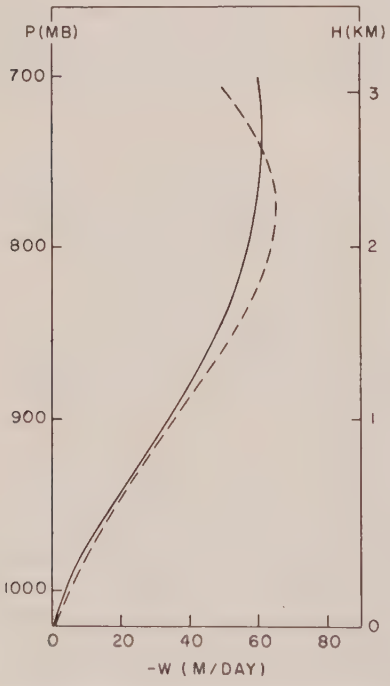

Fig. 6. Solid curve shows mean vertical motions (m/day) as a function of height and pressure calculated from the observed divergence distribution for the section. The dashed curve shows the corresponding vertical motion distribution given by the solution to the differential equation for the two-layer model.

The results for $\partial u'/\partial x$, $d/dz(\partial u'/\partial x)$, and w' are shown and compared with the observations in Figures 5 and 6. On the whole, the agreement is good, although the theoretical divergence shifts over to convergence above 2 km, while the observed curve trails off more slowly. This is believed to be due to the decrease in the two-dimensional character of the flow aloft as the wind steadiness falls off and thus the model begins to break down at higher levels. In practice, an increasing $\partial v'/\partial y$ probably accounts for the difference between the two curves above 2 km. Otherwise, many of the significant aspects of the flow are reproduced and elucidated by the model. Reserving discussion of the pressure field for the section below on shearing stresses, we can now call attention to some important features of the velocity structure: in particular the wind maximum and its location in the vertical.

Rewriting equation (9) in combination with (11), we have

$$\frac{d}{dz}\left(\frac{\partial u'}{\partial x}\right) = F(z) + \frac{gs}{\bar{u}^2} w' \qquad (13)$$

In the subcloud layer $s \cong 0$, $F(z)$ is positive, and the divergence increases rapidly upward. As the cloud base is reached stabilization rather suddenly occurs. The vertical velocity is negative and so a large term abruptly appears on the right to be subtracted from $F(z)$ which at this level is changing only very slowly with elevation. This means that the divergence must start decreasing upward instead of continuing to increase. This point is brought out clearly in Figure 5 b which shows $d/dz(\partial u'/\partial x)$ calculated from the observational curve of Figure 5 a, compared with $d/dz(\partial u'/\partial x)$ computed from the model. The sharp "knee" in the observationally-deduced curve is strikingly reproduced by the theory. It would seem that the average appearance of the trade-wind maximum near cloud base is no coincidence and, barring large changes in the forcing function,

$F(z)$, it would be tied there, at the level where the static stability rather suddenly becomes positive.

The latter conclusion is not sensitive to small changes in the amplitude and exact height dependence of $F(z)$ as a whole. The lower part of the solid curve in Figure 5 b may be approximated by other functions and the main features of the flow field, such as subsidence and wind maximum, derived within the same observational accuracy. The chosen $F(z)$, however, is composed of two subtractive terms and small changes in each individually lead to rather large alterations in their difference. An example is illustrated in Section X, following a discussion relating the components of $F(z)$ to physical processes.

VII. The Distribution of Shearing Stress

The total forcing function $F(z)$ for the differential equation (9) was seen earlier to be physically related to the heating and shearing stresses as follows

$$F(z) = F_1(z) - F_2(z) = \frac{1}{\bar{\varrho}\,\bar{u}} \frac{\partial^2 \tau_{xz}}{\partial z^2} - \frac{gV}{c_p \bar{u}^2 \bar{T}} \quad (14)$$

In solving the differential equation for w', however, this relation was temporarily ignored and a functional form of $F(z)$ was deduced from observations independent of the above. It was found to be well represented by the difference between two exponentials, as written out in equation (12). The second of these exponentials $A_2 e^{-z/a_2}$ is within computational accuracy the same as the heating term $Pe^{-z/h}$ of equation (6 a) evaluated previously in section III. Thus when we make the association between $gV/c_p \bar{u}^2 \bar{T}$ in (14) with the $A_2 e^{-z/a_2}$ in (12), (14) becomes a differential equation for τ_{xz}, namely

$$F_1(z) = \frac{1}{\bar{\varrho}\,\bar{u}} \frac{\partial^2 \tau_{xz}}{\partial z^2} = A_1 e^{-z/a_1} =$$

$$= 1.74 \cdot 10^{-10}\, e^{-z/1.715} \quad (15)$$

Since $\bar{\varrho}$ varies rather little percentually through the height of the section, in most cases integration of this equation may be approximated by two simple quadratures. Two boundary conditions on τ_{xz} are, however, required. We will assume here that the shearing stress (or vertical transport of horizontal momentum) is zero

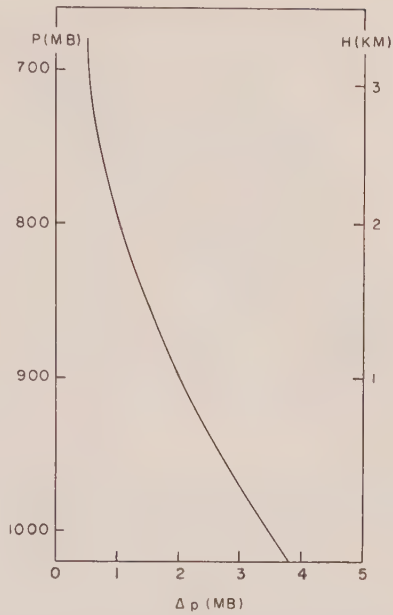

Fig. 7. Theoretical height distribution of downstream pressure drop, $\triangle p$, in mb. $\triangle p$ is the difference between the pressure at the upstream end and that at the downstream end, or over a horizontal distance of 2 500 km along the flow. Observations show a surface pressure drop of just under 5 mb and little or no pressure drop at 3 km (see Fig. 1).

at the height of the trade-wind maximum, a premise well justified by the work of SHEPPARD, CHARNOCK, and FRANCIS (1956), and we will take a value of $\tau_{xz} = 1.0$ dyne/cm^2 at the lower boundary. The latter is consistent with the values used in I for the drag of the sea surface on the lowest air. Under these conditions, τ_{xz}, the shearing stress, and $1/\bar{\varrho}\ \partial\tau_{xz}/\partial z$, the frictional force per unit mass are specified as functions of height. Introducing the latter into equation (1 b) the downstream pressure gradient is also determined. The results are given in Table 2 and Figure 7.

The next-to-last column tests the shearing stress by comparing it to the mean (observed) wind profile. It gives the eddy momentum exchange coefficient, defined as the ratio between the calculated shearing stress and the wind shear at the level considered. Beside it in the last column is shown the eddy coefficient which was required in I to balance the momentum budget. The agreement is within observational and computational error. The results in the two middle columns are also

Table 2. The Stress Distribution and Its Consequences

Height	Calculated τ_{xz}	Calculated $\partial\tau_{xz}/\partial z$	$\Delta p = p_{\text{upstream}} - p_{\text{downstream}}$	μ(from τ_{calc} and du/dz)	μ from momentum budget
m	dyne/cm²	dyne/cm² per 100 m	mb	c.g.s.	c.g.s.
0	1.0	— .149	3.8	330	
500	0.4	— .111	2.8	270	370
900	0	— .088	2.2	indeterminate	
1,500	— 0.4	— .062	1.5	330	630
2,000	— 0.7	— .046	1.1	700	680
2,500	— 0.9	— .035	0.8	600	
3,000	— 1.1	— .026	0.6	700	570

close to observational accuracy. The height derivative of shearing stress, $\partial\tau_{xz}/\partial z$, has a distribution similar to that described by SHEPPARD (1954). It falls off with height in a manner consistent with the hypothesis that the frictional drag is brought about by the same processes which distribute the heating. Due to the small contribution of $\bar{u}\ \partial u'/\partial x$ in equation (1 b), the downstream pressure drop is to all intents and purposes proportional to $\partial\tau_{xz}/\partial z$. It also decays exponentially and has nearly vanished at 3 km.

Although the model says nothing explicitly about the cross-stream pressure gradient (which is given by the y-equation of motion), the disappearance of the large downstream pressure gradient toward the top of the section means that the isobars are rotating with height into parallel orientation with the air trajectory, as observed. This conclusion has been arrived at without any *a priori* assumptions concerning the pressure field or of any simple relation between it and the wind field.

VIII. The Relation between Heating, Shearing Stress, and Convection

So far in this paper the relation between the small scales of motion in the trades and the heating and friction distributions has only been stated as an hypothesis. In the case of the shearing stresses, the hypothesis has received recent observational test in the western Atlantic trade-wind region (SHEPPARD, CHARNOCK, and FRANCIS, 1956; BUNKER, 1955). The shearing stresses contributed by turbulent and convective motions ranging in size from small eddies up to convection cells (10—50 km across) have been obtained and compared with mean wind profiles and the total stresses calculated therefrom. The agreement is sufficiently good to conclude that in the low-level easterlies the vertical transport of horizontal momentum is mainly achieved by scales of motion not larger than convection cells. The percentage contributed by the larger-scale systems apparently becomes greater with height, perhaps discontinuously rapidly through the trade inversion. The increased role played by synoptic systems (present in the trades with less regularity than smaller convective motions) in maintaining the momentum transports aloft may be related to the upward diminution of wind steadiness, as will become clearer in Sections IX—XI.

The production of the heating function V is somewhat more complex. The downstream rise in potential temperature represents a small net difference between opposing processes. Radiation is a heat sink throughout the free atmosphere. In the subcloud layer, the net warming is due to a slight excess of eddy flux convergence over outgoing radiation. In the cloud layer, although the potential temperature increases strongly upward, the direction of the eddy heat flux is not definitely known. In any case it probably plays a small role in the heat balance, which the evidence in I indicates is primarily achieved between a large precipitation source and radiation sink. Connecting the net warming throughout the moist layer to convective processes, therefore, implicitly assumes that the radiational heat sink varies relatively little.

IX. Fluctuations about the Steady State

The pronounced steadiness of the flow has been emphasized as one of the significant features of the trades. The over-all dynamic stability of a Hadley-type meridional cell in the low latitudes of a heated rotating system has been suggested by experimental (FULTZ, 1949) and theoretical (KUO, 1954) investigations of simplified planetary analogs. The present treatment of a limited portion of the real Hadley cell proposes consideration of another kind of stability, which may not be unrelated. The results of the preceding sections indicate a coupling between the small-scale motions occurring within a section along the easterlies and the modifications in the large-scale flow observed between the upstream and downstream ends. It has been shown that the transports effected by the small-scale systems impose a constraint upon the large-scale flow, or alternatively, that the large-scale flow must adjust itself to permit the development of those small scales which transport heat and momentum in the manner indirectly specified here. The response of either scale of motion to an alteration in the other is significant in determining the nature and amplitude of the system's fluctuations about its average condition. In the westerlies, disturbances of certain critical sizes are able, by drawing on stored energy, not only to grow in a self-accelerative fashion, but in so doing often to upset the entire structure of the flow, which thereby fluctuates so widely that an average picture has only very restricted meaning as a "steady state". In the easterlies, by contrast, the average and the daily picture bear a closer resemblance to one another. The infrequency of intense disturbances in the low-level trades, and the reliable presence of trade cumulus clouds suggests that the coupling between small- and large-scale processes is stable and perhaps contributes to the over-all dynamic stability of the meridional circulation.

In the framework of the present model, therefore, we might inquire what happens, for example, if the heating is weakened, presumably through a diminution of convective activity. A stable coupling of the type suggested would be substantiated if we could show that a weakening of the heat source would lead to decreased subsidence. It is well known that subsidence in the trades is one of the most effective brakes upon convection, and even a slight release of this brake would lead to renewed outbreaks of convective activity.

Any such approach, however, patently represents a drastic oversimplification, and its mathematical formulation must be preceded by several reservations. The present theoretical treatment cannot be interpreted to state that the heating within this limited section and the flow within it are cause and effect in a straightforward manner; it merely prescribes relations between the two which must, on the average, be satisfied. To deal with the complete, time-dependent behavior of the trades, the writer believes that much larger circulation branches must be considered.

The present theory can, on the other hand, tell us what other steady or quasi-steady configurations are possible and self-consistent for this section. If such configurations may be interpreted as describing the slow fluctuations about the mean seasonal picture discussed in the foregoing paragraphs, we may profitably inquire whether a given one of these exhibits a structure likely to restore the seasonal mean or to lead to even greater departures from it.

Re-examining equation (9) and temporarily ignoring variations in $gs/\bar{u}^2$, we see that the flow may be restored in two ways, either by a stable interaction between the forcing function as a whole and the motion field, or by readjustment between the two right-hand terms maintaining their difference the same. In both categories, only a few of the possible rearrangements will give a consistent relation between the resulting wind profile and stress distribution; the remainder are therefore excluded. Due to our inadequate knowledge of the dependence of the two right-hand terms both upon one another and upon external influences, only one illustrative calculation is worked out here.

X. An Example with Decreased Heating

Rainfall in the trade stream is the least reliable of its properties. Even casual observers have noted that a skyful of trade cumuli will on some days produce plentiful showers from clouds of all sizes, while on other apparently similar days with an apparently similar cloud distribution, no drop of rain appears. We have seen that the net non-adiabatic heating in the cloud layer is probably controlled by the

Table 3. Results of a 10 % Reduction in Heating

Height	w'	divergence · 10^6	calc. τ_{xz}	calc. $\frac{\partial \tau_{xz}}{\partial z}$	Δp
m	m/day	sec^{-1}	dyne/cm²	dyne/cm² per 100 m	mb
0	0	— 1.1	2.2	—.19	4.8
300	+ 22	— 0.6	1.7	—.17	4.2
650	+ 23	— 0.2	1.2	—.14	3.5
1,000	+ 16	+ 0.6	0.7	—.12	3.0
1,500	— 23	+ 1.2			
1,600			0	—.10	2.6
2,000	— 65	+ 1.1	— 0.4	—.08	2.0
3,000	— 105	+ 0.3	— 1.2	—.07	1.8

amount of precipitation. The evidence in I suggests that precipitation heating in the cloud layer may also be of importance indirectly in the net warming of the air below cloud base (if the eddy heat transports are, in fact, down the potential temperature gradient). It is not impossible, therefore, that we might have significant changes in the V term in equation (9) while the frictional stresses produced by the convective and turbulent elements remain more or less the same. Thus we have chosen as the example case one in which just the net heating is reduced.

The situation is now considered where the amplitude of the heating function is cut by 10 % without altering its height dependence.

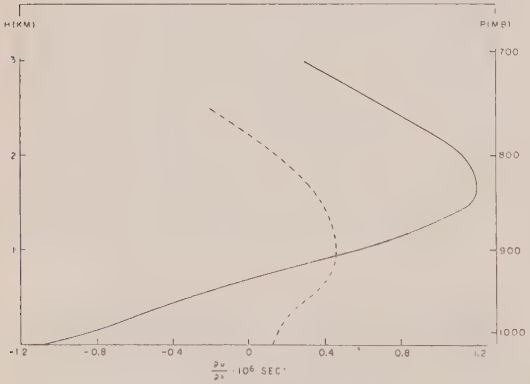

Fig. 8. Solid curve gives the theoretical divergence profile resulting when the heating is reduced by 10 % relative to that used for the average situation. The dashed curve reproduces the theoretical divergence curve for the average situation as a comparison (same as dashed curve of Fig. 5 a). Note that according to the model the wind profiles in the two cases would have shapes similar to the divergence profiles.

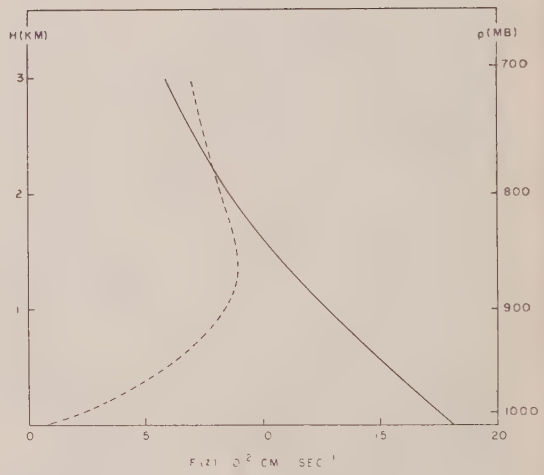

Fig. 9. Solid curve is the new forcing function $F(z)$ appearing (with a negative sign) on the right side of the differential equation for w' when the heating amplitude is reduced by 10 %. The dashed curve is the $F(z)$ used in the model of the mean flow with the heating distribution approximating that observed.

The only change in the corresponding stress term will be that its level of exponential decay is now taken as 1.6 instead of 1.7 km. This slight change is necessary to give consistent results throughout and would presumably allow for a small reduction of mean cloudiness. The solution of equation (9) is now carried through as previously, with the same stabilities in the two layers and the same boundary conditions on w'. The results are presented in Table 3 and Figures 8 and 9.

Since the wind (divergence) maximum now occurs at 1,600 m, the boundary conditions

used here on τ_{xz} were that it be zero there and 2.2 dynes/cm² at the bottom surface. That choice of the lower boundary condition makes a self-consistent model because the surface wind now decreases downstream 2.8 m/sec (in the 2,500 km), while that at 1,600 m increases 3 m/sec, giving a positive wind shear of about 3.5 m/sec per km in the lower part of the section. The calculated τ_{xz} distribution in Table 3 requires an average eddy momentum exchange coefficient in the subcloud layer of about 500 c.g.s., or a substantial increase over the mean situation. This is plausible in view of the intensified eddying anticipated in consequence of replacing the former subsidence by comparable ascent in the low levels. The rate of wind shear up to the wind maximum and the height of the wind maximum are both at the upper limit of average daily values observed by Sheppard et al. in the western Atlantic trade. Thus Table 3 represents a realistic but rather extreme situation.

Although the heating has only been reduced slightly, a comparison of the new total forcing function (Figure 9) with that used previously shows that its average value has been altered by a factor of more than two in the lowest km. Apparently this is near the permissible limit of changes in the total forcing function still giving a flow field in the observed range. The new situation, however, does seem to contain restoring influences. Table 3 shows that sinking has been replaced by mean ascent up to 1 km and that the subsidence is much weaker than normal through most of the cloud layer. Weakening the descent in the cloud layer favors increased cloudiness and precipitation, while ascent in the subcloud layer aids upward transport of sensible heat, both directly and by destabilizing the already nearly neutral lapse rate. Recent observational studies (Malkus, 1955 b) suggest that the processes in the tropical subcloud layer are critically sensitive to slight amounts of subsidence or its removal. In view of this it seems likely that the system would often restore its heating and return to normal even before departing so far as the conditions of Table 3.

XI. Concluding Remarks

Within the moist convective layer the trade stream seems to have at its disposal the mechanisms to adjust: it is able to meet the imposed constraints by mutual rearrangement between heating, stress, and motion field in such a way that the motion field is allowed to fluctuate little from the mean. Above the convective layer, these mechanisms are no longer available and we are not surprised that the steadiness vanishes.

Nevertheless, the reader familiar with the trade-wind system may be disturbed by the egregious unreliability of its precipitation. It was seen that only a 10 % reduction in heating produced, in one test situation, flow patterns in the outer range of those observed. Although the variation percentage-wise in the weekly or monthly rainfall along a 2,500 km oceanic section cannot even be estimated today, we may safely guess that it often exceeds 10 %. In conclusion of this work, therefore, we must briefly examine the consequences of larger variations in heating and inquire whether any plausible shearing stress field can conceivably maintain the flow for short periods. Thus the extreme limiting question to ask of our model is whether the total forcing function (and so the flow) can temporarily remain the same as given in Section VI, without any heating at all. This is readily tested by setting V equal to zero in equation (14) and solving for τ_{xz} under the boundary conditions originally used. An observationally possible distribution of τ_{xz} arises, provided that larger eddy coefficients are occasionally permitted near the section top than those required to balance the average budgets. We find, however, that the downstream pressure drop decreases much more slowly with height than before. Even allowing for the height variation of density in equation (14), $\triangle p$ is about 3 mb at the bottom and 2 mb at the top of the section. Simple hydrostatic reasoning makes this inevitable, for if the lower column is warmed less, it can contribute proportionally less to a pressure fall along the bottom surface. Concomitantly, $\frac{\partial \tau_{xz}}{\partial z}$ shows $^2/_3$ of its surface value at 3 km. Sheppard (1954) has found that such situations are sometimes observed in the trades. It would be highly desirable to determine observationally whether occasions of abnormally slow vertical decay of frictional forces and pressure drop are associated with greatly diminished downstream warming, as the model suggests. This and other valuable tests of the relations between stress, motion

field, and heating could be carried out were a series of weather ships or other sounding devices again placed along a trade-wind air trajectory.

Acknowledgments

The writer would like to acknowledge the enormous contribution made by Dr Herbert Riehl to every phase of this paper. Not only must any endeavor to advance our knowledge of the trades take account of his publications, but the specific lines pursued here largely arose from personal discussions and correspondence with him.

Most of the work described herein was carried out at the Imperial College, London, while the writer was on a Fellowship provided by the Munitalp and Guggenheim Foundations.

REFERENCES

Bunker, A. F., 1955: Turbulence and shearing stresses measured over the North Atlantic Ocean by an airplane-acceleration technique. *J. Meteor.*, **12**, pp. 445—455.

Fultz, D., 1949: A preliminary report on experiments with thermally produced lateral mixing in a rotating hemispherical shell of liquid. *J. Meteor.*, **6**, pp. 17—33.

Kuo, H.-L., 1954: Symmetrical disturbances in a thin layer of fluid subject to a horizontal temperature gradient and rotation. *J. Meteor.*, **11**, pp. 399—411.

Malkus, J. S., 1955 a: Meteorology: On the isolation of tractable problems and an example in variable heating. *Science Prog.*, **171**, pp. 461—475.

Malkus, J. S., 1955 b: The effects of a large island upon the trade-wind air stream. *Q. J. Roy. Met. Soc.*, **81**, pp. 538—550.

Malkus, J. S., and M. E. Stern, 1953: The flow of a stable atmosphere over a heated island, Part I. *J. Meteor.*, **10**, pp. 30—41.

Phillips, N. A., 1956: The general circulation of the atmosphere: A numerical experiment. Unpublished manuscript submitted under Contracts No. N-6-ori-139(01) and No. N-ONR-1358(02) with the U.S. Office of Naval Research and the Geophysics Research Directorate. To be published.

Pisharoty, P. R., 1955: The kinetic energy of the atmosphere. *Investigations of the general circulation of the atmosphere, final report*, Dept. Meteor. U. Calif. at Los Angeles.

Riehl, H., 1956: On the heat balance and maintenance of circulation of the trades. Unpublished manuscript.

Riehl, H., T. C. Yeh, J. S. Malkus, and N. E. La Seur, 1951: The north-east trade of the Pacific Ocean. *Q. J. Roy. Met. Soc.*, **77**, pp. 598—626.

Sheppard, P. A., 1954: The vertical transfer of momentum in the general circulation. *Archiv für Meteorologie, Geophysik und Bioklimatologie*. Serie A. Band 7, pp. 114—124.

Sheppard, P. A., H. Charnock, and J. R. D. Francis, 1956: An investigation of the lower atmosphere in the trades. Unpublished manuscript. To be published.

Smith, R. C., 1955: Theory of airflow over a heated land mass. *Q. J. Roy. Met. Soc.*, **81**, pp. 382—395.

Stern, M. E., 1954: Theory of the mean atmospheric perturbations produced by differential surface heating. *J. Meteor.*, **11**, pp. 495—502.

Differences in Numerical Prognoses Resulting from Differences in Analyses[1]

By Lt.-Col. WILLIAM H. BEST, USAF, Univ. of Stockholm[2]

(Manuscript received November 30, 1955)

Abstract

This paper describes differences in numerical 500 mb prognoses, using the barotropic model, which result from different analyses of the same initial chart. Three synoptic cases are investigated, comparing the results of using routine analyses made by the Deutscher Wetterdienst, Frankfurt, Germany and the Royal Swedish Air Force Weather Service, Stockholm, Sweden.

It is a truism accepted by most forecasters that good chart prognosis starts with an accurate chart analysis. Nowhere should this be more evident than in numerical weather prediction where the forecast evolves, without subjectivity, from solving the applicable forecast equations using initial data extracted from the current analysis. It is also recognized that weather map analysis has a certain non-unique character insofar as different analysts can arrive at different conclusions in drawing a weather chart. There are many reasons for this; varying degrees of analysis skill, our limited understanding of how the atmosphere behaves, an insufficient or inadequate network of observations, and poor communications are a few. Thus, while the state of the atmosphere at a given instant is obviously unique and single-valued, its description on charts in terms of instantaneous fields of wind, temperature and pressure (or pressure-height) is often non-unique.

NEWTON (1954) has given a comprehensive survey of the problems which can arise in numerical prediction from our inability to describe precisely the atmosphere at some initial time. He has suggested certain experiments to determine the observational requirements for numerical prediction, including tests of the effects of different possible interpretations of existing data. Following this suggestion, it is the purpose of this paper to show briefly the differences in numerical, machine prognoses with the barotropic model that can result from differences in analysis. It was planned to do this by experimenting with 500 mb patterns that could be defined analytically, and observing the prognostic differences that could be caused by modifying the descriptive equation. As a prelude, however, it was decided to investigate actual synoptic cases.

[1] The research reported in this document has been sponsored in part by the Geophysics Research Directorate of the Air Force Cambridge Research Center, *Air Research and Development Command*, United States Air Force, under contract No. AF 61 (514)—648—C, through the European Office ARDC,

[2] Present assignment Headquarters, 2nd Weather Wing, Bitburg Air Base, Germany.

It is certainly of operational interest to know the extent of prognostic differences that can result from analysis differences. In this way it may be possible to establish "tolerances", so to speak, that are acceptable in analysis. It has been alleged that the problems of non-unique analysis are made irrelevant with the introduction of objective (i.e. machine) analysis. Of course this is not so, since different objective techniques may, in fact, lead to different analyses. Furthermore it would seem that a good test of a machine analysis method would be how well it can determine those scales of horizontal motion on the current analysis which, in fact, significantly influence the ultimate machine prognosis. It is these scales with which this investigation is concerned.

The investigations described below were made while the writer was a member of the numerical prediction group at the University of Stockholm, Sweden, 1954—55. This group, under the leadership of B. Bolin, has for the past several years concentrated on an exhaustive study of the barotropic model in forecasting for periods up to 72 hours.

The analyses for 3 December, 8 December and 15 December 1954 were chosen for the experiment. Their selection was random insofar as the dates were specified several weeks before they occurred. It is believed, therefore, that the analysis differences observed are typical for the winter. Two sets of analyses were used:

A. The routine 0300GMT analysis made by the Deutscher Wetterdienst, Frankfurt, Germany. This set, including the prognoses derived therefrom, is referred to hereafter as Map A, Analysis A, or Prog A, and is represented on all figures by solid lines. Contour lines are labelled in tens of meters.

B. The routine 0300 GMT analysis made by the weather central of the Royal Swedish Air Force, Stockholm. This set, including prognoses derived therefrom, is referred to as Map B, Analysis B, and Prog B, and is represented on all figures by dashed lines.

It is emphasized that these are routine analyses prepared under operational duress and without benefit of late data and hindsight study.

The forecasts were made on the Swedish electronic computer BESK over a rectangular grid of 30×40 points on a polar stereographic projection (cf Fig 1, Bolin 1955). The grid width interval was 300 km at 50° N. Boundary assumptions consisted of keeping grid point values of height and vorticity constant. Values of the initial vorticity on the boundaries were calculated using height values at the row/column immediately outside the 30×40 grid. As has been pointed out before (Bolin 1955), these boundary assumptions will introduce errors in the forecasts which may be expected to "invade" the forecast area for increasing distances with increasing time. In discussing the prognoses, therefore, we shall confine our attention to exclude boundary areas and consider the east coast of North America, the Atlantic, polar regions, and west Europe.

Case 1, 3 December 1954, was run with 1 hour 12 minute forecast time steps using the barotropic code, the characteristics of which have been described by Bolin (1955). Cases 2 and 3, 8 and 15 December 1954, were run with 1 hour forecast time steps using a barotropic code similar to the one used by Staff Members, University of Stockholm (1954). In the latter a smoothing routine was introduced such that in the initial 500 mb height field and in the prognostic height fields for 24h, 48h and 72h each grid height is replaced by a "smoothed" value:

$$\overline{\phi} = \phi_0 + \frac{1}{16} \overline{\nabla}^2 \phi$$

where $\overline{\nabla}^2$ is the finite difference Laplacian operator. The previous code had no smoothing; smoothing has been introduced to damp the appearance of so-called "wiggles", that is, relatively high amplitude-short wave length oscillations, on some 48h and 72h progs (cf Bolin 1955). It is interesting to note that thus far no such oscillations have been observed using the new code.

Case 1. 0300 GMT, 3 December 1954

Fig. 1 compares the 2 initial 500 mb analyses, A and B. It is seen that the major differences between them occur with respect to the LOW northwest of Greenland, the small LOW over southeast Greenland on Analysis A (solid lines), and in the shape of the several contour lines running from southeast

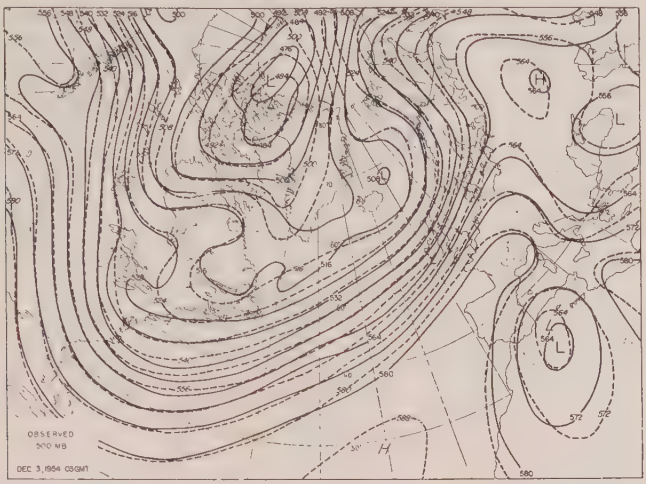

Fig. 1. Observed 500 mb map, Dec. 3, 1954, 03 GMT. Solid lines indicate analysis from Deutscher Wetterdienst. Dashed lines indicate analysis from Swedish Air Force.

Canada to Iceland. Otherwise the analyses are quite similar.

Figs. 2 and 3 compare the 24 h and 72 h prognoses derived from the 2 analyses. It is seen that the major difference between the 2 prog series results from the different evolution of the pattern from southern Greenland to northwestern Europe. At 24h, Prog A shows a small amplitude wave south of Grenland, compared to a uniform southwesterly flow on Prog B. On the 48h (not shown), the wave on Prog A has progressed eastward and increased in amplitude so that a pronounced trough lies west of Scandinavia. No similar development is evident on Prog B. On the 72h, the trough on Prog A has intensified and moved to western Europe. Prog B does not show this development but gives northwesterly flow from Greenland to central Europe.

A striking feature of this prognostic series is the development of an intense subtropical HIGH. This will be discussed later.

The conclusion from Case 1 is that analysis differences of the scale and type shown in Figure 1 lead to prognostic differences that are probably not too significant at 24h from the forecaster's point of view. On the other hand, the resulting prognostic differences at 48h and

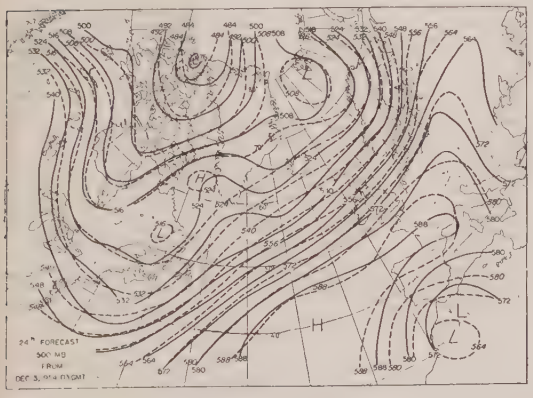

Fig. 2. 24h forecast 500 mb from Dec. 3, 1954, 03 GMT (cf Fig. 1).

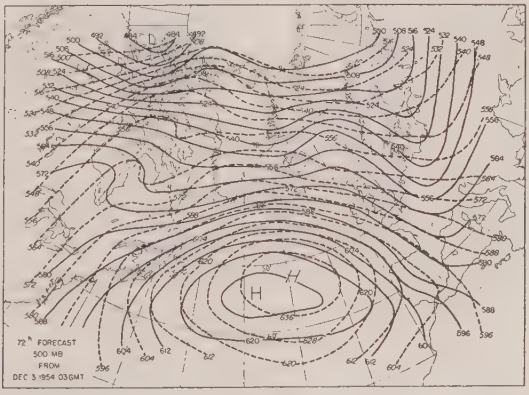

Fig. 3. 72h forecast 500 mb from Dec. 3, 1954, 03 GMT (cf Fig. 1).

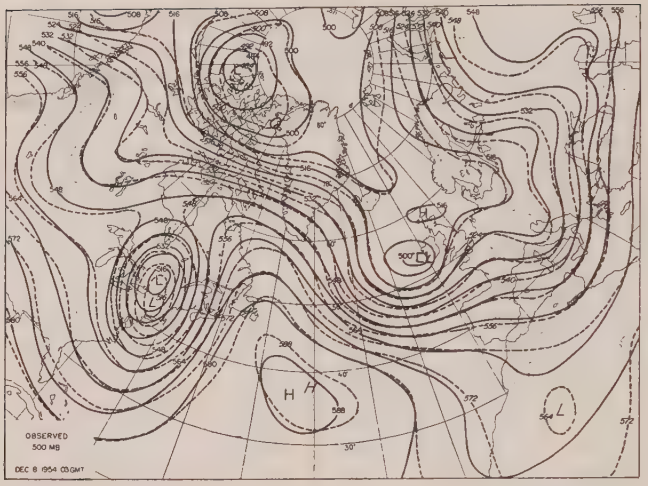

Fig. 4. Observed 500 mb map, Dec. 8, 1954, 03 GMT (cf Fig. 1).

at 72h seem to be of considerable forecast significance over an area far downstream from where the original analysis differences were.

Case 2. 0300 GMT, 8 December 1954

Figure 4, comparing the two 500 mb analyses, shows that the major differences occur in the location and intensity, but not the shape, of the strong cyclone over northeast U.S. A lesser difference is also noticeable, in isopleth curvature over the mid-Atlantic. The analyses over west Europe, showing several small HIGHs and LOWs, are essentially equivalent.

The evolution of the prognoses is shown for 24h and 72h in Figures 5 and 6. The prognosis for 48h is not shown. With regard first to the northeast U.S. LOW, the cyclone moves northeastward on the 24h and 48h progs of both series. By 48h, its central intensity on A is about the same as on B. It is evident that this feature has evolved similarly on both series. The development from 48h to 72h is rather different, however, as the Prog A LOW merges into the main LOW over Greenland and the Prog B LOW proceeds eastward as a small but nevertheless distinct center.

With regard to the pattern over west Europe, the 24h and 48h progs are essentially the same for A and B. However, the 72h progs show some difference; the trough and cut-off LOW appear 1,000 km further east on Prog B than on Prog A.

The conclusion from Case 2 is that analysis differences of the scale and type shown by

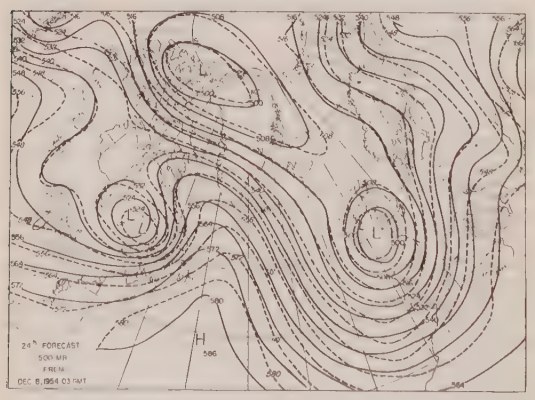

Fig. 5. 24h forecast 500 mb from Dec. 8, 1954, 03 GMT (cf Fig. 1).

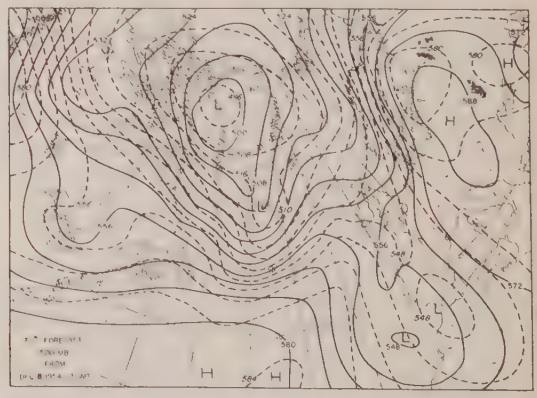

Fig. 6. 72h forecast 500 mb from Dec. 8, 1954, 03 GMT (cf Fig. 1).

Fig. 7. Observed 500 mb map, Dec. 15, 1954, 03 GMT (cf Fig. 1).

Figure 4 cause prognostic differences of not especial significance at 24h and 48h. However, by 72h, the differences appear to become significant for forecasting weather over most of the area under discussion.

Case 3. 0300 GMT, 15 December 1954

Figure 7, comparing the two analyses, shows that the major difference occurs in the mid-Atlantic with respect to the location, intensity and surrounding pattern of the LOW. Of particular interest is the shape of the contours northeast of the LOW center; on Analysis A a ridge is apparent.

At 24h, Figure 8, Prog A shows a strong trough at 25° W and ridging over Britain. On the other hand, the northern portion of the trough on Prog B is flatter, its southern portion is sharper, and the ridge downstream is flatter and further northeast. The 48h (not shown) and 72h progs, Fig. 9, show that A and B evolve quite differently. On Prog A, the trough west of Britain is fairly sharp and a strong closed HIGH appears over eastern Scandinavia and western Finland. In contrast, on Prog B the trough is quite flat; furthermore, the HIGH over Spain and the Bay of Biscay at 24h moves westward. These prognostic differences should be sufficient to give quite different forecasts of wind and weather.

The conclusion from Case 3 is that analysis differences of the scale and type shown cause prognostic differences which are already be-

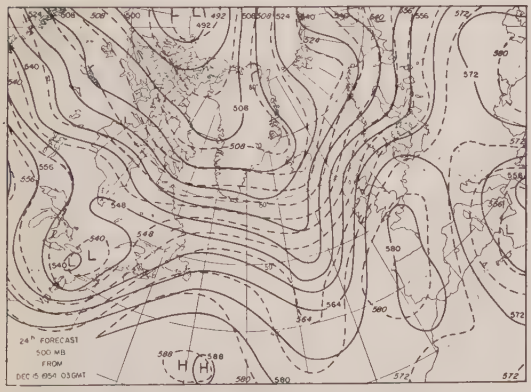

Fig. 8. 24h forecast 500 mb from Dec. 15, 1954, 03 GMT (cf Fig. 1).

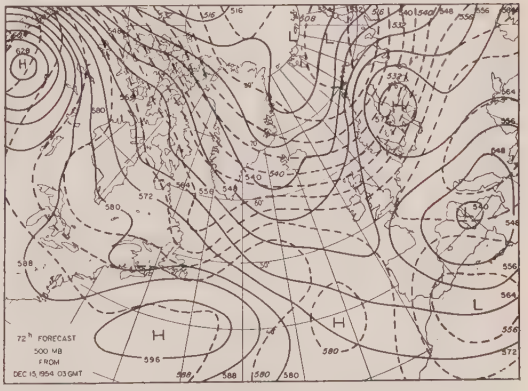

Fig. 9. 72h forecast 500 mb from Dec. 15, 1954, 03 GMT (cf Fig. 1).

coming important at 24h and which are of definite forecast significance at 48h and 72h.

We wish now to compare the behavior of 2 particular LOWS: the large cyclone over northeast U.S. on 8 Dec. and the smaller LOW in the mid-Atlantic on 15 Dec. The analysis differences are quite marked between the A and B maps for both dates. Grid point height differences between analyses, for example, are as high as 120 m on the 8th and over 200 m on the 15th. Yet the ensuing prognoses, A and B, diverge much more rapidly and strikingly on the 15th than on the 8th. Why?

In evaluating the results of these analysis differences, it should be recalled that numerical prediction involves advecting the absolute vorticity field, which is derived from the height field, in the height field itself. Thus, if two LOWs have the same shape, contour curvature and spacing, they should have, disregarding latitudinal changes the Coriolis parameter, the same vorticity distribution and be predicted along parallel paths for the same distance. Thus in the 8 Dec. case, the equivalent motion of the LOWs agrees with their having wind and vorticity distributions that are approxi- mately equivalent. On the other hand, although the 15 Dec. LOW is much smaller than the 8 Dec. LOW, the contours around the former are analyzed quite differently on Analyses A and B (Fig. 7). In particular, Map A places a definite ridge northeast of the LOW while Map B does not.

In Case 3, a striking feature of the prognoses is the intense anticyclogenesis predicted over western North America. The same phenomenon occurred in Case 1, with the spuriously intense anticyclogenesis forecast in the Atlantic. A possible cause of this overdevelopment has been suggested by Bolin (1955) to be the assumption of constant boundary conditions which, in effect, continuously advect anticyclonic vorticity around the west side of a HIGH situated near the boundary. To test this, Analysis A of Case 1 was re-analyzed to give a single-valued height at the lower boundary of the forecast area and hence make approximately zero the advection normal to the boundary. On the prognoses obtained from this re-analysis, intense anticyclogenesis was still present, but the forecast heights were as much as 100 m lower than those predicted by the original analysis. This would suggest that false vorticity advection across the boundary is at least partly responsible for building a synoptically impossible HIGH.

Conclusions

The following conclusions seem indicated by these 3 cases:

1. Differences in analysis over the area studied lead to differences in prognosis. The degree of the prognostic difference increases with the length of the forecast.

2. The prognostic differences do not appear to be of major importance on the 24h forecasts. However, for forecast periods of 48h and 72h, the prognostic differences seem large enough to be operationally significant.

3. Although objective analysis may minimize the effects of analysis differences such as are found here, it would seem that one important test of an objective analysis method is its ability to define those scales of horizontal motion which in fact affect the prognosis. This study indicates that those scales exist down to wavelengths of several grid widths.

4. In view of the numerical forecast procedure and the physical principles of the barotropic model, it appears that analysis differences with regard to the *shape* of the map features have at least as great an effect on prognoses as do analysis differences due to *location* of the features.

5. The present fixed observing network over the North Atlantic is, in certain synoptic situations, too sparse to define the characteristics of the 500 mb flow precisely enough for use with the barotropic model. This does not mean that a numerical forecast with the present net is automatically doomed, but the net is inadequate when LOWs occur over the ocean.

REFERENCES

Bolin, B., 1955: Numerical forecasting with the barotropic model, *Tellus* **7**, pp. 27—49.

Newton, C. W., 1954: Analysis and data problems in relation to numerical prediction, *Bull. Am. Met. Soc.* **35**, pp. 287—294.

Staff Members, Institute of Meteorology, University of Stockholm, 1954: Results of forecasting with the barotropic model on an electronic computer (BESK), *Tellus* **6**, pp. 139—149.

On Conversions between Potential and Kinetic Energy in the Atmosphere

By ROBERT M. WHITE, Air Force Cambridge Research Center, and
BARRY SALTZMAN, Massachusetts Institute of Technology

(Manuscript received February 2, 1956)

From a consideration of the large-scale horizontal variations of individual pressure change and 500 mb temperature in a mid-latitude sector of the Northern Hemisphere, computations are made of the required mean conversion of potential energy into the kinetic energy of the horizontal wind systems. The order of magnitude of the estimate obtained is in agreement with that obtained by Brunt from considerations of the frictional dissipation of kinetic energy. In addition, the role of organized overturnings is investigated. It is indicated that overturnings in east-west vertical planes associated with the large-scale disturbances are of primary importance in effecting the release of potential energy.

1. Introduction

In recent years increasing attention has been given to basic questions relating to the manner in which the energy provided by solar heating is utilized in maintaining the large-scale atmospheric wind systems. In this connection it has been convenient to think in terms of a "cycle" which traces the transformation and flow of energy in the atmosphere. In such an energy cycle, conversions between the potential, internal, and kinetic forms play a vital role. Aspects of this conversion process have been discussed by many authors including EADY (1949), CHARNEY (1951), FJØRTOFT (1951), VAN MIEGHEM (1952, 1955), KUO (1954), LORENZ (1954), PHILLIPS (1954, 1955), PISHAROTY (1954), and STARR (1954).

Although the stages of the energy cycle which involve the partition of available potential energy and kinetic energy into eddy and zonal components have been measured by direct observations (see, for example, STARR and WHITE, 1954), little quantitative observational evidence has been obtained thus far concerning the conversion between potential and kinetic energy. This has been largely due to the difficulties in computing the field of vertical motion, or divergence, on which such measurements critically depend.

It is the purpose of this article to present some observational estimates of the conversion process based on data recently computed by means of a two-parameter model of atmospheric flow, for a grid network covering a portion of the North American continent.

2. The nature of the conversion process

In accordance with the ideas originally expressed by MARGULES (1903) and recently extended by LORENZ (1954), one may conceive of the primary effect of solar heating as being the creation of horizontal temperature differences which represent an "available" potential energy in the atmosphere. Through the action of vertical motions, under conditions closely approximating hydrostatic equilibrium, this available potential energy is released and converted largely into the kinetic energy of the horizontal wind (see KUO, 1954).

In order to obtain a mathematical expression which represents this energy conversion process we may proceed as follows. Taking the

pressure, p, as the vertical coordinate and using the hydrostatic equation we may write the equation of motion for the horizontal wind in the form,

$$\frac{d\mathbf{v}}{dt} + f\mathbf{k} \times \mathbf{v} = -\nabla\phi - \mathbf{F}, \qquad (1)$$

where $\mathbf{v}$ is the horizontal vector wind, f is the Coriolis parameter, $\mathbf{k}$ is the unit vector in the vertical, $\phi = gz$ is the geopotential of an isobaric surface, ∇ is the two-dimensional del-operator in a pressure surface and $\mathbf{F}$ is the vector frictional force per unit mass. If we scalar-multiply this equation by $\mathbf{v}$, and expand the total derivative, we obtain the energy equation for the horizontal motions in the form,

$$\frac{\partial k}{\partial t} + \mathbf{v} \cdot \nabla k + \omega \frac{\partial k}{\partial p} = -\mathbf{v} \cdot \nabla\phi - D, \qquad (2)$$

where $k = \mathbf{v}^2/2$ is the kinetic energy of horizontal motion per unit mass, $D = \mathbf{v} \cdot \mathbf{F}$ is the rate of frictional dissipation of kinetic energy per unit mass, and $\omega = dp/dt$. With the use of the hydrostatic equation,

$$\frac{\partial \phi}{\partial p} = -\alpha, \qquad (3)$$

where $\alpha = 1/\varrho$ is the specific volume, and the continuity equation,

$$\frac{\partial \omega}{\partial p} = -\nabla \cdot \mathbf{v}, \qquad (4)$$

we may rewrite equation (2) in the form,

$$\frac{\partial k}{\partial t} + \nabla \cdot (k + \phi)\mathbf{v} + \frac{\partial}{\partial p}(k + \phi)\omega = -\omega\alpha - D. \qquad (5)$$

Finally, if this equation is integrated over the entire mass of the atmosphere, M, we obtain,

$$\frac{\partial}{\partial t}\int_M k\,dm = -\int_M \omega\alpha\,dm - \int_M D\,dm, \qquad (6)$$

where $dm = g^{-1}\,dx\,dy\,dp$ (x is distance eastward and y is distance northward).

This equation states that for the entire mass of the atmosphere the kinetic energy of the horizontal wind can vary as a result of a frictional dissipation and an effect depending on the product of ω and the specific volume throughout the mass of the fluid.

That this latter effect actually represents a conversion of potential and internal energy may be demonstrated as follows. The first law of thermodynamics may be written in the form,

$$\frac{dQ}{dt} = c_p \frac{dT}{dt} - \omega\alpha \qquad (7)$$

where c_p is the specific heat at constant pressure, T is temperature, and dQ/dt is the rate of heat addition per unit mass (including the generation of heat by friction). With the use of (4), this equation becomes

$$c_p \frac{\partial T}{\partial t} + \nabla \cdot c_p T\mathbf{v} + \frac{\partial}{\partial p} c_p T\omega = \omega\alpha + \frac{dQ}{dt}. \qquad (8)$$

Integrating this equation over the entire atmosphere and recalling that for a vertical column of the atmosphere in hydrostatic equilibrium $c_p g^{-1}\int_0^{p_0} T\,dp$ is equal to the sum of the potential and internal energy of the column,[1] we find that the expression for the time-rate of change of total potential and internal energy, $\int_M (\Phi + I)\,dm$, takes the form,

$$\frac{\partial}{\partial t}\int_M (\Phi + I)\,dm = \int_M \omega\alpha\,dm + \int_M \frac{dQ}{dt}\,dm. \qquad (9)$$

The appearance of $\int_M \omega\alpha\,dm$ with opposite sign in both equations (6) and (9) indicates that this term represents a conversion between potential and kinetic energy, a loss in one representing a gain in the other.

By virtue of the strong relation between ω and the vertical motion it is clear that the effect represented by this term is associated with the process of rising of warm air masses and sinking of cold air masses, which has been connected with the conversion process since the time of Margules.

Since over a long period of time there is no observed change in the total kinetic energy of

[1] Owing to the fact that in a hydrostatic atmosphere the potential energy in a given column bears a fixed ratio to the internal energy, we shall henceforth include both of these forms under "potential" energy.

the horizontal wind, it follows from equation (6) that the conversion integral, $-\int \omega\alpha \, dm$, must be positive in the mean to balance the frictional dissipation. From another point of view, it has been noted by EADY (1949), PHILLIPS (1954), and KUO (1954) that the vertical transport of heat (of which this integral is a close measure) should, in the long-time mean, be positive, in order to maintain the observed stable stratification against radiational losses in the upper levels of the atmosphere.

It may be noted also, that by comparing the long-time averages of equations (6) and (9), the well-known result that the mean rate of heat addition equals the mean rate of frictional dissipation is obtained.

3. Measurement of the conversion term

An evaluation of the conversion term requires a knowledge of the spatial distribution of ω over the entire atmosphere. Although it is impossible at present to obtain such extensive data, computations of ω for limited regions of the atmosphere now being made in connection with numerical weather prediction experiments are becoming available. The reliability and coverage of these new computations are in many respects superior to those provided by other methods. It seems desirable therefore to make use of such data for the present problem.

In the process of carrying out a series of numerical forecasting experiments for each day of January 1953, values of the vertically-averaged individual pressure change were computed by the joint Geophysics Research Directorate—Air Weather Service numerical weather prediction project (THOMPSON and GATES, 1956). These computations were based upon a simple 2-parameter, quasi-geostrophic, baroclinic model developed by THOMPSON (1953). The results of these computations were kindly made available to the authors for the present study.

More specifically, the vertically-averaged individual pressure change, $\tilde{\omega}$, was computed by means of the adiabatic energy equation in the form,

$$\tilde{\omega} = -\frac{g}{f\tilde{\varkappa}}\left[\frac{\partial h}{\partial t} + \frac{g}{f}J(Z, h)\right] \qquad (10)$$

where $\tilde{(\ )} = 1/p_0 \int_0^{p_0} (\ ) dp$, $\varkappa = RTf^{-1}\Theta^{-1}\partial\Theta/\partial p$ (Θ = potential temperature), and $J(Z, h)$ is the two-dimensional Jacobian of the 500 mb height, Z, and the thickness between 1,000 and 500 mb, h. $\tilde{\varkappa}$, which is a measure of the static stability through the depth of the atmosphere, was estimated from a set of observational data for the period 1—10 January, 1953.

The values of the tendency, $\partial h/\partial t$, computed from the thermal vorticity equation for the initial time $t = 0$, and the corresponding values of $J(Z, h)$ were used to evaluate $\tilde{\omega}$ at a network of 204 grid points covering a large part of the North American sector. In the solution of the thermal vorticity equation it is necessary to specify the thickness tendency along the boundaries of the region. This was approximated by assuming that the tendency at the initial time is proportional to the known 24-hour thickness change centered on time $t - 0$.

Since these numerical computations provide *vertically-averaged* values of ω only, it is not possible in the present study to consider the multi-level effects of the horizontal variations of α. Synoptic evidence suggests, however, that the general mid-tropospheric variations of α are of considerable importance in the conversion process. Accordingly, as a simple assumption the horizontal variations of α were estimated by measuring the field of temperature along the 500 mb surface. It is recognized that such an estimate does not necessarily give a representative measure of effects in the upper levels of the atmosphere where the horizontal field of α tends to be somewhat out-of-phase with that in the troposphere.

The 500 mb temperature fields and the corresponding $\tilde{\omega}$-fields were analyzed on separate charts, from which the values of temperature and $\tilde{\omega}$ were extracted at every 5 degree latitude-longitude intersection over the area between latitudes 35° N to 60° N and longitudes 70° W to 120° W. An example of the type of distribution of $\tilde{\omega}$ and temperature which was found is shown in Fig. 1.

It is reasonable to expect that, in the mean, the conditions in the area sampled in this study are similar in their essential features to other middle-latitude areas of the hemisphere. The geographical extent of this area is sufficiently

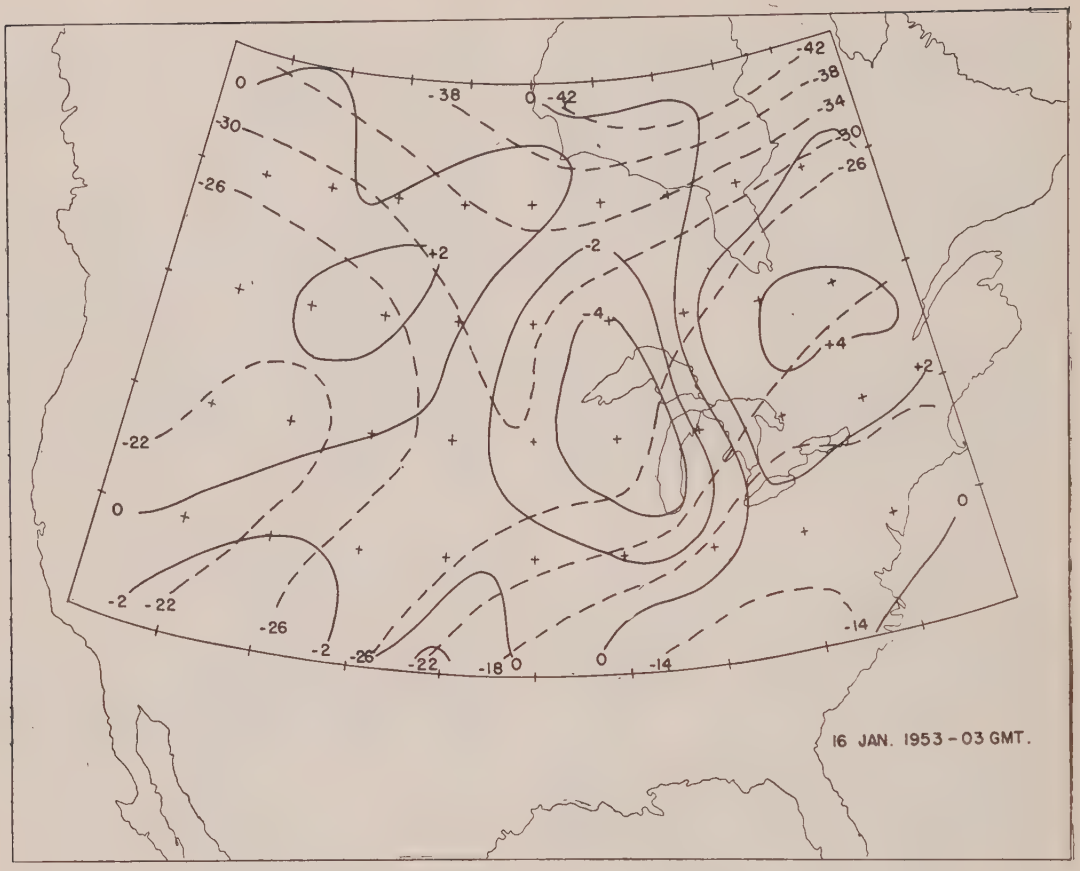

Fig. 1. Map for 16 January 1953. The values of $\tilde{\omega}$, converted to estimates of the vertical velocity (cm sec $^{-1}$) by the formula $w = -\varrho^{-1} g^{-1} \tilde{\omega}$, are represented by the solid lines. The dashed lines represent the 500 mb isotherms in degrees Centigrade.

large so that it always includes at least one synoptic-scale disturbance with associated temperature and $\tilde{\omega}$-fields.

In view of the approximations outlined above and the limited geographical area treated, the computations based on these data can be taken only as a rough measure of the actual conversion process.

4. Analysis of the data

As outlined in the preceding section, estimates of the horizontal variation of the individual pressure change and specific volume were obtained in this study. We henceforth denote these estimates by $\omega^\star(x, y)$ $(=\tilde{\omega})$ and $\alpha^\star(x, y)$ $(\sim 500$ mb temperature) respectively.

We may write the time mean of the space average of the product $\omega^\star\alpha^\star$, in the form, $\overline{\{[\omega^\star\alpha^\star]\}}$, where the brackets, brace and bar represent averages with respect to x, y and t respectively. This quantity may be further resolved into components representing the contributions due to vertical overtunings in $x-p$ "planes", overturnings in the $y-p$ "plane", and the time variations of the space averaged individual pressure change and specific volume. Such a resolution is accomplished by the following expansion,

$$\overline{\{[\omega^\star\alpha^\star]\}} - \overline{\{[\omega^\star]\}}\ \overline{\{[\alpha^\star]\}} = \overline{\{[\omega^\star]''[\alpha^\star]''\}} + \\ + \overline{\{[\omega^{\star\prime}\alpha^{\star\prime}]\}} + \overline{\{[\omega^\star]\}'''\{[\alpha^\star]\}'''}, \qquad (11)$$

where the single, double and triple primes denote deviations from the x-, y- and t-means respectively.

It can be shown that, in the long-time mean, the integral of ω over the entire mass of the atmosphere must vanish. Hence, the second term on the left, which involves $\{\overline{[\omega^*]}\}$, is identically zero if the entire atmosphere is considered. Since only a limited region of the atmosphere is treated in the present study this term can have a significant non-zero value. It is desireable, therefore, to take as a more representative measure of the *hemispheric* conversion process the left-hand side of equation (11) rather than $\{\overline{[\omega^* \alpha^*]}\}$ alone. If the vertical motions associated with the large-scale synoptic features in mid-latitudes are the important ones in effecting the required conversion,[1] and if the region sampled is somewhat representative of other regions of the hemisphere, one would expect this quantity to be negative in accordance with the theory of section 2.

The first term on the right-hand side of (11) represents the contribution resulting from the correlation of $[\omega^*]$ and $[\alpha^*]$ in the north-south direction, associated with overturnings in the $y-p$ "plane". The second term on the right depends on the correlation between ω^* and α^* along a latitude circle and results from overturnings in $x-p$ "planes". The third term depends on the time correlation between the space averages of ω^* and α^*.

More meaningful interpretations of these expressions can be made in terms of the energy cycle of the general circulation conceived by Lorenz (1954). In accordance with his scheme, $y-p$ overturnings are associated with transformations between mean zonal kinetic energy and the "*zonal* available potential energy", while the $x-p$ overturnings represent a transformation between eddy kinetic energy and "*eddy* available potential energy".

[1] It is possible that phenomena of a smaller scale than the grid network used in this study, such as cumulus convection, may be of some importance in the global conversion process.

5. Results

Each of the terms in equation (11) were computed from the data, and their values are given in table 1.

If we consider that the mass of a column of the atmosphere of unit cross-sectional area is approximately 10^3 gm, then an estimate of the net rate of energy conversion for the entire depth of the atmosphere may be obtained from the first column. In accordance with the remarks of section 2, this quantity also represents an estimate of the mean rate of frictional dissipation of kinetic energy per unit area. In the present case the value obtained is 5.0×10^3 ergs cm^{-2} sec^{-1}, representing about two per cent of the effective solar radiation. Considering the approximations made in this study, this estimate agrees well with that obtained by Brunt (1941) from other considerations. This result lends some support to the assumption implicit in this study that the gross-scale horizontal tropospheric variations of ω and α in mid-latitudes are of primary importance in the conversion process.

As previously noted, the total energy conversion is brought about by various kinds of organized atmospheric circulations. The processes represented by the second and third columns of table 1 are those associated with vertical overturnings in north-south and east-west vertical "planes" respectively. On the basis of these data it appears that in middle latitudes the $x-p$ overturnings consistently act to increase the kinetic energy, with $y-p$ overturnings acting in the opposite sense. Thus, in terms of the Lorenz energy cycle, the overturnings result in the conversion of eddy available potential energy into the kinetic energy of the large scale atmospheric disturbances while the $y-p$ overturnings give rise to an increase in the zonal available potential energy at the expense of the zonal kinetic energy.

A more detailed description of the $x-p$ overturning process is given in Fig. 2 where

Table 1. Rate of conversion between potential and kinetic energy based on data for 2—31 January, 1953. A minus sign indicates a conversion from potential to kinetic energy. Units in ergs gm^{-1} sec^{-1}.

$\overline{\{[\omega^*\alpha^*]\}} - \overline{\{[\omega^*]\}}\,\overline{\{[\alpha^*]\}}$	$\overline{\{[\omega^*]''[\alpha^*]''\}}$	$\overline{\{[\omega^{*\prime}\alpha^{*\prime}]\}}$	$\overline{\{[\omega^*]'''\{[\alpha^*]'''}$
— 5.0	+ 2.0	— 6.8	— 0.2

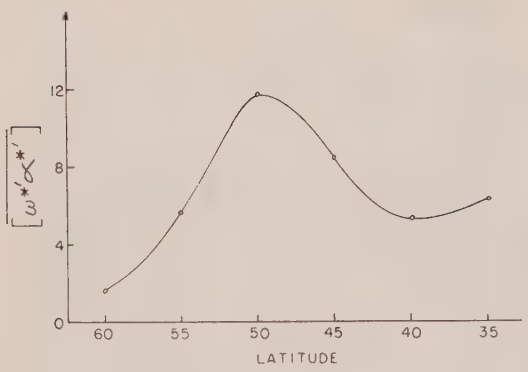

Fig. 2. Latitudinal variation of the mean rate of conversion of eddy available energy into eddy kinetic energy as measured by $[\alpha\star' \omega\star']$, in units of ergs cm^{-2} sec^{-1} $\times$ 10^3.

the latitudinal variation of the mean rate of conversion by this process is shown. It can be seen that kinetic energy conversion from eddy available potential energy due to this process is most intense in the vicinity of 50° N. Interestingly, this is also the region where the horizontal poleward flux of sensible heat, which is a measure of the generation of eddy available potential energy, is a maximum (see, for example, STARR and WHITE, 1954).

The negative contribution of the $y-p$ overturnings result largely from the existence of an indirect mean meridional circulation over the latitudinal belt which has been sampled in this study. It should be noted that observational evidence provided by STARR and WHITE (1954), MINTZ and LANG (1955) and PALMEN (1955) suggest the existence of weak direct meridional circulations in tropical and polar regions. Such circulations convert zonal available potential energy into zonal kinetic energy, tending therefore to counteract the negative contribution from the middle-latitude indirect cell. One would not expect this effect to be appreciable, however, since observations have already revealed that the kinetic energy of the zonal wind is maintained primarily by a transfer of kinetic energy from the disturbances through the action of horizontal eddy stresses (e.g. KUO 1951).

The energy conversion associated with the term in the fourth column of table 1, which depends on the time variations of the space means of $\omega\star$ and $\alpha\star$, appears to be negligibly small.

6. Conclusions

From a consideration of synoptic-scale horizontal variations in a middle-latitude sector of the atmosphere, an estimate of the required mean conversion of potential to kinetic energy has been obtained which appears to be of the correct order of magnitude.

The empirical study has suggested that this total conversion is accomplished mainly by overturnings in east-west vertical planes, in general agreement with the proposals of STARR (1954) and the descriptions of the energy cycle of the general circulation proposed by LORENZ (1954) and PHILLIPS (1955).

As noted earlier, it is recognized that, due to the limitations in data, the results of this study can only be taken as a rough measure of the true global conversion process. When sufficient data become available it would, accordingly, be desirable to extend computations of the type presented here to the entire hemisphere on a multi-level basis.

Acknowledgements

The authors wish to thank Drs. P. D. Thompson and L. W. Gates and Mr. L. Berkofsky of the joint Geophysics Research Directorate—Air Weather Service numerical weather prediction project for permission to use their computations of the field of individual pressure change. We would also like to acknowledge the considerable aid given by Miss F. Seaver who supervised the computations.

REFERENCES

Brunt, D., 1941: *Physical and Dynamical Meteorology.* London, Cambridge University Press.

Charney, J., 1951: On baroclinic instability and the maintenance of the kinetic energy of the westerlies. *Union Géodésique et Géophysique Internationale, Ninth general assembly.*

Eady, E. T., 1949: Long waves and cyclone waves. *Tellus*, **1**, pp. 33—52.

Fjørtoft, R., 1951: The stability properties of large-scale atmospheric disturbances. *Compendium of Meteorology*, pp. 454—463.

Kuo, H. L., 1951: A note on the kinetic energy balance of the zonal wind systems. *Tellus*, **3**, pp. 205—207.

— 1954: Energy releasing processes and stability of thermally driven motions in a rotating fluid. *Sci. Report No. 1, Contract AF 19(604)—1000, Mass. Inst. of Tech., J. Meteor.*, in press.

Lorenz, E. N., 1954: The basis for a theory of the general circulation. *Final Report, Contract AF 19(122)—153, Mass. Inst. of Tech.*

Margules, M., 1905: Über die Energie der Stürme, *Jahrb. (Anh. 1903) Zentralanst. f. Meteor. Geodyn., Wien.* (English translation in "the mechanics of the earth's atmosphere, a collection of translations by Cleveland Abbe", Smithson. Misc. Coll., 51, no. 4, pp. 533—595, 1910.)

Mintz, Y., and Lang, J., 1955: A model of the mean meridional circulation. *Final Report, Contract AF 19(122)—48, Univ. of Calif. at Los Angeles.*

Palmen, E., 1955: On the mean meridional circulation in low latitudes of the northern hemisphere in winter and the associated meridional and vertical flux of angular momentum. *Final Report, Contract AF 19(122)—48, Univ. of Calif. at Los Angeles.*

Phillips, N. A., 1954: Energy transformations and meridional circulations associated with simple baroclinic waves in a two-level, quasi-geostrophic model, *Tellus*, **6**, pp. 273—286.

— 1955: General circulation of the atmosphere: a numerical experiment, Unpublished manuscript (in press).

Pisharoty, P. R., 1954: The kinetic energy of the atmosphere. *Final Report, Contract AF 19(122)—48, Univ. of Calif. at Los Angeles.*

Starr, V. P., 1954: Commentaries concerning research on the general circulation. *Tellus*, **6**, pp. 236—272.

Starr, V. P., and White, R. M., 1954: Balance requirements of the general circulation. *Geophysics Research Papers No. 35*, Air Force Cambridge Research Center, ARDC.

Thompson, P. D., 1953: On the theory of large-scale disturbances in a two-dimensional baroclinic equivalent of the atmosphere. *Q.J.R.M.S.*, **29**, pp. 51—70.

Thompson, P. D., and Gates, W. L., 1956: A systematic test of numerical prediction methods based on the barotropic and two-parameter baroclinic models. *J. Meteor.* (In press.)

Van Mieghem, J., 1952: Energy conversions in the atmosphere on the scale of the general circulation. *Tellus*, **4**, pp. 334—352.

— 1955: Note on energy transfer and conversion in large atmospheric disturbances. *Q.J.R.M.S.*, **81**, pp. 19—22.

A Series Solution for the Barotropic Vorticity Equation and its Application in the Study of Atmospheric Vortices

By JULIÁN ADEM, International Meteorological Institute in Stockholm[1]

(Manuscript received April 17, 1956)

Abstract

A method to obtain a series solution for the barotropic non-divergent, vorticity equation is given and is applied to the case of a vortex.

A formula that gives the development of a symmetrical vortex as a function of radius, maximum velocity and latitude is obtained. A numerical example is worked out.

The convergence of the series solution for the general case is discussed and shown to depend on the scale of motion to be forecast and conclusions are drawn regarding time-steps used in a forecast and the smoothing of the initial map.

The possibility of improving a forecast and reducing the number of time-steps used in it by the application of this series solution, follows as a general conclusion.

Finally, a theorem that gives the scaling of the variables in an experimental model of a barotropic flow is obtained.

I. Introduction

In order to describe the behaviour of the complex atmosphere in the form of equations which can be solved in a practical way, it is necessary to search for the *main* mechanisms responsible for the atmospheric changes and formulate a theoretical model, which takes into account these mechanisms.

The barotropic model of the atmosphere is the only model up till now, which has been extensively tested and subjected to a detailed study and the reports about it (BOLIN, 1955, 1956) are encouraging. In this model the primitive equations of motion can be combined into a single forecasting equation, the well known vorticity equation, which was apparently used for the first time in meteorological applications in 1939 by Rossby and his collaborators.

When considering the integration problem from the point of view of practical applications, one is forced to use the finite difference version of the forecasting differential equations. Consequently, although very much use has been made of the vorticity equation, very little, for example, is known about the nature and properties of its solution from the point of view of differential equations.

[1] The author is a member of the Instituto de Geofísica, Universidad Nacional de México and of the Instituto Nacional de la Investigación Científica, Mexico City. He undertook the investigation reported in this paper when he was on leave in Stockholm.

A technique has been developed in this paper by which a forecasting equation or system of equations can be integrated and it has been applied to the specific case of the non-divergent barotropic equation. The solution obtained by this method is a series in the time variable and should be particularly useful when one wishes to obtain approximate analytical solutions. The method should therefore lead to a better understanding of the influence of the different parameters that enter in a forecast.

The method is specially useful in the study of atmospheric vortices. The paper contains an example of its application in the case of a cyclone embedded in a resting atmosphere.

In the last part of this paper a theoretical study of the nature of the solution of the vorticity equation and its dependence on the scale of motion has been presented and some of the results arrived at have been applied to get information of practical value in numerical forecasting.

II. The solution of the Poisson equation

The solution of an equation of the type

$$\nabla^2 z = F(x, y) \tag{1}$$

where ∇^2 is the Laplace operator $\partial^2/\partial x^2 + \partial^2/\partial y^2$ and $F(x, y)$ is a function of two variables x, y is of fundamental importance in numerical forecasting. We shall start by deriving a solution to such an equation in a form that can be useful to obtain some analytical solutions.

Writing (1) in polar coordinates (r, Θ) and considering that the function $F(x, y)$ can be expressed as a sum of terms of the type $F_1(r) \sin n\Theta$ and $F_2(r) \cos n\Theta$ where n is an integer, we shall deal with an equation of the type

$$\nabla^2 z = F_n(r) \begin{Bmatrix} \cos n\Theta \\ \sin n\Theta \end{Bmatrix} \tag{2}$$

A solution to this equation is

$$z = \left[\frac{r^n}{2n} \int r^{-n+1} F_n(r) dr - \frac{r^{-n}}{2n} \int r^{n+1} F_n(r) dr \right] \cdot \begin{Bmatrix} \cos n\Theta \\ \sin n\Theta \end{Bmatrix} \tag{3}$$

as can be easily checked by direct substitution in (2).

III. Series solution for the barotropic non-divergent vorticity equation

Let[1] $u = -\psi_y$ and $v = \psi_x$ where u and v are the components along the x- and y-axis, respectively, of the horizontal wind, the x-axis points to the east and the y-axis to the north. Substituting these values of u and v in the non-divergent barotropic vorticity equation we obtain

$$\nabla^2 \psi_t = J(\nabla^2 \psi, \psi) - \beta \psi_x \tag{4}$$

where $J(\nabla^2 \psi, \psi) \equiv \psi_y (\nabla^2 \psi)_x - \psi_x (\nabla^2 \psi)_y$ and β is the variation of the Coriolis parameter.

Given the stream function ψ and boundary conditions for the tendency ψ_t, one can compute ψ_t from (4), by solving a Poisson equation.

Differentiating (4) with respect to t one obtains

$$\nabla^2 \psi_{tt} = J(\nabla^2 \psi_t, \psi) + J(\nabla^2 \psi, \psi_t) - \beta \psi_{tx} \tag{5}$$

in which ψ_t can be computed from (4) and which is also a Poisson equation in ψ_{tt}.

Similarly, by successive differentiation with respect to t, we can obtain the equations giving the derivatives of higher order

$$\nabla^2 \psi_{ttt} = J(\nabla^2 \psi_{tt}, \psi) + 2(\nabla^2 \psi_t, \psi_t) + J(\nabla^2 \psi, \psi_{tt}) - \beta \psi_{ttx} \tag{6}$$

$$\nabla^2 \psi_{tttt} = J(\nabla^2 \psi_{ttt}, \psi) + 3J(\nabla^2 \psi_{tt}, \psi_t) + 3J(\nabla^2 \psi_t, \psi_{tt}) + J(\nabla^2 \psi, \psi_{ttt}) - \beta \psi_{ttt} \tag{7}$$

We have therefore a possibility of obtaining a series solution for the vorticity equation by solving equations (4), (5), (6), (7), . . .which are all of type (1) in the highest derivative with respect to t.

The solution is obtained as a Taylor's series:

$$\Psi = \psi + \frac{\partial \psi}{\partial t} t + \frac{1}{2} \frac{\partial^2 \psi}{\partial t^2} t^2 + \frac{1}{3!} \frac{\partial^3 \psi}{\partial t^3} t^3 + \ldots \tag{8}$$

where ψ is the stream function at the initial time, and Ψ the stream function at time t. A general discussion of this solution will be given in section V of this paper.

[1] In this section the subscript notation for derivatives will be employed. For example, $\psi_t = \partial\psi/\partial t$, $\psi_{tx} = \partial^2\psi/\partial x \partial t$, etc.

IV. Series solution for a barotropic vortex

Let (r, Θ) be a polar coordinate system, and the stream function $\psi(r)$ initially be only a function of r, and such that at $r \geq r_0$ it is equal to zero. We assume that $\psi(r)$ and its three first derivatives are continuous differentiable functions.

Substituting $\psi(r)$ in (4) we obtain

$$\nabla^2\psi_t = -\beta \cos\Theta \frac{d\psi}{dr} \tag{9}$$

from which ψ_t can be obtained at once by applying formula (3) and specifying some boundary conditions. If we assume that ψ_t is zero at $r = R_0$ we get

$$\psi_t = -\frac{\beta\cos\Theta}{r}\int_0^r \psi(r)rdr + \frac{\beta r\cos\Theta}{R_0^2}\int_0^{r_0}\psi(r)rdr \tag{10}$$

We shall assume throughout the rest of this paper that $R_0 \gg r_0$ so that the last term of the second member of (10) can be neglected.

Substituting $\psi(r)$, (9) and (10) in (5) we obtain, after simple manipulation

$$\nabla^2\psi_{tt} = \beta\sin\Theta\left[-\frac{1}{r}\left(\frac{d\psi}{dr}\right)^2 + \frac{1}{r^2}\frac{d(\nabla^2\psi)}{dr}\int_0^r \psi(r)rdr\right] + \beta^2\left[\frac{\psi}{2} + \frac{\cos 2\Theta}{2r^2}\int_0^r \frac{d\psi}{dr}r^2dr\right] \tag{11}$$

which, by applying again (3) and boundary conditions of the type used to determine ψ_t, yields ψ_{tt}.

In a similar manner, one can obtain the derivatives of higher order. For example, ψ_{ttt} contains $\beta\cos\Theta$, $\beta^2\sin 2\Theta$ and $\beta^3\cos 3\Theta$ terms.

If in the above computations we consider numerical values within the range of those corresponding to the actual atmospheric motions which we want to study, it can be seen that the terms in higher powers of β are small compared with those in the first power; for example, in (11) the β^2 term is, for practical purposes, negligible compared with the β term. For the purpose of this investigation, it is enough to consider only the β terms.

When solving (5) the terms $J(\nabla^2\psi_t, \psi)$ and $J(\nabla^2\psi, \psi_t)$ give rise to a β term, and $\beta\psi_{tx}$ to a β^2 term.

In (6), similarly, the only β terms are $J(\nabla^2\psi, \psi_{tt})$ and $J(\nabla^2\psi_{tt}, \psi)$; in (7) the β terms are $J(\nabla^2\psi, \psi_{ttt})$ and $J(\nabla^2\psi_{ttt}, \psi)$; and so forth.

It is not difficult in this way to find that the solution can be written in the form

$$\Psi(r, \Theta, t) = \psi(r) + \beta\cos\Theta\left[F_1 t + \frac{F_3}{3!}t^3 + \frac{F_5}{5!}t^5 + \dots\right] - \beta\sin\Theta\left[\frac{F_2}{2}t^2 + \frac{F_4}{4!}t^4 + \frac{F_6}{6!}t^6 + \dots\right] + R \tag{12}$$

where

$$F_n = -\frac{1}{2r}\int_0^r F_n^{\star}r^2dr + \frac{r}{2}\int_{r_0}^r F_n^{\star}dr$$

$$F_1 = -\frac{d\psi}{dr}$$

$$F_n^{\star} = \frac{1}{r}\left[\frac{d(\nabla^2\psi)}{dr}F_{n-1} - \frac{d\psi}{dr}F_{n-1}^{\star}\right]$$

and where R represents the sum of the terms containing β to a higher power than one (i.e. β^m, $m > 1$).

Let

$$\left.\begin{aligned}\psi(r) &= \psi_0\left[1 - \left(\frac{r}{r_0}\right)^2\right]^4 \quad \text{for } r \leq r_0\\ \text{and } \psi(r) &= 0 \qquad\qquad\qquad\quad \text{for } r > r_0\end{aligned}\right\} \tag{13}$$

This stream function represents a cyclone of radius r_0 when $\psi_0 < 0$ (and an anticyclone when $\psi_0 > 0$).

The maximum velocity $v_{\max} = (d\psi/dr)_{\max}$ is at $(r/r_0)^2 = 1/7$ and ψ_0 is given as a function of the radius and of the maximum velocity by

$$\psi_0 = -0.525\, r_0\left(\frac{d\psi}{dr}\right)_{\max}$$

Table 1

Terms in series (14) for $\beta = 1.7 \times 10^{-13}$ sec^{-1} cm^{-1}, $r_0 = 1000$ km, $v_{max} = 30$ m/sec, t in hours.

r/r_0 \ t	2	4	6	8	10	12	14
	βt term for sin $\Theta = 1$						
.0	0×10^{-3}	0×10^{-3}	0×10^{-3}	0×10^{-3}	0×10^{-3}	0×10^{-3}	0×10^{-3}
.2	— 12	— 24	— 36	— 48	— 60	— 72	— 84
.4	— 18	— 36	— 54	— 72	— 90	— 108	— 126
.6	— 19	— 38	— 56	— 76	— 95	— 112	— 133
.8	— 15	— 30	— 45	— 60	— 75	— 90	— 105
1.0	— 13	— 26	— 38	— 52	— 65	— 76	— 91
	βt^2 term for cos $\Theta = 1$						
.0	0×10^{-4}	0×10^{-4}	0×10^{-3}	0×10^{-3}	0×10^{-3}	0×10^{-3}	0×10^{-3}
.2	15	60	14	24	37	54	73
.4	20	80	18	32	50	70	98
.6	12	48	11	19	30	43	59
.8	4	16	2	18	10	10	20
1.0	0	0	0	0	0	0	0
	βt^3 term for sin $\Theta = 1$						
.0	0×10^{-5}	0×10^{-5}	0×10^{-4}	0×10^{-3}	0×10^{-3}	0×10^{-3}	0×10^{-3}
.2	5	40	13	3	6	10	17
.4	8	64	21	5	10	16	27
.6	10	80	26	6	12	21	34
.8	13	104	33	8	16	26	44
1.0	0	0	0	0	0	0	0
	Values of $\psi(r)/\psi_0$						
.0	1.00						
.2	.849						
.4	.498						
.6	.168						
.8	.017						
1.0	.0						

Substituting (13) in (12) we obtain

$$\frac{\Psi}{\psi_0} = \frac{\psi}{\psi_0} + r_0\,\beta\cos\Theta\left[G_1 t + G_3\left(\frac{v_{max}}{r_0}\right)^2 t^3 + \right.$$

$$\left. + G_5\left(\frac{v_{max}}{r_0}\right)^4 t^5 + \ldots\right] + r_0\,\beta\sin\Theta\left[G_2\left(\frac{v_{max}}{r_0}\right) t^2 + \right.$$

$$\left. + G_4\left(\frac{v_{max}}{r_0}\right)^3 t^4 + \ldots\right] + R \qquad (14)$$

where G_1, G_2, G_3, ... are functions of the non-dimensional variable r/r_0.

This solution can be written also in the form

$$\left.\begin{aligned}\frac{\Psi}{\psi_0} &= \frac{\psi}{\psi_0} + A\cos\Theta\left[G_1^{\star}\tau + G_3^{\star}\tau^3 + \ldots\right] + \\ &+ A\sin\Theta\left[G_2^{\star}\tau^2 + G_4^{\star}\tau^4 + \ldots\right] + R\end{aligned}\right\} (14')$$

where $G_1^{\star}$, $G_2^{\star}$, ... are functions of the non-dimensional variable r/r_0 and $\tau = (v_{max}/r_0)t$ (or $\tau = (\psi_0/r_0^2)t$) is a non-dimensional time and $A = r_0^2\beta/v_{max}$ (or $A = r_0^3\beta/\psi_0$).

Solution (14) expresses the behaviour of a vortex as a function of latitude, maximum velocity in the vortex and radius of the vortex, and lends itself to a comparative study of vortices by varying these three parameters.

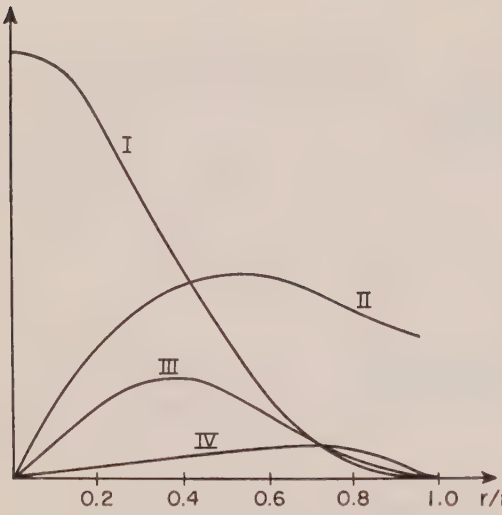

Figure 1. The line I represents the initial stream function used in the example of a vortex as a function of r/r_0; the lines II and IV represent the βt^3 terms of the series for $|\cos\Theta| = 1$ and $t = 10$ hours, and III the βt^2 term evaluated for $\sin\Theta = 1$ and the same time $t = 10$ hours. The initial stream function is represented with a vertical scale one fifth of that used for the other terms.

Let $\beta = 1.7 \times 10^{-13}$ sec^{-1} cm^{-1}, $r_0 = 1{,}000$ km and $v_{max} = 30$ m/s

Some of the results of the computation using these data are summarized in Table 1, which gives the values of the βt, βt^2 and βt^3 terms for different values of r/r_0 and different times.

The results are also shown graphically in Fig. 1, in which the lines II and IV represent the βt and βt^3 terms of the series evaluated for for $|\cos\Theta| = 1$ and $t = 10$ hours. The line III, the βt^2 term for $\sin\Theta = 1$ and the same time $t = 10$ hours. Finally, the line I represents the initial stream function drawn with vertical scale one fifth of that used for the other terms.

These calculations show that a forecast using only the βt term can be obtained up to approximately 2 hours; afterwards the βt^2 term also becomes important, and up to 6 or 8 hours these two terms are the only important ones; afterwards the βt^3 term can no longer be neglected and up to $t = 10$ or 12 hours one can obtain a solution using only these three terms; afterwards other terms become increasingly important. If one wants to continue the forecast, one has to use the above solution up to, for example, 10 hours, and then start again a new series solution now with stream function at $t = 10$ hours as the initial field. This new initial ψ is a sum of terms of the type

$$F_n(r) \left\{ \begin{matrix} \sin n\Theta \\ \cos n\Theta \end{matrix} \right\}$$

and therefore the integration can be continued using the same formula (3) obtained above.

The forecast for $t = 10$ hours is shown in Fig. 2. Fig. 2-a represents the initial stream function and Fig. 2-b the forecast for $t = 10$ hours.

The center of the vortex has moved 65 km in 10 hours, that it to say at the rate of 1.80 m/s.

We have used only the βt, βt^2 and βt^3 terms in this forecast. Fig. 3-a shows the βt term, Fig. 3-b the βt^2 term, Fig. 3-c shows the sum of the βt and βt^2 terms and, finally, Fig. 3-d the sum of the βt, βt^2 and βt^3 terms. Comparison of 3-d and 3-c shows that for $t = 10$ hours the βt^3 term is still not so important. Fig. 3 has been drawn with a scale different from that for Fig. 2.

The following general conclusions can be drawn from formula (14) and from the previous example:

Due to the variation of the Coriolis parameter β, a barotropic non-divergent cyclone embedded in a resting atmosphere moves north-westwards.

Initially, before the symmetrical cyclone gets deformed, it moves westwards and its motion is given by the term $r_0\beta G_1 t \cos\Theta$ in (14); as time increases, it gradually begins to move also northwards the component in this direction being given by $\beta G_2 t^2 v_{max} \sin\Theta$. The initial westward component is, therefore, proportional to the radius of the vortex and the northward component is proportional to the maximum velocity in the cyclone.

It is interesting to note that in our solution, the βt^3 term has sign opposite to that of the βt term, and although we have computed only the terms up to the βt^3 term, it seems as if the terms in the series (14) have alternating signs.

The above results suggest the following physical interpretation:

The variation of the Coriolis parameter induces a resultant acceleration on the cyclone (Rossby, 1949) that tends to drive the material particles northwards; this northward translational motion combined with the rotational motion of the vortex produces the westward

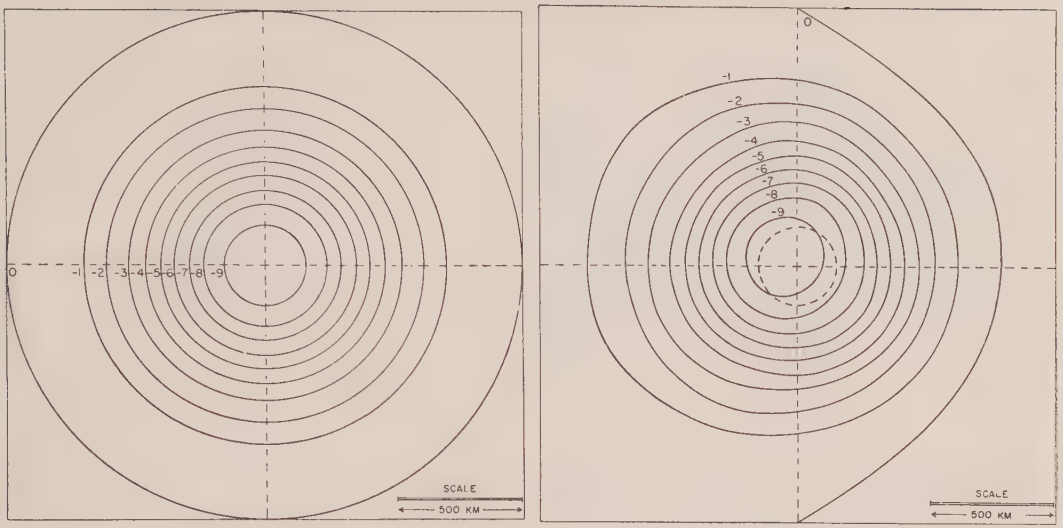

2 a 2 b

Figure 2. Forecast for a cyclone with a maximum velocity of 30 m/s and a radius of 1 000 km. 2-a is initial stream function and 2-b the forecast for $t = 10$ hours.

movement of the vortex. This fact was pointed out by Rossby (1949) and can be seen by adding graphically the stream lines from Figs 2-a and 3-a. The initial westward displacement of the cyclone, apparently, induces the northward displacement represented by the βt^2 term in the series, that in turn induces the eastward component represented by the βt^3 term, and so forth.

The solution for an anticyclone can be obtained by substituting in the above solution a positive value for ψ_0 instead of the negative one that corresponds to a cyclone; and from (14) it can be shown that an anticyclone moves south-westwards and that the above results for a cyclone apply to an anticyclone if the word "north" is replaced by "south".

Solution (14′) shows that the time up to which the series can be used with the first n terms depends on the ratio v_{max}/r_0 (or ψ_0/r_0^2); and because $\tau = (v_{max}/r_0)\ t$, there exists a linear relation between the ratio r_0/v_{max} (or r_0^2/ψ_0) and the time up to which the solution using the first n terms is valid.

In Fig. 4 we have plotted lines $\tau =$ constant in a t, r_0/v_{max} (or r_0^2/ψ_0) diagram, t is the ordinate and r_0/v_{max} is the abscissa. By the side of each line we have written three numbers which are proportional to the magnitude of the maximum velocity that appears in the βt, βt^2 and βt^3 terms when evaluated for the corresponding constant value of τ.

In this diagram, times 2, 8, 12 hours of our previous example, correspond to 8, 32 and 48 hours respectively for a vortex with $r_0 = 2{,}000$ km and $v_{max} = 15$ m/s. In other words, in this case, a forecast with only the βt term can be obtained up to 8 hours, instead of 2 hours; up to 32 hours instead of 8 hours using only two terms and up to 48 hours instead of 12 hours, using three terms. On the other hand for a vortex of radius $r_0 = 500$ km and $v_{max} =$ $= 40$ m/s. one gets 1 hour, 3 hour and 5 hour respectively.

V. Solution for a general non-divergent barotropic flow

A stream function can always be written in the form

$$\psi = \psi_0\, P_1\,(x/r_0,\, y/r_0) \qquad (15)$$

where P_1 is a function of the non-dimensional variables x/r_0 and y/r_0; ψ_0 and r_0 are scaling factors from a normalized height of the stream function and a normalized x—y plane respectively. ψ_0 and r_0 will be considered as variable parameters. For example in the case of a vortex, we have chosen r_0 as the radius of the vortex and ψ_0 as the value of the stream function at the center of the vortex.

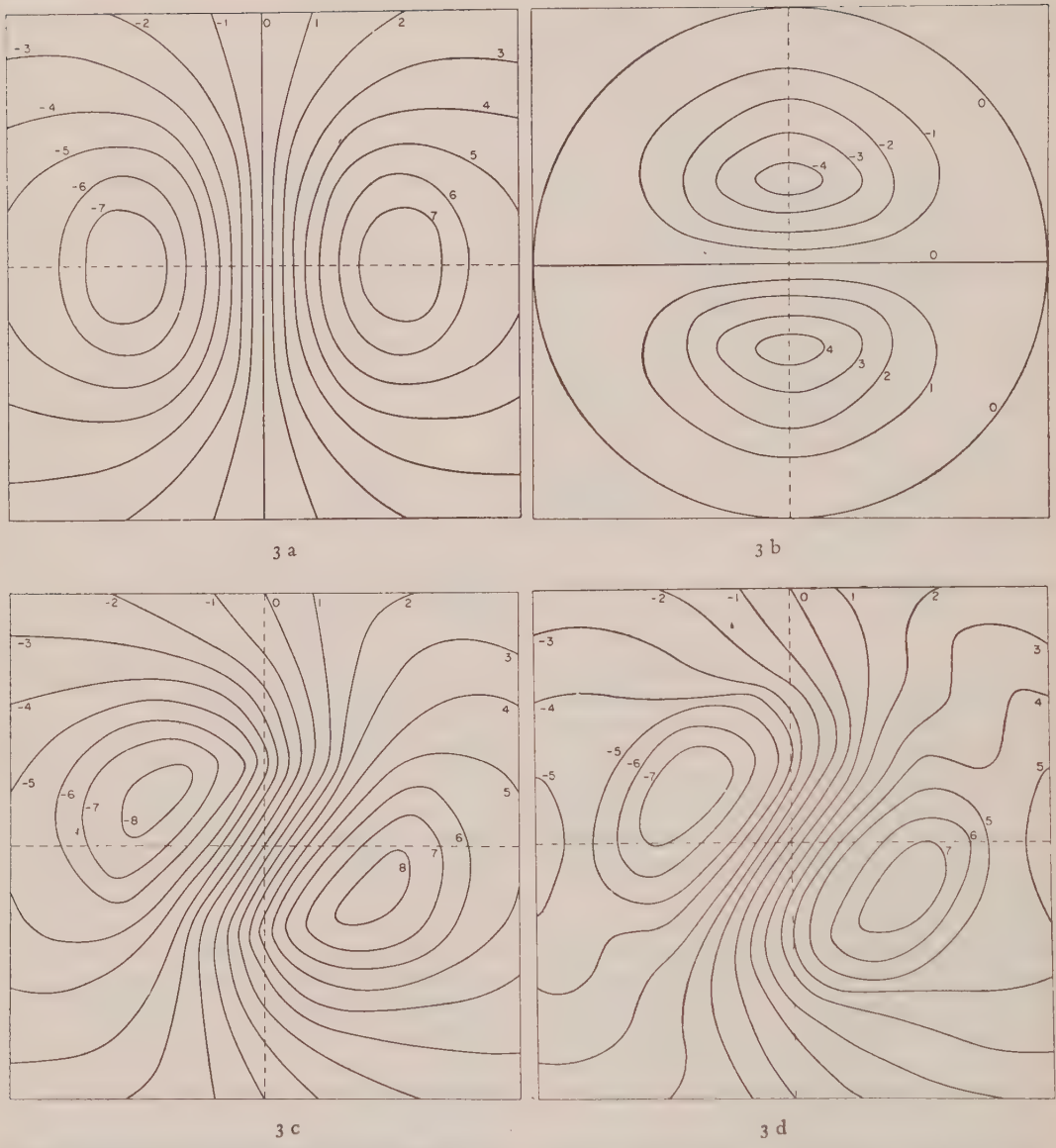

3 a 3 b

3 c 3 d

Figure 3. Graphical representation of the first terms of the series solution for a vortex of radius $r = 1\,000$ km. and maximum velocity equal to 30 m/s., for $t = 10$ hours. 3-a is the βt term, 3-b the βt^2 term; 3-c is the sum of the βt and βt^2 terms; 3-d the sum of the βt, βt^2 and βt^3 terms. The scale is different from that used in Fig. 2-a.

We shall use also as a variable parameter the variation of the Coriolis parameter β, which for the sake of simplicity is considered as a constant.

Substituting (15) in (4) one obtains

$$\nabla^2 \frac{\partial \psi}{\partial t} = \frac{\psi_0^2}{r_0^4} P_3 - \beta \frac{\psi_0}{r_0} P_4 \qquad (16)$$

where P_3 and P_4 are functions in the non-dimensional variables x/r_0 and y/r_0.

If we assume that $(\psi_0/r_0^3\beta) =$ fixed constant, when integrating (16) we obtain

$$\frac{\partial \psi}{\partial t} = \psi_0 s P_5$$

where $s = \psi_0/r_0^2$ and P_5 is a function of x/r_0 and y/r_0.

In a similar way, one can obtain, under the same assumption $(\psi_0/r_0^3\,\beta) =$ constant,

$$\frac{\partial^2\psi}{\partial t^2} = \psi_0 s^2 P_6$$

$$\frac{\partial^3\psi}{\partial t^3} = \psi_0 s^3 P_7$$

. . . . . .

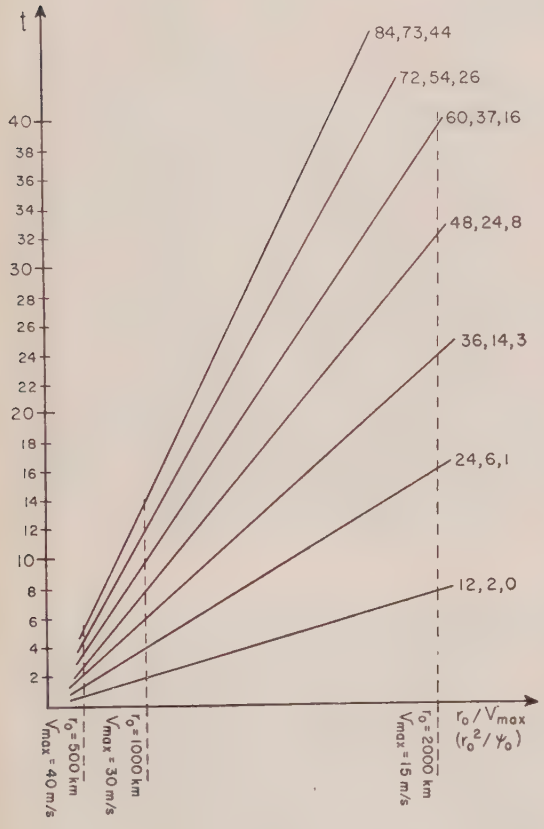

Figure 4 Time-scale of motion, diagram. The ordinate represents the time in hours and the abscisa the ratio r_0/v_{max} where v_{max} is the maximum velocity in the vortex and r_0 is the radius; in general, the abscisa can be taken as r_0^2/ψ_0 where ψ_0 and r_0 are scaling factors for the stream function and the x — y plane respectively. The straight lines represent lines of constant non-dimensional time $\tau = (\psi_0/r_0^3)\,t$ of the series solution. Note that when r_0^2/ψ_0 increases, the permissible time step in a forecast increases. The three numbers on the right hand side of each of these lines are proportional to the magnitude of the maximum velocity that appearts in the βt, βt^2 and βt^3 terms of the series evaluated for the corresponding constant value of τ, for the case of a vortex.

where P_6, P_7, . . . are functions in the non-dimensional variables x/r_0 and y/r_0.

Substituting the above values of $\partial\psi/\partial t$, $\partial^2\psi/\partial t^2$, $\partial^3\psi/\partial t^3$, . . . in the series solution (8) we obtain the following result:

In an incompressible, non-divergent barotropic flow let the initial stream function ψ be given by (15) and let β be a constant. If we choose the variable parameters ψ_0, r_0 and β such that $(\psi_0/r_0^3\beta)$ = constant, then the stream function Ψ at a later time can be written as series in the non-dimensional time $\tau = (\psi_0/r_0^2\,t)$ in the form

$$\frac{\Psi}{\psi_0} = P_1 + P_2\tau + P_3\tau^2 + \ldots .$$

where P_1, P_2, P_3, . . . are functions of the non-dimensional variables x/r_0 and y/r_0.

Since the solution is independent of the arbitrary choice of ψ_0, r_0 and β, we can, without losing generality, always choose such values that $(\psi_0/r_0^2\beta)$ = constant, but still vary ψ_0, r_0 and β for a comparative purpose. We see, therefore, that a figure similar to Fig. 4 can be drawn showing that the time to which the n first terms of the series can approximate the stream function is proportional to the ratio r_0^2/ψ_0.

As a corollary of the above non-dimensional time series solution the following result can be obtained:

Let $\psi = \psi_0 F(x/r_0,\ y/r_0,\ \beta_0)$ represent an initial stream function, where ψ_0, r_0 represent the scaling of normalized quantities and β_0 the variation of Coriolis parameter; then the normalized stream function Ψ/ψ_0 at $t = t_0$ is identical with the one corresponding to an initial stream function $\psi_1 F(x/r_1, y/r_1, \beta_1)$ at time $t = t_1$, where $t_1 = (\beta_0 r_0/\beta_1 r_1)$ and $(r_1^3\beta_1/\psi_1) = (r_0^3\beta_0/\psi_0)$.

This result can be of importance in the construction of experimental models.

VI. Applications to numerical forecasting

Since the solution is a series in the non-dimensional time $\tau = (\psi_0/r_0^2)t$, it is evident that the smoothing of a map from which a forecast of large scale motions is to be made, is a necessity from the point of view of the nature of the solution of the vorticity equation. In fact the smoothing will eliminate small

scale disturbances and motions for which r_0^2/ψ_0 is smaller than a certain value of C and we then forecast large scale motions and disturbances such that $r_0^2/\psi_0 \geq C$.

An important conclusion that can be drawn from our discussion is the dependence of the time step used in a forecast on the scale of motions or disturbances that one wants to forecast. To forecast large scale systems, one needs to forecast from a smoothed initial stream function such that $r_0^2/\psi_0 \geq C$ and use a certain time step which depends on the value of C; while to forecast small scale systems, one needs shorter time steps, since in this case, C is smaller.

There are two meteorologically important cases in which r_0^2/ψ_0 is small; the case of a tropical cyclone, in which one has large velocities concentrated in a small radius; and the case of a jet in which also large velocities are concentrated in a small cross section.

In the case of a cyclone as has already been pointed out when $r_0 = 500$ km and $v_{max} = 40$ m/s the forecast with one term is valid up to one hour, while when $r_0 = 1{,}000$ km and $v_{max} = 30$ m/s it is valid up to 2 hours; and when $r_0 = 2{,}000$ km and $v_{max} = 15$ m/s it is valid up to 8 hours.

An important conclusion that can be drawn from our analysis is the possibility of using longer time steps in a forecast by including in the computational scheme of the forecast the $\partial^2\psi/\partial t^2$ term (and also the higher derivative terms) of the series expansion. In fact, in our example of a vortex of $r_0 = 1{,}000$ km and $v_{max} = 30$ m/s a forecast using only the $\partial\psi/\partial t$ term is valid up to 2 hours, while by considering also the $\partial^2\psi/\partial t^2$ term the forecast can be extended up to 6 or 8 hours, in a single time step.

It may, therefore, be worth suggesting that, instead of using

$$\Psi = \psi + \frac{\partial\psi}{\partial t}\,\Delta t$$

with time steps of 2 hours (for example), we may solve for $\partial\psi/\partial t$ and $\partial^2\psi/\partial t^2$ from the Poisson equations (4) and (5) and then use

$$\Psi = \psi + \frac{\partial\psi}{\partial t}\,\Delta t + \frac{1}{2}\frac{\partial^2\psi}{\partial t^2}(\Delta t)^2$$

with larger time steps (for example 6 or 8 hours).

Another alternative is to use the series solution with as many terms as possible and reduce the number of time steps to a minimum.

Of course the above considerations have not taken into account the limitations set up by the actual practical procedure of using finite difference equations. For example, we know that the distance between grid-points in an actual case sets up a limit to the time steps used in a forecast, and requires special study (Bolin, 1955, p. 28).

In conclusion, it may be stated that this technique for obtaining a series solution for the barotropic non-divergent vorticity equation can also be applied to other forecasting equations or systems of equations. It should thus find application in a wide variety of problems in numerical forecasting.

Acknowledgement

The author wishes to express his indebtedness to professor C.-G. Rossby for giving him the benefit of several stimulating discussions and to Dr B. Bolin for reading most of the manuscript and making some valuable comments.

REFERENCES

Bolin, B., 1955: Numerical forecasting with the barotropic model. *Tellus*, **7**, pp. 27—49 m.

Bolin, B., 1956: An improved barotropic model and some aspects of using the balance equation for three-dimensional flow. *Tellus*, **8**, pp. 1—15.

Rossby, C.-G., 1939: Relation between variations in the intensity of the zonal circulation of the atmosphere and the displacements of the semi-permanent centers of action. *J. Marine Res.*, **2**, pp. 38—55.

Rossby, C.-G., 1949: On a mechanism for the release of potential energy in the atmosphere. *J. Meteor.*, **4**, pp. 135—162.

On Quasi-nondivergent Prognostic Equations and their Integration

By H.-L. KUO
Massachusetts Institute of Technology, Cambridge, Mass.

(Manuscript received September 17, 1955, revised March 5, 1956.)

Abstract

A general two-dimensional wind-pressure relationship is obtained as the first integral of the so-called "balance equation" which requires the horizontal divergence to remain small as compared with the vertical component of the relative vorticity for the large-scale motions. This wind-pressure relationship is used in determining the initial conditions and in deriving the governing equations. The use of this general system removes the error introduced by the quasi-geostrophic approximation.

An influence function is computed for a normal atmosphere. This function represents the reaction of the atmosphere to a point source perturbation and may be used to integrate the three-dimensional governing equation for arbitrary initial disturbances. A set of such functions may be computed, corresponding to different values of the parameter $\bar{f}^2 \cos^2 \varphi / \Gamma$, to meet different situations.

1. Introduction

The synoptically important large-scale motions of the atmosphere are characterized by the fact that at every moment the air is in a near-equilibrium state, with the forces acting on any parcel of air nearly balancing each other so that the wind is given approximately by the geostrophic-wind relation, though not exactly. The equations used in discussing the properties of these large-scale motions and in numerical forecasting are generally derived by making use of the geostrophic approximation, which eliminates the synoptically unimportant but mathematically troublesome sound waves and gravitational waves and lead to a non-homogeneous partial differential equation in the first time-derivative of the pressure or geopotential, and can therefore be solved and extended into the future by iteration. The success of the application of simple equations derived under the geostrophic approximation in forecasting the motion of the upper atmosphere encourages meteorologists to try to improve the simplification in order to obtain still better results. (For references on quasi-geostrophic prognostic equations see Kuo, 1953 a, Charney and Phillips, 1953.) Experiences show that the geostrophic approximation becomes poor in regions of strong wind, especially in the vicinity of intense cyclones (anticyclones) where it gives too high (low) wind and vorticity and therefore incurs fictitious development that does not exist. Since the problem of forecasting is usually more concerned with the development of cyclones and anticyclones, it would seem that the next nontrivial improvement of the quasi-geostrophic approach is to seek an approximation to the wind system better than the geostrophic which, when used as a first approximation in deriving the governing equations for the large scale motions, also eliminates the sound waves

and the gravitational waves. As is usually stated, the synoptically important large-scale motions are characterized by the small value of the ratio between the horizontal divergence D and the relative vorticity ζ while the sound waves and gravitational waves are characterized by large values of the ratio D/ζ, and therefore the small-scale sound and gravitational waves will be excluded if we require the individual change of the horizontal divergence dD/dt to be small, so that it may be neglected in the divergence equation. This equation then reduces to the so called "balance equation", expressing a balance between the horizontal wind and the pressure distribution. Only when the nonlinear terms of this equation are neglected does it reduce to the geostrophic relation. Various attempts have been made to derive forecasting equations satisfying this balance equation: for example, CHARNEY (1955) has proposed to integrate the primitive equations with the balance equation used as an extra condition.

The purpose of this study is two-fold: first we shall obtain the integral of the balance equation in explicit form and then derive the governing equations by making use of this solution, and second: we shall discuss some general methods of integrating these equations.

In contrast to the quasi-geostrophic approximation, the dynamic equations we obtain under the quasi-nondivergent approximation become very complicated when expressed in terms of pressure or geopotential. However, in terms of the stream-function ψ, the equations retain their simple forms. We shall therefore take $\partial\psi/\partial t$ as the dependent variable. This also partly removes the difficulty of using the geostrophic relation at low latitudes, because the large-scale motions can still be represented by the ψ-field if it is nearly horizontal, which is usually the case even near the equator, since the normal atmosphere has a large stable stratification.

In order to derive a single forecasting equation with $\partial\psi/\partial t$ as the dependent variable alone we also express the thermodynamic equation in terms of ψ by making use of the integral of the balance equation. When the absolute vorticity is positive and the stratification is stable, the equation thus obtained is of elliptic type, similar in form with the quasi-geostrophic equation in $\partial\phi/\partial t$. However, since both the wind and the vorticity we use in the non-homogeneous terms are nongeostrophic, the result we obtain represents the nongeostrophic flow.

When the region under consideration is very large, the integration of the three-dimensional elliptic partial differential equation by relaxation or operational methods usually become very difficult. It seems therefore more advantageous to use Green's method for such cases. In numerical applications the advantage of this method depends upon whether standard influence functions can be obtained. The variable coefficient of the elliptic equation depends upon the static stability factor Γ and the latitude. However, experience shows that the solution is not sensitive to variations of these factors. It is therefore permissible to replace the instantaneous distribution of Γ by a function representing a normal distribution. It is then possible to obtain the analytical form of the influence function by suitable transformations. Various sets of such influence functions can be computed corresponding to different values of Γ, which can be used under different situations.

In case the variation of Γ is irregular and therefore cannot be replaced by a normal distribution, the only way of solving the equation is by numerical integration, which amounts to replacing the differential equation by a system of finite difference equations for the various grid points.

2. Dynamic equations for the large-scale motions

Assuming hydrostatic approximation to be valid, and using the pressure p as the vertical coordinate, the equation of motion can be written in the following form

$$\frac{\partial V}{\partial t}+\omega\frac{\partial V}{\partial p}+(f+\zeta)\,k\times V= \\ =-\nabla_s\left(\phi+\frac{1}{2}V^2\right)+\vec{F} \qquad (1)$$

Here $V=ui+vj$ is the horizontal velocity vector, u and v are the two components, $\omega=dp/dt$ is the individual change of pressure, i, j and k are unit vectors in the directions of increasing λ (longitude), φ (latitude) and z (elevation), f is the Coriolis parameter, ϕ is the geopotential of the isobaric surface. $\nabla_s=(a$

$\cos\varphi)^{-1}\ i\ \partial/\partial\lambda + a^{-1}\ j\ \partial/\partial\varphi$ is the spherical gradient operator, a being earth's radius, $\zeta = \nabla_s \times V$ is the vertical component of the relative vorticity and $\vec{F}$ is the frictional force.

For the sake of convenience we separate the horizontal velocity vector V into a nondivergent part V_1 and an irrotational part V_2 such that $V = V_1 + V_2$ and put

$$V_1 = k \times \nabla\psi, \qquad V_2 = \nabla\chi \tag{2}$$

where ψ serves as the stream function for V_1 and χ is the potential function for V_2. The vorticity ζ is then given by $\zeta = \nabla_s{}^2\psi$ and the horizontal divergence D ($\equiv \nabla_s \cdot V$) is given by $D = \nabla_s{}^2\chi$, where $\nabla_s{}^2 = (a\cos\varphi)^{-2}\ \partial^2/\partial\lambda^2 + a^{-2}\ (\cos\varphi)^{-1}\ \partial/\partial\varphi \cos\varphi\ \partial/\partial\varphi$ is the surface spherical Laplacian operator. The continuity equation may now be written as

$$D \equiv \nabla^2\chi = -\frac{\partial\omega}{\partial p}. \tag{3}$$

Applying the Curl operator $\nabla_s\times$ to (1) we obtain the vorticity equation

$$\frac{\partial\zeta}{\partial t} + \frac{1}{a^2\cos\varphi}\left(\frac{\partial\psi}{\partial\lambda}\frac{\partial\zeta}{\partial\varphi} - \frac{\partial\psi}{\partial\varphi}\frac{\partial\zeta}{\partial\lambda}\right) - \\ - (f+\zeta)^2\frac{\partial}{\partial p}\left(\frac{\omega}{f+\zeta}\right) \tag{4}$$

$$+ \frac{1}{a}\frac{\partial f}{\partial\varphi}v + k\times\nabla_s\omega \cdot \frac{\partial V}{\partial p} + V_2 \cdot \nabla_s\zeta - \nabla_s \times F = 0$$

Instead of using the geostrophic approximation we assume V_2 to be always much smaller than V_1 and that the individual change of the horizontal divergence D may be neglected in the divergence equation (see PETTERSSEN, 1953) which is obtained by applying the operator $\nabla_s\cdot$ to (1). Thus our approximate divergence equation is[1]

$$(f+\zeta)\,\zeta - \left(\frac{\partial V}{\partial n}\right)^2 - \frac{1}{a}\cdot\frac{\partial f}{\partial\varphi}u - \nabla^2\phi - \nabla\omega\cdot\frac{\partial V}{\partial p} \\ - \frac{2\tan\varphi}{a^2\cos\varphi}u^2\frac{\partial}{\partial\lambda}\left(\frac{v}{u}\right) - \frac{\sec^2\varphi}{a^2}V^2 = 0 \tag{5}$$

[1] This approximation implies that every term of $\left(\frac{\partial}{\partial t} + V\cdot\nabla + \omega\cdot\frac{\partial}{\partial p}\right) D$ is assumed to be small.

where

$$\left(\frac{\partial V}{\partial n}\right)^2 = (a\cos\varphi)^{-2}\left\{\left(\frac{\partial u}{\partial\lambda}\right)^2 + \left(\frac{\partial v}{\partial\lambda}\right)^2 + \right. \\ \left. + \left(\cos\varphi\frac{\partial u}{\partial\varphi}\right)^2 + \left(\cos\varphi\frac{\partial v}{\partial\varphi}\right)^2\right\}.$$

Since $V_2 \ll V_1$, we may replace V by V_1 in this equation. The last three terms are also much smaller than the other terms and may be neglected. Using plane coordinates we then have

$$(f+\zeta)\,\zeta = \nabla^2\phi + \left(\frac{\partial V_1}{\partial n}\right)^2 + \frac{df}{dy}u_1 \tag{5a}$$

or

$$f\nabla^2\psi + 2(\psi_{xx}\psi_{yy} - \psi_{xy}{}^2) + f_y\psi_y = \nabla^2\phi \tag{5b}$$

where the subscripts denote differentiation. This equation is identical with the so called "balance equation" used by CHARNEY (1955), and BOLIN (1955). In this form the divergence equation has lost its prognostic property; instead it expresses a relation between the stream function ψ and the geopotential ϕ, or between V_1 and ϕ.

The first integrals of (5) are given by

$$(f+\zeta)\frac{\partial\psi}{\partial x} = \frac{\partial}{\partial x}\left(\phi + \frac{1}{2}V_1{}^2\right) \\ (f+\zeta)\frac{\partial\psi}{\partial y} = \frac{\partial}{\partial y}\left(\phi + \frac{1}{2}V_1{}^2\right) \tag{6}$$

where $V_1{}^2 = u_1{}^2 + v_1{}^2 = \psi_x{}^2 + \psi_y{}^2$. It is readily seen that this system represents a general steady state two-dimensional nondivergent flow with convective accelerations. It includes the gradient-wind relation as a particular case, which is obtained by assuming the motion is along circular isobars, such that $V_1 = V_\Theta = \partial\psi/\partial r$, $V_r = \partial\psi/r\partial\Theta = 0$, where r denotes the radius of curvature of the stream lines.

We note that $\frac{\partial u_1}{\partial t} + \omega\frac{\partial u_1}{\partial p} - (f+\zeta)\,v_2$ and $\frac{\partial v_1}{\partial t} + \omega\frac{\partial v_1}{\partial p} + (f+\zeta)\,u_2$ can be subtracted from the left sides of the two equations (6) respectively; the resulting equations are still solutions of the balance equation (5). Thus the balance condition (5), with V replaced by V_1, implies also $(\partial/\partial t + \omega\ \partial/\partial p)\ V_2 \ll \left(\frac{\partial}{\partial t} + \omega\frac{\partial}{\partial p}\right) V_1$, and

therefore we are in essence using the modified equation of motion

$$\left(\frac{\partial}{\partial t}+\omega\frac{\partial}{\partial p}\right)V_1+(f+\zeta)\,k\times V=-$$
$$=-\nabla_s\left(\phi+\frac{1}{2}V^2\right)+\vec{F} \qquad (1')$$

It can readily be shown that the equations (4) and (5) can be derived from this equation.

The equations (5) and (6) can be used to compute the wind and vorticity from the observed pressure distributions. These winds are needed in evaluating the initial transports in the prognostic equations. Such computations of ζ and V_1 can easily be performed by successive approximations, first using a rough estimate of V_1 (for example, the geostrophic wind or the gradient wind) in the right side of (5 a) and obtain $\zeta=\zeta_1$ as the first approximation of ζ, then using ζ_1 and the rough estimate of V_1 in (6) we obtain the first approximations of u_1 and v_1. The computation can be repeated with the result that it will converge rapidly.

It may be remarked that if the motion is exactly two-dimensional and nondivergent ($\omega=0$, $V_2=0$), the vorticity equation (4) alone is sufficient in determining the subsequent motions. The initial data needed are computed from (5 a) and (6) as discussed above, which are more general than the geostrophic approximation. The simple form of the vorticity equation is retained when expressed in terms of the stream function ψ, in analogy with the quasi-geostrophic vorticity equation.

3. The thermodynamic equation

However, we shall investigate the more general case of three-dimensional motions with horizontal divergence present. Since the vorticity equation (4) involves two dependent variables ψ and ω ($V_2=\nabla\chi$ is related to ω by (3)), we need another independent equation in these two variables in order to have a closed system. Such an equation is furnished by the first law of thermodynamics. Assuming that the hydrostatic relation

$$\frac{\partial\phi}{\partial p}=-\frac{1}{\varrho}=-\frac{RT}{p} \qquad (7)$$

holds, the thermodynamic equation may be written as

$$-\frac{p}{R}\left(\frac{\partial}{\partial t}+\frac{u}{a\cos\varphi}\frac{\partial}{\partial\lambda}+\frac{v}{a}\frac{\partial}{\partial\varphi}\right)\frac{\partial\phi}{\partial p}+\Gamma\omega=\frac{Q}{c_p} \qquad (8)$$

where $\Gamma=T\partial\log\Theta/\partial p$, Θ being the potential temperature, R is the gas constant and Q is the heat added to unit mass per unit time. Our immediate problem now is to express also this equation in terms of ψ and ω.

To express $\partial^2\phi/\partial x\partial p$ and $\partial^2\phi/\partial y\partial p$ in terms of ψ we simply differentiate (6) with respect to p and obtain

$$\phi_{xp}=f\psi_{xp}+\frac{\partial}{\partial p}J(\psi,\psi_y) \qquad (9\,a)$$

$$\phi_{yp}=f\psi_{yp}-\frac{\partial}{\partial p}J(\psi,\psi_x) \qquad (9\,b)$$

where $J(a,b)=\partial a/\partial x\;\partial b/\partial y-\partial b/\partial x\;\partial a/\partial y$. On the other hand, to express $\partial^2\phi/\partial t\,\partial p$ in (8) in terms of ψ, we must integrate the relation (6) once again. It is readily seen that the integration of (6) yields,

$$\phi=\bar{f}\psi+\int(\psi_x\psi_{yy}-\psi_y\psi_{xy})\,\delta x+$$
$$+\int(\psi_y\psi_{xx}-\psi_x\psi_{xy})\,\delta y \qquad (10)$$

and therefore

$$\frac{\partial\phi}{\partial p}=\bar{f}\frac{\partial\psi}{\partial p}+\frac{\partial}{\partial p}\int(\psi_x\psi_{yy}-\psi_y\psi_{xy})\,\delta x+$$
$$+\frac{\partial}{\partial p}\int(\psi_y\psi_{xx}-\psi_x\psi_{xy})\,\delta y \qquad (10\,a)$$

Here $\bar{f}$ is the average value of f over a large area.

The last term of (10) do not yield to exact integration except under particular circumstances. However, it can be shown that their contributions in (10 a) are usually much smaller than $\partial\phi/\partial p$ and therefore may be neglected. To demostrate this, let us put

$$\psi_{xx}=\alpha\psi_{yy}$$

and assume α to be a constant. For the large scale motions we are considering in which the horizontal divergence D is much smaller than the vorticity ζ, α is usually positive and is nearly equal to 1. In the case of a circular vortex of uniform vorticity, we have exactly $\alpha=1$. On making use of this assumption in (10 a) we find

$$\frac{\partial\phi}{\partial p}=\bar{f}\frac{\partial\psi}{\partial p}+$$

$$+\frac{1}{2}\frac{\partial}{\partial p}\left\{\frac{1}{\alpha}\triangle_x(\psi_x{}^2-\psi_y{}^2)-\triangle_y(\psi_x{}^2-\alpha\psi_y{}^2)\right\} \tag{10 b}$$

where $\triangle_x$ and $\triangle_y$ are the increments in the x and y-directions, respectively. To estimate the order of magnitude of the last two terms, let us take a strong increase of the horizontal wind, from zero at sea level to 50 m sec^{-1} at 500 mb, so that $\frac{1}{2}\,\partial V_1{}^2/\partial p = 2.5$ m^2 sec^{-2}/mb. On the other hand, taking $T = 260°$ A, we find $\partial\phi/\partial p = -100$ m^2 sec^{-2}/mb. Since $(\psi_x{}^2 - \alpha\psi_y{}^2)$ is much smaller than $V_1{}^2(=\psi_x{}^2+\psi_y{}^2)$, the last two terms on the right side of (10 b) must be very much smaller than $\partial\phi/\partial p$ and therefore may be neglected. The accuracy of this approximation is certainly above that of the other approximations. These arguments apply also to the time derivative of equation (10 b), since the change of the temperature itself at a point is ordinarily not related to the change of $\frac{\partial}{\partial p}(v_1{}^2 - u_1{}^2)$ at that point. Thus we obtain

$$\frac{\partial^2\phi}{\partial t\,\partial p} \equiv -\frac{R}{p}\frac{\partial T}{\partial t} = \bar{f}\frac{\partial^2\psi}{\partial t\,\partial p} \tag{11}$$

Substituting (9 a), (9 b) and (11) in (8) we obtain

$$\frac{\partial^2\psi}{\partial t\,\partial p} + J(\psi,\psi_p) + V_2\cdot\nabla\psi_p + \frac{RQ}{\bar{f}c_p p} + \frac{Y}{\bar{f}} = \frac{R\bar{\Gamma}}{\bar{f}p}\omega \tag{12}$$

where

$$Y = (u_2-\psi_y)\frac{\partial}{\partial p}J(\psi,\psi_y) - (v_2+\psi_x)\frac{\partial}{\partial p}J(\psi_1\psi_x) \tag{13}$$

Since Y is a small correction, we may neglect the terms containing u_2 and v_2 in it.

The vorticity equation (4) and the first law of thermodynamics (12) are the two fundamental equations for the two dependent variables ψ and ω, while V_2 is related to ω by the continuity equation (3).

4. Governing equations in $\partial\psi/\partial t$ and ω

Although the equations (4) and (12) can be solved as two simultaneous equations, their integration will be greatly simplified if we eliminate ω. We then obtain the following forecasting equation in $\psi_t^{\cdot} = \partial\psi/\partial t$

$$\nabla^2\psi_t - \frac{\bar{f}\eta^2}{R}\frac{\partial}{\partial p}\left(\frac{p}{\eta\Gamma}\frac{\partial\psi_t}{\partial p}\right) + \frac{p}{R}\nabla\psi_p\cdot\nabla\left(\frac{\bar{f}}{\bar{\Gamma}}\psi_{pt}\right)$$
$$= -J(\psi,\nabla^2\psi+f) + \frac{\eta^2}{R}\frac{\partial}{\partial p}\left(\frac{Z}{\eta\Gamma}\right) -$$
$$-\frac{1}{R}\nabla\psi_p\cdot\nabla\frac{Z}{\bar{\Gamma}} - V_2\cdot\nabla\zeta + \nabla\times\vec{F} \tag{14}$$

where

$$Z = \bar{f}J(\psi,p\psi_p) + \bar{f}V_2\cdot\nabla(p\psi_p) + \frac{RQ}{c_p} + pY$$

and $\eta = f+\nabla^2\psi$ is the absolute vorticity. Equation (14) is of elliptic type when η and $-\Gamma$ are positive and when the horizontal temperature gradient is below the critical value for overturning or inertial instability.

We note that V_2 is involved in the right side of (14) in the two terms $V_2\cdot\nabla\zeta$ and $V_2\cdot\nabla\psi_p$ of Z. To include the effect of V_2, we may solve the equation for ω, which is obtained by eliminating ψ_t from (4) and (12):

$$\nabla^2\left(\frac{\Gamma}{\bar{f}}\omega\right) - \frac{p}{R}\frac{\partial}{\partial p}\eta^2\frac{\partial}{\partial p}\left(\frac{\omega}{\eta}\right) +$$
$$+\frac{p}{R}\frac{\partial}{\partial p}(\nabla\psi_p\cdot\nabla\omega)$$
$$= -\frac{p}{R}\frac{\partial}{\partial p}\left\{J(\psi,\nabla^2\psi+f) + V_2\cdot\nabla\zeta - \nabla\times\vec{F}\right\} +$$
$$+\frac{1}{R}\nabla^2\left(\frac{Z}{\bar{f}}\right). \tag{15}$$

Thus ω can be determined from the instantaneous velocity and temperature fields, after which we can solve for χ from the continuity equation (3) and obtain $V_2 = \nabla\chi$.

However, although the effect of the transports by V_2 in (14) can be included by the procedure outlined above, too much extra computation is required to incorporate this small correction, since V_2 is assumed to be much smaller than V_1. It seems therefore both profitable and permissible to replace V_2 by a certain approximation in these terms in (14). Since V_1 is considered as the first approximation to the total horizontal velocity vector V and satisfies the equations (6) while V satisfies (1′), we may take

$$fV_2' = \left(\frac{\partial}{\partial t} + \omega\frac{\partial}{\partial p}\right) V_1 \times k = -\left(\frac{\partial}{\partial t} + \omega\frac{\partial}{\partial p}\right)\nabla\psi \tag{16}$$

as an approximation for fV_2, which should be sufficient for these transport terms. We note that the first part of V_2' is equivalent to the isallobaric wind while the second part represents a motion in the direction of the horizontal temperature gradient, toward regions of higher temperature when the air is ascending and toward regions of lower temperature when it is descending. This second part is usually very small and can be neglected, its inclusion in $V_2 \cdot \nabla\psi_p$ of (12) merely changes the stability factor Γ into $\Gamma' = \Gamma\ (1 - 1/Ri)$, where $Ri = g\dfrac{\partial \ln\Theta}{\partial z}\left(\dfrac{\partial V_1}{\partial z}\right)^{-2}$ is the Richardson number, which is usually much larger than 1.

The approximation (16) brings out another interesting property of the large-scale motions. Taken as a part of the horizontal wind, the isallobaric wind represented by the first term is irrotational, which is a pertinent property of V_2. However, since this term is the local acceleration in the equations of motion, the motion produced by it at a later time will be nondivergent. This represents a continuous adjustment between the mass field and the velocity field.

Substituting (16) in (14) we obtain

$$\nabla^2\psi_t - \frac{\bar{f}\eta^2}{R}\frac{\partial}{\partial p}\frac{p}{\eta\Gamma}\frac{\partial\psi_t}{\partial p} + \frac{2\bar{f}+\zeta}{R\Gamma}p\nabla\psi_p\cdot\nabla\psi_{pt} + \\ + \frac{\eta^2}{R}\nabla\left(\frac{\partial}{\partial p}\frac{p}{\eta\Gamma}\frac{\partial\psi}{\partial p}\right)\cdot\nabla\psi_t - \frac{1}{\bar{f}}\nabla\zeta\cdot\nabla\psi_t \tag{17}$$

$$= -J(\psi, \nabla^2\psi + f) + \frac{\eta^2}{R}\frac{\partial}{\partial p}\frac{Z_1}{\eta\Gamma} - \\ - \frac{1}{R}\nabla\psi_p\cdot\nabla\frac{Z_1}{\Gamma} + \nabla\times\vec{F}$$

where

$$Z_1 = \bar{f}J(\psi, p\psi_p) + RQ/c_p + pY.$$

Since no other dependent variable is involved in (17), ψ can be extrapolated into the future by solving this equation alone.

It may be remarked that this equation is capable of representing the slowly varying convective mean meridional circulation in the atmosphere, as can be demonstrated by assuming ψ to be independent of λ and replacing ψ_{yt} by $-fv_2$. The left side of this equation then becomes identical with the equation governing the slowly varying mean meridional circulation (see KUO, 1956).

We note that the second and third terms on the left, which originate partly from the divergence term and partly from the twisting term $\nabla\omega\cdot\nabla\psi_p$ of the vorticity equation, represent an overturning or convective process in a vertical plane perpendicular to the horizontal isotherms. These terms are of some importance in regions of strong horizontal temperature gradient, but under normal conditions are usually small and can therefore be neglected or included through some approximation. They can also be incorporated in the first term by using Θ as the vertical coordinate so as to measure the horizontal differentials along the isentropic surfaces. However, because of the rapid variation of Θ such a coordinate system is not very desirable. Since these terms are usually small, their effect can be included by successive approximations. Denoting the sum of these terms by M and transforming it to the right side of the equation we may write equation (17) in the following form

$$\nabla^2\psi_t - \frac{\bar{f}^2}{R}\frac{\partial}{\partial p}\frac{p}{\Gamma}\frac{\partial\psi_t}{\partial p} = -H(\lambda, \varphi, p) = -\sum_{i=1}^{5} H_i \tag{17 a}$$

with

$$H_1 = J(\psi, \nabla^2\psi + f),$$

$$H_2 = -\frac{\bar{f}\eta^2}{R}\frac{\partial}{\partial p}\frac{p}{\eta\Gamma}J(\psi, \varphi_p)$$

$$H_3 = -\frac{\eta^2}{R}\frac{\partial}{\partial p}\frac{1}{\eta\Gamma}\left(\frac{RQ}{c_p} + pY\right) + \frac{1}{R}\nabla\psi_p\cdot\nabla\frac{Z_1}{\Gamma}$$

$$H_4 = -\nabla\times\vec{F}$$

$$H_5 = -M = \frac{2\bar{f}p}{R\Gamma}\nabla\psi_p\cdot\nabla\frac{\partial\psi_t}{\partial p} + \\ + \nabla\left(\frac{\bar{f}}{R}\frac{\partial}{\partial p}\frac{p}{\Gamma}\frac{\partial\psi}{\partial p} + \frac{1}{\bar{f}}\zeta\right)\cdot\nabla\psi_t - \\ - \frac{\bar{f}\zeta^2}{R}\frac{\partial}{\partial p}\frac{p}{\zeta\Gamma}\frac{\partial\psi_t}{\partial p} \tag{18}$$

The correction M can be included by first solving equation (17 a) with M omitted, then

evaluating M from the solution and then adding it to the right hand side and solving again. Another way of including M is to replace the time derivative in M by that of the immediate past, i.e., $\partial\psi/\partial t)_{t=e\,\Delta t} = \{(\psi)_{t=e\,\Delta t} - -\psi)_{t=(e-1)\Delta t}\}/\Delta t$; in this way M also becomes a known function of space and can therefore be considered as a nonhomogeneous term.

Equation (14) or (17) is linear in ψ_t, with nonhomogeneous terms which also change with ψ, therefore these terms must be determined at frequent time intervals. The stability factor Γ which occurs both in the coefficient of ψ_t and in the nonhomogeneous terms is also related to ψ through the following relation

$$\Gamma = -\frac{\bar{f}}{R}\left(p\,\frac{\partial^2\psi}{\partial p^2} + \frac{c_v}{c_p}\,\frac{\partial\psi}{\partial p}\right).$$

In solving these equations over a large area, it is more convenient to employ a nondimensional horizontal coordinate-system defined by

$$x = \lambda, \quad y = \int \frac{d\varphi}{\cos\varphi} = \log\,(\tan\varphi + \sec\varphi) \quad (19\,a)$$

which represents a Mercator projection. In this projection, a point on the surface of the earth is projected from the center on a cylindrical surface which is tangent to the earth along the equator, with its axis parallel to that of the earth. Denoting the differential operators in the (λ, φ) system by the subscript s and those in the new (x, y) system by the subscript e, we then have

$$\nabla_e = i\,\frac{\partial}{\partial x} + j\,\frac{\partial}{\partial y} = a\,\cos\varphi\,\nabla_s,$$

$$J_e(\alpha_1, \alpha_2) = \frac{\partial\alpha_1}{\partial x}\,\frac{\partial\alpha_2}{\partial y} - \frac{\partial\alpha_2}{\partial x}\,\frac{\partial\alpha_1}{\partial y} =$$

$$= a^2\,\cos^2\varphi\,J_s(\alpha_1, \alpha_2)$$

$$\nabla_e^2 = \frac{\partial^2}{\partial x^2} + \frac{\partial^2}{\partial y^2} = a^2\,\cos^2\varphi\,\nabla_s^2. \quad (19\,b)$$

Thus it is seen that these new operators have the same forms as in a cartesian coordinate-system and that the differentials $\partial/\partial x$ and $\partial/\partial y$ are commutative. When the equations (4), (12), (14) and (17) are multiplied by $a^2\cos^2\varphi$, then all the horizontal differentiations are expressed in terms of the new operators. In particular, eq. (17 a) becomes

$$\left(\frac{\partial^2}{\partial x^2} + \frac{\partial^2}{\partial y^2} - \frac{a^2\bar{f}^2\cos^2\varphi}{R}\,\frac{\partial}{\partial p}\,\frac{p}{\Gamma}\,\frac{\partial}{\partial p}\right)\psi_t =$$

$$= -H_e(x, y, p),$$

$$H_e(x, y, p) = J_e(\psi, \nabla^2\psi + f) - \frac{a^2\cos^2\varphi\,\eta^2}{R}\,\frac{\partial}{\partial p}\,\frac{Z_1}{\eta\Gamma}$$

$$+\frac{1}{R}\,\nabla_e\psi_p\cdot\nabla_e\,\frac{Z_1}{\Gamma} + a\,\cos\varphi\,\nabla_e\times\vec{F} - M_e \quad (20)$$

where all horizontal differentiations are with respect to the new (x, y) system defined by (19 a).

Certain conditions relating the distribution of ψ_t or its normal derivative on the boundaries must be specified in order that the solutions of the elliptic equation (14) or (20) should be unique. On the earth's surface $z = z^\star(x, y)$ or $p = p^\star(x, y)$ we must have

$$w = V\cdot\nabla z^\star \quad (21\,a)$$

Substituting this w and $V = V_1 = k\times\nabla\psi$ in

$$\omega \equiv \frac{dp}{dt} = \varrho\left(\frac{\partial\phi}{\partial t} + V\cdot\nabla\phi - gw\right)$$

we obtain

$$\bar{f}\,\frac{\partial\psi}{\partial t} - J(\psi_1\phi^\star) = \frac{1}{\varrho}\,\omega \quad \text{for } p = p^\star, \quad (21\,b)$$

where $\nabla\phi^\star = g\nabla(z^\star - h)$, $\nabla(z^\star - h)$ being the slope of the earth's surface relative to the isobaric surface. Substituting (21 b) in the thermodynamic equation (12), with the term $V_2\cdot\nabla\partial\psi/\partial p$ omitted, we obtain for $p = p^\star$,

$$\frac{\partial\psi_t}{\partial p} + s\psi_t + J(\psi, \psi_p) - \frac{s}{\bar{f}}\,J(\psi, \phi^\star) + \frac{RQ}{c_0 p_0 \bar{f}} = 0 \quad (21\,c)$$

where

$$s = -\partial\,\ln\,\Theta/\partial p = -\Gamma/T.$$

On the top of the atmosphere $p = 0$ we have

$$\omega|_{p=0} = 0. \quad (22\,a)$$

If we assume the kinetic energy per unit volume vanishes there ($\varrho V^2 \to 0$), we must also have

$$\lim_{p\to 0}\ \varrho^{1/2}\psi_t = 0. \quad (22\,b)$$

Since there is no natural side-boundary in the atmosphere, any physical condition specified on such imaginary boundaries will represent certain restriction on the motion. However, for the investigation of some general physical processes in the atmosphere we may assume symmetry about the equator.

5. Integration by Green's method

When the region under consideration is very large, it is more convenient to integrate the equation (14) or (17) by Green's method. For simplicity, we shall discuss equation (17 a). The form of the Green's function depends upon the stability factor Γ, which usually remains fairly constant in the troposphere but becomes inversely proportional to p in the stratosphere. We shall therefore represent Γ by the formula

$$\Gamma_0 = -\frac{Cp}{(p+\alpha p_0)^2}, \tag{23}$$

and choose $\alpha = 0$ in the stratosphere and $\alpha \simeq 1/2$ in the troposphere. The effect of the departure from this mean Γ can be taken into consideration by transferring the correction to the right side of the equation.

For this stratification, the substitutions

$$\psi_t = (p/p_0+\alpha)^{-1/2}\,\tau \qquad q = \ln\frac{1+\alpha}{p/p_0+\alpha} \tag{24}$$

transfor (17 a), (21 c) and (22 b) into the following forms

$$\frac{\partial^2\tau}{\partial x^2}+\frac{\partial^2\tau}{\partial y^2}+l^2\left(\frac{\partial^2\tau}{\partial q^2}-\frac{1}{4}\tau\right) = -(p/p_0+\alpha)^{1/2}H_e = -H'(x, y, q), \tag{25}$$

$$\frac{\partial\tau}{\partial q}+h\tau = B \quad \text{for } q=0, \tag{25 a}$$

$$\lim_{q\to\infty}\tau = 0. \tag{25 b}$$

where H' is the transformation of H,

$$l^2 = a^2 f^2\cos^2\varphi/RC, \quad h = 1/2+(1+\alpha)\,p_0\frac{\partial\ln\Theta}{\partial p}$$

and $$B = -(1+\alpha)^{1/2}J_s(\psi,\psi_q)+\frac{R}{fc_p}(1+\alpha)^{3/2}Q.$$

To solve this set of equations let us split τ into two parts, τ_1 and τ_2, such that τ_1 satisfies the nonhomogeneous equation (25) and the homogeneous parts of the boundary conditions (25 a) and (25 b), while τ_2 is a particular solution of the homogeneous part of (25) but satisfies the complete nonhomogeneous boundary conditions (25 a) and (25 b). It is easy to see that the sum $\tau_1+\tau_2$ satisfies both the nonhomogeneous equation (25) and the complete conditions (25 a, b). We shall assume that the region of integration covers the entire atmosphere.

The solution τ_1 is readily obtained by Green's method, and is given by $\tau_1 = \int_v GH'dV$, where the integration is to cover the whole atmosphere. The function G has to satisfy the following conditions:

$$\frac{\partial^2 G}{\partial x^2}+\frac{\partial^2 G}{\partial y^2}+l^2\left(\frac{\partial^2 G}{\partial q^2}-\frac{1}{4}G\right) = 0 \text{ for all interior points,} \tag{26 a}$$

$$\frac{\partial G}{\partial q}+h\,G = 0 \quad \text{for } q=0, \tag{26 b}$$

$$\lim_{q\to\infty} G = 0, \tag{26 c}$$

$$\lim_{P\to Q} G(P, Q) \to \frac{1}{4\pi r} \text{ (condition of unit source)}$$

$$r^2 = (x-\xi)^2+(y-\eta)^2+\frac{1}{\bar{l}^2}(q-q')^2. \tag{26 d}$$

$\bar{l}$ being the mean value of l between the two points P and Q. As has been pointed out before, equation (20) is self-adjoint for all forms of Γ, therefore the Green's function G also satisfies the reciprocity relation $G(P, G) = G(Q, P)$. Because of this reciprocity and condition (26 d), let us assume the principal part of G to be a function of r alone. We then find that the one fundamental solution which satisfies both (26 c) and (26 d) is $e^{-\frac{\bar{l}r}{2}}/r$, therefore we shall construct our Green's function by a manipulation of this "principal solution", requiring that G also satisfies the boundary condition (26 b).

An intuitive and direct method of obtaining G is the image method. From the form of the condition (26 b) we notice at once that we need not only an isolated reflected point

source at $q=-q'$, but also a continuous sequence of sources at all points $q<-q'$. The effects of these sources are given by $Ae^{-\frac{\bar{l}r'}{2}}/r'$ and $\int_{q_1}^{\infty} b(\beta)\frac{e^{-\frac{\bar{l}r'}{2}}}{r'(\beta)}\,d\beta$, respectively, where A and $b(\beta)\,d\beta$ are the yields of these sources and

$$r'^2=(x-\xi)^2+(y-\eta)^2+\frac{1}{\bar{l}^2}(q+q')^2,$$

$$r'^2(\beta)=(x-\xi)^2+(y-\eta)^2+\frac{1}{\bar{l}^2}(q+\beta)^2.$$

It is easy to see that these functions satisfy (26 a, c) and the reciprocity requirement. Since they are regular functions for all points occupied by the atmosphere, the function

$$4\pi G=\frac{e^{-\frac{\bar{l}r}{2}}}{r}+A\frac{e^{-\frac{\bar{l}r'}{2}}}{r'}+\int_{q'}^{\infty} b(\beta)\frac{e^{-\frac{\bar{l}r'}{2}(\beta)}}{r'(\beta)}\,d\beta$$

satisfies all the conditions (26 a, c, d, e). We have only to determine the constant A and the function $b(\beta)$ to make it also satisfy (26 b), which requires $A=1$, $(1+A)\,h=b(q')$ and $db/d\beta=hb$. The solution of the last two conditions is $b=2\,h\,e^{-h(\beta+q')}$, therefore the result is

$$4\pi G=\frac{e^{-\frac{\bar{l}r}{2}}}{r}+\frac{e^{-\frac{\bar{l}r'}{2}}}{r'}+2\,h\,e^{-h(q+q')}\cdot I, \quad (27)$$

where $I=\int_{q'}^{\infty} Exp\left\{h(q+\beta)-\frac{lr'(\beta)}{2}\right\}\frac{d\beta}{r'(\beta)}$. This influence function is similar to the one obtained by the writer in the previous study (KUO, 1953 a) under the assumption of a more restricted form of stratification.

For numerical application, the influence function G given by (27) can be computed for different values of the stability factor C of (23) and different latitudes. The first two terms of G are easy to compute. To compute the integral I, it is convenient to put it into another form. Writing $\triangle a$ for $\{(x-\xi)^2+(y-\eta)^2\}^{1/2}$, we distinguish two cases:

(a) $\triangle a=0$ and (b) $\triangle a>0$, where $\triangle a$ is always taken as positive.

(a) $\triangle a=0$. We have $r'(\beta)=q+\beta=\varepsilon$ and

$$I=\int_{q+q'}^{\infty}\frac{e^{-(1/2-h)\varepsilon}}{\varepsilon}\,d\varepsilon=-Ei\,(-\lambda_1) \quad (28\,a)$$

where $\lambda_1=\frac{C}{T_0}\left(\frac{q+q'}{1+\alpha}\right)$. For the tabulation of the exponential integral $-Ei\,(-x)$ see JAKNKE-EMDE (1943).

(b) $\triangle\alpha>0$. For this case we put $q+\beta=\bar{l}\triangle a\tan\alpha$, $r'(\beta)=\triangle a\,\sec\alpha$. The integral I then becomes

$$I=\int_{\alpha_1}^{\frac{\pi}{2}}\sec\alpha\;exp\left\{l\triangle a\,(h\tan\alpha-\frac{1}{2}\sec\alpha)\right\}d\alpha, \quad (28\,b)$$

where $\alpha_1=arc\,\tan\frac{q+q'}{\bar{l}\triangle a}$. This integral can easily be computed for given values of $\bar{l}$ and h.

It may be remarked that the first term of G, i.e., the principal solution $e^{-\frac{\bar{l}r}{2}}/r$, decreases more rapidly with increasing horizontal distance than the corresponding function in two-dimensional motions, so does also the image $e^{-\frac{\bar{l}r'}{2}}/r'$. However, the third term of G decreases more slowly with horizontal distance; therefore it increases the importance of far away points. The contribution from this term depends largely upon the factor $h=\frac{1}{2}-\frac{C}{(1+\alpha)\,T_0}$, and is smaller for an atmosphere with very stable stratification near the ground. We also note that since G is a function of the distance between the two points P and Q in the (x, y, q)-system, it is not symmetric in the linear system (λ, φ, p). Because the north-south distance $\triangle\varphi$ is magnified according to $\triangle y=\triangle\varphi/\cos\varphi$, G decreases more rapidly toward higher latitudes. However, this effect becomes appreciable only for the region beyond latitude 50°.

Some such influence functions have been computed for an atmosphere with $\alpha=0$, $C=C_1=31.5°$ A for $p>250$ mb, and $c=c_2=63°$ A for $p<250$ mb, $\bar{l}h=1.26$ and $\varphi_0=45°$. The values of this function are illustrated in

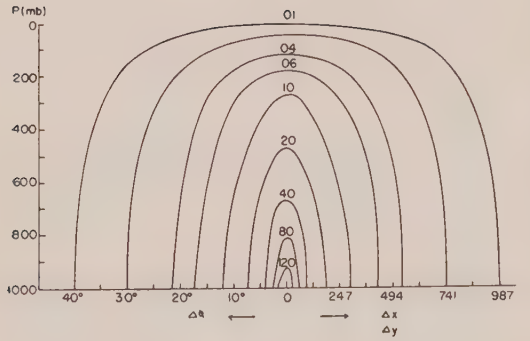

Fig. 1.

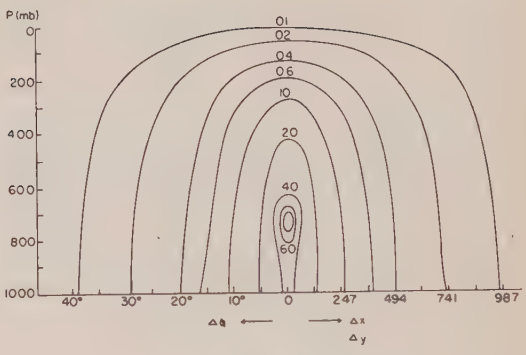

Fig. 2.

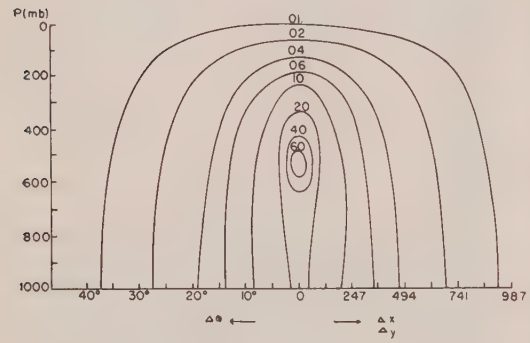

Fig. 3.

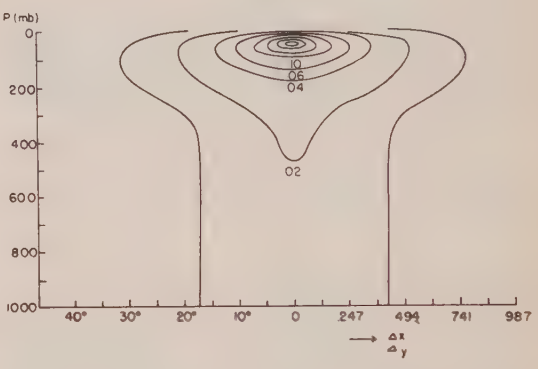

Fig. 4

Fig 1—4. The influence function $K(P, Q) = G(P, Q)/l$ for $c_1 = 31.5°$ C and $c_2 = 63°$ C with source points at $p' = 1\,000$ mb, 700 mb, 500 mb and 50 mb, respectively, and at $\varphi_0 = 45°$.

the figures 1–4, in the form of $K(P, Q) = G(P, Q)/\bar{l}$.

The second part of the solution τ_2 can easily be found by expanding τ_2 and the function B in (25 a) into double Fourier series,

$$\tau_2 = \sum_{m,\,n=-\infty}^{\infty}\sum C_{mn} N_{mn}(q)\, e^{i(mx+ny)} \qquad (29)$$

Equations (25), (25 a) and (25 b) then require

$$\left.\begin{aligned} C_{mn} &= \frac{A_{mn}}{h-\lambda_{mn}},\\ N_{mn}(q) &= e^{-\lambda_{mn} q},\\ \lambda_{mn} &= \frac{1}{4} + \frac{m^2+n^2}{\bar{l}^2},\\ A_{mn} &= \frac{1}{4\pi^2}\iint B(\xi,\eta)\, e^{-i(m\xi+ny)}\, d\xi\, d\eta \end{aligned}\right\} \qquad (30)$$

Therefore τ_2 decreases rapidly with elevation, especially for the high wave-number components.

We may now write down the complete solution of our problem. Returning to the variable ψ_t we have

$$\frac{\partial \psi}{\partial t} = \frac{1}{(p+\alpha p_0)^{\frac{1}{2}}}\iiint K(P,Q)\, H_s(Q)\, \frac{dp'}{(p+\alpha' p_0)^{\frac{1}{2}}}\, dA_s + \sum_{m,\,n=-\infty}^{\infty}\sum \frac{A_{mn}}{h-\lambda_{mn}}\left(\frac{p}{p_0}+\alpha\right)^{\lambda_{mn}-1/2} e^{-i(mx+ny)} \qquad (31)$$

where $K(p, Q) = G(P, Q)/l$ and H_s is the sum of the nonhomogeneous terms given in (18), computed in the surface spherical system, and $dA_s = a^2 \cos\varphi^1\, d\lambda^1\, d\varphi^1$ is the actual area over the spherical earth. The triple integral can be obtained numerically when H_s has been computed. Since the influence function K decreases more rapidly with actual horizontal

distance in higher latitudes, the last form of this equation shows that the polar region has a smaller influence area-wise.

In the treatment above no lateral boundary condition has been assumed, therefore the integral of (31) is to be taken over the entire atmosphere. For some theoretical problems certain lateral boundary conditions can also be specified, even though no such actual boundary exists. Thus if the difference between the two hemispheres is disregarded, we may assume symmetry about the equator, which requires ψ or $\partial\psi/\partial\varphi$ to be zero along the equator. These requirements are satisfied by using $G^1 = G \mp G_1$ as the influence function, where G_1 is the image of G about the equator, a function obtained from G by changing $\gamma - \eta$ into $\gamma + \eta$. When similar conditions are supposed for another latitude circle near the pole, the introduction of one more reflection will be sufficient. On the other hand, if values of ψ_t or its normal derivative are specified along a lateral boundary, then a surface integral has to be added to the solution (32).

In actual computations, the nonhomogeneous term H can be calculated by finite differences. The equations themselves may also be written in finite difference forms and solved by relaxation method (see HINKELMANN 1953, KUO 1955).

REFERENCES

BOLIN, B., 1955: Numerical forecasting with the barotropic model. *Tellus* **7**, pp. 27 – 49.

CHARNEY, J. G., 1955: The use of the primitive equations of motion in numerical prediction. *Tellus* **7**, pp. 22 – 26.

CHARNEY, J. G. and PHILLIPS, N. A. 1953: Numerical integration of the quasi-geostrophic equations for barotropic and simple baroclinic flows. *J. Meteor.*, 10, pp. 71 – 99.

HINKELMANN, K., 1953: Zur numerischen Wettervorhersage mittels Relaxationsmethode unter Einbeziehung barokliner Effect. *Tellus* **5**, pp. 251 – 259; pp. 499 – 512.

KUO, H. L., 1953 a: The development of quasi-geostrophic motions in the atmosphere. *Geophysical research papers*. No. 24, pp. 27 – 52. AF Cambridge Research Center, Cambridge, Mass.

– 1953 b: On the production of mean currents in the atmosphere by large disturbances. *Tellus* **3**, pp. 475 – 493.

– 1955: On quasi-nondivergent prognostic equations and their integration. Scientific report No. 2, M.I.T. General Circulation Project. pp. 1 – 40.

– 1956: Forced and free meridional circulation in the atmosphere. To be published.

PETTERSSEN, SVERRE, 1953: On the relation between vorticity, deformation, and divergence and the configuration of the pressure-field. *Tellus* **5**, pp. 231 – 237.

Optimum Smoothing of Two-Dimensional Fields[1]

By PHILIP DUNCAN THOMPSON, Lt. Col., U.S. Air Force, Joint Numerical Weather Prediction Unit, Washington, D.C.

(Manuscript received August 12, 1955, revised April 24, 1956.)

Abstract

The problem of smoothing out nonsystematic errors in a two-dimensional field of measurements has been studied from the standpoint of finding the type of weighted area average for which the RMS difference between the true field and the weighted average of the field of observations is the least. For fields whose space-autocorrelation functions are invariant with rotation and have a simple and rather typical form, the optimum weighting function is a linear combination of Bessel functions, whose rate of decrease away from the origin depends partially on the so-called "signal-to-noise" ratio, but primarily on the ratio of the scales of the true field and error field. A comparison of optimum averaging with the analyst's subjective process of smoothing indicates that the former is significantly superior in its ability to distinguish between random small-scale fluctuations and minor synoptic features of only slightly greater scale. Finally, the minimum RMS error of linearly smoothed fields is expressed in terms of the statistical properties of the true fields and the observing system itself.

I. Introduction

One of the main functions of synoptic map analysis is that of smoothing out nonsystematic errors in observations taken at a more or less dense network of discrete points. In fact, if the data were to be used exclusively for purposes of numerical weather prediction, and if the observations were taken at a sufficiently dense network of *evenly spaced* points, this would be the only function of synoptic analysis, for, under these conditions, interpolation would be unnecessary.

At the present time, the analyst's process of smoothing is rather subjective and ill-defined ... generally being carried out "by eye" and with no definite weight assigned to each piece of data. Where data coverage is adequate, this process usually consists in drawing continuous isopleths on a horizontal projection (e.g., contours of an isobaric surface), in such a way that they fluctuate as little as possible, but "fit" the data within the tolerances of the probable nonsystematic error of reported measurements. Loosely speaking, the isopleths "fit" the data if the reported measurements are interpolated roughly linearly between the two nearest isopleths *in the direction normal to the isopleths*. The fact that the spacing of the isopleths depends on their local direction means that the isopleths are not positioned by two-point linear interpolation in any *fixed* direction and, accordingly, implies that the value of the smoothed distribution at any single point

[1] Published with permission of the Commander, Air Weather Service, U.S. Air Force.

depends on reported measurements at a number of neighboring points.

In this and other respects, the analyst's smoothed distribution is very similar to a running area average of the field of reported measurements, in which each piece of data is weighted less and less with increasing distance from the point where the average applies. It is not, however, immediately clear how the data should be weighted. If they are "very weakly" weighted (i.e., virtually unweighted), random fluctuations whose scale is comparable with the distance between observation stations are obliterated, but the amplitude of real fluctuations of larger scale is considerably reduced. On the other hand, if the data are "very strongly" weighted (i.e., virtually unaveraged), the large scale synoptic features are unaffected, but so also are random fluctuations of smaller scale. Between these extremes of weighting lies the best compromise between nonsystematic errors of reported observations and systematic errors of "over-averaging".

The purpose of this paper, to state it briefly, is to find the weighting function which is "best" in the sense that the mean square error of the smoothed distribution is the least. To do so, we shall extend Wiener's methods for smoothing functions of one variable to "statistically isotropic" fields or functions of two variables, whose auto- and cross-correlation functions do not depend on the direction in which the fields are shifted. The condition that the RMS difference between the true field and the mean observed field be minimized is expressed in an integral equation, which relates the optimum weighting function to the autocorrelation functions for the true field and the "error" distribution. For Gaussian autocorrelation functions, the weighting function is found to be a linear combination of Bessel functions. The optimum radius of the effective domain of averaging is determined by the distance between observation points, and by the relative wavelengths and amplitudes of the true field and error field.

The optimum averaging process is compared with the "smoothing" process of a skilled synoptic analyst in a case when the spectrum of disturbances was fairly broad. Finally, the minimum RMS error of the smoothed field is expressed as a function of the RMS error of reported measurements and the distance between neighboring observation stations.

II. The Condition for Optimum Smoothing

The problem of averaging or smoothing out nonsystematic error will be recognized as essentially equivalent to that of filtering the "noise" from the output of a communications system . . . a problem that is familiar to the electrical engineer and which has been treated extensively by WIENER (1949) in his theory of stationary time series. Following Wiener, we shall take the minimization of the RMS difference between the true field and the smoothed field of observations as the criterion for optimizing the smoothing process.

We begin by considering a "true" field $g\ (x, y)$ and the corresponding field of observations $f\ (x, y)$, which consists partly of $g\ (x, y)$ and partly of a superimposed "error" $\varepsilon\ (x, y)$. The latter need not be interpreted as genuine error, but may be thought of as any small-scale fluctuation that is random with respect to disturbances of larger scale. We shall also consider a weighted area average $\bar{f}\ (x, y)$, constructed by applying an integral operator to the observed field $f\ (x, y)$. That is,

$$\bar{f}(x, y) = \int\int K(\varrho)\, f(x-\xi, y-\eta)\, d\xi\, d\eta$$

in which x and y are cartesian horizontal coordinates, ξ and η are the corresponding dummy variables of integration, and ϱ is the distance from the origin to the variable point (ξ, η) . . . i. e., $\varrho^2 = \xi^2 + \eta^2$. The indicated area integration generally extends over the entire (ξ, η) plane. The weighting function K is unspecified, except that its area integral is unity. Under some conditions, for example, K may turn out to be a delta function, in which case the integration actually extends over only one point in the (ξ, η) plane.

The mean square difference I between the true field $g\ (x, y)$ and the smoothed field of observations $\bar{f}\ (x, y)$, when taken over the entire (x, y) plane, is

$$I(K) = l.i.m. \int\int [g\ (x, y) - \int\int K(\varrho)\, f\ (x-\xi, y-\eta)\, d\xi\, d\eta]^2 dx\, dy$$

where the symbol "*l.i.m.*" stands for the limit of the area average as the periphery of the

area approaches infinity in all directions. For simplicity, we shall suppose that the autocorrelation functions for g and f and the crosscorrelation between g and f depend only on the magnitude of the shift from (0, 0) to (ξ, η) and not on its direction.[1] Introducing this assumption and inverting the order of integration, we may rewrite the equation above as

$$I(K) = \gamma(0) - 4\pi \int_0^\infty K(\varrho)\chi(\varrho)\varrho d\varrho +$$

$$+ 2\pi \int_0^\infty K(\varrho)\, \varrho d\varrho \int_0^\infty K(R)\, RdR \int_0^{2\pi} \phi(r)\, d\Theta \quad (1)$$

in which $r^2 = R^2 + \varrho^2 - 2R\varrho \cos \Theta$; $\gamma(\varrho)$ is the autocorrelation of g for a shift of magnitude ϱ; χ is the crosscorrelation of f and g; and ϕ is the autocorrelation of f. It should be noted that, according to Eq. (1), the mean square difference between the true field and the smoothed field of observations does not depend on the details of those fields, but is determined entirely by their correlation functions. As will be seen later, these statistics can be expressed in terms of the autocorrelation functions for the true field and the "error" field . . . the former of which probably does not change markedly from one day to the next, and the latter of which (in the case of nonsystematic errors of measurement) depends only on the characteristics of the observing system.

Stated concisely, the mathematical problem is to find the function K for which $I(K)$ is the least, given the correlation functions $\gamma(\varrho)$, $\chi(\varrho)$, and $\phi(\varrho)$ and the condition that the area integral of K is unity. Modifying the argument outlined by Levinson in Appendix C of Wiener (1949), we find that the necessary condition which K must satisfy in order that $I(K)$ be minimized is:

$$\int_0^\infty K(R)\, RdR \int_0^{2\pi} \phi(r)\, d\Theta = \chi(\varrho) \quad (2)$$

This equation completely determines the optimum weighting function if it exists at all.

[1] The fields f and g may each be regarded as the deviation from a linear function, whose derivatives are the unweighted average derivatives of the original field. Since the smoothing operation, when applied to a linear function, yields the same linear function, this interpretation involves no loss of generality.

The remaining problem is to solve the integral equation (2) for $K(R)$, regarding $\phi(r)$ and $\chi(\varrho)$ as known. By rearranging the order of integration and applying the Fourier-Bessel theorem, it can be shown directly that Eq. (2) is satisfied by

$$K(R) = \frac{1}{2\pi} \int_0^\infty \frac{J_0(Ru)X(u)}{F(u)}\, udu \quad (3)$$

where J_0 is the zero-order Bessel function of the first kind, and $X(u)$ and $F(u)$ are the Fourier-Bessel transforms of χ and ϕ, respectively. E.g.,

$$X(u) = \int_0^\infty J_0(\varrho u)\, \chi(\varrho)\, \varrho d\varrho$$

A more revealing form of Eq. (3) may be obtained by normalizing the correlation functions χ and ϕ, and by introducing the fact that the true field g and the error field ε are assumed to be uncorrelated. Thus, according to the definitions of χ and ϕ,

$$K(R) = \frac{1}{2\pi} \int_0^\infty J_0(Ru) \cdot \frac{1}{1 + \dfrac{k^2 \bar{E}(u)}{\bar{\gamma}(u)}} \cdot udu \quad (4)$$

in which $\bar{E}(u)$ and $\bar{\gamma}(u)$ are the Fourier-Bessel transforms of the *normalized* autocorrelation functions for ε and g, respectively, and k^2 is $E(0)/\gamma(0)$. The constant k is the ratio of the *RMS* amplitudes of the "error" field and the true field . . . or, in the language of the electrical engineer, the "noise-to-signal" ratio.

To place the general result stated in Eq. (4) in a familiar setting, we shall consider two special cases. First, if there is no error, k vanishes and the weighting function reduces to:

$$K(R) = \frac{1}{2\pi} \int_0^\infty J_0(Ru)\, udu$$

The integral above is zero except when $R = 0$, and becomes infinite as R approaches zero. Thus, since the area integral of K is unity, K behaves like a delta-function. This implies that, if there is no error, unit weight should be given to the point where the average applies and none to any other point, verifying that an

error-free field of observations should not be smoothed at all. A less obvious conclusion applies when the scale of the true field is the same as that of the error field. In this case, $\bar{E}(u)$ and $\bar{\gamma}(u)$ are sensibly the same, and $K(R)$ again becomes a delta-function. This means that "noise" cannot be filtered out of a "signal" of the same (or smaller) scale by *smoothing*, simply because the signal amplitude is reduced in the same proportion as the error amplitude. It may, of course, be possible to filter out the noise by differentiation . . . rather than by integration or averaging . . . provided the "noise-to-signal" ratio is small enough.

III. The Optimum Smoothing Process for "Gaussian" Correlation Functions

Although Eq. (4) yields the optimum weighting function for any type of "true" field and any uncorrelated "error" field of smaller scale, it is readily appreciated that numerical calculations of the transforms of the correlation functions and the weighting function itself are extremely laborious, if the correlation functions are determined empirically. Accordingly, in order to gain a general understanding of the manner in which the optimum smoothing process depends on the statistical properties of the true field and error field, we shall assign simple and rather realistic analytic forms to the autocorrelation functions $E(\varrho)$ and $\gamma(\varrho)$. By its nature, the normalized autocorrelation function attains a maximum value of unity at $\varrho = 0$, and has zero slope at $\varrho = 0$. Moreover, since the fields under consideration are not genuinely periodic, one would expect that the correlation function decreases monotonically to zero with increasing ϱ. The rate at which it decreases will depend, of course, on the "scale" of the field . . . i.e., a typical distance over which the field has the same sign. These considerations suggest that the "shapes" of the normalized autocorrelation functions might be closely approximated by that of the Gaussian error function. That is,

$$\frac{E(\varrho)}{E(0)} = e^{-a^2\varrho^2} \qquad \frac{\gamma(\varrho)}{\gamma(0)} = e^{-b^2\varrho^2}$$

where a and b are inverse measures of the scale of the fields $\varepsilon(x, y)$ and $g(x, y)$, respectively. For correlation functions of this type, the optimum weighting function is approximately[1]

$$K(R) = \left(\frac{\alpha^2}{2\pi}\right) \frac{1}{\alpha R} J_1(\alpha R) =$$

$$= \frac{\alpha^2}{4\pi} [J_0(\alpha R) + J_2(\alpha R)] \qquad (5)$$

in which $\alpha = (\ln 1/\lambda^2)^{1/2}/p$, $\lambda = kb/a$, and $p^2 = (a^2 - b^2)/4\ a^2b^2$. The formula above gives the weighting function for the types of fields normally encountered.

IV. Dependence of the Degree of Smoothing on Scale and "Noise-to-Signal" Ratio

Since the precise form of the weighting function is probably not critical, the greatest interest centers on the optimum *degree* of smoothing. The latter depends on the scale parameter α, which is inversely proportional to the effective radius of the domain of averaging. The manner in which the degree of smoothing depends on the characteristics of the true field and error field is shown in Fig. 1, on which $5\ \alpha d$ (as computed from Eq. 5) is plotted as a function of the signal-to-noise ratio and the ratio of the scales of the true field and error field. (The length d is a typical distance between adjacent observing stations.) This diagram illustrates the points that were made earlier . . . namely, that the field of observations should not be smoothed if the signal-to-noise ratio is extremely large (i.e., if the error is very small), or when the scales of the true field and the error field are comparable. Otherwise, the most striking feature of these results is that the optimum degree of

[1] This approximation is best when $k \ll 1$ and $a \gg b$. It does not deviate from exact results by more than a few percent when $k = .4$ and $a/b = 4$, except when R is large . . . in which case the weighting function has already become negligibly small. When the "noise-to-signal" ratio k is very large, Eq. (4) reduces to

$$K(R) = \frac{1}{4\pi p^2}\ e^{\exp};\ \exp = \frac{-R^2}{4p^2}$$

This shows that the optimum degree of smoothing is independent of noise level when the "noise-to-signal" ratio is very large. As is intuitively evident, the best strategy in this case is to smooth very strongly . . . provided, of course, that the scale of the true field is greater than that of the error field.

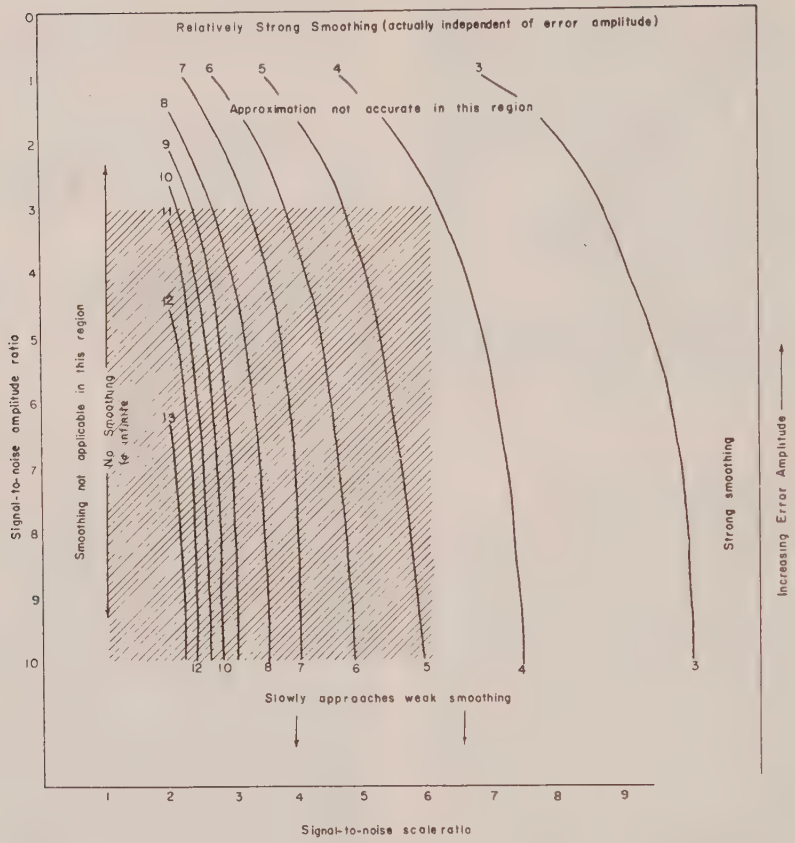
Relatively Strong Smoothing (actually independent of error amplitude)
Approximation not accurate in this region
Smoothing not applicable in this region
No Smoothing (∞ infinite)
Strong smoothing
Increasing Error Amplitude
Slowly approaches weak smoothing
Signal-to-noise amplitude ratio
Signal-to-noise scale ratio

Fig. 1. Reciprocal of effective radius of domain of averaging (in nondimensional units) as a function of scale ratio and signal-to-noise ratio. Shaded area covers a typical range of values under ordinary meteorological conditions.

smoothing depends very strongly on the scale ratio, the effective radius of the domain of averaging being 4 times as great for a scale ratio of 10 as it is for a scale ratio of 2.

With reference to meteorological variables, the ratio of the scale of the true field to that of the error field probably ranges from 3 to about 6 *over areas of good data coverage*, and from 1 or 3 *over the oceans*. The signal-to-noise ratio probably varies from about 10 for the long planetary waves to about 3 for minor synoptic features of shorter wavelength. The region of relative scale and noise level delineated by these ranges is the shaded area in Fig. 1. As is readily seen, the optimum effective radius of the domain of averaging may vary by a factor of 3, a fact that should be taken into account in the analysis of meteorological data. It is also likely, of course, that a skilled analyst introduces qualitative considerations of a similar nature in deciding how much weight is to be assigned to any single piece of data in an irregularly spaced network of observations. It is a matter of some interest, therefore, to compare the results of optimum smoothing with those of the subjective smoothing practiced by an experienced analyst.

V. A Comparison of Optimum Smoothing With Subjective Smoothing

In order to compare the subjective and optimum processes of smoothing from the standpoint of minimizing the RMS difference between the true field and the smoothed data field, both processes were applied to the same synthetic field of "observations", consisting of an artificially constructed "error" field

superimposed on a specified true field. For purposes of isolating differences due to method alone, it is sufficient to deal with an assumed true field that is more or less typical of real meteorological conditions. Accordingly, a set of height values at the points of a square grid, interpolated to the nearest 10 feet between the contours shown in Fig. 2 (a), were regarded as correct. The contours had been drawn to fit real data for 1500Z, 22 April 55 . . . a case that was deliberately selected as one in which the spectrum of wave components was fairly broad.

The "error" field was constructed by matching a random sequence of errors to a predetermined sequence of gridpoints, spaced about 200 miles apart. The sequence of errors was formed by letting each two-digit group in a list of random numbers determine the magnitude and sign of each error in the sequence. The correspondence between the sequences of errors and random numbers was arranged in such a way that the frequency distribution of errors is normal, with an RMS error of 100 feet. The "error" field so formed is fairly typical of the *combined* fields of instrumental, reading, height evaluation, and roundoff errors, although somewhat exaggerated to accentuate differences of method.[1]

The "observations" at the gridpoints were obtained simply by adding the "error" field to the assumed true field. The resulting field of observations was then analyzed by an experienced meteorologist, who was informed that the field contained random errors with a normal frequency distribution and RMS error of 100 feet, but who did not have access to the true field. The same field of observations was also subjected to the process of optimum smoothing, by computing the weighted average for each gridpoint as a weighted sum of the "observed" heights at that point and at the 20 points nearest to it. The weighting factors were calculated from Eq. (5); the scale ratio and signal-to-noise ratio were estimated from the computed autocorrelation functions for the assumed true field and the artificial error field.

The results of this experiment are summarized in Figures 2 (b) and (c), which show the subjectively smoothed and "optimum" averaged fields, respectively. These are to be compared with Figure 2 (a), which shows the

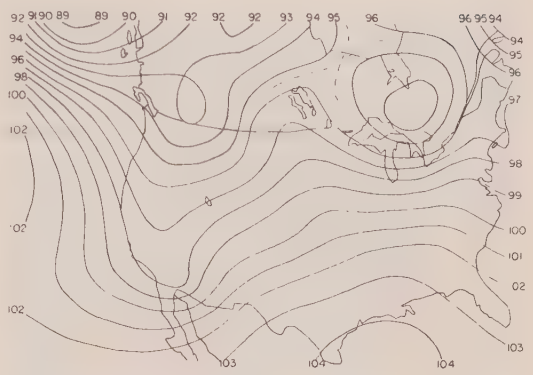

2 a.

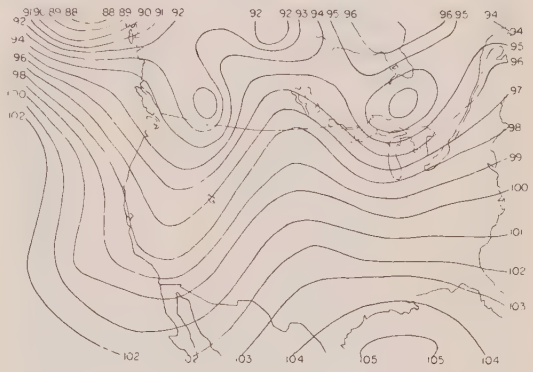

2 b.

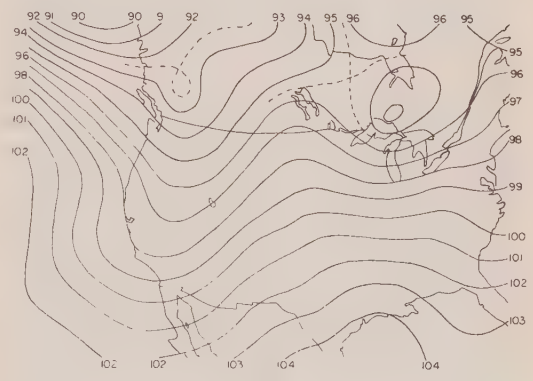

2 c.

Fig. 2. Contours of 700 millibar surface (100 foot height intervals) for 1 500 Z, 22 April 1955 corresponding to: (a) the "true" height field (b) the subjectively smoothed "height-plus-error" field and (c) the optimum averaged "height-plus-error" field.

[1] The mean square total error is approximately the sum of the mean squares of the individual types of error, provided different types of error are not highly correlated.

corresponding "true" field. In general, it appears that the subjective process of "analysis" and the optimum averaging process perform the function of smoothing in approximately the same way, since the subjectively smoothed and optimum averaged fields are quite as similar to each other as either is to the true field. Each of them removes fluctuations whose wave lengths are comparable with twice the distance between observation points (e.g., the component with wavelength about 900 kilometers, associated with the rather "square" trough and ridge over the northwestern U.S.) but retains the large-scale features of greater amplitude. Both produce about the same *degree* of smoothness.

Over most of the area considered, there is no significant and systematic difference between the two smoothed fields. Over the southeastern quadrant, however, the subjectively smoothed field is noticeably smoother than the optimum average ... too smooth, in fact, to reproduce the very weak trough in the southwest flow over western U.S. (where it actually shows anticyclonic contour curvature), or the shallow trough along the east coast. The optimum average, on the other hand, does reflect these minor synoptic features, though with somewhat reduced amplitude. The most obvious reason for this difference is that the scale of the features mentioned above is considerably less than that of the large-scale pattern, but is still somewhat greater than twice the distance between observation points. Even a skilled analyst probably finds it difficult to distinguish qualitatively between random small-scale fluctuations and real disturbances of only slightly larger scale and comparable amplitude and, for this reason, thinks in terms of fluctuations whose amplitude and scale are perceptibly greater. The optimum smoothing process, however, does distinguish between random and real fluctuations ... provided the scale of the latter is greater than that of the error field, and if the existence of small-scale disturbances is reflected in the autocorrelation function for the true field. In short, whatever difference there is between the subjective and optimum processes of smoothing is probably due to differences in the fidelity with which they reproduce fluctuations whose scale is intermediate between that of the error field and the major synoptic features of the true pattern. That there is a significant difference in performance is revealed in the RMS errors of the smoothed fields ... 52 feet in the case of subjective smoothing, and 42 feet for optimum smoothing.

VI. The Information Value of a Network of Data in Smoothing Out Nonsystematic Error

It was emphasized earlier that the mean square error of the smoothed field is expressible in terms of the autocorrelation functions ... which, in the cases studied here, are assumed to have the form of the Gaussian error function. Since the optimum weighting function for this type of autocorrelation function is now known, it is possible to calculate the minimum RMS error attainable by "linear" smoothing, which is a measure of the maximum amount of information about the true field that can be extracted from an error-contaminated field of observations. Substituting from Eq. (5) into Eq. (1), we may write the minimum mean square error $I_{\min}$ of the smoothed field as:

$$I_{\min} = \gamma(0)\left\{\left(\frac{k}{S}\right)^{\frac{2S^2}{S^2-1}} + k^2\left[1 - \left(\frac{k}{S}\right)^{\frac{2}{S^2-1}}\right]\right\} \quad (6)$$

in which $S = a/b$. It has been shown previously that there are two cases in which the data field should not be smoothed ... namely, when there is no error, or when the true field and the error field are of the same scale. In the former case ($k = 0$), Eq. (6) verifies that the mean square error of the "smoothed" field (or, more precisely, the unsmoothed field) is zero. In the latter case ($S = 1$), Eq. (6) reduces to:

$$I_{\min} = k^2\,\gamma(0) = \frac{E(0)\,\gamma(0)}{\gamma(0)} = E(0)$$

This simply shows that the minimum mean square error of the "smoothed" field in the case when $S = 1$ is the mean square error of the reported measurements.

The general way in which the minimum RMS error of the smoothed field depends on the spacing of observation stations is illustrated in Figure 3, on which the RMS error (expressed as a fraction of the RMS error of reported measurements) is plotted as a function

of the scale ratio. Since the optimum weighting function does not change markedly with varying noise-to-signal ratio, the calculations were carried out for a single typical value of k, equal to one-tenth. Figure 3 shows that the minimum RMS error is reduced only slightly by increasing the density of the observing stations if the scale ratio is greater than 6, but indicates that a considerable gain in accuracy is to be made by increasing the scale ratio from 2 to about 5.

In interpreting these results, it should be borne in mind that the foregoing analysis has dealt entirely with a *continuous* true field and an error field that is *simulated* by a continuous field, whose scale is determined by the distance between *discrete* observing points. Application of the smoothing operation to data at a network of discrete points requires that the weighted average of *continuous* observations over a ring-shaped region of finite width be approximated by the unweighted average of the observations at *discrete* points in the ring, multiplied by the integral of the weighting function taken over the ring. This approximation is clearly best when the number of observations in the effective domain of averaging is large enough to constitute a representative sample of nonsystematic errors, and when the width of the ring is much less than the scale of the true field. Both of these conditions, of course, are enhanced by a large scale ratio. Moreover, it is evident that the discrete point approximation is most nearly valid when applied at the observation points, where bona fide data figure most heavily in the smoothed field. This simply means that the use of the smoothing process as a combined operation of smoothing and interpolation does not result in any more real information about the *detail* of the true field than is revealed in the original observations.[1] In short, one must distinguish between the value of a network of observations as a means of resolving the detailed structure of the true field, and its value as a means of reducing nonsystematic error at each point of the network. At present, of course, we are concerned solely with the latter.

[1] This is especially obvious in the case of no error, when the weighting function is zero everywhere, except at the origin.

Despite these cautionary remarks, the results of an analysis of continuous smoothing may be used to estimate the gain of information (reduction of error) that can be expected from averaging data at discrete points. According to Figure 3, a good compromise between accuracy and economy is attained when S is about 5, which corresponds to a linear density of about 15 stations spread over a characteristic wavelength of the true field.

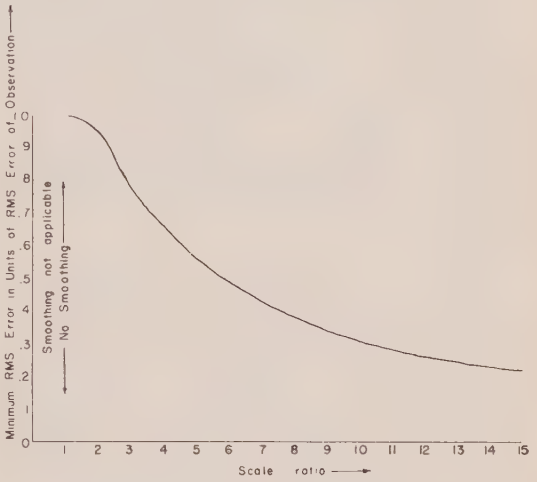

Fig. 3. Residual RMS error of the optimum smoothed field (in units of RMS error of observations) as a function of scale ratio. The signal-to-noise ratio was taken as 10.

For typical wavelengths of disturbances in the flow aloft, a reasonable spacing of stations is around 200 miles. It should be pointed out, however, that it is undoubtedly more economical to reduce the errors of the smoothed field by reducing the errors of reported measurement, rather than by smoothing over a very dense network.

The remaining problem . . . that of estimating the information value of a network of essentially error-free observations . . . clearly involves the details of the use to which the data are put. For example, if the observations are to be used as initial data for a numerical forecast, the information value of the network depends on the errors of approximating derivatives by finite differences over a typical distance between neighboring observation stations. Such considerations are beyond the scope of the present paper.

VII. Summary and Conclusions

This paper has dealt exclusively with the problem of smoothing out nonsystematic errors of reported measurements or other small-scale fluctuations that are random with respect to fields of larger scale. By extending Wiener's methods for smoothing stationary time series to two-dimensional fields whose autocorrelation functions are invariant with rotation, it has been found possible to define and analyze an "optimum" linear smoothing process . . . "optimum" in the sense that the RMS difference between the true and smoothed fields is the least. The optimum smoothed field is essentially a weighted area average, whose weighting function is determined by the "signal-to-noise" ratio and the autocorrelation functions for the true field and "error" field.

The form of the optimum weighting function has been investigated in detail for fields whose autocorrelation functions have the shape of the Gaussian error function . . . a type that is more or less characteristic of aperiodic fields. In this case, the optimum weighting function is a linear combination of Bessel functions, whose rate of decrease away from the origin depends on the signal-to-noise ratio, the ratio of the scales of the true field and "error" field, and the distance between neighboring observation stations. The manner in which the radius of the effective domain of averaging depends on the scale ratio and the signal-to-noise ratio substantiates two conclusions that were previously established under more general conditions . . . namely, that the field of observations should not be smoothed at all if the noise-to-signal ratio is very small (in which case there is obviously nothing to gain by *smoothing*) or if the scale of the true field is the same or less than that of the "error" field (when reduction of error cannot be attained by *smoothing*, without simultaneously reducing the amplitude of the true field in the same or greater degree). When the signal-to-noise ratio is very small, the optimum degree of smoothing approaches a limit that is independent of noise level; in this case, the best strategy is to average over a very large region, whose effective radius is determined by the relative scales of the true field and error field. In the normal range of signal-to-noise ratio, the optimum radius of the effective domain of averaging depends most strongly on the scale ratio, varying by a factor of 3 or 4 from one extreme to another. Although a skilled analyst probably introduces qualitative considerations of a similar nature in smoothing observations over an irregularly spaced network of stations, it is suggested that the objective and quantitative character of the optimum linear smoothing process may prove advantageous from the standpoint of maintaining consistently high performance over a variety of ordinary situations.

The subjective and "optimum" processes of smoothing have been applied to the same synthetic field of "observations", consisting of an artificial field of random errors superimposed on an assumed (but fairly typical) "true" field. Comparisons between the two smoothed fields, and between each smoothed field and the "true" field show that the two different processes accomplish about the same type and degree of smoothing. In the one case presented here, the only significant difference was a reflection of the fact that the optimum smoothing process is more capable of distinguishing small-scale random fluctuations from minor synoptic features of only slightly greater scale. The RMS errors of the subjectively smoothed field and the optimum average were 52 and 42 feet, respectively, indicating that the optimum linear smoothing process can probably match the performance of a skilled analyst, and may exceed it.

Finally, the minimum RMS error of linearly smoothed fields has been expressed in terms of the signal-to-noise ratio, the standard deviation of the "true" field, and the scale ratio (which, in turn, depends on the spacing of observation stations). This result shows that the information value of a network of observations can be enhanced considerably by increasing the linear density of observing stations from 6 to about 15 per wavelength, but is not substantially increased beyond a linear density of 18 stations per wavelength. It is to be emphasized that this conclusion applies only to the information value of a network from the standpoint of smoothing out nonsystematic error, and does not bear directly on the problem of interpolation or of reducing truncation error.

Acknowledgement

The author gratefully acknowledges his indebtedness to Dr H. M. Mott-Smith of Norden Laboratories for several valuable and illuminating discussions of this problem, and particularly for pointing out a number of general properties of the Fourier-Bessel (or Hankel) transforms of correlation functions.

Thanks are also due to Mr E. B. Fawcett of the Joint Numerical Weather Prediction Unit for his careful subjective analysis of the synthetic field of observations referred to in Section 5.

REFERENCE

WIENER, N., 1949: *Extrapolation, Interpolation, and Smoothing of Stationary Time Series*. Technology Press of Massachusetts Institute of Technology, Cambridge, Mass. 163 pp.

A Relation between Meteor Showers and the Rainfall of November and December

By E. G. BOWEN, Division of Radiophysics, Commonwealth Scientific and Industrial Research Organization, Sydney, Australia

(Manuscript received February 8, 1956, revised March 22, 1956)

Abstract

An examination is made of the November and December rainfall of approximately 300 stations distributed over the globe. Six singularities are found, five of which occur about 30 days after prominent meteor showers. This result is similar to one which has already been reported for the month of January. The remaining singularity on November 26 could be due to a daylight meteor stream from the direction of Virgo which has just been discovered in the Southern Hemisphere.

One of the better known meteor showers during the period investigated, namely the Giacobinids is known to have an orbital period of 6.6 years. A similar recurrence tendency is found in the rainfall 30 days later.

1. Introduction

In a recent paper (BOWEN, 1956) the hypothesis was advanced that the rainfall of many parts of the world is influenced by the earth's passage through streams of dust in the solar system. It was shown that if the daily rainfall records of a sufficiently large number of stations were totalled for the month of January, they did not result in a smooth curve approximating to the mean January rainfall, but tended to show well defined maxima on certain calendar dates. The dates of these maxima showed a close correspondence for regions separated both in latitude and longitude and they occurred approximately thirty days after prominent meteor showers. It was suggested that the phenomenon was due to the nucleating effect of the dust associated with meteor streams falling into the cloud systems of the lower atmosphere.

This hypothesis was first put forward in a preliminary note (BOWEN, 1953) which was subsequently criticized in rather severe terms by SWINBANK (1954), MARTYN (1954), NEUMANN (1954) and by M. B. and V. J. OLIVER (1955). The basis of these criticisms was that the variations in rainfall were not real and could be accounted for as normal statistical fluctuations or, alternatively, any variations which did take place could be accounted for in terms of well-known climatological phenomena. It is not proposed to deal with these criticisms in detail in the present paper except to point out that each of these authors based his opinion on an extremely small amount of data. The investigation of a world-wide effect

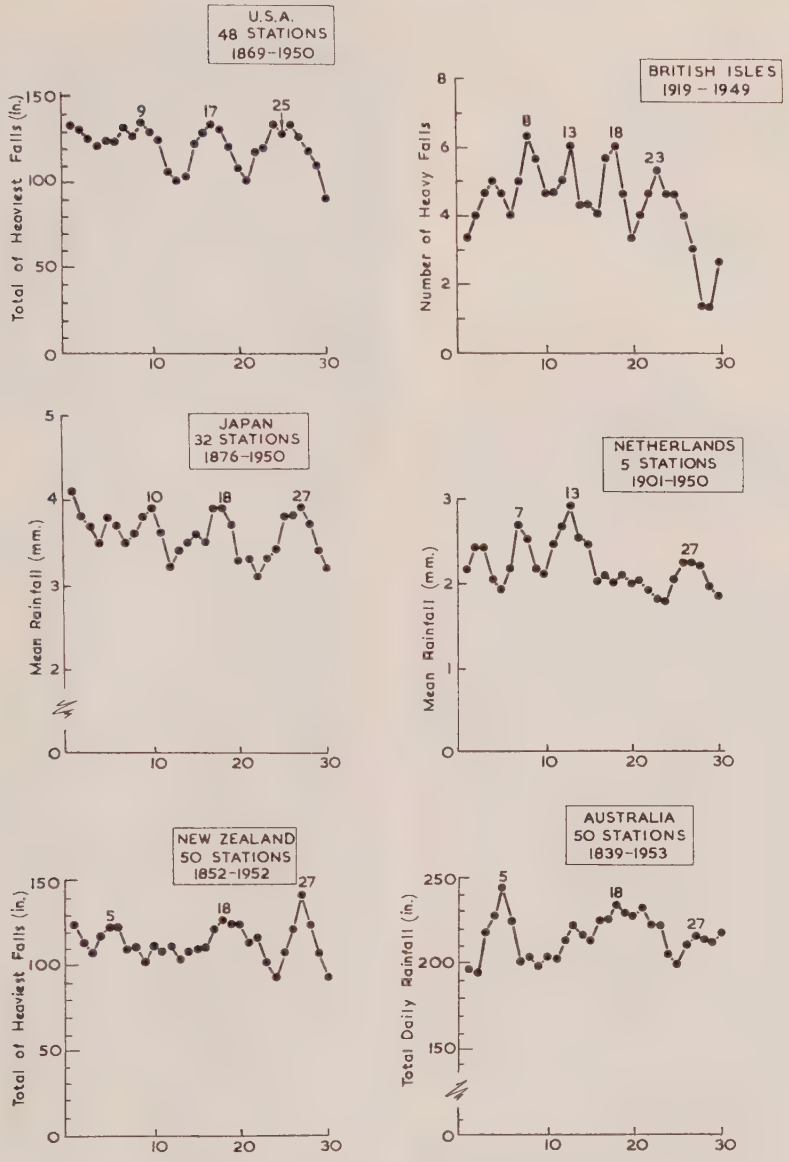

Fig. 1. Rainfall curves for the month of November for U.S.A., Great Britain, Japan, Netherlands, New Zealand and Australia.

calls for the study of a large amount of data from widely separated points. Swinbank, however, referred to the rainfall records of only three stations, Melbourne, Madras and Nagapattinan, while the Olivers used data from a small number of stations in Kenya covering a period of only 10 years. Martyn referred to 8 stations in Australia covering a period of 6 days in one year only, namely 1911. This is approximately 1/10,000th of the amount of data given in Fig. 1 or Fig. 2 of the present paper. Neumann performed a statistical test which violates one of the first rules of time series analysis, namely that under no circumstances should the data be shuffled.

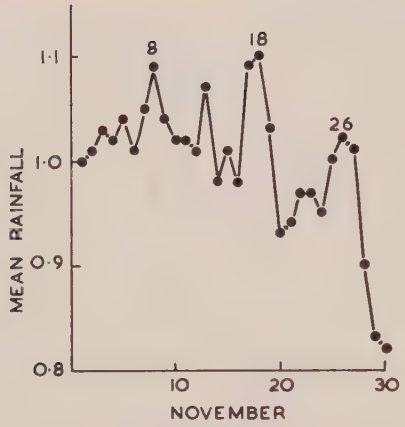

Fig. 2. The mean rainfall curve for November obtained by summing the means of all curves in Fig. 1.

It is only fair to point out that the meteor hypothesis has been commented on less critically by Riehl (1954) and by Browne, Palmer and Wormell (1954). The latter add a warning which might well have been heeded by the previous critics, namely that the "suggestion needs more than a superficial examination before a conclusion can be reached and [the] observations, if they are valid, will be hard to explain by any other theory". Dhar (1954) has published evidence that there might be a similar influence affecting the rainfall in India, while Cwilong (1955), Smith, Kassander and Twomey (1956) and Bigg (1956) have described physical measurements of the entry of meteoritic dust into the top of the atmosphere and observations of the behaviour of freezing nuclei in the lower atmosphere which either support the hypothesis or are consistent with it.

The present paper presents an analysis of the rainfall for the months of November and December which is similar to that already published for January. The choice of these months is dictated by the fact that some of the best known meteor showers occur about this time of year and their properties have been reasonably well established. Because experience has shown that it is difficult to appreciate the details of more than one month's rainfall at any time, it is proposed to treat the months separately and to assemble the results at the end of the paper.

II. Sources of data

In analysing the rainfall records of different parts of the world it would be preferable to use the identical quantity—for example, the daily rainfall or the heaviest fall of the month—for each locality. Unfortunately, records which are in precisely the required form are not easy to obtain and the records used in the present analysis are those which could most readily be obtained by mail from the respective Weather Bureaus. They refer to six widely separated regions of the globe and in every case the stations were selected by officers of the Weather Bureaus concerned. They comprise the following:—

1. The heaviest falls of the month for 48 stations in the U.S.A.
2. The falls exceeding $2^1/_2$ inches in 24 hours recorded on any of the official raingauges in Great Britain.
3. The mean daily rainfall of 32 stations in Japan.
4. The mean daily rainfall of 5 stations in the Netherlands.
5. The heaviest falls of the month for 50 stations in New Zealand.
6. The daily rainfall of 50 stations in Australia.

These data are identical with those used in the previous paper except that, in the case of Australia, figures for 50 stations distributed throughout the continent are now available and have been used in preference to those of 23 stations in the State of New South Wales. A list of stations and periods for which records are available in the first five regions was given in the Appendix to the previous paper. The corresponding list of Australian stations is given in the Appendix to the present paper. Approximately half these records date from 1907 or 1908 and the remainder from about 1880. There are a few longer records, however, notably that of Adelaide which dates from 1839. The whole have been included in the present analysis; it will be observed that the dates assigned to each region in the curves of Fig. 1 are the earliest and latest dates for which any records are available.

III. November rainfall

In Fig. 1 are given the rainfall curves of November for the above regions of the world.

As in the previous paper, these curves and those of Fig. 6 have been smoothed by taking three day running means. During the first ten days of the month the agreement between the curves is not good, but during the latter part of the month there are peaks which are grouped about November 18 in five of the six regions, and peaks grouped about November 26 in all six. Following the procedure in the previous paper, the curves have been normalized and added together giving the curve of Fig. 2. It may be taken to represent the daily variations from the November mean for approximately 300 stations distributed over the globe. It shows distinct maxima on November 18 and 26, as might be expected from the individual curves, and a third peak on November 8. There is a smaller peak on November 13 which must be regarded as of doubtful significance since there is a minimum on three of the curves on this date.

In the previous paper it was shown that the peaks in the January rainfall tend to occur about thirty days after prominent meteor showers. On this hypothesis, the meteor streams which might be expected to affect the November rainfall are the Giacobinids of October 9 and the Orionids which commence on October 20 and continue until the 23rd. It is seen that the rainfall peak of November 8 occurs exactly 30 days after the Giacobinids, and the peak of November 18 is 29 days after the date of the first appearance of the Orionids. This is in good agreement with the January results.

If the hypothesis is correct, one might also expect a meteor shower about October 27, to

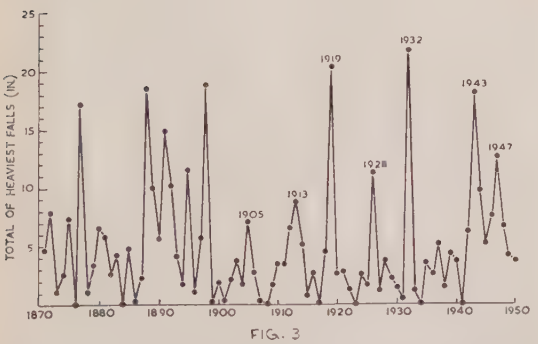

Fig. 3. The heaviest falls of the month for the three days, November 8, 9 and 10, for 48 stations in the U.S.A. from 1870 to 1950.

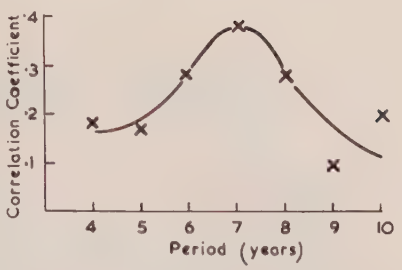

Fig. 4. Cross correlation of rainfall of U.S.A. on November 8, 9 and 10 against a saw-toothed function with period from 4 to 10 years.

account for the rainfall peak on November 26. The day and night time meteor streams of the northern hemisphere, and the night time streams of the southern hemisphere are now reasonably well known, but there is no prominent stream on this date. However, the possibility remains of a day time stream being discovered in the southern hemisphere.

It is interesting to observe that ELLYETT and ROTH (1955), in their radar observations of daytime meteors in the southern hemisphere, appear to have found a stream on about the expected date. They state that "A new shower from the direction of Eridanus is present in late June, and there appears to be a strong and quite enduring shower from the direction of Virgo over the period October 22—November 7 . . . No significant daylight activity has been found over the other months."

It will be interesting to see if future observations confirm the existence of this shower and indicate whether there is a maximum activity about the anticipated date of October 27.

The periodicity associated with the Giacobinids. —The Giacobinids are one of the meteor streams of recent origin which exhibit a marked variation in intensity from one year to the next (LOVELL, 1954). The meteors are associated with the Giacobini-Zinner comet which has an orbital period of 6.6 years. It appeared in 1900 and the earth passed very close to the tail. It was predicted that the earth would pass through the tail on its later appearances and that a display of meteors might be expected. There are reports of such meteors in 1913 and 1914 (DAVIDSON, 1915; DENNING, 1918) which are open to some doubt, but in 1926, 1933 and 1946 there were spectacular appearances which have been extensively

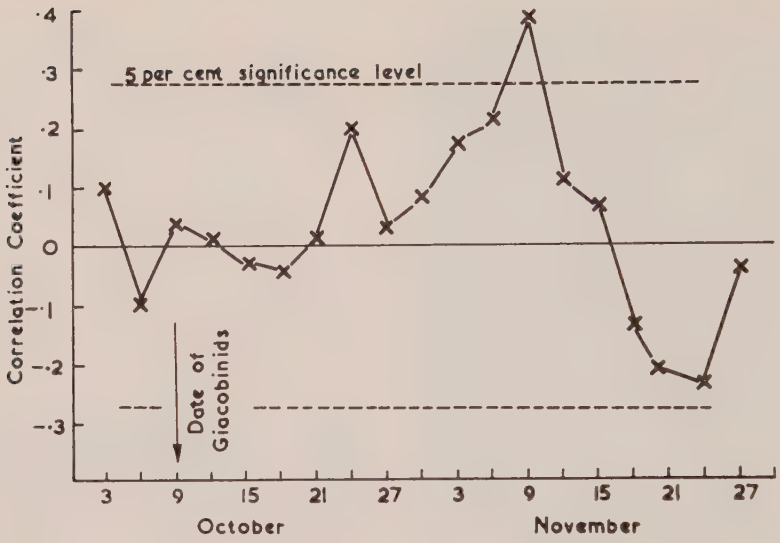

Fig. 5. Cross correlation of rainfall of U.S.A. with a sawtoothed function of period 7 years, for each successive three day period in October and November.

described. The meteors were not observed, however, in 1939.

If the rainfall thirty days after the Giacobinids were influenced by that stream it would be expected to show a similar 6 to 7-year recurrence tendency. The rainfall peak which might correspond to this shower occurs in the U.S.A. on November 9, and in Fig. 3 is given the total of the heaviest falls of the month for the 48 stations in the U.S.A. for the three days November 8, 9 and 10 for each year over the period of records. It will be seen that there is no obvious pattern prior to 1900, but commencing about 1900 the rainfall shows sharp maxima in 1905, 1913, 1919, 1926 and 1932, that is, with approximately the same period and phase as the meteor stream. There is no peak in 1939 when the meteor stream was absent, but there are other peaks in 1943 and 1947.

If there is a relation between the meteor stream and rainfall, the latter would be expected to show a significant 6 or 7-year recurrence tendency. This may be investigated quantitatively by cross correlating the rainfall against a saw-toothed function having successive values 0, 0, $^1/_2$, 1, $^1/_2$, 0, 0 etc. with gradually increasing period. The correlation coefficients between this function and the rainfall of the U.S.A. from the date of appearance of the comet, namely 1900 until 1950, are given in Fig. 4 for periods from 4 to 10 years. They fall on a smooth curve with a maximum value at 7 years. The correlation coefficients at 6 and 8 years each have a value 0.28, which is significant at the 5 per cent level. The value for a recurrence period of 7 years is 0.38, which is significant at the 1 per cent level.

The rainfall for corresponding 3-day periods before and after these three days shows no such recurrence tendency. In Fig. 5 are given the correlation coefficients against the saw-toothed function with a 7-year period, for each successive 3-day period throughout the months of October and November. They are all below the 5 per cent significance level with the exception of November 8, 9 and 10. This may be taken as supporting evidence that the rainfall of November 8, 9 and 10 is related to the Giacobinid meteor shower.

It will be interesting, when more data become available, to examine the geographical distribution of this effect over the northern and southern hemispheres. The Giacobinids are incident on the earth from declination 54° N and it is doubtful whether dust associated with this shower would reach into the southern hemisphere. It appears from the curves of Fig. 1 that the rainfall peak about November 8 is absent in the Australian and New Zeeland

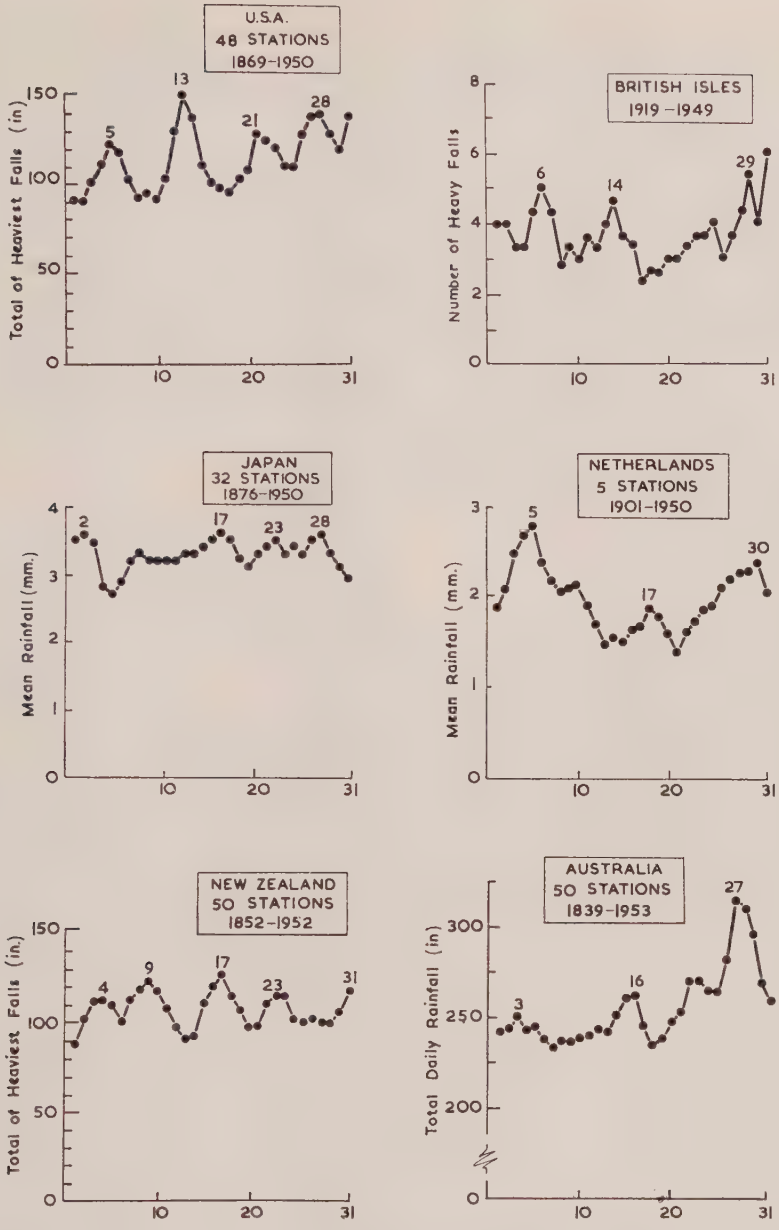

Fig. 6. Rainfall curves for the month of December for U.S.A., Great Britain, Japan, Netherlands, New Zealand and Australia.

records, but it requires data from the other two land masses in the southern hemisphere before this point can be adequately investigated.

Before proceeding, there are several features of Fig. 3 which should be remarked upon. In the first place it is interesting that the effect on rainfall appears to have started about the same time as the appearance of the comet and before visible meteors were observed. This suggests that the dust which is influencing rainfall is not in quite the same orbit as the visible meteors, a result which is similar to that

already obtained with the Bielids (BOWEN, 1956). In the same way, although there is a good statistical relation between the period and phase of the visible meteors and the rainfall, there is not always exact agreement in the dates of the maxima. For example, the visible meteors made a strong appearance in 1933 but the rainfall peak appeared in 1932. This suggests that the earth passed through the dust which was capable of affecting rainfall in 1932 but did not pass through the larger particles which give visible meteors until it had returned to the same position in its orbit a year later.

Finally, it is interesting to observe in Fig. 3 the depth of the rainfall minima during periods when the meteoritic dust is presumably absent, and the exceptional magnitude of the peaks when it is present.

IV. December rainfall

In Fig. 6 are given the rainfall curves for the month of December for the same regions as in Fig. 1. The agreement between the individual curves is not as close as for November and January but peaks appear in five out of the six regions on dates distributed around December 4, and in all six regions about December 29. Combining the curves by addition of the daily means gives the curve of Fig. 7, in which it is seen that three peaks occur on December 5, 14 and 29 respectively.

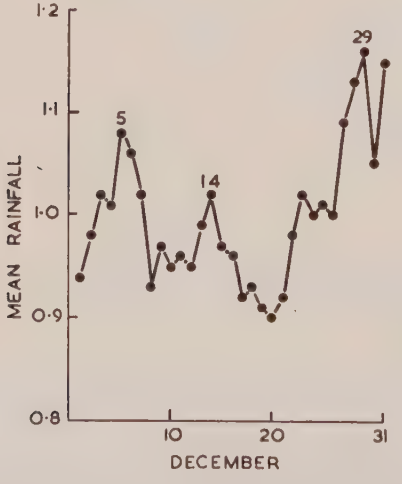

Fig. 7. The mean rainfall of December obtained by summing the means of all curves in Fig. 6.

The meteor showers which might influence the December rainfall are the Taurids, the Leonids and the Bielids. The Taurids are of relatively long duration, commencing on November 3 and continuing until November 10. If the date of commencement is arbitrarily taken as the basis of reference, the rainfall peak on December 5 occurs 32 days later, in fair agreement with the results for November and January. The Leonids have been known for hundreds of years and occur on November 16. This is 28 days before the peak on December 14, also in fair agreement with the previous results. The rainfall peak of December 29 has already been related to the Bielids I (BOWEN, 1956) and will not be discussed further.

V. Summary

It appears therefore that there are peaks in the world rainfall during November and December which occur approximately 30 days after prominent meteor showers. This is consistent with the hypothesis, which was arrived at from a study of the January rainfall, that dust associated with meteor streams is affecting world rainfall.

In Fig. 8 is given a composite curve of the rainfall for the three months November, December and January, obtained by combining Figs. 2 and 7 of the present paper with Fig. 4 of the previous one. It may be taken to represent the departure of daily rainfall from the mean for approximately 300 stations over many parts of the world. In table 1 are listed

Table 1. Comparison of dates of meteor streams and rainfall peaks

Date of rainfall peak		Meteor Stream	Date	Time Difference (days)
November	8	Giacobinids	Oct. 9	30
	18	Orionids	20—23	29
	26	Not known with certainty		—
December	5	Taurids	Nov. 3—10	32
	14	Leonids	16	28
	29	Bielids I	27→15	—
January	1	Bielids II	Dec. 2	30
	12	Geminids	13	30
	22	Ursids	22	31
February	1	Quadrantids	Jan. 3	29

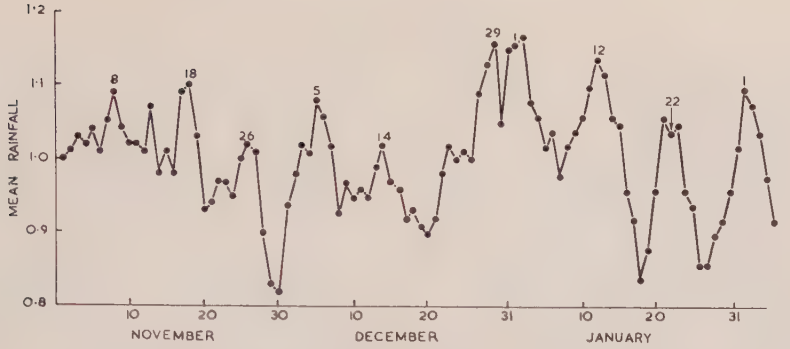

Fig. 8. Composite curve giving the daily mean rainfall of approximately 300 stations over the globe for the three months, November, December and January.

the dates on which rainfall singularities appear, together with the meteor showers which are thought to be associated with them. In the final column is given the time difference between the dates of the meteor showers and that of the rainfall peaks. They have a mean value of 30 days, the greatest departures from this value being ± 2 days.

VI. Discussion

There are many aspects of the present hypothesis which are difficult to accept and many questions arise. How does the amount of dust entering the atmosphere vary from one day to the next, why is the effect on rainfall confined to such a few days and why is the time of fall so consistent from one meteor shower to the next. These questions are without specific answers at the present time and they are all clearly in need of careful physical investigation.

Easily the most unsatisfactory part of the hypothesis is concerned with the fall of the dust through the atmosphere. The particles entering the atmosphere would be expected to have a wide range of sizes and a correspondingly wide distribution of fall times. However, the postulated effect on rainfall is a trigger effect, so that a sharp advancing front in the dust arriving at the lower atmosphere would be adequate to account for a peak in the rainfall.

The variation of only ± 2 days in the fall time given in the last column of table 1 is less difficult to understand. Each observation of the time difference between a meteor shower and a rainfall peak in this table is the mean of some 20,000 individual observations. The variation in any one place and in any one year would obviously exceed this figure.

Whipple (1954) has expressed the opinion that the flux of meteoritic dust entering the atmosphere is almost constant and increases only by a small percentage at the time of meteor showers. However, in a recent publication Bigg (1956) described a simple method of detecting the entry of meteoritic dust into the top of the atmosphere. He showed that there were variations in the amount of this dust of the order of 5 to 1 from one day to the next and that these variations were closely correlated with meteor showers.

This paper has been principally concerned with the information which can be gleaned from a study of rainfall data but there are clearly limitations to this method. For real advances to be made one must look to proper physical investigations of the behaviour of meteoritic dust in the atmosphere. The arrival of the dust at the top of the atmosphere can be detected by Bigg's "twilight" technique. Its behaviour as a nucleating agent in the lower atmosphere can be studied by measuring the freezing nucleus concentration in the manner described by Cwilong (1955) and Smith, Kassander and Twomey (1956). It would seem of greatest importance to the science of meteorology that an intensive study of the time variations of these quantities be made in different parts of the world.

Acknowledgement

The author would like to thank Mrs. Beazley for her great help in analysing the records.

REFERENCES

Bigg, E. K., 1956: The detection of atmospheric dust and temperature inversions by twilight scattering. *Nature*, **177**, pp. 77—79.

Bowen, E. G., 1953: The influence of meteoritic dust on rainfall. *Aust. J. Phys.*, **6**, pp. 490—497.

Bowen, E. G., 1956: The relation between rainfall and meteor showers, *J. Meteor.* **13**, pp, 142—151.

Browne, I. C., Palmer, H. P., and Wormell, T. W., 1954: The physics of rainclouds. *Quart. J. Roy. Meteor. Soc.*, **80**, pp. 291—327.

Cwilong, B. M., 1955: Abnormal freezing nuclei in the atmosphere. *Nature*, **176**, pp. 129—130.

Davidson, M., 1915: Meteor radiants from debris of comets. *J. Brit. Astronom. Assoc.*, **25**, pp. 292—293.

Denning, W. F., 1918: Giacobini's comet of 1900 and a connected meteoric shower. *J. Brit. Astronom. Assoc.*, **28**, p. 229.

Dhar, O. N., 1954: Meteoric dust and rainfall. *Indian J. Meteor. Geophys.*, **5**, pp. 356—357.

Ellyett, C. D., and Roth, K. W., 1955: The radar determination of meteor showers in the Southern Hemisphere. *Aust. J. Phys.*, **8**, pp. 390—401.

Lovell, A. C. B., 1954: *Meteor Astronomy*, Oxford, Clarendon Press, 463 pp.

Martyn, D. F., 1954: Comments on a paper by E. G. Bowen entitled "The influence of meteoritic dust on rainfall". *Aust. J. Phys.*, **7**, pp. 358—364.

Neumann, J., 1954: Fluctuations of long-period accumulations of daily rainfall amounts. *Aust. J. Phys.*, **7**, pp. 522—526.

Oliver, M. B. and V. J., 1955: Rainfall and stardust. *Bull. Amer. Meteor. Soc.*, **36**, pp. 147—151.

Riehl, H., 1954: *Tropical Meteorology*, New York, McGraw-Hill, 392 pp.

Smith, E. J., Kassander, A. R., and Twomey, S., 1956: Measurements of natural freezing nuclei at high altitudes. *Nature*, **177**, pp. 82—83.

Swinbank, W. C., 1954: Comments on a paper by E. G. Bowen entitled "The influence of meteoritic dust on rainfall". *Aust. J. Phys.*, **7**, pp. 354—358.

Whipple, F.: Seminar Discussion at U.S. Weather Bureau, Washington, D.C., January 1954.

Appendix

List of 50 rainfall stations in Australia used in Figs. 1 and 6 and dates for which rainfall figures are available.

New South Wales	
Sydney	1859—1952
Goulburn	1857—1954
Forbes	1875—1954
Armidale	1858—1954
Narrabri	1870—1954
Port Macquarie	1870—1954
Dubbo	1870—1954
Wagga	1871—1950
Bathurst	1858—1954
Cooma	1858—1954
Queensland	
Brisbane	1900—1953
Mackay	1907—1953
Gladstone	1907—1952
Charleville	1907—1953
Roma	1907—1952
Stanthorpe	1907—1952
Aramac	1887—1948
Hughenden	1907—1952
Cunnamulla	1907—1952
Palmerville	1908—1952
Townsville	1913—1952
Camooweal	1907—1952
Burketown	1908—1952
Victoria	
Melbourne	1859—1954
Orbost	1883—1954
Echuca	1881—1954
Wangaratta	1878—1954
Stawell	1865—1954
Tasmania	
Hobart	1908—1954
Lake Leake	1908—1953
Burnie	1908—1953
Cressy	1908—1953
Thule	1908—1953
Queenstown	1908—1953
South Australia	
Adelaide	1839—1954
Clare	1882—1953
Port Lincoln	1884—1954
Streaky Bay	1878—1953
Mount Gambier	1861—1953
Western Australia	
Perth	1880—1952
Albany	1907—1954
Bunbury	1907—1954
Esperance	1907—1954
Geraldton	1907—1952
Marble Bar	1901—1953
Katanning	1907—1953
Wyndham	1907—1953
Mt. Florence	1907—1954
Northern Territory	
Darwin	1869—1951
Daly Waters	1880—1949

Entraînement d'air humide saturé contenant de l'eau liquide dans une masse d'air humide saturé contenant de l'eau liquide

Par L. DUFOUR, Institut Royal Météorologique, Uccle, Belgique

(Manuscript received January 19, 1956)

Abstract.

In the present work, on the basis of the first principle of thermodynamics, we establish the law of variation of temperature with pressure in a saturated mass sphere containing liquid water into which saturated air containing also liquid water penetrates.

Admitting that the considered mass of air and the air which is introduced into it form a closed system, the problem consists in the study of the adiabatic transformations of a polytherm closed system.

Owing to a few hypothesis (cf (24) and (28)), we obtain formula (35) which is a particular case of the formula (36) to which leads the study of the entrainment of non saturated air into a cumulus.

Taking the example of a buble which moves in the middle of a cumulus, we show that the rate of variation of temperature with pressure is, to the first approximation, that of the standard adiabatic.

Pour expliquer la formation des cumulus, SCORER et LUDLAM (1953) ont proposé une théorie dans laquelle ils supposent entre autres que des masses d'air, qu'ils appellent des bulles, se déplacent vers le haut dans le nuage en se mélangeant à l'air ambiant.

L'étude thermodynamique de ce problème peut être envisagée de la façon suivante. Supposons:

1°) que la bulle est composée d'air humide saturé contenant de l'eau liquide et qu'elle constitue un système ouvert;

2°) que l'air ambiant, entraîné dans la bulle, est constitué d'air humide saturé contenant de l'eau liquide et qu'il constitue également un système ouvert;

3°) que l'ensemble formé par ces deux systèmes ouverts constitue un système fermé dans lequel se produisent des échanges d'air sec, de vapeur d'eau et d'eau liquide;

4°) que les transformations de ce système fermé sont adiabatiques.

D'après ces hypothèses, l'étude thermodynamique de l'entraînement de l'air dans une bulle se ramène à celle des transformations adiabatiques d'un système fermé polytherme formé d'un système ouvert prime (bulle) déterminé par la température T', la pression p et les masses m'_a, m'_v, m'_e de l'air sec, de la vapeur d'eau et de l'eau liquide et d'un système ouvert seconde (air entraîné dans la bulle) déterminé par la température T'', la pression p et les masses m''_a, m''_v, m''_e d'air sec, de vapeur d'eau et d'eau liquide.

Posons

$$m_a = m'_a + m''_a, \quad m_v = m'_v + m''_v, \quad m_e = m'_e + m''_e \qquad (1)$$

L'air sec étant un constituant inerte et le système constitué par l'ensemble des deux systèmes prime et seconde étant fermé, on a

$$\left.\begin{aligned} dm_a &= dm'_a + dm''_a = 0, \\ dm_v + dm_e &= dm'_v + dm''_v + dm'_e + dm''_e = 0, \end{aligned}\right\} \qquad (2)$$

d'où il résulte que des six variables massiques déterminant le système polytherme, quatre seulement sont indépendantes.

Désignons par h'_a, h'_v, h'_e et h''_a, h''_v h''_e les enthalpies spécifiques des constituants dans les phases prime et seconde; on a (cf. par exemple, VAN MIEGHEM et DUFOUR, 1948, §22)

$$\left.\begin{aligned} h'_a &= h^\circ_a + c_{pa}(T' - T_0), \\ h'_v &= h^\circ_v + c_{pv}(T' - T_0), \\ h'_e &= h^\circ_e + c_{pe}(T' - T_0), \end{aligned}\right\}$$
$$\left.\begin{aligned} h''_a &= h^\circ_a + c_{pa}(T'' - T_0), \\ h''_v &= h^\circ_v + c_{pv}(T'' - T_0), \\ h''_e &= h^\circ_e + c_{pe}(T'' - T_0), \end{aligned}\right\} \qquad (3)$$

où h°_a, h°_v, h°_e sont les enthalpies spécifiques à la température T_0 et c_{pa}, c_{pv}, c_{pe} sont les chaleurs spécifiques à pression constante de l'air sec, de la vapeur d'eau et de l'eau liquide.

Rappelons que les enthalpies des deux systèmes prime et seconde sont données par les relations

$$\left.\begin{aligned} H' &= m'_a h'_a + m'_v h'_v + m'_e h'_e, \\ H'' &= m''_a h''_a + m''_v h''_v + m''_e h''_e. \end{aligned}\right\} \qquad (4)$$

Rappelons également la forme que prend l'expression de la chaleur de vaporisation de l'eau; on a, à la température T' et à la température T''

$$L'_v = h'_v - h'_e, \quad L''_v = h''_v - h''_e \qquad (5)$$

d'où il résulte, compte tenu de (3), que

$$L''_v = L'_v - (c_{pv} - c_{pa})(T' - T''). \qquad (6)$$

L'équation différentielle des transformations adiabatiques du système fermé s'écrit

$$d(H' + H'') - (V' + V'')dp = 0 \qquad (7)$$

où V' et V'' sont les volumes des systèmes prime et seconde.

Compte tenu de (2), (3), (4) et (5), l'équation (7) prend la forme suivante

$$\begin{aligned} &(m'_a c_{pa} + m'_v c_{pv} + m'_e c_{pe})\,dT' + \\ &+ (m''_a c_{pa} + m''_v c_{pv} + m''_e c_{pe})\,dT'' + \\ &+ L'_v(dm'_v + dm''_v) + (T'' - T') \times \\ &\times (c_{pa}dm''_a + c_{pv}dm''_v + c_{pe}dm''_e) - (V' + V'')dp = 0 \end{aligned} \qquad (8)$$

Négligeons le volume de la phase liquide par rapport à celui de la phase gazeuse dans les systèmes prime et seconde. On a alors, en vertu de l'équation caractéristique des gaz parfaits,

$$V' \cong \frac{m'_a R_a T'}{p - p'_v} \text{ et } V'' \cong \frac{m''_a R_a T''}{p - p''_v} \qquad (9)$$

où R_a est la constante spécifique des gaz parfaits pour l'air sec et p'_v, p''_v les pressions partielles de la vapeur d'eau dans les deux systèmes.

On sait d'autre part que les rapports de mélange dans les systèmes prime et seconde sont donnés par les relations

$$r'_v = \frac{m'_v}{m'_a} = \frac{\varepsilon p'_v}{p - p'_v}, \quad r''_v = \frac{m''_v}{m''_a} = \frac{\varepsilon p''_v}{p - p''_v}, \qquad (10)$$

où ε est la gravité spécifique de la vapeur d'eau.

Posons

$$r'_e = \frac{m'_e}{m'_a}, \quad r''_e = \frac{m''_e}{m''_a}. \qquad (11)$$

En différentiant les relations (10) et (11), on a

$$\left.\begin{aligned} dm'_v &= m'_a dr'_v + r'_v dm'_a, \\ dm''_v &= m''_a dr''_v + r''_v dm''_a, \end{aligned}\right\} \quad \left.\begin{aligned} dm'_e &= m'_a dr'_e + r'_e dm'_a, \\ dm''_e &= m''_a dr''_e + r''_e dm''_a. \end{aligned}\right\} \qquad (12)$$

Eu égard à (2) et (11), l'équation (8) s'écrit

$$\begin{aligned} &(m'_a c_{pa} + m'_v c_{pv} + m'_e c_{pe})dT' + \\ &+ (m''_a c_{pa} + m''_v c_{pv} + m''_e c_{pe})dT'' + \\ &[(c_{pa} + r''_v c_{pv} + r''_e c_{pe})(T'' - T') + L'_v(r''_v - r'_v)] \times \\ &\times dm''_a + m'_a L'_v dr'_v + m''_a[L'_v + c_{pv}(T'' - T')]dr''_v + \\ &+ m''_a c_{pe}(T'' - T')dr''_e - R_a \times \\ &\times \left(\frac{m'_a T'}{p - p'_v} + \frac{m''_a T''}{p - p''_v}\right)dp = 0. \end{aligned} \qquad (13)$$

Remarquons que cette équation est une relation différentielle linéaire à six fonctions inconnues d'une variable indépendante p.

Exprimons maintenant que les systèmes prime et seconde restent saturés au cours de la transformation adiabatique en écrivant que la loi du déplacement de l'équilibre est satisfaite dans les deux systèmes. Cette loi s'écrit comme suit dans le système prime

$$\frac{\varepsilon L'_v}{(T')^2} dT' = R_a \frac{dp'_v}{p'_v}. \tag{14}$$

On a d'autre part, en différentiant la première relation (10),

$$dr'_v = \frac{(\varepsilon + r'_v) dp'_v}{p - p'_v} - \frac{r'_v dp}{p - p'_v} \tag{15}$$

ou encore, compte tenu de (14),

$$dr'_v = \frac{r'_v(\varepsilon + r'_v) L'_v}{R_a (T')^2} dT' - \frac{r'_v dp}{p - p'_v}. \tag{16}$$

On montrerait de même que, pour le système seconde, on a

$$dr''_v = \frac{r''_v(\varepsilon + r''_v) L''_v}{R_a (T'')^2} dT'' - \frac{r''_v dp}{p - p''_v}. \tag{17}$$

En remplaçant dr'_v et dr''_v par leurs valeurs tirées de (16) et (17) dans (13), cette équation prend la forme suivante

$$\frac{dT'}{dp} = \frac{X}{Y} \tag{18}$$

où

$$X = \frac{m'_a R_a T'}{p - p'_v}\left(1 + \frac{r'_v L_v}{R_a T'}\right) + \frac{m''_a R_a T''}{p - p''_v} + \frac{m''_a [L'_v - c_{pv}(T' - T'')] r''_v}{(p - p''_v)} +$$

$$+ \left[(c_{pa} + r''_v c_{pv} + r''_e c_{pe})(T' - T'') + L'_v (r'_v - r''_v)\right] \times \left(\times \frac{dm''_a}{dp} + m''_a c_{pe}(T' - T'') \frac{dr''_e}{dp} - \right.$$

$$\left. - \left[(m''_a c_{pa} + m''_v c_{pv} + m''_e c_{pe}) + [m''_a L'_v - c_{pv}(T' - T'')] \frac{r''_v(\varepsilon + r''_v) L''_v}{R_a (T'')^2}\right] \frac{dT''}{dp}\right. \tag{19}$$

et

$$Y = m'_a c_{pa} + m'_v c_{pv} + m'_e c_{pe} + \frac{m'_a r'_v (\varepsilon + r'_v)(L'_v)^2}{R_a (T')^2}. \tag{20}$$

Remarquons que la relation différentielle (18) ne contient plus que quatre fonctions inconnues (m''_a, r''_e, T', T'') d'une variable indépendante p, deux fonctions ayant été éliminées en exprimant que l'air est saturé dans les systèmes prime et seconde.

Introduisons l'opérateur

$$d = d_i + d_e \tag{21}$$

où le signe différentiel d_i se rapporte aux transformations massiques qui se produisent à l'intérieur d'un système ouvert et le signe différentiel d_e aux échanges de masse du système avec l'extérieur.

On a

$$d_i m'_a = 0, \quad d_i m'_v + d_i m'_e = 0, \tag{22}$$

et

$$d_i m''_a = 0, \quad d_i m''_v + d_i m''_e = 0. \tag{23}$$

L'expression (18) se simplifie considérablement si l'on fait les hypothèses suivantes.

La *première* hypothèse est que l'entraînement de l'air sec, de la vapeur d'eau et de l'eau liquide dans la bulle (système prime) est proportionnel aux masses de ces constituants dans l'air ambiant, c'est-à-dire que

$$\frac{d_e m''_a}{m''_a} = \frac{d_e m''_v}{m''_v} = \frac{d_e m''_e}{m''_e}. \tag{24}$$

Différentions logarithmiquement les secondes relations (10) et (11), nous obtenons

$$\frac{d_e r''_v}{r''_v} = \frac{d_e m''_v}{m''_v} - \frac{d_e m''_a}{m''_a} \tag{25}$$

et

$$\frac{d_e r''_e}{r''_e} = \frac{d_e m''_e}{m''_e} - \frac{d_e m''_a}{m''_a}, \tag{26}$$

d'où, (24),

$$d_e r''_v = 0, \quad d_e r''_e = 0. \tag{27}$$

La *seconde* hypothèse consiste à supposer que les transformations du système ouvert seconde sont pseudoadiabatiques, c'est-à-dire que (cf. Van Mieghem et Dufour, 1948, § 41)

$$dH'' - V'' dp - h''_a d_e m''_a - h''_v d_e m''_v - h''_e d_e m''_e = 0, \tag{28}$$

ou encore, compte tenu de (3), (4), (5) et (21), que

$$\left.\begin{aligned}(m''_a c_{pa} + m''_v c_{pv} + m''_e c_{pe}) dT'' - \\ - V'' dp + L''_v d_i m''_v = 0.\end{aligned}\right\} \tag{29}$$

Mais, eu égard à (10), (11), (21), (23) et (27),

$$d_i m_v'' = m_a'' d_i r_v'' = m_a'' dr_v'' \qquad (30)$$

et

$$d_i m_e'' = m_a'' d_i r_e'' = m_a'' dr_e'' \,. \qquad (31)$$

En ajoutant les équations (30) et (31) membre à membre, on trouve, compte tenu de (23), que

$$dr_v'' = -\,dr_e'' \,. \qquad (32)$$

Eu égard à (1), (17) et (30), l'équation (29) prend alors la forme suivante

$$\left[m_a'' c_{pa} + m_v'' c_{pv} + m_e'' c_{pe} + m_a'' \frac{r_v''(\varepsilon + r_v'')(L_v'')^2}{R_a (T'')^2}\right] \times \frac{dT''}{dp} = \frac{m_a'' R_a T''}{p - p_v''} + \frac{m_a'' L_v'' r_v''}{p - p_v''} \,. \qquad (33)$$

Revenons à l'équation (18) qui s'écrit, compte tenu de (32) et (33),

$$\frac{dT'}{dp} = \frac{\dfrac{m_a' R_a T'}{p - p_v'}\left(1 + \dfrac{r_v' L_v'}{R_a T'}\right) + \left[(c_{pa} + r_v'' c_{pv} + r_e'' c_{pe})(T' - T'') + L_v'(r_v' - r_v'')\right]\dfrac{dm_a''}{dp}}{m_a' c_{pa} + m_v' c_{pv} + m_e' c_{pe} + \dfrac{m_a' r_v'(\varepsilon + r_v')(L_v')^2}{R_a (T')^2}} \,. \qquad (34)$$

En première approximation, p_v' est négligeable devant p et il en est de même de $r_v'' c_{pv} + r_e'' c_{pe}$ devant c_{pa}, de $m_v' c_{pv} + m_e' c_{pe}$ devant $m_a' c_{pa}$ et de r_v' devant ε. En tenant compte de ces approximations, l'équation (34) prend la forme suivante

$$\frac{dT'}{dp} \cong \frac{\dfrac{R_a T'}{c_{pa} p}\left(1 + \dfrac{r_v' L_v'}{R_a T'}\right) + \left[(T' - T'') + \dfrac{L_v'}{c_{pa}}(r_v' - r_v'')\right]\dfrac{1}{m_a'}\dfrac{dm_a''}{dp}}{1 + \dfrac{r_v'(L_v')^2}{c_{pa} R_a (T')^2}} \,. \qquad (35)$$

Cette équation approchée a la même forme que l'équation approchée à laquelle on arrive en étudiant l'entraînement d'air humide non saturé dans de l'air humide saturé (Dufour 1956). Cette équation s'écrit, avec les notations utilisées ci-dessus

$$\frac{dT'}{dp} \cong \frac{\dfrac{R_a T'}{c_{pa} p}\left(1 + \dfrac{r_v' L_v'}{R_a T'}\right) + \left[(T' - T'') + \dfrac{L_v'}{c_{pa}}\left(r_v' - \dfrac{U''}{100} r_v''\right)\right]\dfrac{1}{m_a'}\dfrac{dm_a''}{dp}}{1 + \dfrac{r_v'(L_v')^2}{c_{pa} R_a (T')^2}} \,. \qquad (36)$$

où U'' est l'humidité relative du système seconde. On voit ainsi que (35) est un cas particulier de (36), celui où $U'' = 100$ % et où l'air entraîné est donc saturé.

Lorsque $dm_a''/dp = 0$, c'est-à-dire lorsqu'il n'y a pas d'entraînement, l'équation (35) prend la forme classique du taux de variation individuelle de la température par unité de pression lors d'une transformation adiabatique de saturation, à savoir

$$\frac{dT'}{dp} = \frac{\dfrac{R_a T'}{c_{pa} p}\left(1 + \dfrac{r_v' L_v'}{R_a T'}\right)}{1 + \dfrac{\varepsilon r_v'(L_v')^2}{c_{pa} R_a (T')^2}} \,. \qquad (37)$$

Posons

$$\frac{1}{m_a'}\frac{dm_a''}{dp} = k \qquad (38)$$

où k est ce que nous appellerons le coefficient d'entraînement dont on ne connaît malheureusement pas la valeur.

Pour se faire une idée de cette valeur, partons d'un fait d'observation, à savoir que les cumulus se dissipent continuellement dans leur partie latérale. Ce phénomène est expliqué en admettant que de l'air ambiant non saturé est entraîné dans l'air saturé du nuage, ce qui provoque l'évaporation des gouttelettes nuageuses. Dans le cas considéré, l'entraînement est donc tel que dT'/dp est, en première

approximation, égal au taux de variation individuelle de la température lors d'une transformation adiabatique d'air sec. En introduisant ce taux dans la formule (36), il est alors possible de déterminer la valeur de k.

Considérons le cas où, à la pression de 900 mb, de l'air humide non saturé dont la température $T'' = 282$ °K et l'humidité relative $U'' = 50$ % est entraîné dans de l'air humide saturé dont la température $T' = 283$ °K.

Calculons, à l'aide de la formule (37), où nous avons posé $r'_v = 0$, le taux de variation individuelle de la température lors d'une transformation adiabatique d'air sec. On trouve[1]

$$\left(\frac{dT'}{dp}\right)_1 = 8{,}98 \times 10^{-2} \text{ °C, } mb^{-1}. \quad (39)$$

En portant la valeur (39) dans l'équation (36), on a dans le cas considéré,

$$k = 8{,}56 \times 10^{-3} mb^{-1} \quad (40)$$

ce qui correspond à peu près au doublement de la masse d'air par entraînement pour une variation de pression de 100 mb.

En admettant que le coefficient d'entraînement soit le même au cœur du nuage que sur les bords, on trouve, compte tenu de (40) et de (35), que

$$\left(\frac{dT'}{dp}\right)_2 = 5{,}48 \times 10^{-2} \text{ °C, } mb^{-1} \quad (41)$$

lorsque l'air entraîné est saturé.

S'il n'y avait pas d'entraînement, on aurait, d'après (37), dans le cas considéré

$$\left(\frac{dT'}{dp}\right)_3 = 4{,}64 \times 10^{-2} \text{ °C, } mb^{-1}. \quad (42)$$

La comparaison des valeurs (41) et (42) montre que l'entraînement d'air humide saturé ambiant affecte peu le taux de variation de la température en fonction de la pression dans une masse d'air humide saturé qui se déplace au cœur d'un cumulus.

En première approximation, on peut donc admettre, comme on l'a fait jusqu'ici sans le prouver, que le taux de variation de la température en fonction de la pression dans les masses d'air qui se déplacent au cœur d'un cumulus est celui qui résulte des transformations adiabatiques de l'air humide saturé.

C'est grâce au Fonds National de la Recherche Scientifique que j'ai pu effectuer cette recherche lors d'un séjour à l'Institut international de météorologie à Stockholm. Je remercie vivement le Professeur C. G. Rossby et mes collègues étrangers de l'accueil qu'ils m'ont réservé et le Fonds national de la recherche scientifique de l'appui qu'il a bien voulu m'accorder.

[1] Dans ce calcul et dans le suivant nous avons utilisé es valeurs données dans la Publication n° 79 de l'Organisation météorologique mondiale.

BIBLIOGRAPHIE

DUFOUR, L., 1956: Thermodynamical study of the entrainment of air into a cumulus. *Tellus*, **8**, p. 202.

SCORER, R. S. et LUDLAM, F. H., 1953: Bubble theory of penetrative convection. *Quart. J. R. Meteor. Soc.*, **79**, pp. 94—103.

VAN MIEGHEM, J., et DUFOUR, L., 1948: Thermodynamique de l'atmosphère. *Inst. roy. mét. Belgique, Mémoires*, vol. XXX.

Letters to the Editor

Electrodynamic Effects connected with the Motion of a Satellite of the Earth

Dear Sir,

During the International Geophysical Year a number of artificial satellites are planned to be launched into the earth's upper atmosphere. A satellite of the proposed type will move with a velocity of about 7.7×10^3 metres/sec. In the American project the motion is expected to take place in an orbit which has its nearest approach to the earth's surface at an altitude around 500 km. The satellite will have the shape of a sphere, about 0.5 metres in diameter.

A short discussion will be given here on the electrodynamic effects connected with the motion of such a satellite. From accepted data on the ionosphere (KUIPER 1954, ALLEN 1955) is concluded that the mean free path of charged and of neutral particles is much greater than the dimensions of the satellite. The ions at altitudes of 500 km have a thermal velocity of 1.7×10^3 metres/sec., a radius of curvature in the earth's magnetic field of 7 metres and a corresponding gyro time of 0.02 sec., approximately. CHAPMAN and COWLING (1939) state that the mean energy of electrons is likely to exceed the value corresponding to thermal equilibrium at the altitudes in question. The cross section for photo ionization of air is considerable down to wave lengths of about 300 Ångströms (VON ENGEL 1955). A large fraction of the electrons will be released with kinetic energies of the order of the ionization potentials of oxygen and nitrogen, i.e., of the order of 15 eV. The lifetime of electrons at these altitudes is about 10^5 sec. The mean collision time of electrons is approximately in the range from 0.1 to 10 sec., corresponding to between 10^4 and 10^6 collisions during the lifetime of an electron. NICOLET (1953) has shown that Coulomb scattering dominates the collision processes at high altitudes. However, even if inelastic collisions occur less frequently, they are more effective in reducing the electron energy. Thus, the mean energy of electrons should be somewhere between the ionization potential and the value corresponding to thermal equilibrium (0.26 eV at 2000° K), and probably closer to the latter value than to the former. On the night side the mean energy will be brought down by means of collisions to a value somewhat greater than that corresponding to thermal equilibrium. The gyro time of electrons is about 10^{-6} sec. Electrons with energies of the order of 1 eV have velocities of 6×10^5 metres/sec. and a radius of curvature in the earth's magnetic field of 0.07 metres.

An electrically neutral and unpolarized satellite is fed with an ion current directed towards its front half sphere. The electron current is directed mainly along the magnetic field lines and reaches the whole surface of the sphere. It is about 150 times greater than the ion current. Thus, the satellite will be charged to a negative potential such as to cut off almost the whole electron current. i.e., to a potential of the order of — 1 volt at least, i.e., to a potential slightly lower than — 0.7 volts which would be reached in a situation of thermal equilibrium. This value is hardly affected by the ion current which changes very little with potentials of this magnitude. Photo emission of electrons from the surface of the satellite may change its potential. This depends upon the special material which will be used for the construction and cannot be discussed here in detail. Further, the electric field caused by a polarization of the satellite in the earth's magnetic field can be neglected as compared to the field generated by the negative charge.

First consider the separate interaction between the charged satellite and each charged particle in its surroundings. Most of the momentum is transferred to the charged particles during a time which is short as compared to the gyro time of ions, and which is long as compared to that of electrons. This will cause a momentum transfer to ions in a direction perpendicular to the path of the satellite, and to electrons in a direction along the magnetic field lines (cf BOHR 1913, 1915 and FERMI 1951). For the sake of simplicity we assume the satellite to move in a direction nearly perpendicular to the magnetic field lines. When it passes through the ionosphere it repells the electrons in directions along the magnetic field lines and attracts ions in directions nearly perpendicular to its path. If space charge effects are neglected the charge of the satellite will be sufficiently large to cause a full momentum transfer to the scattered particles within a certain distance from its centre. This implies that, inside this distance, the scattered particles are given a momentum as if they were colliding with a rigid wall. In the region further out the momentum transfer decreases with

the distance from the satellite. At large distances the collision times of electrons and ions will be longer than the pulse time, i.e., the time during which the greater part of momentum is transferred in the scattering process. In such a situation we assume that, on the average, the charged particles lose all their systematically directed velocity at each collision and start a new free flight with zero systematical velocity. The energy losses, W_e and W_i, caused per unit time by electron and ion scattering are compared to the energy loss, W_m, caused per unit time by the mechanical drag. On the day side the corresponding ratios become.

$$W_e/W_m \approx 40\ X \text{ and } W_i/W_m \approx 0.16\ X,$$

where the ionization degree, X, is likely to be in the range from 10^{-2} to 10^{-1}. A detailed description of the derivation of these expressions requires too much space to be given here.

These results seem to indicate that the electrodynamic effects should be of considerable importance. However, for a satellite of the present size, they are applicable to regions having very low densities only, and not to the ionosphere around altitudes of 500 km. The charge of the satellite is large enough to "blast off" electrons in front of it in directions along the magnetic field lines. The remaining positive ion charge generates an electric field which screens off the field from the satellite. At an altitude of 500 km the charge of the satellite becomes equal to the total electron charge within a volume of the ionosphere comparable to that of the satellite. This indicates that momentum transfer will take place in its immediate neighbourhood only, essentially inside the Debye distance from the satellite (cf. SPITZER 1956). Thus, the ratios W_e/W_m and W_i/W_m given by the expressions above will be reduced appreciably.

The separation of charge caused by the motion gives rise to an increase in electrostatic energy and in plasma oscillations. Further, the interaction with the ionized gas in the neigbourhood will generate magneto-ionic waves propagated into the external regions (ÅSTRÖM 1950). Electrodynamic forces caused by the interaction between the earth's magnetic field and electric currents will be of the same order as the mechanical drag, provided that a current density of 0.2 amp./metre^2 exists within a volume comparable to that of the satellite. This is a very high value which can hardly be obtained by moving all the charges within the volume with velocities corresponding to the ionization energy. Further investigations are necessary for a definite answer to these questions.

An acknowledgement is gratefully addressed to Prof. H. Alfvén for drawing the author's attention to these problems.

Yours sincerely,

B. LEHNERT
The Royal Institute of Technology, Stockholm

July 11, 1956.

REFERENCES

ALLEN, C. W., 1955: *Astrophysical quantities*, Univ. of London, The Athlone Press.

ÅSTRÖM, E., 1950: On waves in an ionized gas. *Ark. f. fysik*, **2**, p. 443.

BOHR, N., 1913: On the theory of the decrease of velocity of moving electrified particles on passing through matter. *Phil. Mag.* [6], **25**, p. 10.

— 1915: On the decrease of velocity of swiftly moving electrified particles in passing through matter, *ibid.*, **30**, p. 581.

CHAPMAN, S., and COWLING, T. G., 1939: *The mathematical theory of non-uniform gases*, Cambridge Univ. Press, p. 346.

ENGEL, A. VON, 1955: *Ionized gases*, Oxford, Clarendon Press, p. 60—65.

FERMI, E., 1951: *Nuclear physics*, Univ. of Chicago Press, p. 27.

KUIPER, G. P., 1954: *The earth as a planet*, Univ. of Chicago Press.

NICOLET, M., 1953: The collision frequency of electrons in the ionosphere. *J. Atmosph. Terr. Phys.*, **3**, p. 200.

SPITZER, L., 1956: *Physics of fully ionized gases*, Interscience Publ., N.Y.

The reader is also referred to:

SINGER, S. F., 1956 a: Measurements of interplanetary dust, Physics Dept. *Techn. Rep. No. 33, Univ. of Maryland.*

— 1956 b: Studies of a minimum orbital unmanned satellite of the earth (MOUSE). Part II. Orbits and lifetimes of minimum satellites. *Astronautica Acta*, **2**, p. 125.

International Geophysical Year, A special report prepared by the National Academy of Sciences for the Committee on Appropriations of the United States Senate, presented by Mr. Hayden, May 28, 1956, United States Government Printing Office, Washington: 1956.

Blue Suns

Dear Sir,

A note on a blue sun in the Canadian Arctic in September 1951 may be an addition of some interest to the series of observations made about the same time as reported in papers in Tellus 3.

About noon on Sept. 27, 1951 near Resolute, 74.5°N, 59°W in the Canadian Arctic, I observed a distinctly (darkish) blue sun shining through thin alto-stratus (accompanied by two mock suns). It persisted for about half an hour after I first noticed it, after which the sun was hidden by thickening alto-stratus.

The date is that of the appearances of blue suns in Denmark, S. France. NW. Spain, and at Stockholm. The sun may have been blue on previous days in the Arctic but not noticed; I have not seen any such report in the logs of the Canadian Stations or from elsewhere in the Arctic.

Toronto, May 20, 1956

W. E. KENDREW
Meteorological Office

Errata

Volume 8, number 2. Page 126, Fig 14, Line 2: for "ca. 1.5 curies" read "ca. 0.5 curies".

Current Data on the Chemical Composition of Air and Precipitation VII

(For further information see Egnér, H., Eriksson, E., *Tellus* **7**, pp. 134—139, and *Tellus* **8**,p. 285.)

Code	D 602												L 602						
	mm	mg/m²							pH	HCO_3^- $\frac{\mu val}{l}$	$\frac{\varkappa \cdot 10^6}{\Omega \cdot cm}$	$\mu g/m^3$ (= kg/km³)						
		S	Cl	NO_3–N	NH_3–N	Na	K	Mg	Ca				S	Cl	NH_3–N	Na	K	Mg	Ca
Ri	21	10	71	2	3	37	3	6	19	6.2	25	20	3.7	1.4	2.0	3.1	5.7	2.0	19.
Ki	15	11	7	1	1	6	1	3	33	5.5	0	13	1.3	6.7	0.8	0.9	1.5	0.5	4.6
Ar	17	17	24	3	2	9	3	4	17	5.4	0	16	8.0	5.7	1.9	2.0	1.0	2.0	5.8
Öj	17	21	21	4	2	24	5	7	62	6.9	98	33	*	*	*	*	*	*	*
Rö	20	23	24	5	2	26	2	5	37	6.5	28	22	*	*	*	*	*	*	*
Of	27	37	127	7	23	103	57	6	46	6.9	118	51	5.5	8.7	1.6	0.8	0.8	0.7	6.7
Br	13	15	43	3	5	24	2	10	10	6.1	15	25	2.3	3.5	0.5	1.1	0.3	0.5	0.4
ÅF	29	32	51	2	2	30	2	5	16	5.7	0	13	11.	2.2	1.8	2.0	1.0	0.8	4.5
ÅH	—	—	—	—	—	—	—	—	—	—	—	—	—	—	—	—	—	—	—
Sv	39	36	18	5	2	21	9	6	48	5.2	0	18	—	—	—	—	—	—	—
Rä	11	18	20	4	1	10	4	4	129	7.5	*	74	14.	9.5	1.5	0.7	0.5	0.3	6.6
Åm	31	29	48	7	14	28	17	7	28	5.7	0	22	*	*	*	*	*	*	*
Sa	19	47	43	8	8	23	9	14	72	6.0	11	45	16.	1.2	2.1	0.8	0.4	0.8	2.7
Ul	18	16	17	4	4	10	1	5	18	4.9	0	21	11.	2.7	1.2	0.4	0.3	0.6	0.0
Er	21	19	26	3	2	17	3	5	18	4.9	0	21	*	*	*	*	*	*	*
St	19	22	14	4	1	19	7	5	44	6.4	28	24	13.	2.8	1.6	1.4	0.7	0.1	2.6
Fo	10	15	29	3	2	14	7	5	20	6.0	11	31	10.	3.3	1.9	2.8	3.5	0.5	6.0
Kv1	2	147	17	5	17	15	8	12	205	3.9	*	646	55.	0.0	5.8	0.7	0.5	3.0	10.
Kv7	13	34	21	5	6	11	2	5	29	4.3	0	53	9.5	0.0	2.5	0.6	0.2	1.4	3.7
VN	3	12	12	2	1	11	3	4	19	*	*	85	—	—	—	—	—	—	—
La	5	11	10	2	1	8	1	4	16	*	*	44	0.0	1.6	0.7	2.2	2.7	0.7	6.3
Bo	2	8	28	3	1	13	0	5	3	*	*	82	*	*	*	*	*	*	*
Vi	3	39	505	5	4	276	12	36	25	*	*	761	46.	480.	3.1	220.	14.	29.	51.
Fa	26	24	32	4	4	19	2	5	7	4.6	0	24	7.6	0.0	4.1	1.4	2.0	2.1	15.
Fl	8	13	40	3	5	21	13	4	12	6.5	52	49	*	*	*	*	*	*	*
Am	12	18	14	2	1	17	7	5	25	6.6	54	26	—	—	—	—	—	—	—
Si	32	40	89	6	8	45	11	7	2	4.8	0	27	—	—	—	—	—	—	—
Pl	10	33	73	6	25	44	7	6	24	6.3	44	82	16.	6.5	18.	5.0	1.2	0.9	2.2
Sö	10	43	27	5	6	14	12	6	73	6.3	24	68	—	—	—	—	—	—	—
Sm	24	25	54	5	6	22	2	5	17	4.5	0	30	11.	5.4	1.9	1.5	0.3	0.8	7.7
Sy	22	13	36	6	7	25	4	5	33	6.2	24	22	*	*	*	*	*	*	*
BH	9	23	18	5	3	15	1	4	13	4.9	0	37	*	*	*	*	*	*	*
Ha	8	30	43	8	15	25	5	5	25	5.3	0	72	—	—	—	—	—	—	—
Al	15	37	36	8	10	23	3	7	34	4.9	0	44	21.	7.6	2.7	2.1	0.6	0.0	4.7
Hi	0.4	*	*	*	*	*	*	*	*	*	*	100	—	—	—	—	—	—	—
Ås	0	0	0	0	0	0	0	0	0	—	0	0	*	*	*	*	*	*	*
Vå	5	8	4	2	2	4	1	3	10	*	*	26	*	*	*	*	*	*	*
Li	20	31	376	8	3	207	9	26	21	4.9	0	87	14.	15.	1.2	6.5	0.7	1.1	7.6
Ka	10	14	33	3	4	7	7	2	28	6.3	29	33	9.4	50.	4.1	5.0	11.	1.2	2.8
Ku	1	*	*	*	*	*	*	*	*	*	*	93	0.0	14.	3.9	1.4	0.5	1.0	14.
Jy	5	19	31	4	7	22	18	3	16	*	*	87	5.6	4.2	0.9	0.3	0.2	0.4	4.4
Tv	10	12	74	4	2	41	4	6	13	5.5	0	45	*	*	*	*	*	*	*
Öd	6	28	74	6	17	42	6	7	12	4.8	0	112	14.	41.	5.5	19.	3.4	2.9	5.1
As	16	46	187	7	14	52	21	9	65	4.8	0	80	*	*	*	*	*	*	*
Ty	13	42	110	9	21	55	5	10	15	5.3	0	69	18.	17.	4.1	3.8	0.0	1.1	9.2
Ab	46	80	722	8	10	372	19	48	40	4.4	0	89	18.	25.	3.2	18.	2.0	2.9	19.
Ed	28	72	242	9	21	141	12	21	38	5.4	0	59	*	*	*	*	*	*	*
Le	11	54	308	9	32	148	9	21	46	4.4	0	173	41.	260.	8.3	100.	6.7	16.	16.
Ro	4	23	128	9	5	55	7	10	51	*	*	203	*	*	*	*	*	*	*
NA	4	9	33	4	6	21	3	3	11	*	*	79	26.	7.9	7.5	2.6	0.1	0.1	6.0
Au	1	*	86	*	*	27	*	*	*	*	*	*	25.	0.5	2.6	1.3	1.5	5.1	5.5
Gü	16	28	22	12	6	8	2	10	42	5.2	0	34	39.	7.6	4.0	1.0	1.2	0.5	14.
Fe	20	84	19	15	28	16	13	7	30	4.1	0	84	9.2	0.0	1.8	2.1	1.3	0.4	1.7

— No sampling
* Sample discarded

Code	D 603												L 603						
	mg/m²												µg/m³ (= kg/km³)						
	mm	S	Cl	NO_3–N	NH_3–N	Na	K	Mg	Ca	pH	$HCO_3 - \frac{\mu val}{l}$	$\frac{\varkappa \cdot 10^6}{\Omega \cdot cm}$	S	Cl	NH_3–N	Na	K	Mg	Ca
Ri	52	31	114	4	4	60	6	10	20	5.6	0	16	7.8	4.2	1·3	2.1	2.4	1.5	14.
Ki	1	*	*	*	*	*	*	*	*	*	*	25	0.0	1.5	0.1	0.3	0.0	0.4	0.0
Ar	3	*	12	*	*	8	*	*	*	*	*	*	3.5	4.0	3.1	1.4	0.7	0.2	4.3
Öj	0	0	0	0	0	0	0	0	0	—	0	0	4.7	1.0	2.7	0.8	1.0	3.6	5.9
Rö	0	0	0	0	0	0	0	0	0	—	0	0	14.	6.2	2.2	1.4	0.8	0.1	7.0
Of	5	13	11	1	2	10	1	8	10	*	*	35	6.7	14.	4.4	3.4	2.3	0.4	8.2
Br	4	6	24	1	3	15	13	1	6	*	*	53	3.1	1.5	1.0	0.5	0.0	0.1	2.6
ÅF	24	24	44	3	5	30	3	5	12	5.8	4	19	7.7	4.1	1.4	0.3	0.0	0.6	5.3
ÅH	—	—	—	—	—	—	—	—	—	—	—	—	—	—	—	—	—	—	—
Sv	4	*	16	*	*	49	*	*	*	*	*	*	—	—	—	—	—	—	—
Rä	4	18	7	3	0	2	9	1	73	*	*	133	5.3	6.4	2.2	1.3	1.1	1.7	11.
Åm	5	5	2	1	0	4	0	1	3	*	*	19	*	*	*	*	*	*	*
Sa	7	5	10	1	1	6	1	1	6	6.5	*	20	9.1	4.7	2.3	0.7	0.5	0.2	4.5
Ul	6	7	8	1	3	4	0	1	2	5.0	*	24	9.3	3.3	2.0	0.5	0.1	0.0	0.0
Er	3	*	14	*	*	22	*	*	*	*	*	*	*	*	*	*	*	*	*
St	4	3	4	0	0	8	0	1	9	*	*	31	9.7	3.2	2.4	0.8	0.4	0.2	5.9
Fo	7	12	13	2	2	12	1	1	14	6.7	44	33	1.8	4.2	1.7	2.5	1.3	0.3	6.3
Kv1	4	128	5	3	8	44	6	5	154	*	*	328	62.	6.7	6.2	1.0	0.6	1.0	15.
Kv7	3	11	3	2	3	3	0	14	9	*	*	52	8.9	3.0	6.2	1.0	0.1	1.3	8.8
VN	9	14	10	3	4	9	2	2	16	6.3	39	29	—	—	—	—	—	—	—
La	0	0	0	0	0	0	0	0	0	—	0	0	*	*	*	*	*	*	*
Bo	16	24	73	5	4	57	10	13	48	6.7	99	55	6.7	4.9	2.1	2.8	1.9	0.4	0.5
Vi	4	18	152	5	3	95	5	77	9	*	*	185	19.	23.	3.1	5.3	0.0	1.1	6.5
Fa	7	12	14	2	2	14	0	3	10	5.9	*	34	0.0	14.	3.9	4.5	2.7	14.	22.
Fl	12	15	37	3	4	26	3	9	15	6.3	38	29	8.0	0.0	2.2	1.9	1.6	0.4	4.6
Am	20	24	171	2	0	94	6	14	15	6.3	21	44	—	—	—	—	—	—	—
Si	20	22	62	4	6	40	4	7	16	5.7	6	25	—	—	—	—	—	—	—
Pl	8	30	128	5	20	76	1	12	23	6.7	79	122	8.5	9.1	9.2	2.3	0.4	0.3	7.5
Sö	16	26	56	6	8	33	4	6	44	6.3	28	38	—	—	—	—	—	—	—
Sm	6	8	20	1	1	21	2	2	11	6.9	*	40	7.0	4.2	2.6	0.7	0.2	4.2	5.7
Sy	9	5	11	1	2	11	0	2	6	6.4	28	17	*	*	*	*	*	*	*
BH	21	26	76	6	10	44	3	8	19	4.9	0	36	8.4	6.4	3.5	0.9	0.1	0.3	3.7
Ha	5	25	76	4	10	47	4	48	27	*	*	118	—	—	—	—	—	—	—
Al	17	31	79	3	10	48	5	76	29	5.8	6	43	3.0	4.9	3.0	1.0	0.0	4.3	3.5
Hi	5	25	45	6	1	76	4	15	13	*	*	107	—	—	—	—	—	—	—
Ås	23	33	10	8	13	15	3	4	24	5.0	0	28	8.3	14.	5.6	1.2	0.8	0.8	3.5
Vå	2	*	*	*	*	*	*	*	*	*	*	56	*	*	*	*	*	*	*
Li	19	33	1630	7	5	850	33	101	59	5.6	5	333	4.4	21.	1.8	12.	0.6	3.2	2.5
Ka	1	*	*	*	*	*	*	*	*	*	*	87	*	*	*	*	*	*	*
Ku	8	9	3	2	2	2	0	2	10	5.7	12	18	8.6	5.9	4.4	2.4	0.0	0.1	0.0
Jy	6	7	8	1	3	9	4	1	9	6.5	*	28	1.0	1.5	0.7	0.3	0.0	0.0	2.9
Tv	4	4	13	1	1	9	0	2	5	*	*	32	2.0	2.6	0.6	0.5	0.2	0.0	2.3
Öd	19	39	160	8	20	76	6	12	28	5.1	0	63	8.4	1.9	4.6	2.1	0.6	0.1	7.9
As	31	56	386	10	20	206	16	26	46	4.9	0	74	11.	5.6	4.9	1.9	0.0	0.2	2.7
Ty	10	17	113	3	5	65	3	39	32	6.7	110	71	16.	10.	7.1	3.3	0.2	0.5	13.
Ab	34	73	614	38	56	347	20	44	53	4.6	0	122	31.	19.	5.3	5.2	1.2	2.5	29.
Ed	33	37	231	13	17	111	9	19	37	5.5	0	46	11.	1.8	4.3	1.6	0.1	0.2	12.
Le	16	63	202	23	29	84	11	19	84	4.8	0	115	29.	47.	6.7	28.	2.0	4.3	15.
Ro	22	54	77	18	12	37	14	29	76	5.1	0	56	27.	13.	5.4	3.2	1.2	0.6	17.
NA	39	89	450	25	48	233	17	31	90	5.9	23	76	14.	17.	7.8	4.2	0.2	0.0	5.1
Au	20	57	31	15	20	20	9	31	68	5.9	14	48	39.	6.9	11.	1.6	2.8	8.6	23.
Gü	32	51	22	22	34	12	7	7	37	4.7	0	36	37.	2.4	5.3	1.6	1.1	8.9	7.4
Fe	53	48	35	12	17	26	5	10	39	5.6	7	16	7.6	0.0	2.5	2.2	1.2	1.4	2.5

— No sampling
* Sample discarded

Uppsala, May 29, 1956
G. Brodin
Agricultural College

CO_2-values Febr.—April 1956 in Scandinavia.

(Cf. FONSELIUS, KOROLEFF: *Tellus* **7**, pp. 258—265).

Station	February					March					April				
	Date	°C	Wind		Weather	ml/10 l.	Date	°C	Wind		Weather	ml/10 l.	Date	°C	Wind		Weather	ml/10 l.
Ab	1	— 9.0	SSE	0	⚹° 10	3.25	1	—5.0	NW	4	0	3.24	1	— 3.0	WNW	6	⚹² 10	3.35
	10	— 14.0	SW	2	≡ 10	3.01	10	4.5	WNW	5	10	3.26	10	— 5.0	E	6	⚹° 10	3.34
	20	— 10.0	SSW	4	0	3.25	20	—8.0	NNW	2	= 3	3.25	20	— 1.0	SSW	4	4	3.16
Öj	1	— 6.2	W	2	10	3.01	1	—0.1	NW	1	2	3.20	1	2.4	NE	2	9	3.27
	10	— 27.6	Calm		=° 0	2.95	10	8.5	W	4	8	3.23	10	— 1.4	NE	1	⚹ 10	3.42
	20	— 11.6	»		⚹° 10	3.30	20	—1.5	SSW	3	1	3.20	20	4.9	N	3	0	3.26
Br	1	— 12.0	N	5	10	3.21	1	0.0	W	1	⚹° 5	3.20	1	3.0	NNW	5	8	3.28
	10	— 8.0	W	1	⚹° 10	3.03	10	5.0	SW	1	1	3.19	10	0.0	NE	1	10	3.33
	20	— 15.0	E	1	0	3.25	20	—2.0	SSE	5	2	3.14	20	7.0	NW	1	0	3.30
Ul	1	— 12.9	N	4	⚹ 10	3.45	1	4.8	SW	4	0	3.29	1	7.0	NNW	4	4	3.24
	10	— 16.0	N	4	0	3.31	10	0.6	SSW	3	8	3.20	10	1.9	SE	2	= 10	3.35
	20	— 1.6	SE	2		3.37	20	4.3	SSE	3	0	3.21	20					
Fl	1	— 12.6	N	2	7	3.17	1	3.0	NW	2	0	3.14	1	4.4	NE	1	4	3.20
	10	— 16.2	NE	2	0	3.19	10	0.6	N	1	0	3.19	10	3.2	SW	1	, 10	3.36
	20	— 2.8	E	2	0	3.30	20	4.6	ESE	2	0	3.17	20	6.4	NE	2	0	3.40
Pl	1	— 13.0	NE	2	0	3.21	1						1	5.0	NW	3	●° 10	3.21
	10	— 13.0	NE	3	3	3.28	10	2.0	Calm		7	3.25	10	4.0	W	3	●° 10	3.34
	20	— 1.0	NE	1	10	3.22	20	4.0	SE	7	1	3.16	20	9.0	E	2	4	3.31
Ka	1	— 11.6	NNE	3	5	3.27	1	—1.0	N	4	5	3.25	1	1.5	NNW	3	0	3.30
	10	— 23.0	SSW	3	5	3.21	10	—0.1	SW	4	5	3.41	10	1.0	S	3	⚹ 10	3.16
	20	— 6.4	S	6	5	3.19	20						20	0.1	NE	0	6	3.33
Ri	1	— 4.9	N	4	5	3.17	1	0.3	SW	1	5	3.33	1	— 2.0	WNW	2	5	3.28
	10	— 21.5	N	1	0	3.12	10	—1.8	SSW	3	5	3.39	10	0.6	E	2	● 10	3.50
	20	— 7.9	SE	4	5	3.29	20	—1.0	SW	2	0	3.27	20	1.5	NW	2	0	3.47
Lu	1	— 8.8	N	3	5	3.40	1	—0.4	SSW	2	5	3.28	1	— 2.2	W	3	⚹ 10	3.25
	10	— 21.9	N	3	0	3.16	10	—1.6	SW	3	0	3.31	10	1.4	ESE	2	0	3.36
	20	— 8.0	S	4	5	3.26	20						20	3.3	NNW	3	5	3.44
Tv	1	— 12.0	N	4	5	3.19	1	3.0	WSW	1	0	3.29	1	2.0	W	3	0	3.19
	10	— 20.0	NE	1	0	3.34	10	—1.5	W	1	5	3.35	10	2.0	SE	0	≡ 10	3.22
	20	— 7.0	SE	1	0	3.41	20						20	4.5	S	1	5	3.42
Bo	1	— 7.8	ENE	3	4	3.06	1	0.4	NE	2	=° 9	3.15	1	0.4	NNE	4	=° 3	3.28
	10	— 2.5	ENE	3	=° 10	2.92	10	4.2	NNW	4	● ▽ 10	3.26	10	1.8	NNE	5	=° 9	3.19
	20						20	0.2	ENE	1	1	3.18	20	4.8	NNE	2	=° 7	3.47
Vå	1	— 18.2	E	1	5	3.23	1	—1.1	SW	8	⚹° 5	3.23	1	9.0	SSW	1	=° 0	3.33
	10	— 10.4	W	1	5	3.24	10	—4.5	SW	1	0	3.19	10	4.6	W	2	10	3.29
	20	— 15.4	WNW		=° 2	3.31	20	—1.5	NE	2	6	3.29	20	12.6	E	1	4	3.27
Be	1	— 5.4	ENE	2	4	3.32	1	4.3	WNW	4	10	3.30	1	6.0	SW	1	● 6	3.35
	10	— 0.4	SE	1	⚹° 10	3.29	10	8.1	SSE	3	0	3.43	10	3.0	N	4	=▽ 10	3.31
	20	— 1.0	Calm		4	3.43	20	5.1	Calm		5	3.49	20	8.7	N	0	8	3.49
Öd	1	— 12.0	NE	3	⚹° 4	3.32	1	5.0	W	5	8	3.27	1	1.6	NNE	3	8	3.27
	10	— 11.0	NE	2	2	3.23	10	2.0	SSE	1	= 10	3.27	10	6.4	SW	4	= 9	3.35
	20	— 3.2	NE	2	⚹° 9	3.31	20	1.8	ENE	4	2	3.26	20	13.0	NNE	2	0	3.32
As	1	— 10.1	ENE	5	⚹ 10	3.29	1	3.8	NW	5	6	3.25	1					
	10	— 11.6	NE	3	0	3.49	10	1.7	NE	1	=° 10	3.27	10	6.2	W	5	●° 10	3.39
	20	— 7.8	SE	2	0	3.36	20	1.8	SE	6	5	3.33	20	14.2	NW	2	4	3.27

Symbols used for description of weather conditions, are those, internationally used. The numbers in the weather column give the cloudiness.